Development of bioorthogonal synthetic strategies towards hybrid macromolecular conjugates with tailored properties

TECHNISCHE UNIVERSITÄT DARMSTADT

Vom Fachbereich Chemie
der Technischen Universität Darmstadt

zur Erlangung des akademischen Grades eines
Doktor-Ingenieurs (Dr.-Ing.)

genehmigte
kumulative Dissertation

vorgelegt von

Dipl.-Ing. Christina Uth
aus Seoul (Südkorea)

Referent:	Prof. Dr. Harald Kolmar
Korreferent:	Prof. Dr. Siegfried Neumann

Tag der Einreichung:	19. September 2016
Tag der mündlichen Prüfung:	07. November 2016

Darmstadt 2016

D 17

Die vorliegende Arbeit wurde unter der Leitung von Herrn Prof. Dr. Harald Kolmar am Clemens-Schöpf-Institut für Organische Chemie und Biochemie der Technischen Universität Darmstadt von September 2011 bis August 2016 angefertigt.

A fin de alcanzar lo imposible, hay que intentar lo absurdo.

Miguel de Cervantes

Die Ergebnisse der vorliegenden Arbeit wurden an folgenden Stellen vorgestellt, veröffentlicht oder zur Veröffentlichung eingereicht:

C. Uth, S. Zielonka, S. Hörner, N. Rasche, A. Plog, H. Orelma, O. Avrutina, K. Zhang, H. Kolmar, A chemoenzymatic approach to protein immobilization onto crystalline cellulose nanoscaffolds., *Angew. Chem. Int. Ed.,* **2014**, *53*, 2618-12623.
See also: **C. Uth** *et al.*, *Angew. Chem.,* **2014**, *126*, 12826-2832.

S. Hörner,‡ **C. Uth**,‡ O. Avrutina, H. Frauendorf, M. Wiessler and H. Kolmar, Combination of inverse electron-demand Diels-Alder reaction with highly efficient oxime ligation expands the toolbox of site-selective peptide conjugations., *Chem. Commun.,* **2015**, *51*, 11130-11133.

S. Hörner,‡ S. Knauer,‡ **C. Uth**,‡ M. Jöst, V. Schmidts, H. Frauendorf, C. M. Thiele, O. Avrutina, and H. Kolmar, Nanoscale biodegradable organic-inorganic hybrids for efficient cell penetration and drug delivery., *Angew. Chem. Int. Ed.*, **2016**, *55*, 14842–14846.
See also: S. Hörner *et al.*, *Angew. Chem.*, **2016**, *128*, 15063–15068.

‡ Authors contributed equally

Weitere Publikationen und Patente, die im Rahmen dieser Dissertation eingereicht oder veröffentlicht wurden:

S. Zielonka, N. Weber, S. Becker, A. Doerner, A. Christmann, C. Christmann, **C. Uth**, J. Fritz, E. Schäfer, B. Steinmann, M. Empting, P. Ockelmann, M. Lierz, H. Kolmar, Shark attack: High affinity binding proteins derived from shark vNAR domains by stepwise *in vitro* affinity maturation., *J. Biotechnol.*, **2014**, *191*, 236-245.

T. Hofmeyer, S. I. Bulani, J. Grzeschik, S. Krah, B. Glotzbach, **C. Uth**, O. Avrutina, M. Brecht, H. U. Göringer, P. van Zyl, H. Kolmar, Protein production in *Yarrowia lipolytica via* fusion to the secreted lipase Lip2p., *Mol. Biotechnol.*, **2014**, *56*, 1, 79-90.

Knauer, S.; Roese, T. M. L.; Avrutina, O.; Kolmar, H.; **Uth, C., 2016**, Method for peptide synthesis and apparatus for carrying out a method for solid phase synthesis of peptides., Technische Universität Darmstadt, WO/2016/050764.

Konferenzbeiträge

· 12th German Peptide Symposium, Darmstadt, March 18th -21st 2015 (poster)

· Bioorthogonal Chemistry, Berlin, July 16th -18th 2014 (poster)

· 11th German Peptide Symposium, Munich, March 18th -21st 2013 (poster and short talk)

· PEGS Europe, Vienna, November 6th -8th 2012 (poster)

Table of Contents

Zielsetzung und Zusammenfassung

Über die letzten Jahrzehnte wurde eine große Anzahl von chemischen Reaktionen entwickelt, die kompatibel mit bioinspirierten, biotechnologischen und biomimetischen Molekülen sind und den gegenwärtigen Anforderungen des kontinuierlich wachsenden Repertoires von Konjugationstechniken entsprechen. Die Wahl des geeigneten Ansatzes aus der *Toolbox* der sogenannten bioorthogonalen Methoden ist allerdings immer einzelfallabhängig. Das zentrale Ziel der vorgestellten kumulativen Arbeit war deshalb die Konzeption und Entwicklung von neuen kombinierten „orthogonalen bioorthogonalen“[1] Synthesestrategien, d.h. die Entwicklung von bestimmten chemo- und regioselektiven Reaktionen für die Synthese von makromolekularen Konjugaten mit maßgeschneiderten Eigenschaften. Dazu wurde eine Vielzahl von Verbindungen aus verschiedenen molekularen Klassen untersucht, darunter kleine Zytotoxine und Oligopeptide, hoch geordnete kubisch-oktamerische Silsesquioxane (COSS), kristalline Nanocellulose und funktionelle Proteine. Für jedes, in dieser Arbeit beschriebene Konjugat wurde eine individuelle bioorthogonale Synthesestrategie entwickelt, die die intrinsischen Eigenschaften, speziellen Anforderungen und verschiedenen Restriktionen der jeweiligen Reaktionspartner berücksichtigt.

Um eine tragfähige und reproduzierbare Syntheseplattform zu etablieren, wurden drei eigenständige Studien durchgeführt, die jeweils eine Reihe von selektiven chemischen Reaktionen zwischen speziellen funktionellen Molekülen mit den jeweiligen Gegenstücken enthielten. Unter Berücksichtigung, dass Bio-(makro)moleküle sehr komplex und vielfältig sind, sollte der Konjugationsansatz die erforderliche Bioorthogonalität, sowie Flexibilität hinsichtlich Effizienz, Erschwinglichkeit und Leichtigkeit des Zugangs bieten.

Jede individuelle Studie im Rahmen dieser Arbeit adressierte die Kupplung von zwei oder mehr molekularen Strukturen zur Erzeugung molekularer definierter Konstrukte. Alle drei vorgestellten Studien enthielten drei wesentliche Zielsetzungen:

- das Design eines Strukturgerüst-Liganden Systems;
- die Ausarbeitung/Konzeption und Anwendung einer speziellen Synthesestrategie;
- die Untersuchung der Bioaktivität, falls erforderlich.

Das Ziel der ersten Studie war die Immobilisierung von Proteinen unterschiedlicher Größe und Komplexität auf ein kristallines Nanocellulose Strukturgerüst. Als Liganden wurden drei Biomakromoleküle ausgewählt: ein grün- fluoreszierendes Protein, ein Enzym, Galaktose Oxidase und ein anti-Lysozym Haiantikörper. Die spezifischen Konjugate sollten die Eigenschaften der immobilisierten Proteinen mit den intrinsischen Charakteristika der Cellulose Nanokristalle, wie niedrige Toxizität, Wasser- und Biokompatiblität sowie die, durch ihr nanoskaliges Format bedingten offensichtlichen Vorteile, vereinen.

Die zweite Arbeit zielte auf die Entwicklung einer tragfähigen Strategie für die Biofunktionalisierung eines der kleinsten bekannten Nanopartikel, kubisch-oktamerische Silsequioxane (COSS), mit Peptiden. Zunächst sollte eine Vorstudie für die passende Konjugationsplattform mit verschiedenen peptidischen Reaktionspartnern durchgeführt werden. Peptide von unterschiedlicher Länge und Architektur wurden untersucht, darunter eine enzymatische Erkennungssequenz, Cystin-Knoten Miniproteine, ein Integrin bindendes und ein antimikrobielles Peptid, sowie ein Inhibitor einer therapeutischen Protease. Das Design der Synthese, vor allem die Wahl eines geeigneten bioorthogonalen Verfahrens sollte unter der Prämisse erfolgen, dass das COSS-Gerüst in Gegenwart von bestimmten Nukleophilen instabil ist

Die dritte Studie war auf die Synthese eines Wirkstofftransportmoduls fokussiert, das aus einem kubisch-oktamerisches Silsesquioxan (COSS) Gerüstmolekül mit zellpenetrierenden Eigenschaften und Doxorubicin, ein cytotoxischen Anthracyclin Antibiotikum, besteht. Dieses komplexe Konstrukt sollte die Zellaufnahme des Wirkstoffes erleichtern und diesen in der Zelle freisetzen. Die Einschränkungen bezüglich der Stabilität des COSS-Gerüstes sollten ebenfalls berücksichtigt werden.

Die Ergebnisse der kumulativen Forschungsarbeit sind in **Schema 1** zusammengefasst.

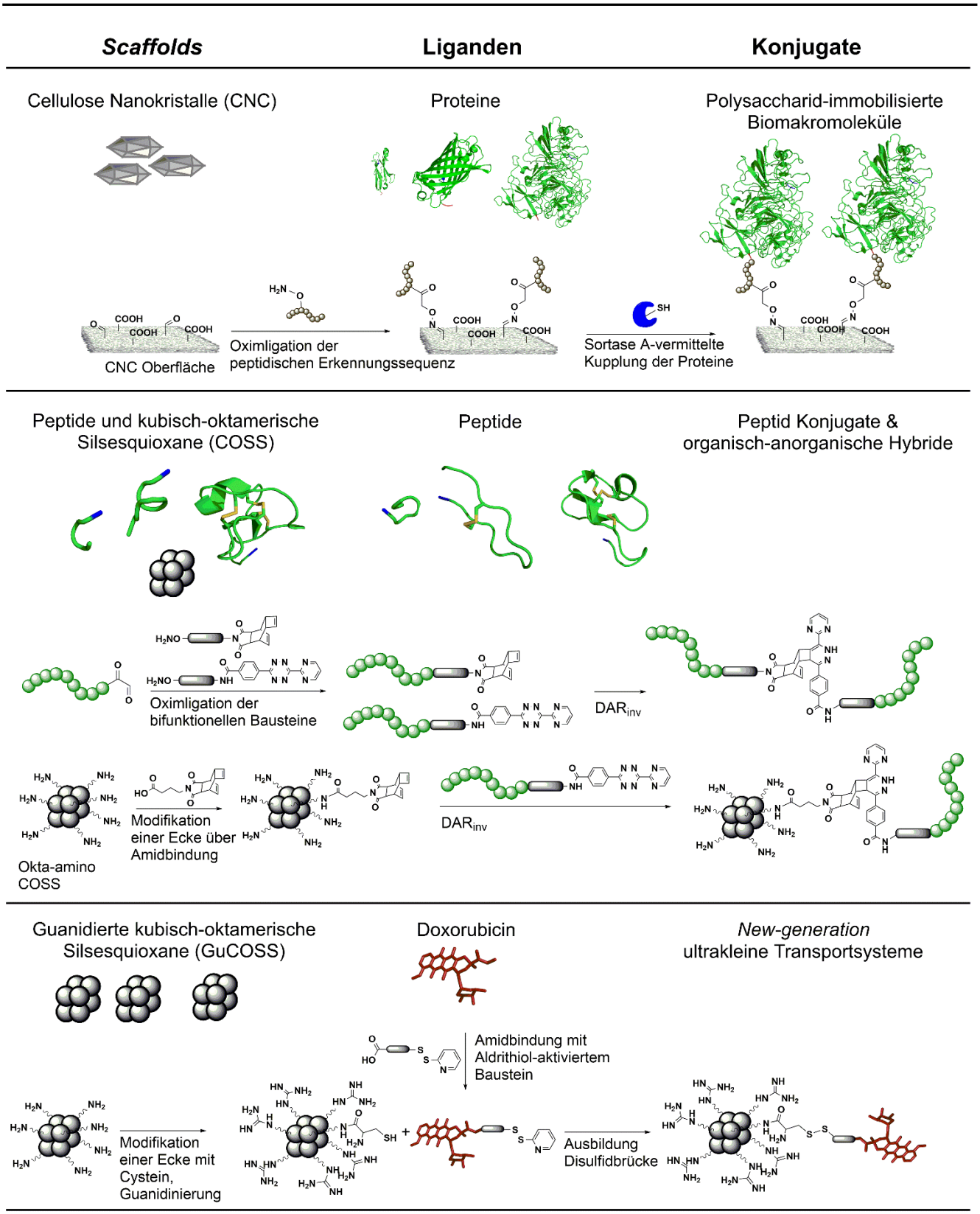

Schema 1: Übersicht über die Gerüstmolekül-Liganden Paare und die jeweilige Ligationsstrategie, die für die Synthese der gewünschten Konjugate entwickelt wurde.

Die erste Studie (*Angew. Chem. Int. Ed.*, **2014**, *53*, 12618-12623) adressierte die Entwicklung eines ortsgerichteten, bioorthogonalen und modularen Syntheseansatzes für die Immobilisierung von Biomolekülen auf einer kristallinen Nanocellulose (CNC) Plattform (**Schema 1, oben**). Das ultimative Ziel war die kovalente, chemoselektive Immobilisierung von bioaktiven Proteinen auf der Oberfläche von CNC – einer nachhaltigen, natürlichen makromolekularen Verbindung.

Die Herausforderung dieser Studie war, die allgemeinen Nachteile der üblicherweise verwendeten Proteinkonjugationsmethoden bezüglich verbesserter Selektivität und Einsatz unter physiologischen Bedingungen in wässrigem Milieu zu vermeiden. Zu diesem Zweck wurde ein generisches Zweistufenverfahren entwickelt, das auf einer Reihe von effizienten orthogonalen Reaktionen basiert, die Notwendigkeit von organischen Lösungsmitteln vermeidet und dadurch kompatibel mit physiologischen Systemen ist. Unter Verwendung von effizienter Oximligation und anschließender Sortase-vermittelter Konjugation zeigte die Synthesestrategie die erforderliche Regiospezifität und Biokompatibilität, die die Anwendung auf eine große Anzahl von funktionellen Proteinen ermöglicht. Durch die TEMPO-vermittelte Oxidation der oberflächenexponierten CNC-Hydroxylgruppen konnte zunächst ein kleiner Fluorophor immobilisiert werden, der die Detektion von Aminooxy-adressierbaren Oberflächenaldehyden ermöglichte. Die anschließende Oximierung mit dem peptidischen Linker wurde validiert und führte zu Sortase A adressierbaren Positionen auf dem CNC-Träger. Anschließend wurde die Enzym-vermittelte Oberflächenimmobilisierung mit drei Proteinen aus unterschiedlichen Klassen, von verschiedener Größe, Komplexität und Bioaktivität unter Erhalt ihrer biologischen Funktion durchgeführt.

In dieser Arbeit wurde, aufgrund erhöhter katalytischer Eigenschaften, eine gentechnisch mutierte Variante der Sortase A (eSrtA) verwendet. Zusätzlich konnte gezeigt werden, dass die definierte Orientierung durch die ortsselektive Kupplung der Proteinliganden, im Vergleich zu zufällig immobilisierten Proteinen, in einer verbesserten Bioaktivität resultierte. Unter Berücksichtigung dieser Erkenntnisse, kann zusammenfassend gesagt werden, dass diese nachhaltigen, nanoskaligen Biomaterialien eine exzellente Plattform für die spezifische Immobilisierung von anspruchsvollen Makromolekülen für biomedizinische Zwecke, Wirkstofftransport oder –ablagerung darstellen.

Die zweite Studie (*Chem. Commun.*, **2015**, *51*, 11130-11133) widmete sich der Entwicklung einer Synthesestrategie für die Generierung eines hybriden organisch-anorganischen Konstruktes, unter Verwendung eines der kleinsten bekannten kubisch-oktamerischen Nanopartikel (COSS) und eines funktionellen, peptidischen Konjugationspartners (**Schema 1, mittig**). In den *Proof-of-Concept* Experimenten wurde die Anwendbarkeit des modularen synthetischen Ansatzes, der die Generierung von *N*-terminalen Peptidaldehyden, effiziente Oximligation und Diels-Alder Reaktion mit inversem Elektronenbedarf (DAR_{inv}) kombiniert, anhand der Konjugationen von linearen, Cystin-cyclisierten und multi-Disulfid-verbrückten funktionellen Peptiden demonstriert. Zusätzlich wurde die Strategie auf die Synthese von Konstrukten mit komplexen Strukturen erweitert.

Im Rahmen dieser Arbeit wurde die Diels-Alder Reaktion mit inversem Elektronenbedarf (DAR_{inv}) wegen ihrer Biokompatibilität und schnellen Reaktionskinetik für die Synthese von Biokonjugaten, bestehend aus Peptiden mit unterschiedlicher Länge, molekularer Komplexität und biologischen Eigenschaften, ausgewählt. Zudem hat diese spezielle Reaktion den Vorteil, dass ihr zweiter Schritt aufgrund der Abspaltung von molekularem Stickstoff irreversibel ist und somit das Gleichgewicht auf die Seite der Produktbildung verschiebt.

Um die orthogonal adressierbaren Funktionalitäten zu erzeugen, enthielten die synthetisierten Bausteine eine Aminooxy-Einheit jeweilig kombiniert mit einem Tetrazin oder Reppeanhydrid. Diese bifunktionellen Einheiten waren synthetisch leicht zugänglich und wurden in eine Vielzahl von molekularen Konstrukten installiert, ohne deren strukturelle Eigenschaften zu beeinträchtigen. Sukzessive Reaktion über die DAR_{inv} resultierte in definierten Konjugaten mit gutem bis quantitativen Umsatz. Die Modularität dieses synthetischen Zweistufenverfahrens bietet den Vorteil, dass sobald die DAR_{inv}-Einheit in das Molekül von Interesse installiert wurde, es mit jedem gewünschten Reaktionspartner reagieren kann. Somit ist dieses Verfahren für die Generierung von Peptidkonjugaten, sowohl mit synthetischen als auch rekombinanten Peptiden, anwendbar.

Die dritte Studie, die im Rahmen dieser Arbeit durchgeführt wurde, (*Angew. Chem. Int. Ed.,* **2016***, 55,* 14842–14846) zielte auf die Ausarbeitung einer synthetischen Strategie für hybride organisch-anorganische kubisch-oktamerische Silsesquioxan-Derivate und deren Anwendung als Gerüstmolekül für die Generierung eines zellpenetrierenden Transportsystems (**Schema 1, unten**). In einer vorherigen Studie wurden die zellpenetrierenden Eigenschaften von Ammonium-funktionalisierten COSS-Nanopartikeln und ihre Akkumulation im Nukleoli nachgewiesen. Basierend auf diesen Ergebnissen war der nächste Schritt die Entwicklung von neuen COSS-Partikeln mit positiv geladenen flankierenden Armen und die Untersuchung ihrer zellpenetrierenden Eigenschaften. Der Transport eines therapeutischen Wirkstoffes in lebende Zellen sollte die Funktionsfähigkeit der neuen Generation von molekularen Transportern zeigen.

Im Rahmen dieser Studie wurde gezeigt, dass die entwickelten guanidierten COSS-Nanopartikel (GuCOSS) eine viel höhere und schnellere Zellaufnahme zeigten als die üblicherweise verwendeten zellpenetrierenden Peptide (z.B. TAT, Penetratin, Hepta- und Dekaarginine). Diese Effizienz (78-fach höher als bei Heptaarginin, das die gleiche Art und Anzahl von geladenen Gruppen trägt) kann durch die geringe Größe und die dadurch bedingte hohe Ladungsdichte um den COSS-Kern erklärt werden.

Interessanterweise zeigten sich unsere neuartigen, zellgängigen Module promiskuitiv hinsichtlich der Zielzellen. Tatsächlich wurde eine effiziente zelluläre Aufnahme in verschiedene Zellarten beobachtet, darunter Gram-negative Bakterien (*Escherichia coli*), Hefe (*Saccharomyces cerevisiae*) und Archeen (*Sulfolobus islandicus, Sulfolobus tokodaii, Halobacterium salinarum*) sowie humane Krebszelllinien. Da die Zellaufnahme bei 4°C im Vergleich zu der bei 37°C nur unwesentlich reduziert war, wurde ein energieunabhängiger Mechanismus vorgeschlagen. Zusätzlich degradiert der COSS-Kern innerhalb der Zelle und für die Einzelkomponenten an sich wurde keine bis niedrige Toxizität vorhergesagt. Diese Erwartung wurde durch die Untersuchung der Zellaufnahme, Toxizität und Degradation des GuCOSS-Moduls bestätigt.

Als *Proof-of-Concept Cargo* für den intrazellulären Transport wurde der therapeutische Wirkstoff Doxorubicin verwendet, da dieser in freier Form nur sehr langsam durch passive Diffusion in die Zelle permeieren kann. Doxorubicin wurde über eine Disulfidbrücke an den hocheffizient-zellpenetrierenden heptaguanidierten COSS-Nanopartikel konjugiert. Das jeweilige Oktaammonium COSS-Derivat wurde dafür an einer Ecke mit einem Cystein, funktionalisiert. Anschließende Guanidinylierung der verbleibenden Amine, gefolgt von der Bildung einer Disulfidbindung über das Aldrithiol™-2-modifizierte Zytotoxin resultierte in einem hybriden zellpenetrierenden Konjugat an das ein Wirkstoff eine Disulfidbrücke angebunden ist. Die Disulfidbrücke sollte in dem reduzierenden Milieu des Zytoplasmas gespalten werden und das Zytotoxin freigeben. Die durchgeführten Zytotoxizitätsstudien der Hybride zeigten eine erhöhte Toxizität gegenüber dem freien Wirkstoff. Zusätzlich konnte die Inkubationszeit durch die schnelle Zellaufnahme signifikant reduziert werden. Da es viele Wirkstoffe gibt, die nicht zellgängig sind und/oder schlecht wasserlöslich, z.B. Hygromycin, Ispinesib etc. eröffnet der GuCOSS-basierte molekulare Transporter neue Wege für die erleichterte Aufnahme dieser Therapeutika.

Zusammengenommen leisten die Ergebnisse dieser kumulativen Forschungsarbeit, im Hinblick auf die Anwendbarkeit, Vielseitigkeit, Zuverlässigkeit und Kompatibilität mit komplexen molekularen Strukturen, unabhängig ihres Ursprungs, einen Beitrag zur *Toolbox* der modernen, bioorthogonalen Methoden. Darüber hinaus erweitert die Kombination von klassischer Chemie mit modernen, biokompatiblen Ligationsmethoden, darunter beispielsweise Enzym-unterstützte Reaktionen, das Spektrum bioorthogonaler Konjugationsstrategien.

1. Introduction

"Bioconjugate chemistry is the study of linking one molecule to another by chemical or biological means. The resulting complexes will typically be formed from at least one biomolecule, though they can also be purely synthetic molecules with a biological application."[2]

One of the main goals in a broad range of chemical disciplines and applied areas of chemistry, among them medical biology, material sciences, physical chemistry, biochemistry, chemical engineering, *etc.* is the generation of complex molecular constructs with tailored properties and predetermined activity. Within the wide spectrum of such constructs, the architectures comprising biomolecular or biocompatible counterparts are at the top of hierarchy in frames of molecular complexity, structural variety, and functional diversity. Today's challenges faced by modern research comprise the conjugation of molecules of different classes and origin, with surface immobilization of nanomaterials or the modification of insoluble polymers being the prominent examples.[3] Since no conventional methods of chemical synthesis match these sophisticated design formats, different classes of building blocks with unique characteristics are required. Depending on the properties and the chemical sensitivity of the respective reaction partners, the development of conjugation strategies based on the suitable chemical transformations is of high scientific interest and applicative demand.

2. Objective

The presented cumulative work was focused on the development of a multivariable synthetic strategy enabling covalent attachment of functional biomolecules to the molecular scaffolds of interest under preservation of their structural features and activity. To establish a viable and reproducible synthetic platform, three self-contained studies were envisaged, each comprising a set of selective chemical reactions between particular functional molecules with respective counterparts. Taking into consideration that bio(macro)molecules are rather complex and diverse, the respective conjugation approach had to provide the required bioorthogonality and versatility in frames of efficiency, affordability and facility of access.

Each individual research within the scope of this thesis addressed the coupling of two or more molecular architectures for the synthesis of highly defined molecular constructs. Every presented study comprised three major objectives:

- design of a scaffold-ligand system;
- elaboration and application of a particular synthetic strategy;
- assessment of bioactivity if required.

The first study was aimed at the immobilization of proteins of different size and complexity on a crystalline nanocellulose (CNC) scaffold. As ligands, three biomacromolecules were chosen: a green fluorescent protein, an enzyme galactose oxidase, and an anti-lysozyme shark antibody. These specific conjugates should combine the properties of the immobilized proteins with the intrinsic characteristics of the cellulose nanocrystals, such as low toxicity, water- and biocompatibility as well as obvious advantages given by their nanosize.

The second investigation was devoted to the development of a viable strategy for the biofunctionalization of one of the smallest known nanoparticle, cube-octameric silsesquioxane (COSS), with peptides. As a preliminary study, a suitable conjugation platform should be examined using reaction partners of peptidic nature. Various peptides featuring different length and architecture must be investigated, among them an enzyme recognition motif, cystine-knot miniproteins, an integrin-binding and an antimicrobial peptide as well as an engineered inhibitor of a therapeutic protease. Synthesis design, especially considering the choice of an appropriate bioorthogonal method, proceeded from a premise that COSS core is not stable in basic milieu and in the presence of certain nucleophiles.

The third work was focused on the synthesis of a drug delivery module comprising a cube-octameric silsesquioxane (COSS) scaffold with cell-penetrating properties and doxorubicin, a cytotoxic anthracycline antibiotic. Furthermore, this sophisticated construct should release the doxorubicin

payload upon cellular uptake. The restrictions of COSS template considering its stability issues should be taken into account as well.

2.1. Preface: Toolbox of conjugation chemistry

Generally, conjugations of molecular partners can be divided into three main groups: 1) the linkage of molecules of the same class, involving biomolecular, polymeric, or small-molecule conjugates; 2) the linkage of macro- and small molecules, e.g. antibody-drug or protein-peptide conjugates; and 3) linkage of macromolecules from different classes, e.g. hybrid constructs such as polymer-biomolecule/drug/peptide conjugates, or the marriage of nanoparticles with biomolecules. Typically, these linkages of two or more molecular partners are classified considering their nature of binding, namely, non-covalent interactions or covalent connections.[3b] Although non-covalent immobilization techniques comprising adsorption, affinity-driven, electrostatic or hydrophobic interactions[4] have been extensively explored and optimized, they were not considered for this work focused on the generation of highly defined constructs. The covalent conjugations, which can also be subdivided into site-selective transformations and "*random grafting*" approaches, have to be carefully considered for each individual case as every reaction partner usually exhibits unique intrinsic properties. Consequently, reliable chemistries besides the common reactions, which make use of inherent functionalities, are of high demand.

To address this problem, numerous (bio-)conjugation methods have been explored and established throughout the past decades, expanding the toolbox of orthogonal, posttranslational modifications of biological and polymeric macromolecules.[5] Typically, such bioorthogonal reactions are chemical transformations featuring compatibility with and inertness towards biological systems. The term or the concept of bioorthogonality was introduced in 2004 by Bertozzi *et al.*: *"Selective chemical reactions that are orthogonal to the diverse functionality of biological systems are now recognized as important tools in chemical biology…these bioorthogonal reactions have inspired new strategies."*[6]

The bioorthogonal modifications can be achieved either by applying the inherent functionalities naturally present in biomolecules or by chemical or biosynthetic derivatization with non-natural addressable groups or recognition units exhibiting site- and, moreover, chemoselectivity towards their coupling partners. Additionally, the respective chemical transformation involving such functionalities should be highly efficient under physiological conditions.[7] The required solitary reactive non-natural moieties are introduced genetically or incorporated *via* post-synthetic modifications as a complementary strategy to recombinant options. However, chemical modifications are often a method of choice for the manufacturing of highly defined macromolecular constructs with tailored properties.

To date, various strategies have been reported to modify side chains of canonic amino acids in biomacromolecules, especially those bearing primary amines or thiols. Nonetheless, the scope of this chemistry is rather limited and it often lacks the adequate selectivity. Therefore, a number of alternative approaches have been developed to selectively address a single moiety within proteins or enzymes while preserving the orthogonality towards the inherent functional groups. To date, a plethora of related bioconjugation techniques classified as chemical ligations and enzymatic transformations have been reported. Chemical methods involve e.g. periodate oxidation of β-amino alcohols towards highly reactive *N*-terminal glyoxylyl moieties, hydrazide and hydrazone formation, oximation, Staudinger ligation as well as numerous "click" reactions, among them copper-catalyzed or copper-free cycloadditions.[8]

However, most chemical methods can be hardly applied to biomacromolecules. Indeed, these highly ordered, sophisticated architectures, most of them possessing a peculiar fold, are often not compatible with organic solvents, metal catalysts or strongly acidic/basic milieu. Therefore, protein modifications have been established that involved site-specific manipulations such as *N*- or *C*-terminal protein derivatization, modification of non-native functionalities, recombinant protein ligation, and side-chain functionalization of amino acids.[9] Plenty of conjugates have been synthesized *via* orthogonal ligation

methods, ranging from rather trivial fluorescently, radiolabeled or small-molecule-marked peptides to complex multifunctional architectures like antibody-drug conjugates or even organic-inorganic hybrids.

The following chapter will give a brief introduction to the conjugation methods as well as the respective scaffold-ligand pairs relevant for this work. Recent developments and applications will be outlined as well.

2.2. Chemical modification of macromolecules

Orthogonal reactions targeting non-natural functional groups in biomacromolecules often make use of carbonyl (ketone and/or aldehyde) chemistry. The introduction of these highly electrophilic groups can be achieved upon recombinant expression (*via* a recognition tag for enzymatic transformations[10] or by the incorporation of unnatural amino acids[11]), during the course of chemical synthesis (introduction of non-natural building blocks) as well as upon chemical transformation of inherent groups (periodate or pyridoxal phosphate oxidation). Obviously, biomolecules of a certain size are beyond the scope of chemical synthesis. The enzymatic transformations will be discussed in chapter 1.3.

2.2.1. Introduction of reactive carbonyls

Sodium periodate is known for decades to oxidize vicinal diols,[12] sugars and sugar-based polymers[13] as well as threonine and serine[14] to aldehydic moieties. In case of peptides and proteins it is often the method of choice allowing to selectively generate an *N*-terminal glyoxylyl moiety under very mild conditions. Indeed, this reaction does not interfere with the structural elements of biomolecules or affect their biological activity. Nevertheless, short reaction time and moderate excess of periodate are required to avoid over-oxidation of sulfide-bearing side chains.[15] The reaction is usually performed in aqueous media at neutral pH; low concentrations of sodium periodate are required.[16] However, oxidation has to be performed in the dark, as the dissolved sodium periodate is known to slowly evolve ozone in course of a photochemical reaction.[17] The mechanism of $NaIO_4$ oxidation involves a cyclic intermediate and proceeds under the loss of formaldehyde and ammonia (**figure 1**).[14]

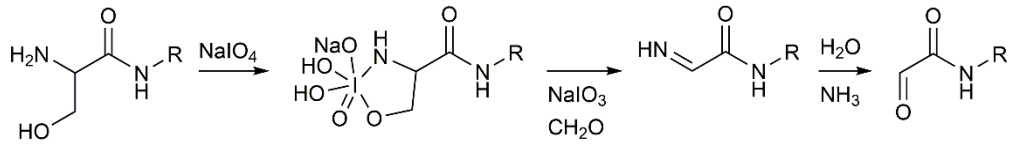

Figure 1: Reaction mechanism of serine oxidation by sodium periodate. Modified after Agten *et al.*[18]

Since its discovery, the periodate oxidation method has been used for a vast number of conjugation approaches, including the ligation of peptidic molecules,[16, 19] the synthesis of antibody-drug conjugates (ADCs)[20] or the oxidation of sugar moieties, e.g. in therapeutic cytotoxins doxorubicin and daunomycin, to crosslink them to immunoglobulins under the preservation of both antibody and drug activities.[21]

Particularly the *N*-terminal serines have been found to be well accessible in synthetic peptides and proteins since they can be easily introduced both during the course of solid-phase peptide synthesis (SPPS) and upon recombinant production *via* a genetically encoded TEV-site. The TEV protease is a cysteine protease derived from the *Tobacco Etch Virus*, which cleaves the peptide bond between the glutamine and serine or glycine, respectively, within its peptidic recognition sequence ENLYFQ|S or G. It is often used for the release of affinity tags or the cleavage of fusion proteins.[22] Synthetically accessible compounds, like peptides or small molecules, can be easily decorated with aldehydic functionalities during the course of synthesis *via* the introduction of non-natural amino acids or chemical building blocks.[23]

Another well-examined, more promiscuous/universally applicable methodology for the generation of *N*-terminal ketone or aldehyde moieties is the pyridoxal 5`-phosphate (PLP)-assisted biomimetic

transamination.[24] The first step of this reaction is the addition of the aldehyde functionality of PLP to the *N*-terminus of the peptide or protein forming a Schiff base that tautomerizes to the respective imine derivative. Subsequent hydrolytic cleavage leads to the release of pyridoxamine and the corresponding aldehyde or ketone moiety.[24-25] However, the PLP-mediated transamination depends on the amino acid at the *N*-terminus and requires long incubation times and elevated temperature.[24, 26] Moreover, it exhibits only low to moderate conversion rates.[27]

The enzymatic generation of aldehydic functionalities *via* the formyl glycine-generating enzyme (FGE) will be discussed in **chapter 1.3**.

In the following chapter the bioorthogonal reactions of carbonyl electrophiles will be discussed in detail.

2.2.2. Aldehyde/ketone-based ligation strategies

Nucleophilic reactions of biomolecules containing aldehyde or ketone electrophiles require a respective counterpart, usually hydrazides, thiosemicarbazides, and aminooxy functionalities (**figure 2**). These so-called dynamic covalent-coupling reactions follow a classical imine mechanism under acid catalysis yielding respective hydrazones, thiosemicarbazones or oximes.[28] Due to the higher hydrolytic stability of the oxime bond, oxime chemistry is often the method of choice.[29]

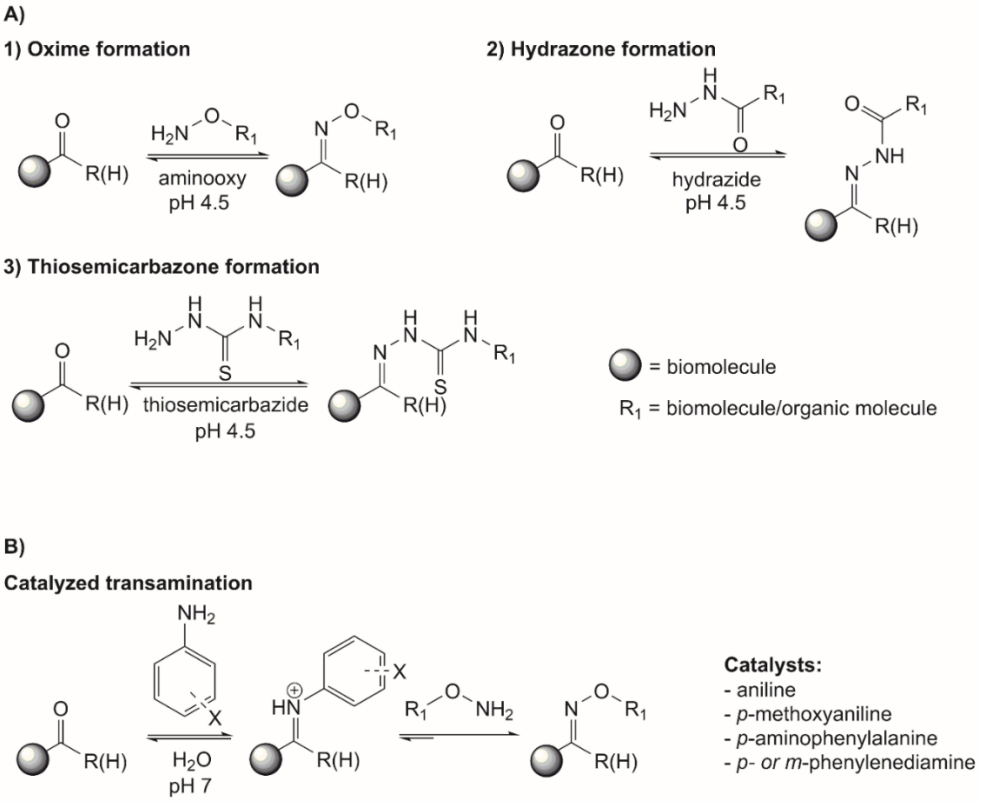

Figure 2: A) Conjugations involving aldehydes or ketones. B) Catalyzed transamination.

The oxime ligation (**figure 2**) represents a common ketone/aldehyde-based modification strategy as aminooxy compounds exhibit a higher reactivity than hydrazides or thiosemicarbazides.[30] However, the oximation has its highest conversion rate at pH 4.5, thus posing a challenge if applied to the modification of proteins. Indeed, at such pH many proteins aggregate or even degrade. To overcome this handicap, Dirksen *et al.* made use of an alternative two-step transamination mechanism, applying nucleophilic catalysis to dramatically amplify reaction rate at physiological pH. First, similar to a classic imine mechanism, aniline (or its derivative) forms a hemiaminal which after dehydration undergoes transimination yielding the thermodynamically stable oxime.[31] To date, various nucleophilic catalysts have been reported, among them *p*-aminophenylalanine, *p*-methoxyaniline, and

p-/*o*-/*m*-phenylenediamine.[32] Interestingly, *p*-phenylenediamine has been found a superior catalyst compared to aniline due to its high performance over a wide range of pH. Moreover, as it accelerates oximation at 4°C as well as at ambient temperature,[32a] it has been applied to a vast number of bioconjugations where preservation of structural features was essential.[32b, 33] Recently reported carboxylate-driven activation in tandem with nucleophilic catalysis allowed to significantly increase the rate of oxime reaction, making oximation of less reactive ketones possible at physiological pH. Presumably, formation of hydrogen bonds between a ketone and a carboxylic acid plays a crucial role for the nucleophilic addition to the carbonyl group.[31b]

2.2.3. Click chemistry and cycloadditions

Azide-alkyne cycloaddition

Another class of orthogonal reactions often applied to bioconjugations are the cycloadditions between azide and alkyne moieties. In 2001, K. B. Sharpless *et al.* introduced the term "click chemistry" describing the modular approach to generate new entities by connecting small units *via* heteroatom linkages.[34] Furthermore, they postulated that these so-called "click reactions" had to fulfill certain requirements, among them very high yields, the generation of solely harmless byproducts and/or stereospecificity.[34]

The most prominent variant of these pericyclic reactions is the copper(I)-catalyzed azide-alkyne cycloaddition (CuAAC), commonly referred to as "click reaction", where bioorthogonal alkyne and azide moieties react to a 1,4-disubstituted triazole (**figure 3A**). In the presence of a ruthenium catalyst the 1,5-disubstituted product in formed (RuAAC).[35] However, requiring elevated temperatures and organic solvents, this reaction does not fully meet the demands of a "click reaction".

In the course of metal-catalyzed cycloadditions, severe cytotoxic effects could be expected. For example, copper(I) promotes generation of reactive oxygen species (ROS) from molecular oxygen, thus limiting the scope of CuAAC to non-living systems.[36] Therefore, several approaches have been developed over the last years to circumvent this problem, among them the synthesis of water-soluble copper-complexing agents preventing the formation of copper species in higher oxidation states (e.g. TBTA, THPTA or BTTAA),[37] the development of copper-chelating azides[37b] or the introduction of strain-promoted "click" compounds allowing to discard metal catalyst.[38] Though lacking regioselectivity, the strain-promoted azide-alkyne cycloaddition, SPAAC, is driven by ring strain of an unsaturated carbocycle, usually cyclooctyne, and does not require catalysis. SPAAC has already been applied to the covalent modification of living cells,[39] the labeling of RNA,[40] DNA[41] or peptides for PET imaging.[42] As an alternative, the so-called traceless (azide) Staudinger ligation makes use of triarylphosphines reacting with an azide to an amide-linked product (**figure 3D**).[43]

Though the required azide or alkyne functionalities are not present in natural biomolecules, they can be introduced genetically by non-natural amino acids,[44] postsynthetically *via* the ligation of azide-modified linker molecules[45] or *via* an aqueous diazotransfer on inherent amines.[46]

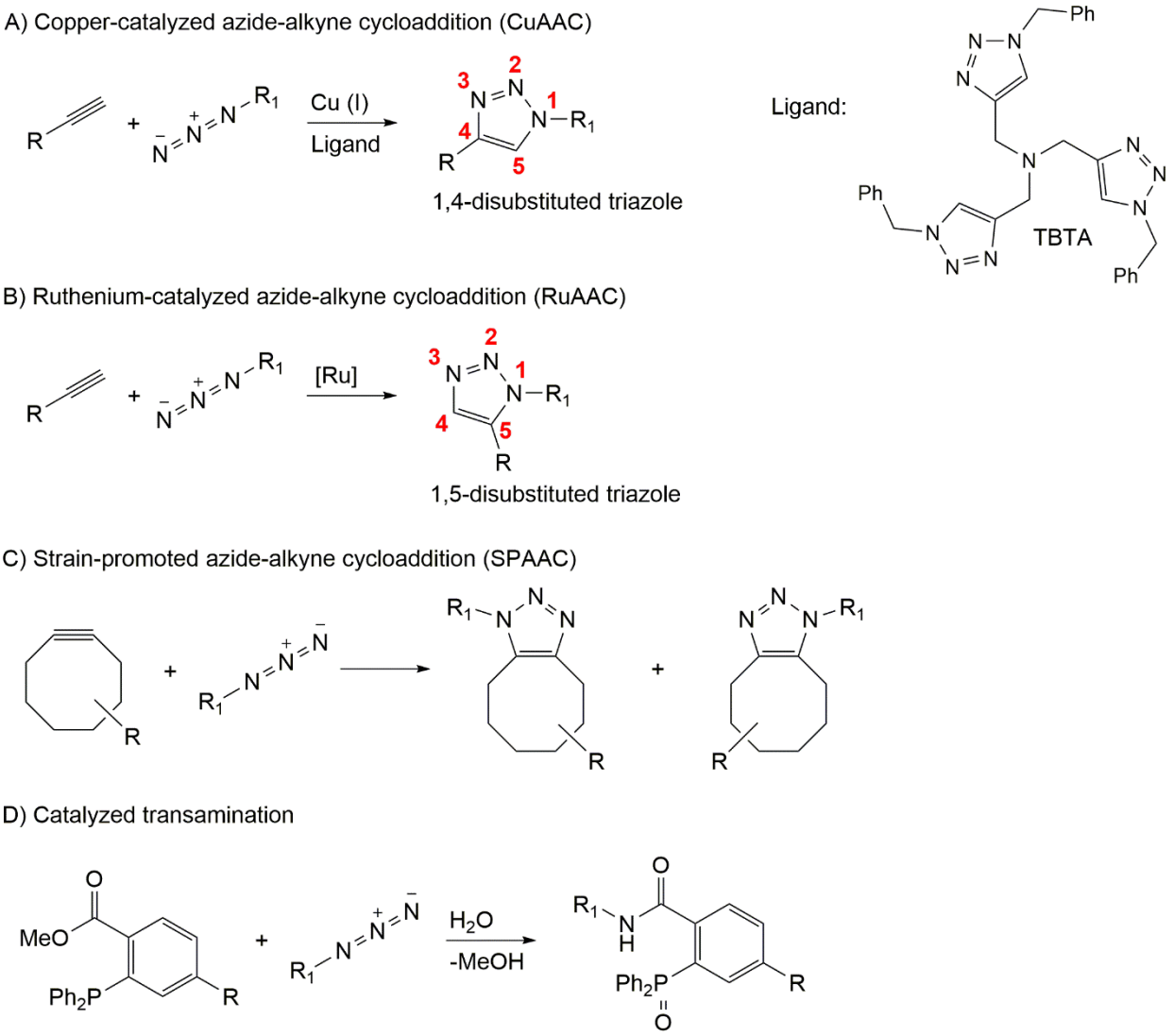

Figure 3: Overview of the most common "click reactions" involving azides.

Inverse electron-demand Diels-Alder reaction (DAR_{inv})

What most of the previously described methods have in common is the requirement of a catalyst like a metal salt (CuAAC, RuAAC), an acid (oxime or hydrazine ligation), or a nucleophile (catalyzed transamination). Over the last decades, the introduction of catalyst-free bioorthogonal reactions has brought the chemical modifications of biomacromolecules to a new level of sophistication. However, widely applied to modification of biomolecules SPAAC has a shortcoming in terms of regioselectivity.

A very powerful method, devoid of mentioned drawbacks, is the inverse electron-demand Diels-Alder reaction (DAR_{inv}) of electron-deficient heterocycles.[47] This reaction involves a tetrazine diene bearing residues with a –I and/or a +M effect decreasing the electron density, and a dienophile containing a residue with a +M effect increasing electron density, among them Reppe anhydride,[48] norbornene,[49] transcyclooctene or transcyclooctyne derivatives.[50] It follows a concerted mechanism possessing second-order kinetics, with the reversible cycloaddition between the tetrazine and the dienophile being the rate-determining step (**figure 4**).[47, 48b] The DAR_{inv} represents an attractive method for the conjugation of biomolecules since it is compatible with organic solvents as well as with aqueous media, exhibits fast reaction rates, tolerates a broad range of biological functionalities and is irreversible due to the loss of molecular nitrogen, which is the only byproduct.[50a, 51] Moreover, due to the optical properties of the tetrazine derivatives (absorbance maximum around 500-540 nm) the reaction progress can be monitored photometrically.[47, 50c, 52] So far, it has been explored extensively for the

introduction of radiolabels to antibodies or hormones,[53] for the modification of DNA, RNA or PNA,[48c, 54] the fluorescent labeling of living cells,[50b] derivatization of peptides[55] as well as in animal model studies,[56] thus demonstrating its versatile applicability and biocompatibility.

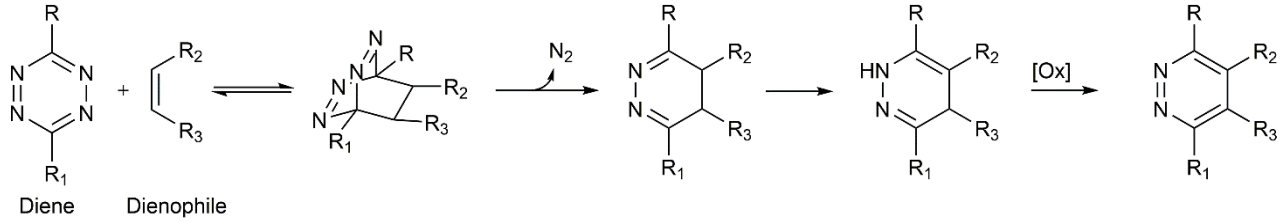

Figure 4: Reaction scheme of the inverse electron-demand Diels-Alder reaction involving a tetrazine as diene. Modified after Knall *et al.* [47]

2.3. Enzyme-promoted bioconjugations: Sortase A

Next to chemical modifications, the development of enzyme-mediated approaches to bioorthogonal ligations has been in the scientific spotlight as well. Naturally occurring enzymes which are known to modify the cell walls,[57] catalyze the splicing process[58] or crosslink proteins[59] have gained more and more attention over the past years. Their original function was utilized for the functionalization of biomacromolecules, among them proteins, peptides, DNA and RNA.[10]

One of the prominent examples of such enzymes is the calcium-dependent transpeptidase Sortase A (SrtA) derived from the gram-positive bacteria *Staphylococcus aureus*. In Nature, it catalyzes the covalent linkage of surface proteins to the bacterial peptidoglycan cell wall.[57] To be recognized by SrtA, the conjugation partners need a conserved *C*-terminal LPXTG-*OH* motif, with X representing any canonical amino acid, and the respective oligoglycine counterpart.[60] During surface attachment of the proteins, Sortase A catalyzes the cleavage of the peptide bond between threonine and glycine of the recognition tag with a subsequent formation of a new amide bond between the carboxylic end of threonine and the *N*-terminus of the oligoglycine.[61] Recent studies have demonstrated that the Ca^{2+} ions are required for the activation of the enzyme, since they are complexed by glutamates of the β3/β4 pocket in spatial proximity to the active site, thereby provoking a structural fluctuation of the β6/β7 loop between an open, flexible state and a closed, binding form (**figure 5**).[62]

The active site of Sortase A comprises the side chains of cysteine 184, histidine 120 and arginine 197 (**figure 5**), with that of C184 being essential for the catalytic activity as the thiolate enables the nucleophilic attack on the carboxylic group of the threonine to yield a thioester enzyme-substrate intermediate. Subsequently, a new amide bond is formed between both peptidic recognition motifs (**figure 6**).[62b, 63]

Due to mild reaction conditions and fast kinetics, SrtA-assisted ligation has been used in a number of conjugation approaches involving the generation of antibody-drug conjugates,[64] surface modifications,[65] peptide or protein conjugations [66] or even the surface labeling of live cells.[67]

Recent research is focused on improving the catalytic activity and altering substrate selectivity of Sortase A.[68] It has been discovered that truncation of up to 59 *N*-terminal amino acids has no effect on catalytic activity. The so-called evolved variant of Sortase A, eSrtA, has been recently generated that possessed five mutated amino acids and exhibited a 40-fold increase in LPETG-coupling activity as well as faster reaction kinetics compared to the wild-type enzyme.[69] Moreover, sortase variants with different substrate specificity were generated, with respect to simultaneous orthogonal applications.[70]

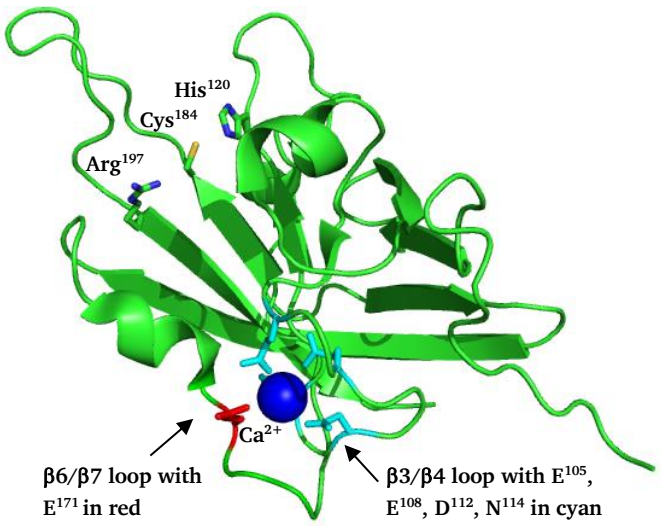

Fig. 5: Crystal structure of Sortase A with the catalytic center comprising histidine 120, cysteine 184 and arginine 197 and the residues from β3/β4 and β6/β7 loop complexing a Ca^{2+} ion. Modified after PDB database entry 2KID. [71]

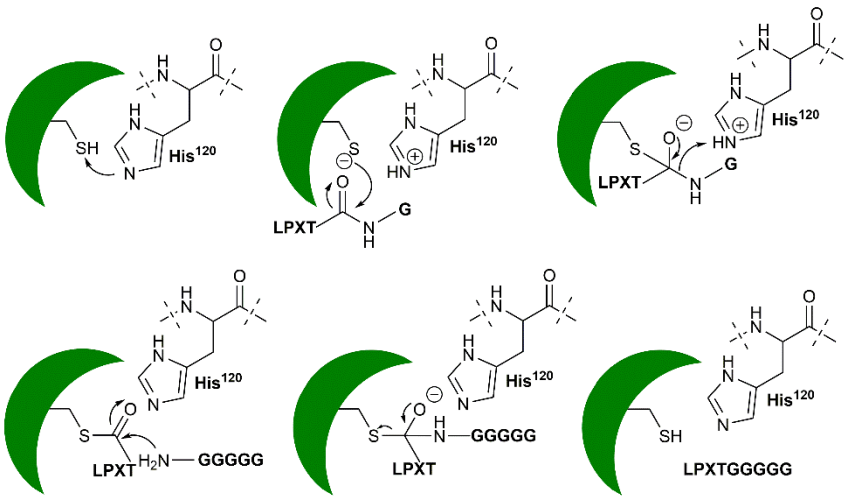

Figure. 6: Proposed reaction mechanism of Sortase A catalysis.

Alternative enzyme-mediated ligation methods reported so far involve e.g. the formylglycine generating enzyme (FGE) derived from *Mycobacterium tuberculosis*,[72] which recognizes a pentapeptidic motif CxPxR (x stands for any amino acid) and specifically converts the cysteine into an aldehyde-bearing formylglycine, which can then be addressed by hydrazides or aminooxy groups.[73] Usually, the recognition sequence is genetically encoded and the protein of interest is produced recombinantly. FGE can either be co-expressed, oxidizing the cysteine in the cell, or it can be expressed separately altering the cysteine after isolation of the respective protein.[73]

Further developments of enzymatic conjugation strategies include split inteins which have been used for the labeling of proteins,[74] immobilization of proteins on solid support,[75] macrocyclization of proteins and peptides,[76] lipoic acid ligase (LplA) that catalyzes the attachment of lipoic acid moieties to alkyl derivatives[77] or transglutaminase (TGase) that promotes the attachment of primary amines to biomolecules containing a glutamine-bearing recognition sequence.[78]

2.4. Scaffolds and Ligands

"Though the term 'scaffold' is used broadly in chemistry, the precise meaning of the word is context- and chemist-dependent."[79] In Biochemistry and related disciplines, as well as in this work, the term "scaffold" is used to describe a defined (nano-)molecular construct, serving as a template or platform for the covalent immobilization and/or oligomerization of biomacromolecules of different size and complexity. Over the last years, defined multifunctional scaffolds of high symmetry have gained

increasing biomedical and biosynthetic attention.[80] A vast number of small organic molecules with diverse structure, flexibility and valence, among them cubane,[81] porphyrins,[82] calix[4]arene,[83] adamantane[84] or even cyclic decapeptides,[45a] (**figure 7**) has been reported to date. In addition, biodegradable and sustainable polymeric scaffolds, e.g. cellulose and its nanocrystalline variants, have been in the focus of scientific attention as they often show low toxicity and are compatible with aqueous milieu. Due to these properties, such scaffolds have emerged as a powerful tool for the synthesis of well-defined customized constructs with particular orientation of ligands, among them proteins, peptides, toxins, dyes or radioactive labels.[85] In general, biological compatibility, low toxicity and number of reaction sites along with application purposes and geometry play a major role upon the choice of a scaffold.

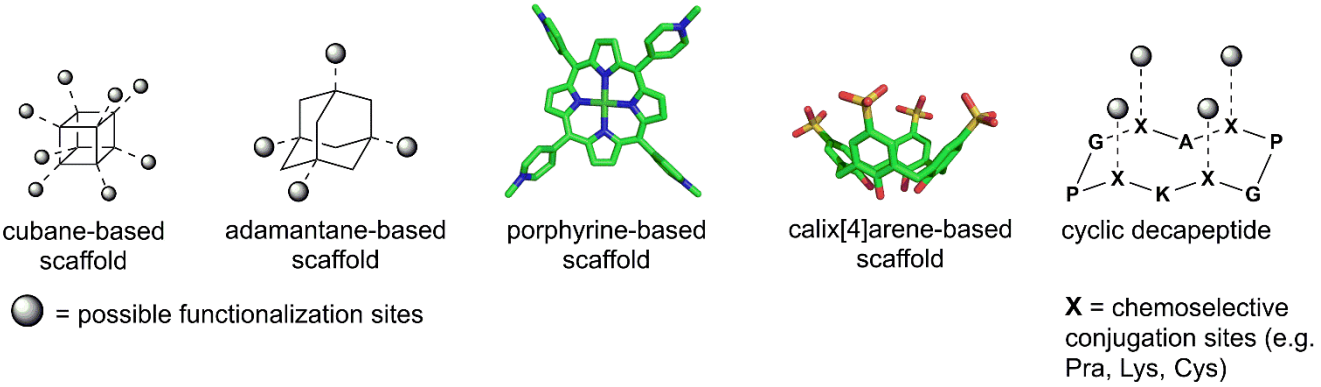

Figure 7: Symmetric scaffold cores. Modified from PDB database entries 1EM0 and 3TYI.[86]

2.4.1. Cellulose nanocrystals (CNC)

Cellulose, the most abundant natural building block in the biosphere,[87] was isolated and characterized by the French chemist Anselme Payen in 1838.[88] In Nature, it is synthesized by plants, bacteria, sea animals, fungi, and amoebae.[89] The cellulose polymer consists of β-1,4-linked D-glucopyranose units forming a linear homopolysaccharide (**figure 8**). These cross-linked microfibrils congregate to cellulose fibers.[90]

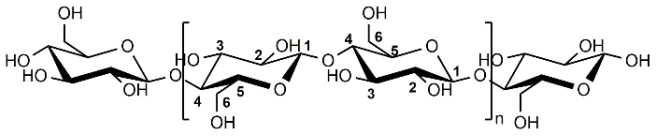

Figure 8: Structural units of cellulose.

In recent years, the nanocrystalline modification of cellulose has gained growing scientific attention as it possesses fascinating mechanical, optical, chemical, and rheological properties.[91] Already in 1920, the Swedish scientist Bengt Ranby described the "liberation of crystallites" *via* the treatment of native cellulose fibers with strong acids.[92] Even today, cellulose nanocrystals (CNCs) are primarily obtained from cellulose microfibrils or microcrystalline cellulose using the acidic hydrolytic cleavage of the lower-ordered amorphous regions (**figure 9**).[87, 93] Depending on the cleavage conditions and the cellulose origin, the formed whisker-shaped nanocrystals exhibit a length of approximately 0.1-1μm (**figure 10**).[87, 94]

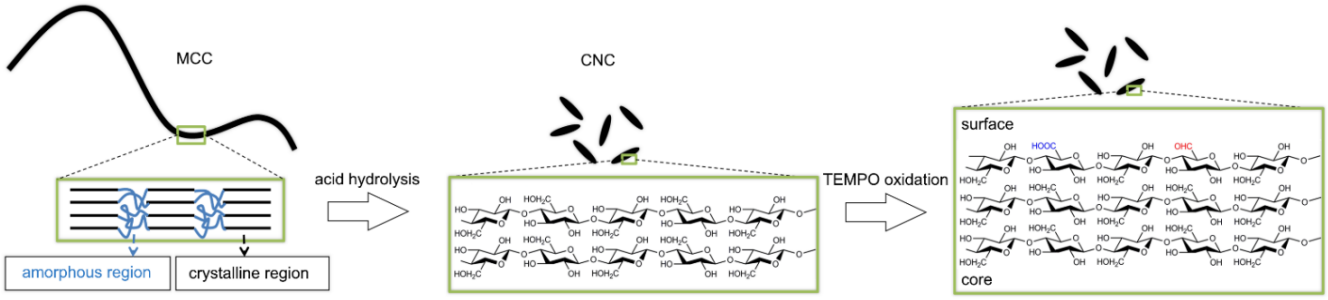

Figure 9: Schematic representation of the generation of cellulose nanocrystals.

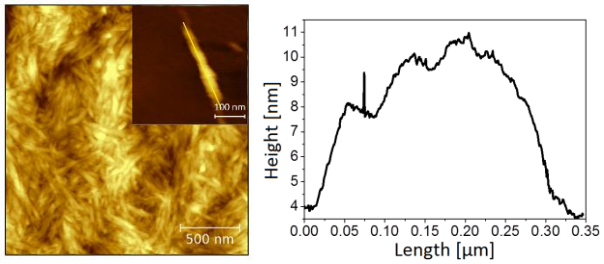

Figure 10: Atomic force micrograph of nanocrystalline cellulose whiskers (left) with the corresponding height profile (right).

Furthermore, the surface-exposed primary hydroxyls can be selectively converted into their respective aldehydes or carboxyl groups upon TEMPO(2,2,6,6-tetramethylpiperidine-1-oxyl)-mediated oxidation (**figure 11**).[95] Depending on the oxidation conditions, a mixture of both oxidation products can be generated, whereby the ratio of carboxylic-to-aldehydic groups is determined by electric conductivity titration. The resulting functional groups can be selectively addressed in a broad range of chemical modifications (see **chapter 1.2.2.**). Depending on the application purpose, the surface modifications can be either of covalent or non-covalent (adsorption-driven) nature.

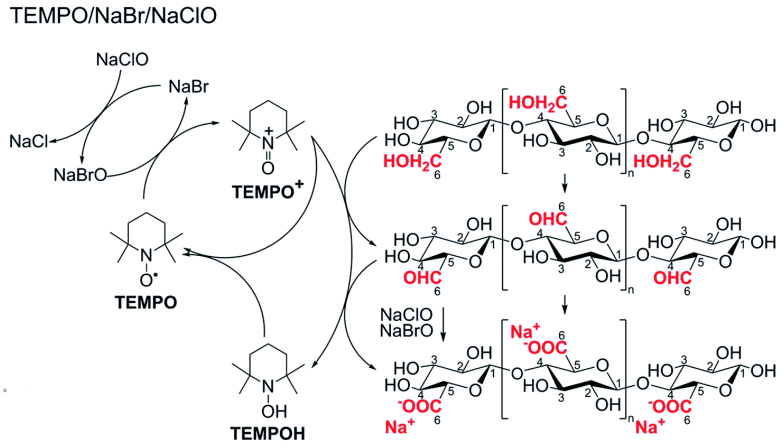

Figure 11: TEMPO-mediated oxidation of cellulose. Modified after Carlsson *et al.* [96]

So far, CNCs have found numerous applications, e.g. in nanocomposites such as films, hydrogels or biopolymers, as template materials for the generation of hybrid catalysts or biosensors, and medical drug carriers for therapeutic and diagnostic purposes.[97] Additionally, due to their intrinsic nanoscale dimensions combined with a large surface area and a highly ordered structure, CNC is an excellent scaffold candidate for biological, biochemical, or biomedical applications. Furthermore, CNCs exhibit water-compatibility, are biodegradable, low-toxic, bioavailable, and inexpensive.[98] Recently, it has been shown that, depending on their surface charge, CNCs can also enter the membrane of human cells.[99] This makes CNCs an attractive scaffold for drug delivery and deposition.[99-100] Indeed, these polysaccharide compounds have been employed as grafting platform for various drugs, e.g. doxorubicin and tetracycline, which are released within the cell due to disruption of the electrostatic interactions,[101] as well as hydroquinone for topical medication and the treatment of hyperpigmentation,[102] or folic acid for cancer targeting.[103] The immobilization of enzymes and proteins has been reported as well.[104]

2.4.2. Cube-octameric silsesquioxanes (COSS)

As mentioned above, scaffolds of high symmetry providing multiple reactive functionalities have evolved as templates for the presentation of molecular domains of biological relevance.[80a]

To date, the cube-octameric silsesquioxane (COSS) scaffold $[R(SiO_{1.5})]_8$ (R = organic residue) represents the smallest known nanoparticle with a core size of approximately 0.5 nm.[105] The rigid siloxane core enabling its high symmetry can be easily synthesized *via* controlled hydrolytic condensation of the respective organotrichlorosilanes.[105-106]

Due to their biocompatibility, COSS have been in the center of scientific attention with respect to biomedical applications. Today, these nanoparticles as well as their monomers possessing different chemical modifications and functional groups are commercially available (*Hybrid Plastic Inc.)*.[107] Low toxicity of COSS made them excellent candidates for the generation of nanocomposites, particularly in combination with polymers. For example, POSS (polyhedral oligomeric silsesquioxanes) in poly(carbonate-urea)urethane (PCU) are used in cardiovascular applications and tissue engineering.[108] Additionally, due to their multiple reaction sites and, depending on the flanking functional groups, cell-penetrating properties, they have high potential as drug carriers or drug delivery vehicles.[109] In 2013, the COSS particle bearing seven ammonium groups has been found to be cell-penetrating.[109a] Moreover, it has been successfully applied for the delivery of a peptidic cargo into the nucleus of living HeLa cells.[109a] Nevertheless, it has to be considered that the stability of COSS particles is highly dependent on their environment: the nature of the solvent, the presence of nucleophiles and the character of the corner modifications. However, for the application as a drug delivery unit the instability poses an advantage as the drug can be easily released inside the cell.

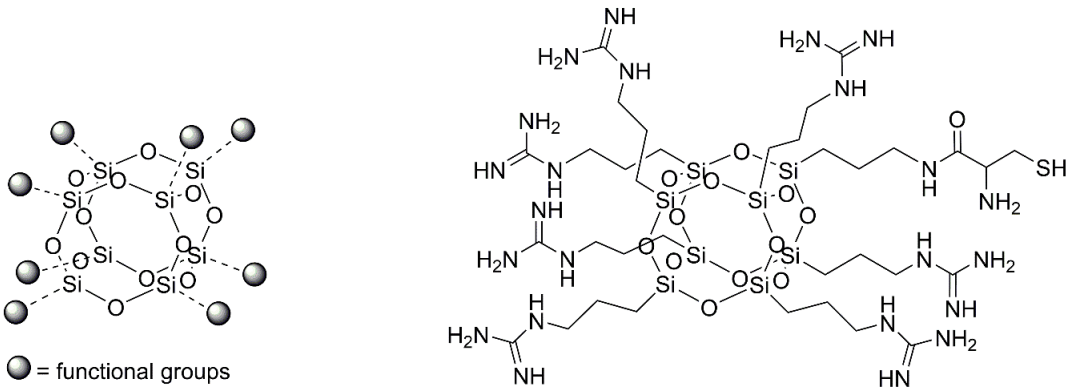

Figure 12: Chemical structure of the COSS core with potential functional groups (left) and cell-penetrating single-corner cysteine-modified heptaguanidinium COSS (right).

2.4.3. Anthracycline antibiotic doxorubicin

Doxorubicin (DOX) also referred to as Adriamycin or hydroxyldaunorubicin (**figure 13, middle**) is a cytotoxic anthracycline antibiotic isolated in 1967 from a mutated strain of the bacteria *Streptomyces peucetius,* namely *Streptomyces peucetius var. caesius.*[110] It is used in antimitotic chemotherapy for the treatment of Hodgkin disease, non-Hodgkin lymphoma, leukemia and various other cancers.[111]

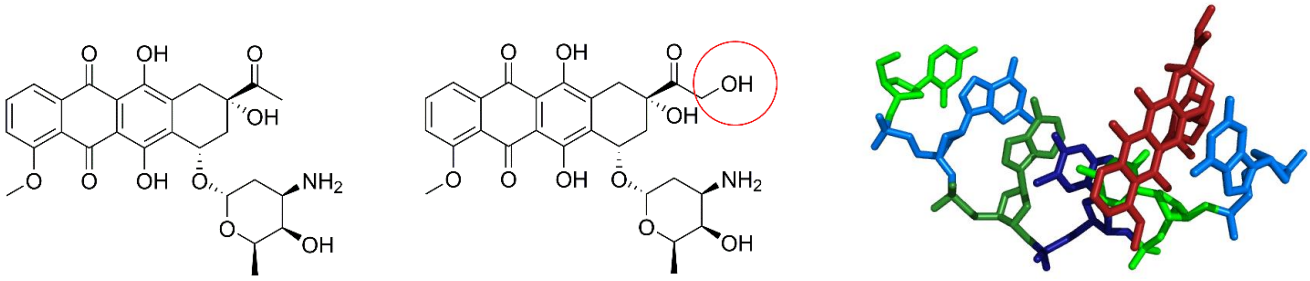

Figure 13: Chemical structure of daunomycin (left) and doxorubicin (middle). Right: Intercalation of doxorubicin (shown in red) with a single-strand DNA sequence CGATCG after PDB file 1D12.[112] (dC in light green, dG in light blue, dA in dark green and dT in dark blue.)

Previously, *Streptomyces peucetius* was discovered to produce daunomycin (DNR), the dehydroxylated derivative of doxorubicin (**figure 13, left**), which was also applied to the treatment of acute leukemia and lymphoma. Although it is supposed that the cytotoxicity of doxorubicin and daunomycin arises

from their intercalation with DNA (**figure 13, right**), thereby inducing DNA damage and the interference with the enzyme topoisomerase II inhibiting DNA replication, the exact mode of action still remains controversial.[113] However, both very potent and effective anticancer drugs were found to evoke severe dose-dependent cardiotoxicity.[114]

Doxorubicin, like most drugs of small size, is only capable to penetrate cells or tissues *via* passive diffusion.[115] Therefore, distribution occurs almost indiscriminately to organs and tissues. Moreover, as doxorubicin is known to be accumulated preferentially in the heart, cardiotoxicity is its dose-limiting factor.[116] Despite extensive research, doxorubicin cardiomyopathy is still the major adverse effect with a mortality of approximately 50%, once congestive heart failure has developed.[117] Additionally, due to its small size free doxorubicin exhibits fast renal clearance and short plasma half-life. The formulation in PEGylated nano-liposomes, namely Doxil®, the first FDA-approved nanodrug (1995), prolonged the half-life as well as blood circulation.[118]

To overcome the limitations and side effects associated with free doxorubicin, namely, the toxicity on noncancerous cells within the body,[115] cardiotoxicity and nephrotoxicity,[119] several conjugation approaches have been developed over the past decades, involving formulations with albumin-conjugated liposomes,[119-120] ADCs,[121] hydrogels,[122] dendrimers[123] or combinations of the mentioned methods. A very recently reported study involves the liposomal coencapsulation of doxorubicin with listeriolysin O.[124] Although this formulation enhanced the nuclear targeting in certain carcinoma cell lines, it is supposed to be highly immunogenic.[124-125]

Due to the fact that doxorubicin, its mode of action as well as its administration and distribution, have been extensively studied and analyzed, it is often used as a proof-of-principle/standard drug for cellular delivery experiments.

3. Summary & Outlook

To date, a vast number of chemical reactions compatible with bioinspired, bioengineered, and biomimetic molecules has been elaborated in response to the demands of the steadily growing repertoire of conjugation techniques. However, the choice of the suitable approach from the toolbox of these so-called bioorthogonal methods still remains case-sensitive. Therefore, the central goal of the presented cumulative work was the design and elaboration of new combined *orthogonal bioorthogonal*[1] synthetic strategies comprising the combination of certain chemo- and site-selective reactions, and their application to the generation of macromolecular conjugates with tailor-made properties. For each hybrid construct a customized bioorthogonal synthetic strategy was developed, carefully considering the intrinsic properties, special requirements, and distinct constraints of the reaction partners. A vast number of compounds from different molecular classes were investigated, ranging from rather small cytotoxic drugs, oligopeptides and highly ordered cube-octameric silsesquioxanes (COSS) to crystalline nanocellulose and full-size functional proteins. The results of the cumulative research are summarized in **scheme 1**.

The first study (*Angew. Chem. Int. Ed.,* **2014**, *53*, 12618-12623) addressed the development of a site-directed, bioorthogonal and modular approach towards the immobilization of biomolecules on a crystalline nanocellulose (CNC) platform (**scheme 1, top**). The ultimate goal was the covalent chemoselective coupling of bioactive proteins to the surface of CNC – a sustainable, nature-derived macromolecular compound. These constructs should combine the properties of the immobilized biomolecules with the intrinsic characteristics of the cellulose nanocrystals, such as low toxicity, water- and biocompatibility as well as obvious advantages given by their nanosize.

The challenge of this investigation was to circumvent the general drawbacks of commonly used protein conjugation methods, with respect to enhanced selectivity and operability under physiological conditions in aqueous milieu. To that end, a generic two-step procedure was developed that implied a set of solely efficient orthogonal reactions, avoiding the need of organic solvents and compatible with physiological systems. Making use of efficient oxime ligation and subsequent sortase-mediated conjugation, the synthetic strategy exhibited the required regiospecificity and biocompatibility, which favored its application to a vast number of functional proteins. Thus, following TEMPO-mediated oxidation of CNC hydroxyls, first a small fluorophore moiety was immobilized, enabling the detection of aminooxy-addressable surface aldehydes. Subsequently, oximation with the peptidic linker was established leading to sortase-addressable sites on CNC carrier. Afterwards, the enzyme-mediated surface immobilization proceeded using three proteins of different classes, diverse size, complexity and bioactivity under preservation of their biological function.

In this work, an engineered Sortase A (eSrtA) variant was used as it exhibited improved catalytic properties. Moreover, it has been demonstrated that the well-defined orientation of the proteinaceous ligands ensured by the site-selective coupling resulted in an enhanced, compared to randomly grafted proteins, bioactivity. Taken these findings into account, it could be concluded that sustainable nanosized biomaterials represent excellent platforms for the customized immobilization of high-profile macromolecules for biomedical purposes, drug delivery or deposition. It might even be interesting to investigate their applicability as platforms for the immobilization of proteins of interest with subsequent application in affinity chromatography.

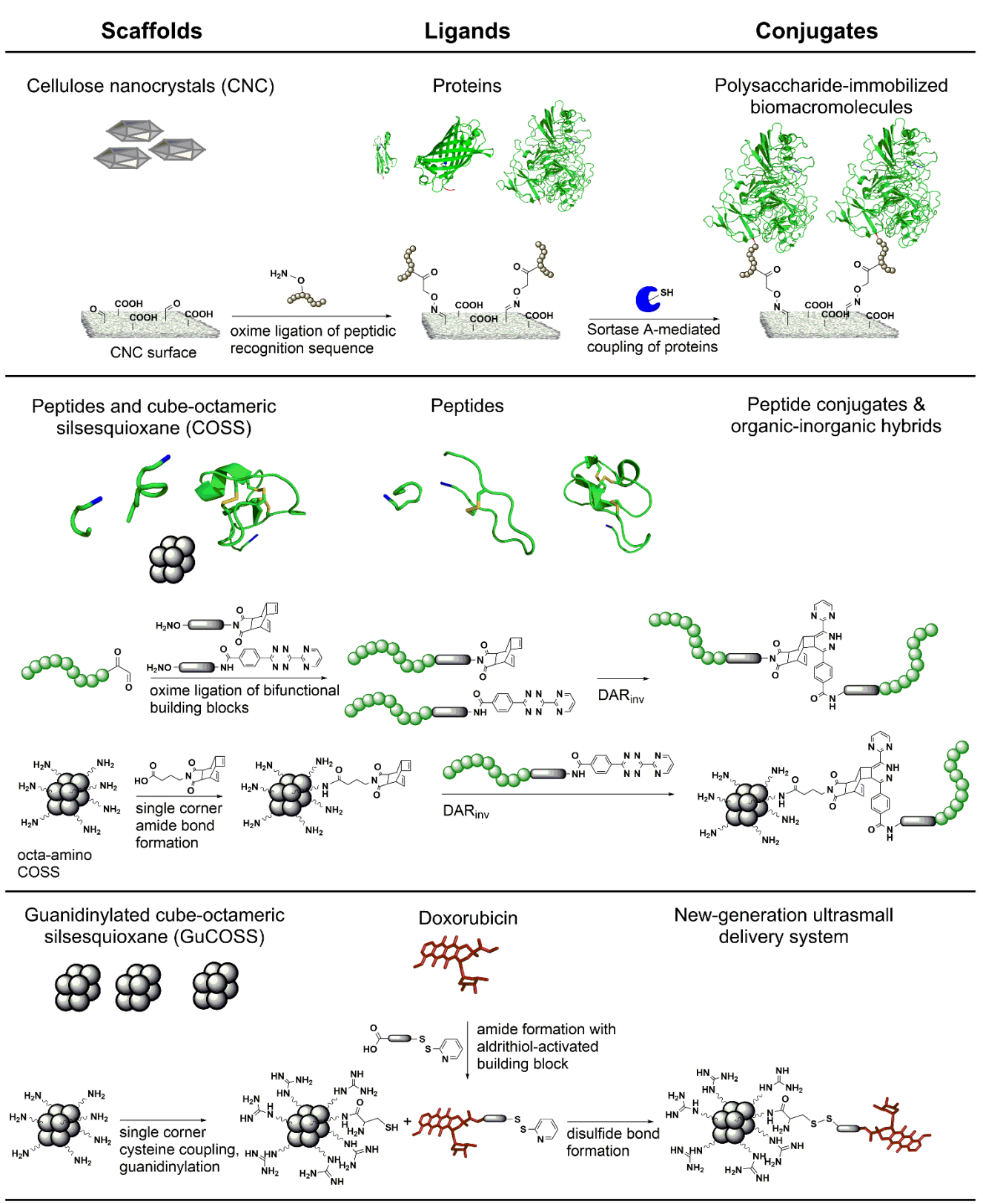

Scheme 1: Overview of the scaffold-ligand pairs and the respective ligation strategies developed for the generation of the desired conjugates.

The second study (*Chem. Commun.,* **2015**, *51*, 11130-11133) was devoted to the development of a synthetic strategy for the ultimate generation of a hybrid organic-inorganic construct comprising one of the smallest known cube-octameric silsesquioxane nanoparticle and a functional peptidic counterpart (**scheme 1, middle**). Synthesis design, especially considering the choice of an appropriate bioorthogonal method, proceeded from a premise that COSS core is not stable in the presence of nucleophiles. In the proof-of-concept experiments, the applicability of a modular synthetic approach combining generation of an *N*-terminal peptide aldehyde, efficient oxime ligation and inverse electron-demand Diels-Alder reaction (DAR_{inv}) was demonstrated upon conjugation of linear, cystine-cyclized, and multi-disulfide functional peptides of diverse size. Further the strategy was expanded to the synthesis of constructs with more sophisticated architecture.

In the scope of this work the DAR_{inv} was chosen for the synthesis of the bioconjugates containing peptides of different length, molecular complexity and biological properties due to its reported biocompatibility and fast reaction kinetics.[52] Moreover, this particular reaction has the advantage that its second step is irreversible due to the loss of molecular nitrogen, which shifts the equilibrium towards the product formation.[126] To achieve orthogonally addressable sites, the synthesized building blocks contained an aminooxy moiety in a combination with a tetrazine or Reppe anhydride, respectively. These bifunctional units appeared easy accessible and were installed into a variety of molecular constructs without compromising their structural features. Successive transformation using the DAR_{inv} yielded defined conjugates with good to quantitative conversion. The modularity of this synthetic two-step procedure offers the advantage that, once the DAR_{inv} moiety has been installed into the molecule of interest, it can react with every desired counterpart. It is feasible for the generation of peptidic conjugates, including synthetic peptides as well as the recombinant ones.

The third study discussed in the course of this thesis (*Angew. Chem. Int. Ed.,* **2016***, 55,* 14842–14846) was aimed on the elaboration of a synthetic strategy towards hybrid organic-inorganic cube-octameric silsesquioxane derivatives and their application as a scaffold upon construction of a cell-penetrating delivery system (**scheme 1, bottom**). This sophisticated construct should be equipped with a cytotoxic drug releasable upon cellular uptake. The restrictions of COSS template considering its stability issues should be taken into account as well. In the preceding study, the cell-penetrating properties of ammonium-functionalized COSS nanoparticles and their accumulation in the nucleoli have been demonstrated.[109a] Based on these findings, the next step was the engineering of additional COSS particles bearing positively charged flanking arms, and investigation of their cell-penetrating features. The delivery of a therapeutic cargo in the living cell should proof the viability of this new-generation molecular transporter.

In the scope of this study it was shown that engineered guanidinylated COSS nanoparticle (GuCOSS) exhibited much higher and faster cellular uptake than the respective commonly used cell-penetrating peptides (e.g. TAT, penetratin, hepta- and decaarginine). This efficacy (78-fold more potent as heptaarginine bearing the same sort and amount of charged groups) can be rationalized taking into consideration the significantly smaller size and, therefore, higher charge density around the COSS core.

Interestingly, our novel cell-permeation module appeared rather promiscuous to targeted cells. Indeed, an efficient cellular uptake was observed in different species, among them Gram-negative bacteria (*Escherichia coli)*, yeast (*Saccharomyces cerevisiae)*, and archaea (*Sulfolobus islandicus, Sulfolobus tokodaii, Halobacterium salinarum*) as well as in human cancer cell lines. As the uptake was only negligibly reduced at 4°C, compared to that at 37°C, an energy-independent mechanism was proposed. Moreover, the COSS core degrades inside the cell and the components themselves are predicted to exhibit non to low toxicity. This expectation was corroborated upon thorough analysis of the cellular uptake, toxicity, and degradation of a GuCOSS module.

The therapeutic drug doxorubicin was chosen as proof-of-concept cargo for intracellular delivery as, being applied solely, it can only enter the cell slowly *via* passive diffusion. Therefore, doxorubicin was conjugated to a highly efficient cell-penetrating heptaguanidinylated COSS nanoparticle. To that end,

the respective octaammonium COSS derivative was single-corner equipped with a cysteine. Subsequent guanidinylation of the remaining amines followed by disulfide bond formation with an aldrithiol™-2-modified doxorubicin resulted in a cell-penetrating module carrying a releasable cytotoxic cargo. Indeed, the disulfide bridge breaks in the reducing milieu of the cytoplasm, thus liberating the active drug. The cytotoxicity studies of the hybrids showed an enhanced toxicity of the conjugate compared to the free compound. Moreover, due the fast cellular uptake, the incubation time was significantly reduced. As there are plenty of drugs lacking cell permeation and/or water solubility, e.g. hygromycin, ispinesib *etc.,* the GuCOSS-based molecular transporter can open new avenues towards facilitated cellular uptake of these therapeutics.

Taken together, the outcome of this cumulative research contributes to the toolbox of modern bioorthogonal methods in view of applicability, versatility, reliability, and compatibility with complex molecular architectures irrespectively on their natural or manmade origin. Moreover, combination of traditional chemistry with modern biocompatible ligation methods, among them enzyme-assisted transformations, expand the spectrum of bioorthogonal conjugation strategies.

4. References

[1] D. M. Patterson, J. A. Prescher, *Curr Opin Chem Biol* **2015**, *28*, 141-149.

[2] http://www.nature.com/subjects/bioconjugate-chemistry.

[3] a) S. K. Jaganathan, A. Balaji, M. V. Vellayappan, A. P. Subramanian, A. A. John, M. K. Asokan, E. Supriyanto, *J Mater Sci* **2015**, *50*, 2007-2018; b) J. M. Goddard, J. H. Hotchkiss, *Prog Polym Sci* **2007**, *32*, 698-725; c) Y. Ikada, *Biomaterials* **1994**, *15*, 725-736; d) K. S. Raja, Q. Wang, M. J. Gonzalez, M. Manchester, J. E. Johnson, M. G. Finn, *Biomacromolecules* **2003**, *4*, 472-476; e) P. G. Holder, D. T. Finley, N. Stephanopoulos, R. Walton, D. S. Clark, M. B. Francis, *Langmuir* **2010**, *26*, 17383-17388; f) Z. Chen, N. Li, S. Li, M. Dharmarwardana, A. Schlimme, J. J. Gassensmith, *Interdiscip Rev Nanomed Nanobiotechnol* **2015**.

[4] M. K. Yu, J. Park, S. Jon, *Theranostics* **2012**, *2*, 3-44.

[5] H. W. Shih, D. N. Kamber, J. A. Prescher, *Curr Opin Chem Biol* **2014**, *21C*, 103-111.

[6] N. J. Agard, J. A. Prescher, C. R. Bertozzi, *J Am Chem Soc* **2004**, *126*, 15046-15047.

[7] E. M. Sletten, C. R. Bertozzi, *Acc Chem Res* **2011**, *44*, 666-676.

[8] a) P. V. Chang, J. A. Prescher, E. M. Sletten, J. M. Baskin, I. A. Miller, N. J. Agard, A. Lo, C. R. Bertozzi, *P Natl Acad Sci* **2010**, *107*, 1821-1826; b) D. X. Zeng, B. M. Zeglis, J. S. Lewis, C. J. Anderson, *Journal of Nuclear Medicine* **2013**, *54*, 829-832; c) M. M. Heravi, M. Tamimi, H. Yahyavi, T. Hosseinnejad, *Curr Org Chem* **2016**, *20*, 1591-1647.

[9] I. S. Carrico, *Chem Soc Rev* **2008**, *37*, 1423-1431.

[10] T. Matsumoto, T. Tanaka, A. Kondo, *Biotechnol J* **2012**, *7*, 1137-1146.

[11] a) T. Hohsaka, M. Sisido, *Curr Opin Chem Biol* **2002**, *6*, 809-815; b) N. Hino, A. Hayashi, K. Sakamoto, S. Yokoyama, *Nat Protoc* **2006**, *1*, 2957-2962.

[12] a) B. Sklarz, *Q Rev Chem Soc* **1967**, *21*, 3-28; b) A. J. Fatiadi, *Synthesis-Stuttgart* **1974**, 229-272.

[13] a) U. J. Kim, S. Kuga, M. Wada, T. Okano, T. Kondo, *Biomacromolecules* **2000**, *1*, 488-492; b) K. A. Kristiansen, A. Potthast, B. E. Christensen, *Carbohydr Res* **2010**, *345*, 1264-1271.

[14] R. Pascual, M. A. Herraez, *Can J Chem* **1985**, *63*, 2349-2353.

[15] a) R. Fields, H. B. F. Dixon, *Biochem J* **1968**, *108*, 883-887; b) H. F. Gaertner, K. Rose, R. Cotton, D. Timms, R. Camble, R. E. Offord, *Bioconjug Chem* **1992**, *3*, 262-268.

[16] K. F. Geoghegan, J. G. Stroh, *Bioconjug Chem* **1992**, *3*, 138-146.

[17] G. Dryhurst, *Periodate oxidation of diol and other functional groups; analytical and structural applications*, 1st ed., Pergamon Press, Oxford, New York,, **1970**.

[18] a) S. M. Agten, P. E. Dawson, T. M. Hackeng, *J Pept Sci* **2016**, *22*, 271-279; b) J. R. Clamp, L. Hough, *Biochem J* **1965**, *94*, 17-24.

[19] T. Kawakami, K. Akaji, S. Aimoto, *Org Lett* **2001**, *3*, 1403-1405.

[20] P. Thompson, B. Bezabeh, R. Fleming, M. Pruitt, S. L. Mao, P. Strout, C. Chen, S. Cho, H. H. Zhong, H. Wu, C. S. Gao, N. Dimasi, *Bioconjug Chem* **2015**, *26*, 2085-2096.

[21] E. Hurwitz, R. Levy, R. Maron, M. Wilchek, R. Arnon, M. Sela, *Cancer Res* **1975**, *35*, 1175-1181.

[22] C. Renicke, R. Spadaccini, C. Taxis, *Plos One* **2013**, *8*, e67915.

[23] A. Moulin, J. Martinez, J. A. Fehrentz, *J Pept Sci* **2007**, *13*, 1-15.

[24] J. M. Gilmore, R. A. Scheck, A. P. Esser-Kahn, N. S. Joshi, M. B. Francis, *Angew Chem Int Ed* **2006**, *45*, 5307-5311.

[25] R. A. Scheck, M. B. Francis, *ACS Chem Biol* **2007**, *2*, 247-251.

[26] R. A. Scheck, M. T. Dedeo, A. T. Lavarone, M. B. Francis, *J Am Chem Soc* **2008**, *130*, 11762-11770.

[27] E. H. M. Lempens, B. A. Helms, M. Merkx, E. W. Meijer, *Chembiochem* **2009**, *10*, 658-662.

[28] a) V. T. Bhat, A. M. Caniard, T. Luksch, R. Brenk, D. J. Campopiano, M. F. Greaney, *Nat Chem* **2010**, *2*, 490-497; bT. P. King, S. W. Zhao, T. Lam, *Biochemistry* **1986**, *25*, 5774-5779.

[29] J. Kalia, R. T. Raines, *Angew Chem Int Ed* **2008**, *47*, 7523-7526.

[30] S. Ulrich, D. Boturyn, A. Marra, O. Renaudet, P. Dumy, *Chemistry* **2014**, *20*, 34-41.

[31] a) A. Dirksen, T. M. Hackeng, P. E. Dawson, *Angew Chem Int Ed* **2006**, *45*, 7581-7584; b) S. J. Wang, D. Gurav, O. P. Oommen, O. P. Varghese, *Chem-Eur J* **2015**, *21*, 5980-5985.

[32] a) M. Wendeler, L. Grinberg, X. Wang, P. E. Dawson, M. Baca, *Bioconjug Chem* **2014**, *25*, 93-101; b) A. R. Blanden, K. Mukherjee, O. Dilek, M. Loew, S. L. Bane, *Bioconjug Chem* **2011**, *22*, 1954-1961.
[33] A. Dirksen, P. E. Dawson, *Bioconjug Chem* **2008**, *19*, 2543-2548.
[34] H. C. Kolb, M. G. Finn, K. B. Sharpless, *Angew Chem Int Ed* **2001**, *40*, 2004-2021.
[35] L. Zhang, X. G. Chen, P. Xue, H. H. Y. Sun, I. D. Williams, K. B. Sharpless, V. V. Fokin, G. C. Jia, *J Am Chem Soc* **2005**, *127*, 15998-15999.
[36] V. Hong, N. F. Steinmetz, M. Manchester, M. G. Finn, *Bioconjug Chem* **2010**, *21*, 1912-1916.
[37] a) T. R. Chan, R. Hilgraf, K. B. Sharpless, V. V. Fokin, *Org Lett* **2004**, *6*, 2853-2855; b) C. Uttamapinant, A. Tangpeerachaikul, S. Grecian, S. Clarke, U. Singh, P. Slade, K. R. Gee, A. Y. Ting, *Angew Chem Int Ed* **2012**, *51*, 5852-5856.
[38] N. J. Agard, J. A. Prescher, C. R. Bertozzi, *J Am Chem Soc* **2004**, *126*, 15046-15047.
[39] a) J. A. Codelli, J. M. Baskin, N. J. Agard, C. R. Berozzi, *J Am Chem Soc* **2008**, *130*, 11486-11493; b) I. Nikic, J. H. Kang, G. E. Girona, I. V. Aramburu, E. A. Lemke, *Nat Protoc* **2015**, *10*, 780-791.
[40] F. H. Li, J. S. Dong, X. S. Hu, W. M. Gong, J. S. Li, J. Shen, H. F. Tian, J. Y. Wang, *Angew Chem Int Ed* **2015**, *54*, 4597-4602.
[41] I. S. Marks, J. S. Kang, B. T. Jones, K. J. Landmark, A. J. Cleland, T. A. Taton, *Bioconjug Chem* **2011**, *22*, 1259-1263.
[42] a) Z. Cai, Q. Ouyang, D. Zeng, K. N. Nguyen, J. Modi, L. Wang, A. G. White, B. E. Rogers, X. Q. Xie, C. J. Anderson, *J Med Chem* **2014**, *57*, 6019-6029; b) H. L. Kim, K. Sachin, H. J. Jeong, W. Choi, H. S. Lee, D. W. Kim, *ACS Med Chem Lett* **2015**, *6*, 402-407.
[43] a) J. A. Prescher, C. R. Bertozzi, *Nat Chem Biol* **2005**, *1*, 13-21; b) B. L. Nilsson, L. L. Kiessling, R. T. Raines, *Org Lett* **2000**, *2*, 1939-1941; c) E. Saxon, J. I. Armstrong, C. R. Bertozzi, *Org Lett* **2000**, *2*, 2141-2143.
[44] a) J. W. Chin, S. W. Santoro, A. B. Martin, D. S. King, L. Wang, P. G. Schultz, *J Am Chem Soc* **2002**, *124*, 9026-9027; b) A. Deiters, P. G. Schultz, *Bioorg Med Chem Lett* **2005**, *15*, 1521-1524; c) J. C. Maza, J. R. McKenna, B. K. Raliski, M. T. Freedman, D. D. Young, *Bioconjug Chem* **2015**, *26*, 1884-1889.
[45] a) O. Avrutina, M. Empting, S. Fabritz, M. Daneschdar, H. Frauendorf, U. Diederichsen, H. Kolmar, *Org Biomol Chem* **2009**, *7*, 4177-4185; b) E. Oueis, M. Jaspars, N. J. Westwood, J. H. Naismith, *Angew Chem Int Ed* **2016**, *55*, 5842-5845.
[46] a) S. Schoffelen, M. B. van Eldijk, B. Rooijakkers, R. Raijmakers, A. J. R. Heck, J. C. M. van Hest, *Chem Sci* **2011**, *2*, 701-705; b) S. F. M. van Dongen, R. L. M. Teeuwen, M. Nallani, S. S. van Berkel, J. J. L. M. Cornelissen, R. J. M. Nolte, J. C. M. van Hest, *Bioconjug Chem* **2009**, *20*, 20-23.
[47] A. C. Knall, C. Slugovc, *Chem Soc Rev* **2013**, *42*, 5131-5142.
[48] a) R. Pipkorn, W. Waldeck, B. Didinger, M. Koch, G. Mueller, M. Wiessler, K. Braun, *J Pept Sci* **2009**, *15*, 235-241; b) M. Wiessler, W. Waldeck, C. Kliem, R. Pipkorn, K. Braun, *Int J Med Sci* **2009**, *7*, 19-28; c) M. Wiessler, W. Waldeck, R. Pipkorn, C. Kliem, P. Lorenz, H. Fleischhacker, M. Hafner, K. Braun, *Int J Med Sci* **2010**, *7*, 213-223.
[49] a) J. Schoch, S. Ameta, A. Jaschke, *Chem Commun* **2011**, *47*, 12536-12537; b) M. Vrabel, P. Kolle, K. M. Brunner, M. J. Gattner, V. Lopez-Carrillo, R. de Vivie-Riedle, T. Carell, *Chemistry* **2013**, *19*, 13309-13312; c) M. Best, A. Degen, M. Baalmann, T. T. Schmidt, R. Wombacher, *Chembiochem* **2015**, *16*, 1158-1162.
[50] a) M. L. Blackman, M. Royzen, J. M. Fox, *J Am Chem Soc* **2008**, *130*, 13518-13519; b) N. K. Devaraj, R. Upadhyay, J. B. Hatin, S. A. Hilderbrand, R. Weissleder, *Angew Chem Int Ed* **2009**, *48*, 7013-7016; c) N. K. Devaraj, S. Hilderbrand, R. Upadhyay, R. Mazitschek, R. Weissleder, *Angew Chem Int Ed* **2010**, *49*, 2869-2872; d) K. Lang, L. Davis, S. Wallace, M. Mahesh, D. J. Cox, M. L. Blackman, J. M. Fox, J. W. Chin, *J Am Chem Soc* **2012**, *134*, 10317-10320.
[51] F. Liu, R. S. Paton, S. Kim, Y. Liang, K. N. Houk, *J Am Chem Soc* **2013**, *135*, 15642-15649.
[52] W. X. Chen, D. Z. Wang, C. F. Dai, D. Hamelberg, B. H. Wang, *Chem Commun* **2012**, *48*, 1736-1738.

[53] S. A. Albu, S. A. Al-Karmi, A. Vito, J. P. K. Dzandzi, A. Zlitni, D. Beckford-Vera, M. Blacker, N. Janzen, R. M. Patel, A. Capretta, J. F. Valliant, *Bioconjug Chem* **2016**, *27*, 207-216.
[54] a) S. Ameta, J. Becker, A. Jaschke, *Org Biomol Chem* **2014**, *12*, 4701-4707; b) J. Schoch, M. Wiessler, A. Jaschke, *J Am Chem Soc* **2010**, *132*, 8846-+.
[55] a) M. Pagel, R. Meier, K. Braun, M. Wiessler, A. G. Beck-Sickinger, *Org Biomol Chem* **2016**, *14*, 4809-4816; b) M. Wiessler, U. Hennrich, R. Pipkorn, W. Waldeck, L. J. Cao, J. Peter, V. Ehemann, W. Semmler, T. Lammers, K. Braun, *Theranostics* **2011**, *1*, 381-394.
[56] a) J. Seckute, N. K. Devaraj, *Curr Opin Chem Biol* **2013**, *17*, 761-767; b) R. Rossin, P. R. Verkerk, S. M. van den Bosch, R. C. Vulders, I. Verel, J. Lub, M. S. Robillard, *Angew Chem Int Ed* **2010**, *49*, 3375-3378.
[57] S. K. Mazmanian, G. Liu, H. Ton-That, O. Schneewind, *Science* **1999**, *285*, 760-763.
[58] S. W. Lockless, T. W. Muir, *Proc Natl Acad Sci U S A* **2009**, *106*, 10999-11004.
[59] C. S. Greenberg, P. J. Birckbichler, R. H. Rice, *Faseb J* **1991**, *5*, 3071-3077.
[60] a) R. P. Novick, *Trends Microbiol* **2000**, *8*, 148-151; b) H. Ton-That, S. K. Mazmanian, K. F. Faull, O. Schneewind, *J Biol Chem* **2000**, *275*, 9876-9881.
[61] a) U. Ilangovan, H. Ton-That, J. Iwahara, O. Schneewind, R. T. Clubb, *Proc Natl Acad Sci* **2001**, *98*, 6056-6061; b) S. K. Mazmanian, H. Ton-That, O. Schneewind, *Mol Microbiol* **2001**, *40*, 1049-1057.
[62] a) M. L. Bentley, H. Gaweska, J. M. Kielec, D. G. McCafferty, *J Biol Chem* **2007**, *282*, 6571-6581; b) M. T. Naik, N. Suree, U. Ilangovan, C. K. Liew, W. Thieu, D. O. Campbell, J. J. Clemens, M. E. Jung, R. T. Clubb, *J Biol Chem* **2006**, *281*, 1817-1826.
[63] K. Kappel, J. Wereszczynski, R. T. Clubb, J. A. McCammon, *Protein Sci* **2012**, *21*, 1858-1871.
[64] R. R. Beerli, T. Hell, A. S. Merkel, U. Grawunder, *Plos One* **2015**, *10*, e0131177.
[65] T. Sijbrandij, N. Cukkemane, K. Nazmi, E. C. Veerman, F. J. Bikker, *Bioconjug Chem* **2013**, *24*, 828-831.
[66] a) T. Matsumoto, S. Sawamoto, T. Sakamoto, T. Tanaka, H. Fukuda, A. Kondo, *J Biotechnol* **2011**, *152*, 37-42; b) R. Parthasarathy, S. Subramanian, E. T. Boder, *Bioconjug Chem* **2007**, *18*, 469-476; c) Q. Chen, Q. Sun, N. M. Molino, S. W. Wang, E. T. Boder, W. Chen, *Chem Commun* **2015**, *51*, 12107-12110; d) S. Pritz, Y. Wolf, O. Kraetke, J. Klose, M. Bienert, M. Beyermann, *J Org Chem* **2007**, *72*, 3909-3912.
[67] a) T. Tanaka, T. Yamamoto, S. Tsukiji, T. Nagamune, *Chembiochem* **2008**, *9*, 802-807; bK. Park, J. Jung, J. Son, S. H. Kim, B. H. Chung, *Chem Commun (Camb)* **2013**, *49*, 9585-9587.
[68] B. M. Dorr, H. O. Ham, C. H. An, E. L. Chaikof, D. R. Liu, *P Natl Acad Sci USA* **2014**, *111*, 13343-13348.
[69] a) I. Chen, B. M. Dorr, D. R. Liu, *Proc Natl Acad Sci* **2011**, *108*, 11399-11404; b) M. W. Popp, J. M. Antos, H. L. Ploegh, *Current protocols in protein science* **2009**, *Chapter 15*, Unit 15 13; c) C. S. Theile, M. D. Witte, A. E. Blom, L. Kundrat, H. L. Ploegh, C. P. Guimaraes, *Nat Protoc* **2013**, *8*, 1800-1807.
[70] K. Piotukh, B. Geltinger, N. Heinrich, F. Gerth, M. Beyermann, C. Freund, D. Schwarzer, *J Am Chem Soc* **2011**, *133*, 17536-17539.
[71] N. Suree, C. K. Liew, V. A. Villareal, W. Thieu, E. A. Fadeev, J. J. Clemens, M. E. Jung, R. T. Clubb, *J Biol Chem* **2009**, *284*, 24465-24477.
[72] B. L. Carlson, E. R. Ballister, E. Skordalakes, D. S. King, M. A. Breidenbach, S. A. Gilmore, J. M. Berger, C. R. Bertozzi, *J Biol Chem* **2008**, *283*, 20117-20125.
[73] D. Rabuka, J. S. Rush, G. W. deHart, P. Wu, C. R. Bertozzi, *Nat Protoc* **2012**, *7*, 1052-1067.
[74] G. Volkmann, X. Q. Liu, *Plos One* **2009**, *4*.
[75] Y. Kwon, M. A. Coleman, J. A. Camarero, *Angew Chem Int Ed* **2006**, *45*, 1726-1729.
[76] M. Q. Xu, T. C. Evans, *Methods* **2001**, *24*, 257-277.
[77] a) M. Fernandez-Suarez, H. Baruah, L. Martinez-Hernandez, K. T. Xie, J. M. Baskin, C. R. Bertozzi, A. Y. Ting, *Nat Biotechnol* **2007**, *25*, 1483-1487; b) J. D. Cohen, P. Zou, A. Y. Ting, *Chembiochem* **2012**, *13*, 888-894; c) D. S. Liu, W. S. Phipps, K. H. Loh, M. Howarth, A. Y. Ting, *ACS Nano* **2012**, *6*, 11080-11087.

[78] a) B. Spolaore, S. Raboni, A. R. Molina, A. Satwekar, N. Damiano, A. Fontana, *Biochemistry* **2012**, *51*, 8679-8689; b) P. Dennler, A. Chiotellis, E. Fischer, D. Bregeon, C. Belmant, L. Gauthier, F. Lhospice, F. Romagne, R. Schibli, *Bioconjug Chem* **2014**, *25*, 569-578.
[79] A. A. Shelat, R. K. Guy, *Nat Chem Biol* **2007**, *3*, 442-446.
[80] a) F. J. Feher, K. D. Wyndham, M. A. Scialdone, Y. Hamuro, *Chem Commun* **1998**, 1469-1470; b) V. Martos, P. Castreno, J. Valero, J. de Mendoza, *Curr Opin Chem Biol* **2008**, *12*, 698-706.
[81] a) T. Carell, E. A. Wintner, A. Bashirhashemi, J. Rebek, *Angew Chem Int Ed* **1994**, *33*, 2059-2061; b) T. Carell, E. A. Wintner, J. Rebek, *Angew Chem Int Ed* **1994**, *33*, 2061-2064.
[82] a) M. Okada, Y. Kishibe, K. Ide, T. Takahashi, T. Hasegawa, *Int J Carbohydr Chem* **2009**, *2009*, 9; b) G. R. Geier, T. Sasaki, *Tetrahedron Lett* **1997**, *38*, 3821-3824.
[83] M. Fiore, A. Chambery, A. Marra, A. Dondoni, *Org Biomol Chem* **2009**, *7*, 3910-3913.
[84] A. Dondoni, A. Marra, *J Org Chem* **2006**, *71*, 7546-7557.
[85] S. Barazzouk, C. Daneault, *Cellulose* **2012**, *19*, 481-493.
[86] a) M. Bennett, A. Krah, F. Wien, E. Garman, R. Mckenna, M. Sanderson, S. Neidle, *P Natl Acad Sci* **2000**, *97*, 9476-9481; b) R. E. McGovern, H. Fernandes, A. R. Khan, N. P. Power, P. B. Crowley, *Nat Chem* **2012**, *4*, 527-533.
[87] J. George, S. N. Sabapathi, *Nanotechnol Sci Appl* **2015**, *8*, 45-54.
[88] a) D. N. S. Hon, *Cellulose* **1994**, *1*, 1-25; b) J. Zhou, N. Butchosa, H. S. N. Jayawardena, J. Park, Q. Zhou, M. D. Yan, O. Ramstrom, *Biomacromolecules* **2015**, *16*, 1426-1432.
[89] J. T. McNamara, J. L. Morgan, J. Zimmer, *Annu Rev Biochem* **2015**, *84*, 895-921.
[90] X. Xu, F. Liu, L. Jiang, J. Y. Zhu, D. Haagenson, D. P. Wiesenborn, *ACS Appl Mater Interfaces* **2013**, *5*, 2999-3009.
[91] B. Li, W. Xu, D. Kronlund, A. Maattanen, J. Liu, J. H. Smatt, J. Peltonen, S. Willfor, X. Mu, C. Xu, *Carbohydr Polym* **2015**, *133*, 605-612.
[92] B. G. Ranby, *Acta Chem Scand* **1949**, *3*, 649-650.
[93] Z. Hanif, F. R. Ahmed, S. W. Shin, Y. K. Kim, S. H. Um, *Colloids Surf B Biointerfaces* **2014**, *119*, 162-165.
[94] G. Siqueira, J. Bras, A. Dufresne, *Polymers-Basel* **2010**, *2*, 728-765.
[95] Y. Habibi, L. A. Lucia, O. J. Rojas, *Chem Rev* **2010**, *110*, 3479-3500.
[96] D. O. Carlsson, J. Lindh, L. Nyholm, M. Stromme, A. Mihranyan, *Rsc Advances* **2014**, *4*, 52289-52298.
[97] a) E. Lam, K. B. Male, J. H. Chong, A. C. W. Leung, J. H. T. Luong, *Trends Biotechnol* **2012**, *30*, 283-290; b) D. Feldman, *J Macromol Sci* **2015**, *52*, 322-329.
[98] N. Lin, A. Dufresne, *Eur Polym J* **2014**, *59*, 302-325.
[99] K. A. Mahmoud, J. A. Mena, K. B. Male, S. Hrapovic, A. Kamen, J. H. Luong, *ACS Appl Mater Interfaces* **2010**, *2*, 2924-2932.
[100] S. Dong, M. Roman, *J Am Chem Soc* **2007**, *129*, 13810-13811.
[101] a) H. R. Wang, J. L. He, M. Z. Zhang, K. C. Tam, P. H. Ni, *Polym Chem* **2015**, *6*, 4206-4209; b) J. K. Jackson, K. Letchford, B. Z. Wasserman, L. Ye, W. Y. Hamad, H. M. Burt, *Int J Nanomedicine* **2011**, *6*, 321-330.
[102] A. Taheri, M. Mohammadi, *Chem Biol Drug Des* **2015**, *86*, 882-886.
[103] S. Dong, H. J. Cho, Y. W. Lee, M. Roman, *Biomacromolecules* **2014**, *15*, 1560-1567.
[104] a) V. Incani, C. Danumah, Y. Boluk, *Cellulose* **2013**, *20*, 191-200; b) M. A. Karaaslan, G. Z. Gao, J. F. Kadla, *Cellulose* **2013**, *20*, 2655-2665.
[105] H. Mori, Y. Miyamura, T. Endo, *Langmuir* **2007**, *23*, 9014-9023.
[106] G. Z. Li, L. C. Wang, H. L. Ni, C. U. Pittman, *J Inorg Organomet P* **2001**, *11*, 123-154.
[107] B. Trastoy, M. E. Perez-Ojeda, R. Sastre, J. L. Chiara, *Chemistry* **2010**, *16*, 3833-3841.
[108] H. Ghanbari, A. de Mel, A. M. Seifalian, *Int J Nanomedicine* **2011**, *6*, 775-786.
[109] a) S. Hörner, S. Fabritz, H. D. Herce, O. Avrutina, C. Dietz, R. W. Stark, M. C. Cardoso, H. Kolmar, *Org Biomol Chem* **2013**, *11*, 2258-2265; b) C. McCusker, J. B. Carroll, V. M. Rotello, *Chem Commun* **2005**, 996-998.
[110] G. Bonadonna, S. Monfardini, M. De Lena, F. Fossati-Bellani, *Br Med J* **1969**, *3*, 503-506.
[111] *Rep Carcinog* **2004**, *11*, III8.

[112] C. A. Frederick, L. D. Williams, G. Ughetto, G. A. van der Marel, J. H. van Boom, A. Rich, A. H. Wang, *Biochemistry* **1990**, *29*, 2538-2549.
[113] a) C. Perez-Arnaiz, N. Busto, J. M. Leal, B. Garcia, *J Phys Chem B* **2014**, *118*, 1288-1295; b) G. Minotti, P. Menna, E. Salvatorelli, G. Cairo, L. Gianni, *Pharmacol Rev* **2004**, *56*, 185-229; c) S. Zhang, X. Liu, T. Bawa-Khalfe, L. S. Lu, Y. L. Lyu, L. F. Liu, E. T. Yeh, *Nat Med* **2012**, *18*, 1639-1642; d) F. Yang, S. S. Teves, C. J. Kemp, S. Henikoff, *Bba-Rev Cancer* **2014**, *1845*, 84-89.
[114] M. M. Haq, S. S. Legha, J. Choksi, G. N. Hortobagyi, R. S. Benjamin, M. Ewer, M. Ali, *Cancer* **1985**, *56*, 1361-1365.
[115] O. Tacar, P. Sriamornsak, C. R. Dass, *Journal of Pharmacy and Pharmacology* **2013**, *65*, 157-170.
[116] K. Greish, T. Sawa, J. Fang, T. Akaike, H. Maeda, *J Control Release* **2004**, *97*, 219-230.
[117] K. Chatterjee, J. Zhang, N. Honbo, J. S. Karliner, *Cardiology* **2010**, *115*, 155-162.
[118] Y. Barenholz, *J Control Release* **2012**, *160*, 117-134.
[119] I. Lentacker, B. Geers, J. Demeester, S. C. De Smedt, N. N. Sanders, *Mol Ther* **2010**, *18*, 101-108.
[120] Y. Liu, J. Fang, Y. J. Kim, M. K. Wong, P. Wang, *Mol Pharm* **2014**, *11*, 1651-1661.
[121] a) H. D. King, D. Yurgaitis, D. Willner, R. A. Firestone, M. B. Yang, S. J. Lasch, K. E. Hellstrom, P. A. Trail, *Bioconjug Chem* **1999**, *10*, 279-288; b) S. C. Jeffrey, M. T. Nguyen, J. B. Andreyka, D. L. Meyer, S. O. Doronina, P. D. Senter, *Bioorg Med Chem Lett* **2006**, *16*, 358-362.
[122] a) H. Ma, C. He, Y. Cheng, Z. Yang, J. Zang, J. Liu, X. Chen, *ACS Appl Mater Interfaces* **2015**, *7*, 27040-27048; b) F. P. Seib, E. M. Pritchard, D. L. Kaplan, *Adv Funct Mater* **2013**, *23*, 58-65.
[123] a) F. Fu, S. Wen, J. Zhu, X. Shi, *J Control Release* **2015**, *213*, e31-32; b) N. G. Yabbarov, G. A. Posypanova, E. A. Vorontsov, O. N. Popova, E. S. Severin, *Biochemistry* **2013**, *78*, 884-894.
[124] Z. F. Walls, H. Gong, R. J. Wilson, *Mol Pharm* **2016**, *13*, 1185-1190.
[125] J. A. Carrero, H. Vivanco-Cid, E. R. Unanue, *Plos One* **2012**, *7*.
[126] A. C. Knall, M. Hollauf, C. Slugovc, *Tetrahedron Lett* **2014**, *55*, 4763-4766.

5. Cumulative Part

5.1. A Chemoenzymatic Approach to Protein Immobilization onto Crystalline Cellulose Nanoscaffolds

Christina Uth, Stefan Zielonka, Sebastian Hörner, Nicolas Rasche, Andreas Plog, Hannes Orelma, Olga. Avrutina, Kai Zhang, Harald Kolmar, A Chemoenzymatic Approach to Protein Immobilization onto Crystalline Cellulose Nanoscaffolds, *Angewandte Chemie International Edition*, **2014**, *53*, 12618–12623.

Title:
A Chemoenzymatic Approach to Protein Immobilization onto Crystalline Cellulose Nanoscaffolds

Authors:
Christina Uth, Stefan Zielonka, Sebastian Hörner, Dr. Nicolas Rasche, Andreas Plog, Dr. Hannes Orelma, Dr. Olga Avrutina, Dr. Kai Zhang and Prof. Dr. Harald Kolmar

Bibliographic data:
Angewandte Chemie International Edition
Volume 53, Issue 46, November 10, 2014, Pages 12618–12623.
Article first published online: 28 JUL 2014 | DOI: 10.1002/anie.201404616
See also: *Angewandte Chemie*, Volume 126, Issue 46, November 10, 2014, Pages 12826–12832.

Graphical abstract:

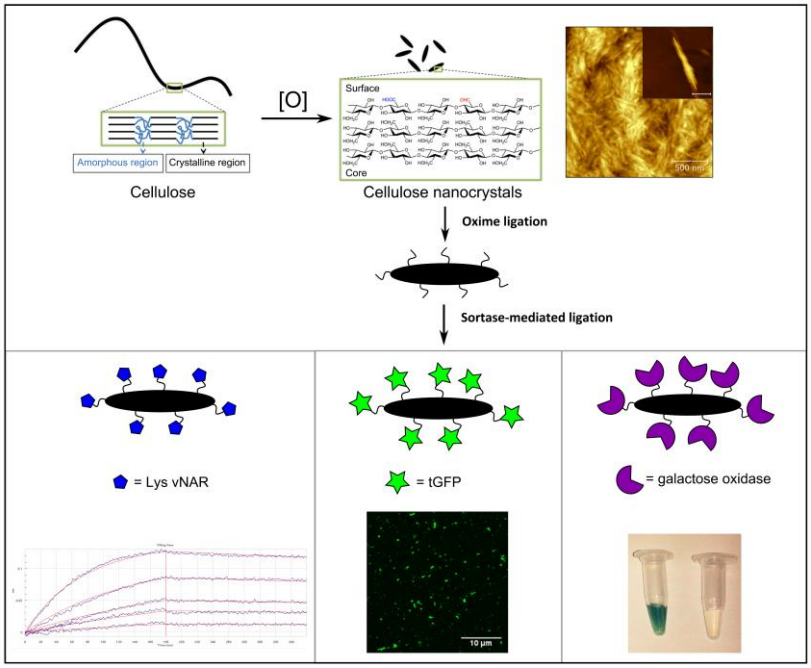

A modular approach was used for site-directed, bioorthogonal protein immobilization. The combination of enzyme-mediated ligation with highly efficient oxime ligation makes it possible to decorate sustainable nanocellulose platforms with fully functional proteins from different families.

Contributions by C. Uth:

- Synthesis and analysis of peptides and production of proteins and enzymes
- Synthesis and analysis of conjugates
- Conducted GOase activity assay
- Prepared figures for manuscript
- Prepared manuscript with O. Avrutina

Angewandte
Communications

Bioconjugation

DOI: 10.1002/anie.201404616

A Chemoenzymatic Approach to Protein Immobilization onto Crystalline Cellulose Nanoscaffolds**

Christina Uth, Stefan Zielonka, Sebastian Hörner, Nicolas Rasche, Andreas Plog, Hannes Orelma, Olga Avrutina, Kai Zhang, and Harald Kolmar**

Abstract: *The immobilization of bioactive molecules onto nanocellulose leads to constructs that combine the properties of the grafted compounds with the biocompatibility and low cytotoxicity of cellulose carriers and the advantages given by their nanometer dimensions. However, the methods commonly used for protein grafting suffer from lack of selectivity, long reaction times, nonphysiological pH ranges and solvents, and the necessity to develop a tailor-made reaction strategy for each individual case. To overcome these restrictions, a generic two-step procedure was developed that takes advantage of the highly efficient oxime ligation combined with enzyme-mediated protein coupling onto the surface of peptide-modified crystalline nanocellulose. The described method is based on efficient and orthogonal transformations, requires no organic solvents, and takes place under physiological conditions. Being site-directed and regiospecific, it could be applied to a vast number of functional proteins.*

In recent years, the development of novel nanocellulose-based materials has attracted growing scientific interest. Since it is a major building block of the biosphere, cellulose is considered as a renewable natural resource and could become a substitute for nonrenewable synthetic polymers.[1] Cellulose-based new materials possess fascinating properties and have been used recently in a vast number of life-science and technical applications.[2]

Contributing to the expanding field of novel sustainable compounds, crystalline nanocellulose has been in the focus of various interdisciplinary studies.[3] Generally, cellulose nanocrystals (CNCs) or nanofibrils are formed upon elimination of amorphous parts from native cellulose fibers and can be prepared following different strategies, among them acid hydrolysis, microfluidization, and TEMPO-mediated oxidation (Figure 1 a).[3b,4] With a diameter of up to 20 nm and a length between 100 nm and 1 μm,[3b,4] CNCs have a significantly more expanded surface area than native cellulose, thus allowing for stronger multiple interactions. Moreover, they can be dispersed in diverse solvents, including water, rendering CNCs as a nanoscale substrate for the immobilization of various compounds that require physiological conditions for their proper function, among them DNA, proteins, and peptides.[5] The resulting constructs combine the properties of grafted compounds with the biocompatibility and low cytotoxicity of cellulose carriers[1,2a,6] and the advantages given by their nanosize.

The methods for protein immobilization onto nanocellulose surfaces can be broadly divided into three main groups according to the molecular forces that mediate binding: a) physical interactions between the protein and the particle surface; b) affinity interactions between the protein and the ligand; c) covalent interactions. In view of covalent protein immobilization two important issues have to be addressed: the preservation of the structural and dimensional properties of nanocellulose and the maintenance of the bioactivity of the immobilized biomolecule. Due to the inherent bioinertness of nanocellulose scaffolds, their surface requires activation or modification to enable interaction with the addressable sites within macromolecules.[5d–f,7] To this end, the free, superficial hydroxy groups are often transformed into the respective carboxylic acids by TEMPO-mediated oxidation, thus allowing for direct amide coupling or other further modifications.[5d,e,7a,b] To date, a number of peptides and proteins have been immobilized onto the surface of nanoscaled cellulose, for example, tryptophan-based oligopeptides comprising two to eight amino acid residues,[5b,c] a human neutrophil elastase tripeptide substrate,[5e] the enzyme alkaline phosphatase, and anti-hydrocortisone antibodies.[5d]

As the *N*-terminus and all surface-exposed lysine residues of proteins provide reactive amino groups, their linkage to the nanoparticle occurs in an uncontrolled fashion, which may result in the attachment at a site of the protein that affects its structure, stability, or bioactivity (see Figure S11 in the Supporting Information).[8] Therefore, several approaches have been developed to assure better selectivity and bio-orthogonality, among them a noncovalent specific binding between an antibody of interest and its peptidic ligand coupled to the surface through a copolymer spacer[6b] and the

[*] Dr. H. Orelma, Dr. K. Zhang
Ernst-Berl-Institut für Technische und Makromolekulare Chemie
Technische Universität Darmstadt
Alarich-Weiss-Strasse 8, 64287 Darmstadt (Germany)
E-mail: zhang@cellulose.tu-darmstadt.de
A. Plog
Center of Smart Interfaces
Technische Universität Darmstadt (Germany)
C. Uth, S. Zielonka, S. Hörner, Dr. N. Rasche, Dr. O. Avrutina, Prof. Dr. H. Kolmar
Clemens-Schöpf-Institut für Organische Chemie und Biochemie
Technische Universität Darmstadt
Alarich-Weiss-Strasse 4, 64287 Darmstadt (Germany)
E-mail: kolmar@biochemie-tud.de

[**] We thank the Hessische Exzellenz Initiative LOEWE—Forschungscluster SOFT CONTROL and the Kooperative Forschungskolleg NANOKAT and DFG priority program 1623 for financial support and Brent Dorr (Harvard University) for providing the plasmid for the sortase expression.

Supporting information for this article is available on the WWW under http://dx.doi.org/10.1002/anie.201404616.

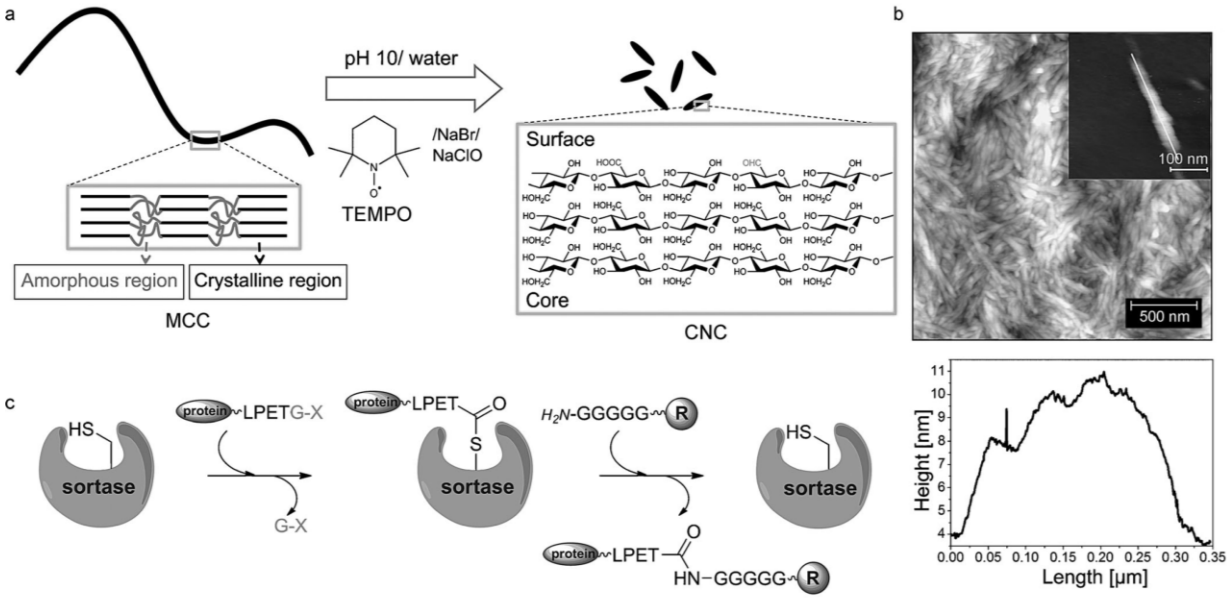

Figure 1. a) Schematic representation of the synthesis of CNCs from microcrystalline cellulose (MCC) through TEMPO-mediated oxidation. b) Top: AFM image of obtained CNCs. The inset presents the AFM image of a single CNC. Bottom: height profile. c) Illustration of sortase-mediated ligation. R represents the moiety of choice, X any amino acid. Amino acids are indicated as one-letter code with the amino terminus shown.

deposition of nanogold on polyethyleneimine-coated nanocellulose allowing for the functionalization with respective thiols.[7c] Site-specific azide–alkyne cycloaddition has been used for immobilization as well, but the reaction procedure was rather sophisticated and could not be applied to functional proteins.[7d] Although these approaches allowed the grafting of human immunoglobulin G (IgG),[5f] glucose oxidase,[9] and β-casein[7d] as well as avidin–biotin complexes, bovine serum albumin, and antihuman IgG[5f,10] onto nanocellulose scaffolds, the procedures suffer from lack of selectivity, long reaction times, nonphysiological pH ranges or solvents, and the necessity to develop a particular reaction strategy for each individual case. To overcome these restrictions, we decided to take advantage of enzyme-mediated biotransformations for covalent bioconjugations.[11]

Over the last decade, the transpeptidase sortase A found in Gram-positive bacteria (where it is used to covalently attach proteins to peptidoglycan layers) has emerged as a powerful tool for the modification of various nature-derived and engineered molecular constructs.[11b,c,12] This enzyme requires two short recognition sequences and generates a native amide bond upon ligation.

The ultimate goal of the present research was the covalent regioselective grafting of bioactive proteins on the surface of CNCs decorated with orthogonally addressable functionalities, for example, aldehyde units. In general, these groups provide the possibility to apply highly efficient and selective oxime ligation using the respective aminooxy function as a reaction partner.[13] Although this moiety can be easily introduced into oligopeptides, both on solid support and in solution, oximation has its highest turnover rate at nonphysiological pH (4–5). As most bioactive proteins lose their proper fold at these pH ranges, near-physiological pH should be applied, leading to prolonged duration of the oxime ligation. As a consequence, the conjugation of full-size proteins is obviously restricted. Therefore, we designed a peptidic linker that combined the required aminooxy function (allowing the prior attachment on CNCs) with a recognition sequence enabling enzyme-catalyzed protein ligation under physiological conditions.

For the anchoring of bioactive proteins on the CNC surface, sortase A mediated ligation was chosen (Figure 2). This calcium-dependent transpeptidase recognizes two short peptidic motifs, LPXTG and oligo-Gly, and catalyzes cleavage at the *C*-terminus of threonine (Figure 1c). Subsequent coupling to the *N*-terminus of the oligo-Gly partner results in a newly formed inter- or intramolecular amide bond, depending on the position of the recognition units. An oligo-Gly sequence was grafted onto the CNC surface, and an LPETG motif was genetically introduced into the respective protein counterparts (Figure 3).

CNCs were prepared from microcrystalline cellulose through TEMPO-mediated oxidation.[4a,14] During this two-step procedure, the primary hydroxy groups at the C6-position were converted into the respective aldehydes as precursors of carboxylic acids. The resulting CNC surface was decorated with both carboxy and aldehyde groups,[15] and their content was determined to be 1.386 mmol g^{-1} and 0.072 mmol g^{-1}, respectively (see Figure S1 and Section 1.3 in the Supporting Information). AFM measurements showed that the obtained CNCs had the form of whiskers with a diameter of around 7 nm and a length of around 300 nm (Figure 1b).[4c,16]

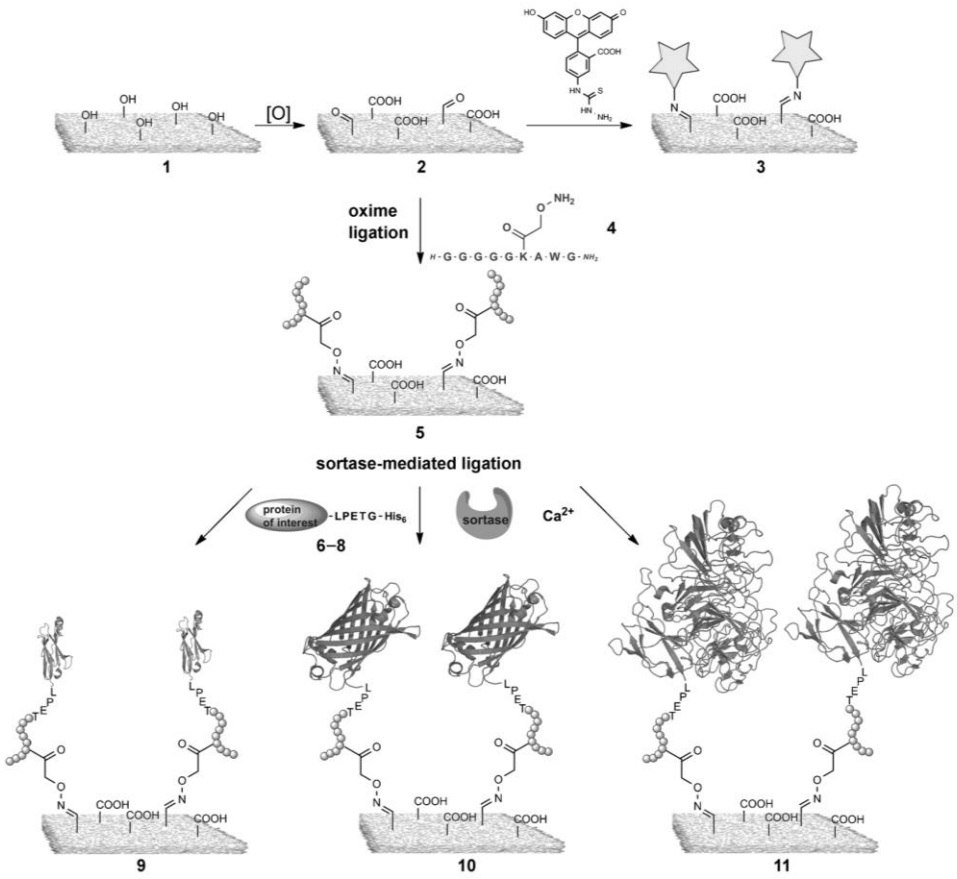

Figure 2. General synthetic strategy. CNC surfaces with the respective groups are shown as gray panels; fluorescein moieties are depicted as stars; peptide **4** is written in one-letter code and schematically drawn as a chain; immobilized proteins are derived from the respective Protein Data Base (PDB) images 2I24, 2WQ8, and 2G6X.

reference sample. These data suggest that modified CNC can be now functionalized with any suitable partner that bears carbonyl-reactive moieties, among them hydrazines, hydrazides, and hydroxylamines. It is important to note that a direct coupling of proteins to aldehyde-bearing CNCs through Schiff base formation with surface-exposed amino groups of lysine residues only occurred to a very low extent (see Figure S12C in the Supporting Information).

To ensure bioconjugation with functional proteins, the surface of carbonyl-bearing CNCs was modified with an oligopeptide module comprising the sortase recognition sequence penta-Gly. To facilitate spectroscopic analysis and purifica-

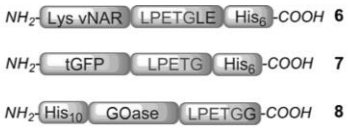

Figure 3. Design of recombinant proteins. **6**: shark antibody Lys-vNAR, **7**: tGFP, **8**: GOase. All proteins comprise the LPETG sortase A recognition sequence as well as His_n tags; $n = 6$ (**6**, **7**) or 10 (**8**).

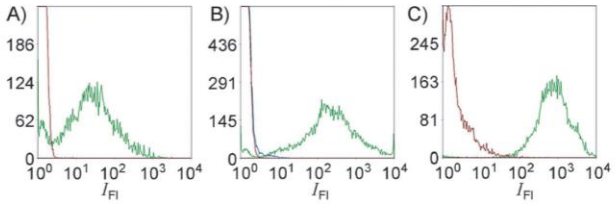

Figure 4. Flow cytometric analysis of CNC conjugates. A) Fluorophore-bearing conjugate **3**; B) tGFP–CNC conjugate **10**; C) Lys-vNAR–CNC conjugate **9**. Red curves: Unlabeled CNCs. Blue curve: CNC lacking the sortase recognition peptide. Green curves: fluorescently labeled CNCs.

On average, the obtained CNCs are smaller than cellulose nanofibrils derived from native cellulose fibers by TEMPO-mediated oxidation.[14,17] This can be explained easily considering that the applied microcrystalline cellulose precursor is in general much smaller than the native counterpart.

To visualize the surface-exposed carbonyl groups, the aldehyde-reactive fluorescein-5-thiosemicarbazide (5FTSC), a fluorescent probe applied in a number of life-science applications, was attached. CNC particles were reacted with 5FTSC in the dark in phosphate-buffered saline (PBS) at ambient temperature, washed, and analyzed by flow cytometry. The diagram in Figure 4A clearly shows the pronounced fluorescent signal of 5FTSC-labeled CNC **3**, compared to the

tion of peptide **4** (see Figure 2), a tryptophan residue was introduced at the *C*-terminal portion. The linker was covalently attached through a carbonyl-reactive aminooxy group, which was installed through the orthogonally protected side chain of lysine. To this end, the peptide was assembled on Rink amide resin using manual Fmoc-SPPS (see Figure S2 in the Supporting Information) and NHS-activated ethoxyethylidene (Eei)-protected aminooxy acetic acid was coupled to the free ε-amino group of the lysine residue after acidolytic

removal of its methyltrityl (Mtt) protecting group. After the chain assembly was completed, the peptide was cleaved from the resin using a mixture of trifluoroacetic acid (TFA, 92%) and respective scavengers (see Section 1.8 in the Supporting Information) with simultaneous cleavage of all protecting groups.

The peptidic linker **4** was covalently grafted on the CNC surface upon formation of a stable oxime bond in ammonium acetate buffer (pH 4.75).[18] We used 3 equiv of the peptidic module relative to the surface carbonyl groups. According to the elemental analysis (see Table S1 in the Supporting Information), 69% of the surface aldehyde groups were decorated with **4**. After the exchange of reaction buffer for a buffer at physiological pH (7.5) by dialysis or by centrifugation, the modified CNC is ready for the enzyme-mediated biofunctionalization.

Three functional proteins differing in size, shape, and biological activity were chosen for grafting. Our main task was to obtain the CNC molecular constructs bearing functional, fully active proteins that are covalently attached to the CNC surface in a regioselective manner, that is, at their exposed carboxy terminus. Although a number of methods making use of nanocellulose as a platform to graft biological ligands have already been developed,[11b] our novel immobilization format implies highly specific, site-directed covalent coupling, in contrast to commonly used noncovalent and/or random methods.

In the initial experiment we used a 27 kDa derivative of green fluorescent protein (tGFP) which has become a standard tool for "proof-of-concept" protein conjugations due to its pronounced autofluorescence.[19] The second protein used in our study belongs to the family of the smallest known antigen-binding antibody-like domains, namely, the shark variable domains of the New Antigen Receptor, where the antigen-binding site (paratope) is formed by one single domain, referred to as vNAR domain.[20] The 13 kDa Lys-vNAR[21] construct **6** can be detected through the interaction with its fluorescently labeled target, namely, hen egg lysozyme. Since in the present study a modified version of Lys-vNAR bearing an LPETGLE extension was used, maintenance of the binding properties of this construct was verified using biolayer interferometry. To this end, the kinetic parameters of the binding of **6** to hen egg lysozyme were determined giving a K_d value of (4.0 ± 0.16) nM (see Figure S9 in the Supporting Information). Hence, the affinities of the modified Lys-vNAR were consistent with those obtained for its parent molecule.[22] The third model protein used in this study was a 70 kDa galactose oxidase (GOase) enzyme, belonging to the family of oxidoreductases. It utilizes two substrates, D-galactose and oxygen, converting them into hexodialdose and hydrogen peroxide, respectively, that could be easily detected in colorimetric assays.

All three proteins were expressed recombinantly in *E. coli* and were engineered to bear the sortase recognition sequence LPETG *C*-terminally. To facilitate their isolation and purification through affinity chromatography, the proteins were decorated at the *N*- or *C*-terminus with His-tags for convenient purification on Ni-loaded NTA resin (Figure 3). We took an evolved variant of sortase A (referred to as eSrtA) for the conjugations, as it demonstrated enhanced catalytic properties (reaction kinetics) than the wild-type.[23]

A typical protein-grafting experiment was conducted in Tris/NaCl buffer (pH 7.5) containing $CaCl_2$ (5 mM). After overnight reaction the dispersed CNC–protein conjugates **9**, **10**, and **11** (see Figure 2) were isolated from the reaction mixtures by sedimentation and purified by repeated washing (see Section 4 in the Supporting Information). The resulting modified CNCs were analyzed by AFM verifying that the overall length and shape of the nanocellulose particles was maintained, while, depending on the molecular mass of the attached proteins, an increase in particle height was observed (Figure 5). The activity of the immobilized proteins was then examined in the respective assays.

The CNC–tGFP conjugate was analyzed using fluorescence microscopy and flow cytometry. In the initial microscopic study, the tGFP-functionalized nanocellulose whiskers **10** were clearly visible as fluorescent green spots in the micrographs (see Figure S13 in the Supporting Information) indicating that the protein was successfully grafted. Flow cytometry, a well-established technique used to analyze microscopic particles by sensing their optical properties, was used to resolve individual CNCs through probe-conferred fluorescence. Thus, the CNC particles **10** exhibit a fluorescent signal that is about 100 times stronger than that for the reference (unmodified CNC), confirming the attachment of tGFP (Figure 4B). Detailed data of flow cytometric experiments are summarized in Figure S12 in the Supporting Information.

To verify that the shark vNAR has been conjugated with the CNC surface and retained its activity in construct **9**, its binding to the fluorescently labeled target, hen egg lysozyme, was visualized by flow cytometry (Figure 4C). The fluorescence profile showed clear evidence of the protein's activity attributed to the target binding. However, it must be mentioned that the analysis of **9** was more complicated than that of **10**, due to the tendency of lysozyme to form nonspecific interactions with CNCs (see Figure S12C in the Supporting Information).

Oxidation of D-galactose to the respective D-*galacto*-hexodialdose is catalyzed by the enzyme GOase and associated with the formation of hydrogen peroxide. Therefore, the catalytic activity of GOase could be easily monitored by coupling the production of hydrogen peroxide to a horseradish peroxidase catalyzed transformation of ABTS (Figure 6A). A soluble green final product can be detected photometrically at $\lambda = 405$ nm. The analysis of conjugate **11** showed that the immobilized GOase retained its activity upon grafting onto CNC (Figure 6B).

To compare the efficacy of our site-directed coupling strategy compared to the commonly used formation of amide bonds from primary amines of grafted proteins and carboxylic groups of the cellulose support, *N*-hydroxysuccinimide active ester (NHS)-mediated attachment of GOase (the largest protein in our experiments) was conducted. To this end, the proportion of surface carboxylate groups equal to the molar ratio of oximated carbonyl groups was activated by EDC/NHS (see Section 5.1 in the Supporting Information) and reacted with equimolar amount of GOase (the proportions

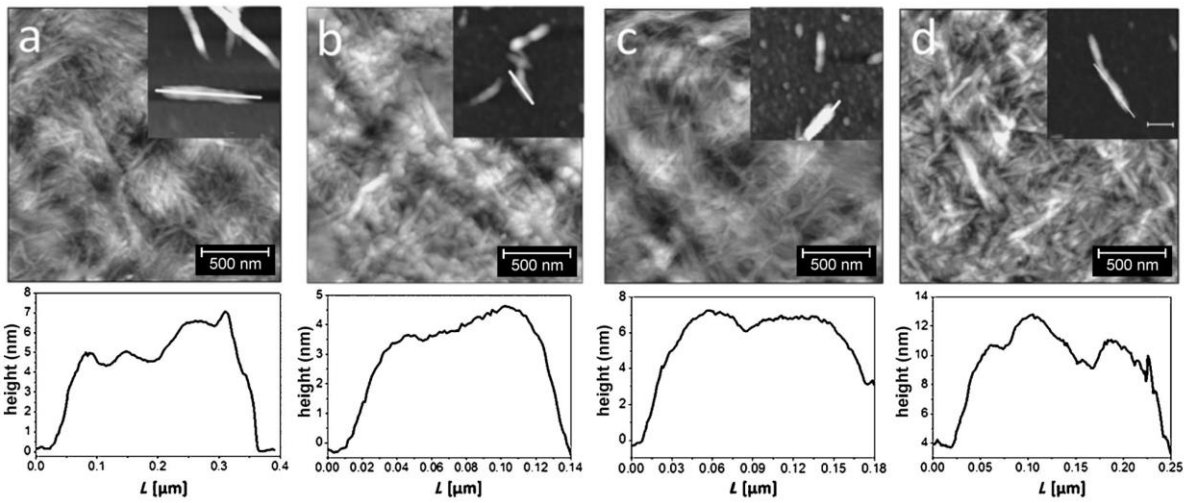

Construct	Height (nm)	Construct	Height (nm)
CNC **2**	5.83±1.13	CNC-tGFP **10**	7.26±0.26
CNC-recognition peptide **5**	5.77±1.07	CNC-GOase **11**	7.72±1.12
CNC-Lys vNAR **9**	6.21±1.15		

Figure 5. Top: AFM images of functionalized CNCs. a) **5** (conjugate with **4**); b) **9** (conjugate with **6**); c) **10** (conjugate with **7**); d) **11** (conjugate with **8**). The insets are magnified images of individual CNCs. The height profiles of the modified CNCs are shown under each AFM image. Bottom: The corresponding heights.

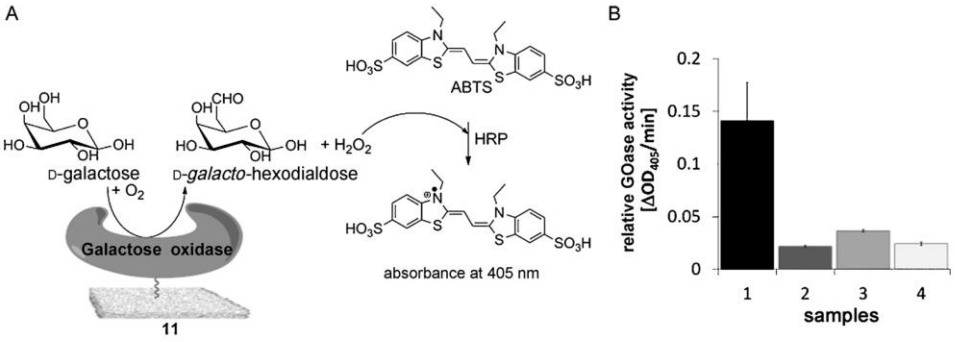

Figure 6. Assessment of the activity of immobilized GOase. A) Schematic depiction of ABTS assay. B) Photometric monitoring of GOase activity in conjugate **11** (1) compared to controls (2: reaction mixture lacking Ca^{2+}, 3: reaction mixture lacking recognition peptide **4**; 4: reaction mixture lacking sortase). Error bars were calculated from a triple determination.

were similar to those for the coupling of peptidic linker **4**). The relative enzyme activity of the immobilized protein was verified using the colorimetric ABTS assay. Thus, compared to the relative GOase activity calculated for the sortase-mediated coupling, the NHS-mediated procedure led to a reduced activity of the surface-immobilized enzyme (ca. 60% of that achieved for the sortase-mediated grafting) (see Figure S10 in the Supporting Information). This outcome could be explained taking into consideration that the NHS-promoted immobilization is random, and all available amino functions of the enzyme are utilized, which could result in restricted access to its active site. On the other hand, the sortase-mediated ligation results in protein-loaded surfaces where all biomacromolecules are grafted exclusively through their *C*-termini (see Figure S11 in the Supporting Information). However, the efficacy of this direct NHS-mediated immobilization also depends on the size and the isoelectric point of the grafted protein and therefore may vary for enzymes other than GOase.

CNC is doubtlessly considered to be a valuable substrate for the deposition of bioactive compounds with different properties. Unlike traditional supports, it provides a large surface area, can be easily prepared from a renewable source, cellulose, and can be chemically modified yielding an extensive nanorelief bearing surface-exposed active groups. The introduction of orthogonally addressable aldehyde units allows for the application of chemical and/or enzymatic methods compatible with biomacromolecules, thus making CNC an advantageous nanoplatform for the immobilization of biological compounds.

We successfully transformed primary alcohols on the surface of CNCs into the respective aldehyde functions,[24] thus enabling the application of highly efficient oxime ligation to immobilize bioactive modules. Since the aldehyde groups are orthogonal to the reactive groups of peptides, we could

couple oligopeptidic motifs that are recognized by the transpeptidase sortase A for further CNC modification by proteins of choice.

Our approach provides a number of obvious advantages over other methods for protein immobilization onto cellulose-derived scaffolds. First, smooth oxidation of surface hydroxy groups to the respective aldehyde units enables orthogonal couplings, ergo, no protection is required upon oxime ligation. Second, sortase-mediated protein grafting takes place under physiological conditions leaving the protein structure, hence activity, intact. Third, the coupling is site-directed, regiospecific, and covalent, and could be easily controlled leading to the formation of tailor-made constructs. Generally, these new G_5-CNCs combine the intrinsic properties of CNC scaffolds, for example low toxicity and water compatibility, with the advantages of recombinantly produced proteins of choice. Moreover, as a cleavable site can be easily installed into recombinant proteins, the controlled detachment of bioactive proteins from the cellulose surface becomes possible, making these conjugates good candidates for, for example, drug deposition and delivery. Of course, our approach is not limited to proteins and could be applied to a vast number of bioactive molecules.

Received: April 23, 2014
Published online: July 28, 2014

Keywords: bioorthogonal protein immobilization · cellulose nanocrystals · enzyme catalysis · immobilization · ligation

[1] D. Klemm, B. Heublein, H. P. Fink, A. Bohn, *Angew. Chem.* **2005**, *117*, 3422 – 3458; *Angew. Chem. Int. Ed.* **2005**, *44*, 3358 – 3393.

[2] a) D. Peschel, K. Zhang, S. Fischer, T. Groth, *Acta Biomater.* **2012**, *8*, 183 – 193; b) H. Jin, M. Kettunen, A. Laiho, H. Pynnonen, J. Paltakari, A. Marmur, O. Ikkala, R. H. A. Ras, *Langmuir* **2011**, *27*, 1930 – 1934; c) G. Y. Yun, J. Kim, J. H. Kim, S. Y. Kim, *Sens. Actuators A* **2010**, *164*, 68 – 73; d) T. Wandowski, P. Malinowski, W. M. Ostachowicz, *Smart Mater. Struct.* **2011**, *20*, 025002; e) D. Sinha, S. Pisana, A. J. Flewitt, *Smart Mater. Struct.* **2011**, *20*, 025016.

[3] a) R. J. Moon, A. Martini, J. Nairn, J. Simonsen, J. Youngblood, *Chem. Soc. Rev.* **2011**, *40*, 3941 – 3994; b) Y. Habibi, L. A. Lucia, O. J. Rojas, *Chem. Rev.* **2010**, *110*, 3479 – 3500; c) D. Klemm, F. Kramer, S. Moritz, T. Lindstrom, M. Ankerfors, D. Gray, A. Dorris, *Angew. Chem.* **2011**, *123*, 5550 – 5580; *Angew. Chem. Int. Ed.* **2011**, *50*, 5438 – 5466.

[4] a) M. Hirota, K. Furihata, T. Saito, T. Kawada, A. Isogai, *Angew. Chem.* **2010**, *122*, 7836 – 7838; *Angew. Chem. Int. Ed.* **2010**, *49*, 7670 – 7672; b) S. C. Espinosa, T. Kuhnt, E. J. Foster, C. Weder, *Biomacromolecules* **2013**, *14*, 1223 – 1230; c) D. Bondeson, A. Mathew, K. Oksman, *Cellulose* **2006**, *13*, 171 – 180; d) K. Abe, S. Iwamoto, H. Yano, *Biomacromolecules* **2007**, *8*, 3276 – 3278.

[5] a) A. P. Mangalam, J. Simonsen, A. S. Benight, *Biomacromolecules* **2009**, *10*, 497 – 504; b) S. Barazzouk, C. Daneault, *Nanomaterials* **2012**, *2*, 187 – 205; c) S. Barazzouk, C. Daneault, *Cellulose* **2012**, *19*, 481 – 493; d) S. Arola, T. Tammelin, H. Setala, A. Tullila, M. B. Linder, *Biomacromolecules* **2012**, *13*, 594 – 603; e) J. V. Edwards, N. Prevost, K. Sethumadhavan, A. Ullah, B. Condon, *Cellulose* **2013**, *20*, 1223 – 1235; f) Y. X. Zhang, R. G. Carbonell, O. J. Rojas, *Biomacromolecules* **2013**, *14*, 4161 – 4168.

[6] a) M. J. Clift, E. J. Foster, D. Vanhecke, D. Studer, P. Wick, P. Gehr, B. Rothen-Rutishauser, C. Weder, *Biomacromolecules* **2011**, *12*, 3666 – 3673; b) X. Yang, E. Bakaic, T. Hoare, E. D. Cranston, *Biomacromolecules* **2013**, *14*, 4447 – 4455.

[7] a) S. Barazzouk, C. Daneault, *Cellulose* **2011**, *18*, 643 – 653; b) S. Barazzouk, C. Daneault, *Cellulose* **2012**, *19*, 481 – 493; c) V. Incani, C. Danumah, Y. Boluk, *Cellulose* **2013**, *20*, 191 – 200; d) M. A. Karaaslan, G. Z. Gao, J. F. Kadla, *Cellulose* **2013**, *20*, 2655 – 2665.

[8] S. V. Rao, K. W. Anderson, L. G. Bachas, *Mikrochim. Acta* **1998**, *128*, 127 – 143.

[9] V. Incani, C. Danumah, Y. Boluk, *Cellulose* **2013**, *20*, 191 – 200.

[10] a) H. Orelma, L. S. Johansson, I. Filpponen, O. J. Rojas, J. Laine, *Biomacromolecules* **2012**, *13*, 2802 – 2810; b) H. Orelma, I. Filpponen, L. S. Johansson, M. Osterberg, O. J. Rojas, J. Laine, *Biointerphases* **2012**, *7*, 61; c) H. Brumer, Q. Zhou, M. J. Baumann, K. Carlsson, T. T. Teeri, *J. Am. Chem. Soc.* **2004**, *126*, 5715 – 5721.

[11] a) D. Rabuka, J. S. Rush, G. W. deHart, P. Wu, C. R. Bertozzi, *Nat. Protoc.* **2012**, *7*, 1052 – 1067; b) M. K. M. Leung, C. E. Hagemeyer, A. P. R. Johnston, C. Gonzales, M. M. J. Kamphuis, K. Ardipradja, G. K. Such, K. Peter, F. Caruso, *Angew. Chem.* **2012**, *124*, 7244 – 7248; *Angew. Chem. Int. Ed.* **2012**, *51*, 7132 – 7136; c) T. Matsumoto, T. Tanaka, A. Kondo, *Langmuir* **2012**, *28*, 3553 – 3557.

[12] a) T. Proft, *Biotechnol. Lett.* **2010**, *32*, 1 – 10; b) M. W. L. Popp, H. L. Ploegh, *Angew. Chem.* **2011**, *123*, 5128 – 5137; *Angew. Chem. Int. Ed.* **2011**, *50*, 5024 – 5032.

[13] J. E. Hudak, R. M. Barfield, G. W. de Hart, P. Grob, E. Nogales, C. R. Bertozzi, D. Rabuka, *Angew. Chem.* **2012**, *124*, 4237 – 4241; *Angew. Chem. Int. Ed.* **2012**, *51*, 4161 – 4165.

[14] T. Saito, A. Isogai, *Biomacromolecules* **2004**, *5*, 1983 – 1989.

[15] a) A. Isogai, T. Saito, H. Fukuzumi, *Nanoscale* **2011**, *3*, 71 – 85; b) K. Zhang, S. Fischer, A. Geissler, E. Brendler, *Carbohydr. Polym.* **2012**, *87*, 894 – 900.

[16] a) S. Dong, M. Roman, *J. Am. Chem. Soc.* **2007**, *129*, 13810 – 13811; b) S. Beck-Candanedo, M. Roman, D. G. Gray, *Biomacromolecules* **2005**, *6*, 1048 – 1054.

[17] T. Saito, S. Kimura, Y. Nishiyama, A. Isogai, *Biomacromolecules* **2007**, *8*, 2485 – 2491.

[18] a) S. Fabritz, S. Hörner, O. Avrutina, H. Kolmar, *Org. Biomol. Chem.* **2013**, *11*, 2224 – 2236; b) A. Dirksen, T. M. Hackeng, P. E. Dawson, *Angew. Chem.* **2006**, *118*, 7743 – 7746; *Angew. Chem. Int. Ed.* **2006**, *45*, 7581 – 7584; c) H. Salo, P. Virta, H. Hakala, T. P. Prakash, A. M. Kawasaki, M. Manoharan, H. Lonnberg, *Bioconjugate Chem.* **1999**, *10*, 815 – 823.

[19] a) T. Misteli, D. L. Spector, *Nat. Biotechnol.* **1997**, *15*, 961 – 964; b) H. Niwa, S. Inouye, T. Hirano, T. Matsuno, S. Kojima, M. Kubota, M. Ohashi, F. I. Tsuji, *Proc. Natl. Acad. Sci. USA* **1996**, *93*, 13617 – 13622.

[20] V. A. Streltsov, J. N. Varghese, J. A. Carmichael, R. A. Irving, P. J. Hudson, S. D. Nuttall, *Proc. Natl. Acad. Sci. USA* **2004**, *101*, 12444 – 12449.

[21] R. L. Stanfield, H. Dooley, M. F. Flajnik, I. A. Wilson, *Science* **2004**, *305*, 1770 – 1773.

[22] H. Dooley, R. L. Stanfield, R. A. Brady, M. F. Flajnik, *Proc. Natl. Acad. Sci. USA* **2006**, *103*, 1846 – 1851.

[23] a) I. Chen, B. M. Dorr, D. R. Liu, *Proc. Natl. Acad. Sci. USA* **2011**, *108*, 11399 – 11404; b) M. W.-L. Popp, J. M. Antos, H. L. Ploegh, *Current Protocols in Protein Science*, Supplement 56, *Unit 15.3*, **2009**; c) C. S. Theile, M. D. Witte, A. E. M. Blom, L. Kundrat, H. L. Ploegh, C. P. Guimaraes, *Nat. Protoc.* **2013**, *8*, 1800 – 1807.

[24] T. Saito, M. Hirota, N. Tamura, S. Kimura, H. Fukuzumi, L. Heux, A. Isogai, *Biomacromolecules* **2009**, *10*, 1992 – 1996.

5.2. Combination of inverse electron-demand Diels-Alder reaction with highly efficient oxime ligation expands the toolbox of site-selective peptide conjugations

Reproduced from Chem. Commun., **2015**, *51*, 11130-11133 (DOI: 10.1039/C5CC03434E) with permission from the Royal Society of Chemistry.

Title:

Combination of inverse electron-demand Diels-Alder reaction with highly efficient oxime ligation expands the toolbox of site-selective peptide conjugations

Authors:

Sebastian Hörner,‡ Christina Uth,‡ Olga Avrutina, Holm Frauendorf, Manfred Wiessler and H. Kolmar*

‡ Authors contributed equally

Bibliographic Data:

Chemical Communications
Volume 51, Issue 55, July 14, 2015, Pages 11130-11133.
First published online 10 Jun 2015| DOI: 10.1039/C5CC03434E

Graphical abstract:

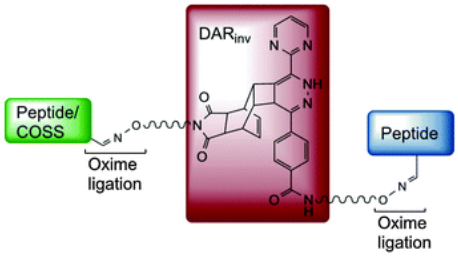

A modular bioconjugation strategy based on stepwise oxime ligation and inverse electron-demand Diels–Alder reaction.

Contributions of C. Uth:

- Conception of experiments with S. Hörner
- Synthesis and analysis of peptides with S. Hörner
- Synthesis and analysis of Reppe-anhydride linker
- Synthesis and analysis of peptide-COSS conjugate
- Prepared manuscript and figures with O. Avrutina and S. Hörner

ChemComm

CORRECTION

View Article Online
View Journal | View Issue

Cite this: *Chem. Commun.*, 2015, **51**, 11727

Correction: Combination of inverse electron-demand Diels–Alder reaction with highly efficient oxime ligation expands the toolbox of site-selective peptide conjugations

S. Hörner,[a] C. Uth,[a] O. Avrutina,[a] H. Frauendorf,[b] M. Wiessler[c] and H. Kolmar*[a]

DOI: 10.1039/c5cc90302e

www.rsc.org/chemcomm

Correction for 'Combination of inverse electron-demand Diels–Alder reaction with highly efficient oxime ligation expands the toolbox of site-selective peptide conjugations' by S. Hörner, *et al.*, *Chem. Commun.*, 2015, DOI: 10.1039/c5cc03434e.

In Fig. 1 of the published article the structures for compound **4** were displayed incorrectly. Fig. 1 should appear as follows:

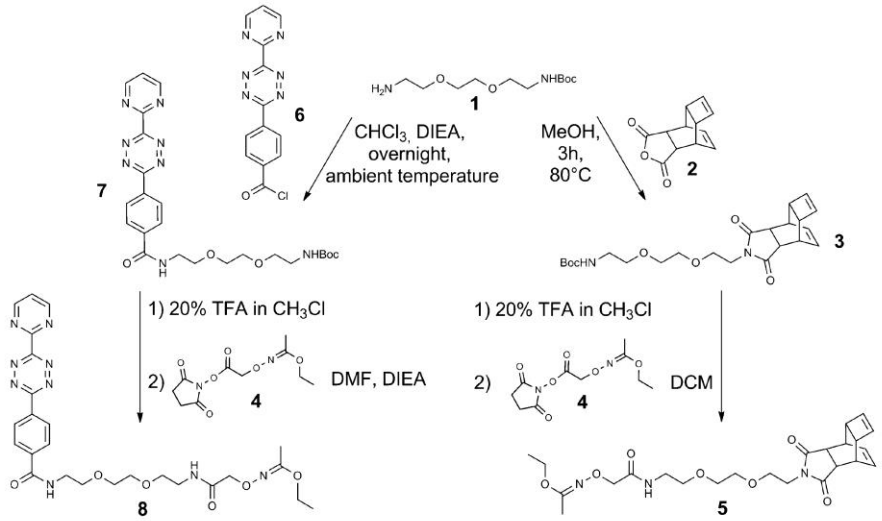

The Royal Society of Chemistry apologises for these errors and any consequent inconvenience to authors and readers.

[a] *Technische Universität Darmstadt, Clemens-Schöpf-Institut für Organische Chemie und Biochemie, Alarich-Weiss Straße 4, 64287 Darmstadt, Germany. E-mail: kolmar@biochemie-tud.de*

[b] *Georg-August-Universität Göttingen, Institut für Organische und Biomolekulare Chemie, Zentrale Analytik/Massenspektrometrie, Tammannstraße 2, 37077 Göttingen, Germany*

[c] *Deutsches Krebsforschungszentrum, Medizinische Physik in der Radiologie, Projektgruppe Biologische Chemie E020, Im Neuenheimer Feld, 69120 Heidelberg, Germany*

ChemComm

COMMUNICATION

View Article Online
View Journal | View Issue

Cite this: *Chem. Commun.*, 2015, **51**, 11130

Received 24th April 2015,
Accepted 10th June 2015

DOI: 10.1039/c5cc03434e

www.rsc.org/chemcomm

Combination of inverse electron-demand Diels–Alder reaction with highly efficient oxime ligation expands the toolbox of site-selective peptide conjugations†

S. Hörner,‡[a] C. Uth,‡[a] O. Avrutina,[a] H. Frauendorf,[b] M. Wiessler[c] and H. Kolmar*[a]

A modular approach combining inverse electron-demand Diels–Alder coupling (DAR_{inv}) and oxime ligation expands the toolbox of bioorthogonal peptide chemistry. Applicability of versatile site-specific bifunctional building blocks is demonstrated by generation of defined conjugates comprising linear, cystine-bridged and multi-disulfide functional peptides as well as their conjugation with hybrid silsesquioxane nanoparticles.

Covalent linkage of certain peptidic units, being an alternative or a complementary strategy to recombinant production, often becomes a method of choice for the synthesis of sophisticated macromolecular constructs with tailored properties.[1] Indeed, to date a vast number of bioconjugates and the respective techniques have been reported,[2] ranging from relatively simple fluorescently[3] or small-molecule-labelled peptides[4] to complex, multifunctional architectures like antibody–drug conjugates.[5] Obviously, chemical transformations suitable for bioconjugations must satisfy at least two obligatory requirements, chemoselectivity and efficiency.[6] In view of the variety of inherent functional groups present in peptidic molecules, the development of a viable orthogonal chemistry for their effective junction at a certain position still remains a challenge.

Generally, the strategy towards site-specific bioconjugations[7] relies on incorporation of a uniquely addressable group at the desired position in the molecule of interest followed by its peculiar reaction with the respective counterpart. Such a uniquely addressable moiety could be incorporated into peptidic molecules through a vast number of post-synthetic modifications, *e.g.* periodate oxidation of β-aminoalcohols,[8,9] or *via* the non-natural building blocks[10] either upon recombinant production[11] or in the course of chemical synthesis. Bioorthogonal reactions to target these non-natural functional groups often make use of rich ketone and aldehyde chemistry[12] as well as numerous click-type reactions,[3,13] with the azide–alkyne cycloaddition being the most prominent representative.[14–16] During the last decade, a special class of pericyclic reactions has got the highest priority as they utilize the ring strain to promote increased reactivity upon cycloaddition.[17–19] In particular, the Diels–Alder reaction with inverse electron-demand (DAR_{inv})[20–22] between numerous dienophiles[23–25] and tetrazines[21,26,27] was found to be a valuable tool for effective bioorthogonal conjugations.[28–30] Followed by a retro-Diels–Alder reaction to eliminate nitrogen gas, this so-called tetrazine ligation is characterized by extremely fast kinetics with second-order rate constants up to 2×10^3 M^{-1} s^{-1} and has been already used in a number of both *in situ* and *in vivo* studies.[25,31,32]

In this study we present a modular approach to the conjugation of biomolecules based on the combination of two efficient chemical transformations, oxime ligation and DAR_{inv}. For the proof-of-concept experiments we designed bifunctional building blocks to incorporate the bioorthogonal DAR_{inv} coupling site in a peptide site-specifically *via* oximation of the respective aldehyde. Following this step, attachment of a DAR_{inv} counterpart would accomplish a desired conjugate. The choice of the strategy was specified by two arguments, feasible generation of required aldehydes in biomolecules[8,9,33] and fast kinetics of an irreversible DAR_{inv}. We reasoned that our approach, initially investigated on peptides of different size and molecular complexity, could be further extended to orthogonal conjugations featuring a broad spectrum of biomacromolecules, *i.e.* proteins, sugars, or other biopolymers.

Here it is important to mention that, while having been used for numerous labeling approaches,[34,35] the DAR_{inv} reaction was surprisingly rarely applied to connect functional peptides site-specifically.[28,36] This could be explained taking into account that both the diene and the dienophile counterparts have been

[a] *Technische Universität Darmstadt, Clemens-Schöpf-Institut für Organische Chemie und Biochemie, Alarich-Weiss Straße 4, 64287 Darmstadt, Germany. E-mail: kolmar@biochemie-tud.de*
[b] *Georg-August-Universität Göttingen, Institut für Organische und Biomolekulare Chemie, Zentrale Analytik/Massenspektrometrie, Tammannstraße 2, 37077 Göttingen, Germany*
[c] *Deutsches Krebsforschungszentrum, Medizinische Physik in der Radiologie, Projektgruppe Biologische Chemie E020, Im Neuenheimer Feld, 69120 Heidelberg, Germany*

† Electronic supplementary information (ESI) available: Combination of inverse electron-demand Diels–Alder reaction with highly efficient oxime ligation expands the toolbox of site-selective peptide conjugations. See DOI: 10.1039/c5cc03434e

‡ These authors contributed equally to this work.

to date installed into partner biomolecules using either amide[37,38] or maleimide chemistry[39] which cannot provide the required orthogonality, especially with regard to cysteine/cystine-bearing molecules. Though the installation of DAR_{inv} building blocks into peptide-like molecules on solid support has been reported, this approach did not find broad application. Moreover, the on-resin assembly is very rarely used for the production of full-size proteins.

Since oxime ligation has been applied to couple *exo*-norbornene as a dienophile handle onto aldehydes of the reducing ends of oligosaccharides[40] and taking into consideration that this moiety is easily generated in both recombinant and synthetic peptides[41] without interference with functional side chains, we decided to use this highly efficient reaction to decorate the peptides of interest with the respective diene and dienophile partners.

Our modular approach relies on the tailor-made bifunctional building blocks equipped with an aminooxy moiety for the primary incorporation into peptidic counterparts along with the DAR_{inv} site for the successive ligation (Fig. 1). In our proof-of-concept study we installed the DAR_{inv} building blocks **5** and **8** into the next functional peptides: a Sortase A recognition heptapeptide **12**,[42,43] an integrin-binding RGD decapeptide **9**,[12] an antimicrobial decapeptide Jelleine derivative **13**,[44] a disulfide-bridged pentadecapeptide matriptase inhibitor **10**,[45] and two cystine knots comprising three disulfides and a backbone of more than thirty amino acids **11**, **14**[46] (Scheme S2, ESI†). An additional *N*-terminal serine was introduced into each peptide to provide the orthogonally addressable site upon post-synthetic modification.[9] The resulted glyoxylyl moieties generated by periodate oxidation (Scheme S1, ESI†) were oximated by the aminooxy-bearing derivatives of Reppe anhydride **5** and tetrazine **8**, respectively (Fig. 1 and 2). The dienes **15–17** were synthesized from peptide-glyoxals **9–11**, and the dienophiles **18–20** – from peptide-glyoxals **12–14** (Fig. 2 and ESI 1.2.12†). Peptides were assembled by microwave-assisted Fmoc-SPPS.[47] Following cleavage from the support with successive oxidative folding if required, the *N*-terminal serines were oxidized by $NaIO_4$ to generate the aminooxy-reactive glyoxals **9–14** for further conjugations (ESI 1.2.9–1.2.11†).

Prior to the installation into synthetic peptides, the bifunctional DAR_{inv} building blocks were synthesized following a two-step procedure as illustrated in Fig. 1.

Thus, mono-Boc-protected miniPEG **1** was reacted with Reppe anhydride **2** or tetrazine derivative **6**, respectively, and the resulting constructs **3** and **7** were transformed into *N*-ethoxyethylidene (Eei)-protected aminooxy building blocks **5** and **8** upon acidolytic cleavage of *N*-Boc protection followed by the *N*-acylation with *N*-hydroxysuccinimide-activated (NHS) Eei-protected aminooxy acetic acid **4** (Fig. 1 and ESI 1.2.1–1.2.8†).[48] The oxime ligation was performed in 50% (v:v) aqueous TFA overnight leading to peptide-tetrazines **15–17** and peptide-dienophiles **18–20** (Fig. 2 and ESI 1.2.12†).

After the conjugation partners have been decorated with the respective DAR_{inv} building blocks, the resulted diene and dienophile counterparts were reacted with each other in 10% aq. acetonitrile containing 0.1% TFA overnight at ambient temperature giving conjugates **21–29** (Fig. 3 and 4, ESI 1.2.15†). The exemplified monitoring of DAR_{inv} reaction progress presented in Fig. 4 and in ESI 1.2.15† clearly indicates that conversion into the desired

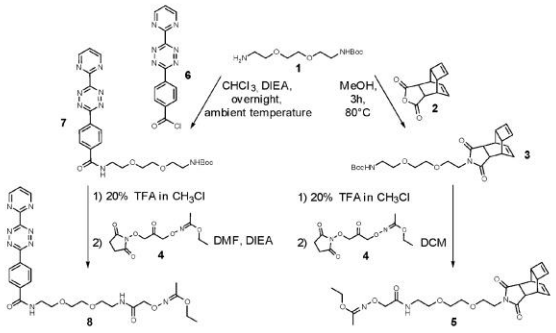

Fig. 1 Synthesis of DAR_{inv} building blocks.

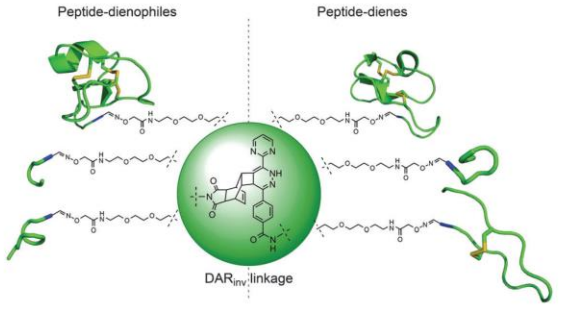

Fig. 3 Schematic representation of peptide conjugates synthesized by DAR_{inv} between the counterparts depicted on the left and the right panels.

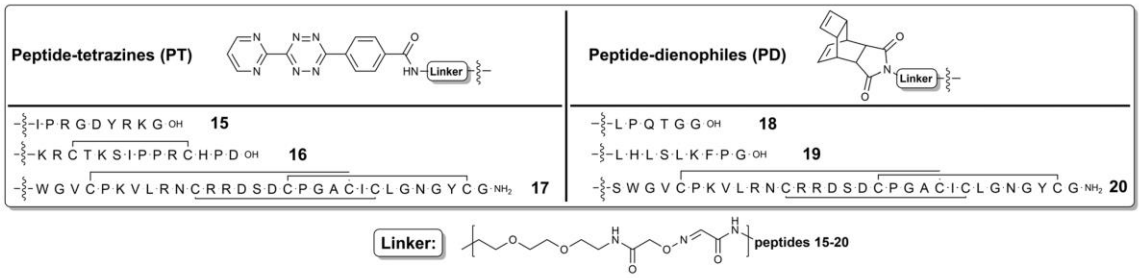

Fig. 2 Synthesized peptidic ligands for successive DAR_{inv} conjugations.

A)

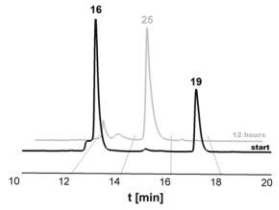

B)

	15	16	17
18	**21** (73.3%)	**24** (87.7%)	**27** (n.d.)
19	**22** (85%)	**25** (100%)	**28** (93.8%)
20	**23** (92.5%)	**26** (87%)	**29** (n.d.)

Fig. 4 (A) HPLC monitoring of an exemplified DAR_{inv} conjugation between Jelleine–Reppe construct **19** and SDMI-3 tetrazine partner **16**. (B) Conversion rate for DAR_{inv} conjugations calculated from the HPLC traces (n.d.: not determined).

products has been achieved for all constructs. Interestingly, upon evaluation of the mass spectrometric data, we observed for some DAR_{inv} conjugates the recovery of the aromatic system in the tetrazine, as previously reported.[49,50] The mass spectra can be seen in Fig. 5 as well as in ESI 1.2.21–1.2.29.†

As the proof-of-concept study showed the viability of our approach, it was further expanded towards a more sophisticated (in view of architecture and functional properties) molecular construct. Thus, we attached a peptidic cargo to the smallest nanoparticle known, a cell-penetrating organic–inorganic hybrid molecule comprising cube-octameric silsesquioxane (COSS).[44] This highly symmetric octavalent compound has recently attracted keen attention, being used as a scaffold in a number of biomedical applications, including delivery of

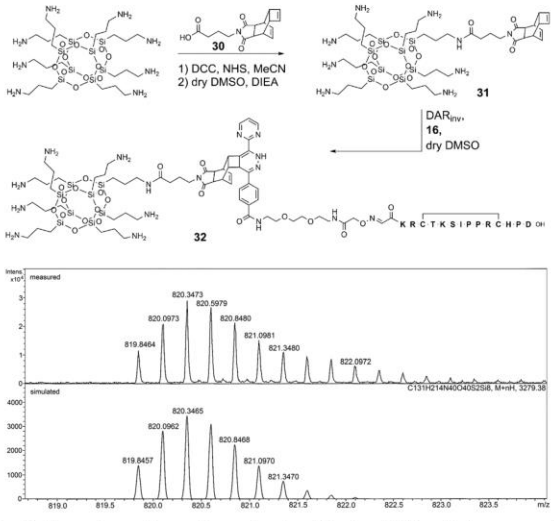

Fig. 5 Top: formation of conjugate **32** by DAR_{inv} between cell-penetrating COSS **31** and peptide **16**. Bottom: exemplary ESI-HR-MS analysis of conjugate **32** $[M + 4H]^{4+}$.

bioactive payloads into cancer cells and development of novel tailor-made conjugates of pharmacological interest.[44]

Compared to the modification of peptides with a dienophile, a different procedure was applied. Thus, Reppe anhydride **2** was equipped with a linker comprising the NHS-activated γ-amino-butyric acid (ESI 1.2.13†). Building block **30** was attached to a single corner of octaamino COSS through an amide bond (Fig. 5 and ESI 1.2.14†) resulting in COSS-dienophile **31** which was reacted with peptide-diene **16** giving conjugate **32**. The reaction was carried out in dry DMSO to assure stability of the siloxane core in the presence of the pendant propylamine groups (Fig. 5).

The combination of oxime ligation and DAR_{inv} is a convenient method for site-specific conjugation of complex peptidic molecules. What is the rationale behind using the set of two transformations rather than the individual reactions, each of which is bioorthogonal, selective, and fast *per se*? First, at physiological pH oxime ligation is rather slow and requires catalysis. This could pose a problem if two functional biological macromolecules are ligated directly, whereas the introduction of small bifunctional linker proceeds unhampered, and the next step is irreversible and uncatalyzed. Second, although the direct introduction of DAR_{inv} moieties on solid support has been reported for short peptides,[21,30,36,51] their introduction in recombinant proteins requires extensive modification of the cellular translation machinery.[10,32,52] And, third, our approach provides certain modularity, giving an option to choose between the reactive sites according to reaction environment and nature of the conjugation partners.

In general, our bifunctional building blocks are readily synthetically accessible and can be introduced into peptides site-selectively, without affecting their architecture. The generation of the required carbonyl moieties in peptidic macromolecules is a routine procedure as it proceeds smoothly both upon post-synthetic modification[8] and in the course of recombinant production.[33] Successive oxime ligation was highly efficient and orthogonal to the side-chain functionalities. Subsequently, the generated DAR_{inv}-modified peptides were reacted without a catalyst with the respective counterpart giving defined peptidic constructs with good to quantitative conversion rates. So far, only few DAR_{inv} site-specific conjugations of peptides have been reported restricted either to junction of rather short peptidic sequences[28] or to the generation of macromolecular constructs of undefined stoichiometry.[34,36] Our approach offers the advantage of being suitable for all synthetic peptides, particularly the recombinant ones.

In our hands, being incorporated into peptides and hybrid silsesquioxanes, the strained four-membered ring system of the Reppe anhydride reacted with the respective tetrazine, smoothly converting it into the desired product. This reactivity can be easily explained considering the non-reversible character of DAR_{inv} coupling and the fact that cyclobutene is amongst the most reactive species classified *via* their activation free energies.[53]

Interestingly, for some peptide conjugates we observed the regeneration of the aromatic system within the tetrazine moiety after DAR_{inv} reaction. This observation has previously been reported, but detailed study of the mechanism is still required.[49,50]

To demonstrate modularity and versatility of our approach, we applied it to covalently graft a bioactive peptide[45] onto a

cell-penetrating COSS nanoparticle. The success of this reaction opens new avenues for the facile generation of peptide–COSS conjugates for intracellular delivery, thus expanding the toolbox for the chemical modifications of these promising compounds. In a perspective, our system could be applied to the generation of peptide–protein conjugates under physiological conditions.[54] Taking into consideration that stability of oxime linkage is context-dependent and at physiological pH a catalyst is required to assure efficient transformation, an adequately high-performance chemistry should be considered to replace this ligation step. To this end, recently reported trapped Knoevenagel condensation[55] could be applied as an alternative strategy.

This work was partially funded by the DFG priority program SPP 1623. The authors thank Peter Lorenz (DKFZ, Heidelberg) for his advice regarding tetrazine synthesis.

Notes and references

1 A. Angelini and C. Heinis, *Curr. Opin. Chem. Biol.*, 2011, **15**, 355–361.
2 J. Kalia and R. T. Raines, *Curr. Org. Chem.*, 2010, **14**, 138–147.
3 A. Chakraborty, D. Wang, Y. W. Ebright and R. H. Ebright, *Methods Enzymol.*, 2010, **472**, 19–30.
4 N. K. Devaraj, S. Hilderbrand, R. Upadhyay, R. Mazitschek and R. Weissleder, *Angew. Chem.*, 2010, **49**, 2869–2872.
5 B. M. Zeglis, P. Mohindra, G. I. Weissmann, V. Divilov, S. A. Hilderbrand, R. Weissleder and J. S. Lewis, *Bioconjugate Chem.*, 2011, **22**, 2048–2059.
6 J. C. Jewett and C. R. Bertozzi, *Chem. Soc. Rev.*, 2010, **39**, 1272–1279.
7 G. C. Rudolf, W. Heydenreuter and S. A. Sieber, *Curr. Opin. Chem. Biol.*, 2013, **17**, 110–117.
8 D. Chelius and T. A. Shaler, *Bioconjugate Chem.*, 2003, **14**, 205–211.
9 K. F. Geoghegan and J. G. Stroh, *Bioconjugate Chem.*, 1992, **3**, 138–146.
10 C. H. Kim, J. Y. Axup and P. G. Schultz, *Curr. Opin. Chem. Biol.*, 2013, **17**, 412–419.
11 W. P. Heal, S. R. Wickramasinghe, P. W. Bowyer, A. A. Holder, D. F. Smith, R. J. Leatherbarrow and E. W. Tate, *Chem. Commun.*, 2008, 480–482.
12 S. Fabritz, S. Horner, D. Konning, M. Empting, M. Reinwarth, C. Dietz, B. Glotzbach, H. Frauendorf, H. Kolmar and O. Avrutina, *Org. Biomol. Chem.*, 2012, **10**, 6287–6293.
13 P. V. Chang, J. A. Prescher, E. M. Sletten, J. M. Baskin, I. A. Miller, N. J. Agard, A. Lo and C. R. Bertozzi, *Proc. Natl. Acad. Sci. U. S. A.*, 2010, **107**, 1821–1826.
14 M. Meldal and C. W. Tornoe, *Chem. Rev.*, 2008, **108**, 2952–3015.
15 J. E. Moses and A. D. Moorhouse, *Chem. Soc. Rev.*, 2007, **36**, 1249–1262.
16 K. Nwe and M. W. Brechbiel, *Cancer Biother. Radiopharm.*, 2009, **24**, 289–302.
17 N. J. Agard, J. A. Prescher and C. R. Bertozzi, *J. Am. Chem. Soc.*, 2004, **126**, 15046–15047.
18 X. Ning, R. P. Temming, J. Dommerholt, J. Guo, D. B. Ania, M. F. Debets, M. A. Wolfert, G. J. Boons and F. L. van Delft, *Angew. Chem.*, 2010, **49**, 3065–3068.
19 N. E. Mbua, J. Guo, M. A. Wolfert, R. Steet and G. J. Boons, *ChemBioChem*, 2011, **12**, 1912–1921.
20 M. Wiessler, W. Waldeck, C. Kliem, R. Pipkorn and K. Braun, *Int. J. Med. Sci.*, 2009, **7**, 19–28.
21 R. Pipkorn, W. Waldeck, B. Didinger, M. Koch, G. Mueller, M. Wiessler and K. Braun, *J. Pept. Sci.*, 2009, **15**, 235–241.
22 A. Niederwieser, A. K. Spate, L. D. Nguyen, C. Jungst, W. Reutter and V. Wittmann, *Angew. Chem.*, 2013, **52**, 4265–4268.
23 S. B. Engelsma, L. I. Willems, C. E. van Paaschen, S. I. van Kasteren, G. A. van der Marel, H. S. Overkleeft and D. V. Filippov, *Org. Lett.*, 2014, **16**, 2744–2747.
24 D. N. Kamber, L. A. Nazarova, Y. Liang, S. A. Lopez, D. M. Patterson, H. W. Shih, K. N. Houk and J. A. Prescher, *J. Am. Chem. Soc.*, 2013, **135**, 13680–13683.
25 M. L. Blackman, M. Royzen and J. M. Fox, *J. Am. Chem. Soc.*, 2008, **130**, 13518–13519.
26 Z. Li, H. Cai, M. Hassink, M. L. Blackman, R. C. Brown, P. S. Conti and J. M. Fox, *Chem. Commun.*, 2010, **46**, 8043–8045.
27 M. R. Karver, R. Weissleder and S. A. Hilderbrand, *Bioconjugate Chem.*, 2011, **22**, 2263–2270.
28 S. Ameta, J. Becker and A. Jaschke, *Org. Biomol. Chem.*, 2014, **12**, 4701–4707.
29 T. S. Elliott, F. M. Townsley, A. Bianco, R. J. Ernst, A. Sachdeva, S. J. Elsasser, L. Davis, K. Lang, R. Pisa, S. Greiss, K. S. Lilley and J. W. Chin, *Nat. Biotechnol.*, 2014, **32**, 465–472.
30 B. M. Zeglis, F. Emmetiere, N. Pillarsetty, R. Weissleder, J. S. Lewis and T. Reiner, *ChemistryOpen*, 2014, **3**, 48–53.
31 J. Seckute and N. K. Devaraj, *Curr. Opin. Chem. Biol.*, 2013, **17**, 761–767.
32 J. L. Seitchik, J. C. Peeler, M. T. Taylor, M. L. Blackman, T. W. Rhoads, R. B. Cooley, C. Refakis, J. M. Fox and R. A. Mehl, *J. Am. Chem. Soc.*, 2012, **134**, 2898–2901.
33 D. Rabuka, J. S. Rush, G. W. deHart, P. Wu and C. R. Bertozzi, *Nat. Protoc.*, 2012, **7**, 1052–1067.
34 F. Emmetiere, C. Irwin, N. T. Viola-Villegas, V. Longo, S. M. Cheal, P. Zanzonico, N. Pillarsetty, W. A. Weber, J. S. Lewis and T. Reiner, *Bioconjugate Chem.*, 2013, **24**, 1784–1789.
35 K. S. Yang, G. Budin, C. Tassa, O. Kister and R. Weissleder, *Angew. Chem.*, 2013, **52**, 10593–10597.
36 R. Hassert, M. Pagel, Z. Ming, T. Haupl, B. Abel, K. Braun, M. Wiessler and A. G. Beck-Sickinger, *Bioconjugate Chem.*, 2012, **23**, 2129–2137.
37 J. B. Haun, N. K. Devaraj, S. A. Hilderbrand, H. Lee and R. Weissleder, *Nat. Nanotechnol.*, 2010, **5**, 660–665.
38 R. Rossin, P. R. Verkerk, S. M. van den Bosch, R. C. Vulders, I. Verel, J. Lub and M. S. Robillard, *Angew. Chem.*, 2010, **49**, 3375–3378.
39 J. D. Thomas, H. Cui, P. J. North, T. Hofer, C. Rader and T. R. Burke, Jr., *Bioconjugate Chem.*, 2012, **23**, 2007–2013.
40 H. S. Beckmann, A. Niederwieser, M. Wiessler and V. Wittmann, *Chemistry*, 2012, **18**, 6548–6554.
41 O. El-Mahdi and O. Melnyk, *Bioconjugate Chem.*, 2013, **24**, 735–765.
42 R. G. Kruger, B. Otvos, B. A. Frankel, M. Bentley, P. Dostal and D. G. McCafferty, *Biochemistry*, 2004, **43**, 1541–1551.
43 C. Uth, S. Zielonka, S. Hörner, N. Rasche, A. Plog, H. Orelma, O. Avrutina, K. Zhang and H. Kolmar, *Angew. Chem.*, 2014, **53**, 12618–12623.
44 S. Fabritz, S. Horner, O. Avrutina and H. Kolmar, *Org. Biomol. Chem.*, 2013, **11**, 2224–2236.
45 H. Fittler, O. Avrutina, M. Empting and H. Kolmar, *J. Pept. Sci.*, 2014, **20**, 415–420.
46 B. Glotzbach, M. Reinwarth, N. Weber, S. Fabritz, M. Tomaszowski, H. Fittler, A. Christmann, O. Avrutina and H. Kolmar, *PLoS One*, 2013, **8**, e76956.
47 R. B. Merrifield, *J. Am. Chem. Soc.*, 1963, **85**, 2149–2154.
48 S. Foillard, M. O. Rasmussen, J. Razkin, D. Boturyn and P. Dumy, *J. Org. Chem.*, 2008, **73**, 983–991.
49 A. C. Knall and C. Slugovc, *Chem. Soc. Rev.*, 2013, **42**, 5131–5142.
50 R. Hoogenboom, B. C. Moore and U. S. Schubert, *J. Org. Chem.*, 2006, **71**, 4903–4909.
51 M. Wiessler, W. Waldeck, R. Pipkorn, C. Kliem, P. Lorenz, H. Fleischhacker, M. Hafner and K. Braun, *Int. J. Med. Sci.*, 2010, **7**, 213–223.
52 K. Lang, L. Davis, S. Wallace, M. Mahesh, D. J. Cox, M. L. Blackman, J. M. Fox and J. W. Chin, *J. Am. Chem. Soc.*, 2012, **134**, 10317–10320.
53 F. Liu, Y. Liang and K. N. Houk, *J. Am. Chem. Soc.*, 2014, **136**, 11483–11493.
54 E. M. Sletten and C. R. Bertozzi, *Angew. Chem.*, 2009, **48**, 6974–6998.
55 R. Kudirka, R. M. Barfield, J. McFarland, A. E. Albers, G. W. de Hart, P. M. Drake, P. G. Holder, S. Banas, L. C. Jones, A. W. Garofalo and D. Rabuka, *Chem. Biol.*, 2015, **22**, 293–298.

5.3. Nanoscale biodegradable organic-inorganic hybrids for efficient cell penetration and drug delivery

Sebastian Hörner, Sascha Knauer, Christina Uth, Marina Jöst, Volker Schmidts, Holm Frauendorf, Christina Marie Thiele, Olga Avrutina, Harald Kolmar, Nanoscale biodegradable organic-inorganic hybrids for efficient cell penetration and drug delivery, *Angewandte Chemie International Edition,* **2016***, 55,* 14842–14846.

Title:
Nanoscale biodegradable organic-inorganic hybrids for efficient cell penetration and drug delivery

Authors:
Sebastian Hörner,‡ Sascha Knauer,‡ Christina Uth,‡ Marina Jöst, Volker Schmidts, Holm Frauendorf, Christina Marie Thiele, Olga Avrutina and Harald Kolmar*

‡ Authors contributed equally

Bibliographic Data:
Angewandte Chemie International Edition
Volume 55, Issue 47, November 14, 2016, Pages 14842–14846.
Article first published online: 24 OCT 201 | DOI: 10.1002/anie.201606065
See also: *Angewandte Chemie*, Volume 128, Issue 47, November 14, 2016, Pages 15063–15068.

Graphical abstract:

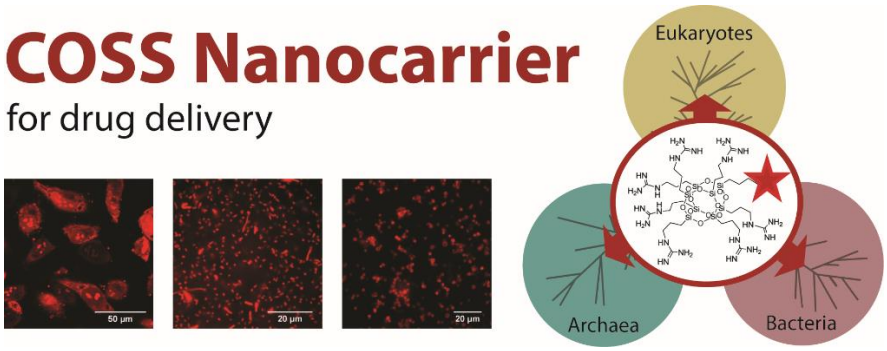

COSS and effect:
New-generation molecular transporters are based on cell-penetrating cube-octameric silsesquioxanes (COSS). These nanoscale hybrid carriers are biodegradable, low-toxic, and show efficient uptake in living cells of all three domains of life.

Contributions of C. Uth:
- Synthesis and analysis of GuCOSS-doxorubicin
- Conducted cytotoxic assays
- Conducted cellular uptake studies in *E.coli* and prepared fluorescence micrographs
- Conducted FACS experiments with 10% FBS with S. Hörner
- Prepared manuscript with O. Avrutina and S. Hörner

Drug Delivery

International Edition: DOI: 10.1002/anie.201606065
German Edition: DOI: 10.1002/ange.201606065

Nanoscale Biodegradable Organic–Inorganic Hybrids for Efficient Cell Penetration and Drug Delivery

*Sebastian Hörner[+], Sascha Knauer[+], Christina Uth[+], Marina Jöst, Volker Schmidts, Holm Frauendorf, Christina Marie Thiele, Olga Avrutina, and Harald Kolmar**

Abstract: *We report a comprehensive study on novel, highly efficient, and biodegradable hybrid molecular transporters. To this end, we designed a series of cell-penetrating, cube-octameric silsesquioxanes (COSS), and investigated cellular uptake by confocal microscopy and flow cytometry. A COSS with dense spatial arrangement of guanidinium groups displayed fast uptake kinetics and cell permeation at nanomolar concentrations in living HeLa cells. Efficient uptake was also observed in bacteria, yeasts, and archaea. The COSS-based carrier was significantly more potent than cell-penetrating peptides (CPPs) and displayed low toxicity. It efficiently delivered a covalently attached cytotoxic drug, doxorubicin, to living tumor cells. As the uptake of fluorescently labeled carrier remained in the presence of serum, the system could be considered particularly attractive for the in vivo delivery of therapeutics.*

Since Linus Pauling's groundbreaking publication in *Science*[1] in 1949, achievements in the rapidly advancing field of molecular medicine and related areas are very impressive. However, while today a vast arsenal of potent and selective drugs is available, an efficient strategy to deliver these therapeutic compounds inside the cell, in particular, in the cell nucleus, has become as important as the design and optimization of the pharmacophore itself. Considering that promising newly developed potential drug candidates, such as peptides and proteins, are water-soluble, a bottleneck in their application in living systems is the passage across the cellular membrane. As a consequence, drug delivery has emerged as one of the major fields in biomedical research. In 1994, the first cell-penetrating peptide (CPP) penetratin was described as a vehicle for cargo delivery into cells.[2] Since then, CPPs were thoroughly investigated and improved.[3] However, several issues associated with toxicity, stability, and efficacy of cellular uptake still require work. As the peptidic structure of CPPs intrinsically limits the scope of improvements, recent efforts are focused on nanoparticles or small non-peptidic molecular scaffolds.[4] These simple, uniform molecular architectures can be easily tailored, leading to cell-penetrating molecules with entirely new properties. In contrast to the macromolecular delivery systems, such as (bio)polymers, dendrimers, lipid-based or viral-like carriers, some of which are actually on the market or under clinical trials,[4c] the next-generation molecular transporters still require optimization.

General strategies towards the improvement of cellular uptake include the reduction of conformational freedom by backbone cyclization of cell-penetrating peptides or by the usage of scaffolds which induce spatial organization of the uptake-mediating functional groups.[3a,4d,5] Interestingly, the proximity of the charged groups to the backbone was found to influence the efficiency of cell uptake as well.[3c,d,5c,6]

Herein, we chose the cube-octameric silsesquioxane scaffold (COSS) as the starting point for the development of new-generation cell-penetrating compounds. COSS are highly ordered organic–inorganic hybrid molecules with a cage-like core of alternating silicon and oxygen atoms surrounded by eight pendant organic residues. Such an architecture with charged groups located at the flanking arms tethered to a compact (0.7 nm)[7] core ensures a compact, rigid, and symmetric construct. Generally, COSS are used in certain medical fields, for example, tissue engineering, or for the oligomerization of bioactive ligands, among them peptides and carbohydrates.[7,8] They are considered non-toxic and the hydrolytic degradation of the inorganic core under physiological conditions has been thoroughly investigated.[7]

COSS bearing seven ammonium groups were found to penetrate cells.[7,9] We have previously shown that these molecules enable the delivery of a functional peptidic cargo into living HeLa cells.[10] To improve this drug delivery system, we synthesized a series of COSS-based molecular transporters and investigated the uptake efficacy of a covalently attached cytotoxic drug.

Compounds **2**–**7** were synthesized following a two-step procedure (Scheme 1). Thus, inexpensive octaammonium COSS hydrochloride **1** was functionalized with a) guanidinium groups positively charged under physiological conditions or b) permanent positive charges installed by quaternary amines. Additionally, we investigated the influence of the flanking arm's length on cellular uptake. To visualize the constructs in cell assays, tetramethylrhodamine (TAMRA) was attached to a single corner of COSS **1** in a stoichiometri-

[*] S. Hörner,[+] S. Knauer,[+] C. Uth,[+] M. Jöst, Dr. O. Avrutina, Prof. Dr. H. Kolmar
Clemens-Schöpf-Institut für Organische Chemie und Biochemie
Technische Universität Darmstadt
Alarich-Weiss-Strasse 4, 64287 Darmstadt (Germany)
E-mail: kolmar@biochemie-tud.de
Dr. V. Schmidts, Prof. Dr. C. M. Thiele
Clemens-Schöpf-Institut für Organische Chemie und Biochemie
Technische Universität Darmstadt
Alarich-Weiss-Strasse 16, 64287 Darmstadt (Germany)
Dr. H. Frauendorf
Institut für Organische und Biomolekulare Chemie
Georg-August Universität Göttingen
Tammannstrasse 2, 37077 Göttingen (Germany)
[+] These authors contributed equally to this work.
Supporting information for this article can be found under: http://dx.doi.org/10.1002/anie.201606065.

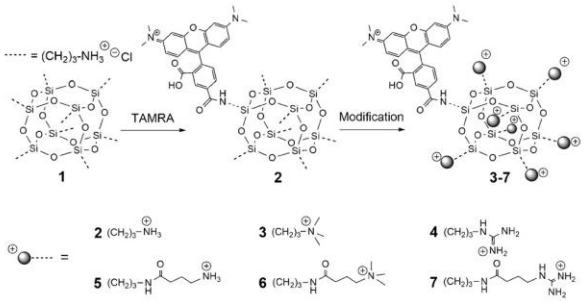

Scheme 1. Synthesis of fluorescently labeled cell-penetrating COSS derivatives **2–7** equipped with cationic functional groups separated from the core by spacers of different lengths. Counterions are excluded for clarity. Sequences of CPPs are shown in Supporting Information 5.2.

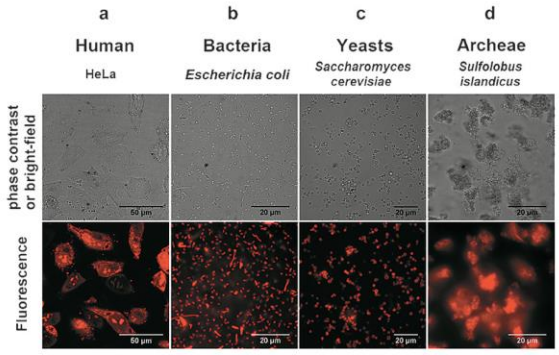

Figure 1. Cell uptake of TAMRA-GuCOSS (**4**). a) Live-cell laser scanning confocal microscopy imaging of HeLa cells incubated with **4** at 37 °C; b)–d) fluorescence microscopy imaging of cells incubated with **4**; b) Gram-negative bacterium (*E. coli*); c) yeast (*Saccharomyces cerevisiae*), both incubated at 37 °C; d) archaeon (*Sulfolobus islandicus*) incubated at 80 °C.

cally controlled reaction leading to TAMRA-aminoCOSS (**2**). Subsequently, the remaining seven amine functionalities of **2** were converted into the corresponding quaternary amines by N-methylation (TAMRA-quartCOSS **3**) or guanidinylation (TAMRA-GuCOSS **4**). Alternatively, for the introduction of a linker separating the siloxane core and the charged elements, 4-aminobutyric, 4-trimethylaminobutyric, or 4-guanidinobutyric acids were installed via amide coupling leading to, respectively, TAMRA-aminoCOSS-L (**5**), TAMRA-quartCOSS-L (**6**), and TAMRA-GuCOSS-L (**7**) (Scheme 1). To investigate toxicity of molecular transporters we synthesized amino-GuCOSS (**8**) lacking a fluorescent label (Supporting Information 5.2). Fluorescein-TAMRA-GuCOSS (**9**) was designed to assess biodegradation of the carriers (Figure 3a). The integrity of the cage-like siloxane core was confirmed by NMR spectroscopy (compounds **2–7**; Supporting Information 5.3).

Fluorescently labeled derivatives **2–7** were investigated for their ability to penetrate living cells. To qualitatively estimate the uptake, we performed live-cell imaging using confocal laser scanning microscopy. Thus, HeLa cells were incubated with compounds **2–7** at a concentration of 20 μM in serum-free Dulbecco's modified eagle medium (DMEM) for 30 min. The cells were washed three times with phosphate buffered saline (PBS) and imaged in DMEM with fetal bovine serum (FBS). Compounds **2–4** bearing shorter linkers (Figure 1a, Figure S1) demonstrated enhanced cellular uptake and prominent accumulation inside the nucleus, the nucleoli, and the cytoplasm, whereas an increase of the spacer's length led to reduced cellular uptake and primarily cytoplasmic localization (compounds **5–7**, Figure S1). In view of predominant accumulation in the nucleus, molecular transporters **2–4** are particularly attractive for the delivery of drugs addressing this cellular compartment.

As the guanidinylated carrier TAMRA-GuCOSS (**4**) exhibited the highest uptake in HeLa cells, its ability to penetrate cells from all three domains of life was further studied. The microscopic images obtained suggest that it is able to enter both eukaryotic and prokaryotic cells, among them yeast (*S. cerevisiae*) and mammalian cells (HeLa), as well as bacteria (*E. coli*) and archaea (*S. islandicus*, *S. tokodaii*, *Halobacterium salinarum*) (Figure 1b–d, Figure S2). These observations are of particular interest in view of the exceptional membrane composition of archaea.[11] As guanidinylated COSS could be of interest for the delivery of antibiotics, we investigated its uptake in *E. coli* in detail (Figure S2c).

To quantify the cellular uptake in eukaryotic cells, we performed comprehensive flow-cytometric experiments with COSS derivatives **2–7** and TAMRA-labeled cell-penetrating peptides: TAT (**10**), penetratin (**11**), heptaarginine (**12**), and decaarginine (**13**).[12] We incubated HeLa cells with these compounds at a final concentration of 20 μM in serum-free DMEM at 37 °C up to 60 min. To remove surface-bound carrier molecules, cells were trypsinized (Supporting Information 5.1). Assays were performed in triplicate, the results were verified in three independent experiments (Figure S3a–g) with carrier **4** having shown the best cellular uptake. Indeed, the intensity of the fluorescence signal was found 155 times higher than that for the TAT peptide **10**. Interestingly, compound **4** carrying seven guanidinium groups displayed a 78-fold higher cellular uptake than heptaarginine (**12**; Figure 2a). In agreement with our microscopy studies, shorter linkers correlated with enhanced fluorescence intensity (Figure S4). Similar results were obtained for HEK 293 and CHO cells (Figure S5a–c). This higher uptake of **4** can be attributed to its more compact arrangement, hence increased density of uptake-mediating functional groups. Indeed, cyclization of CPPs, leading to more constrained and rigid structures, is an efficient strategy to improve cellular uptake.[5c]

To evaluate whether the cellular uptake is energy-dependent, we compared the fluorescence intensity of HeLa cells incubated with **4** at 37 °C and at 4 °C (Figure 2d). As the uptake was only negligibly decreased at 4 °C, an energy-independent mechanism was assumed. Time-resolved flow cytometry indicated fast uptake kinetics with a first shift of the population within an incubation time of 1 min at 37 °C (Figure S6). To determine the minimal internalization threshold, cells were incubated with **4** at different concentrations. Even at the lowest concentration (80 nM) a shift in fluores-

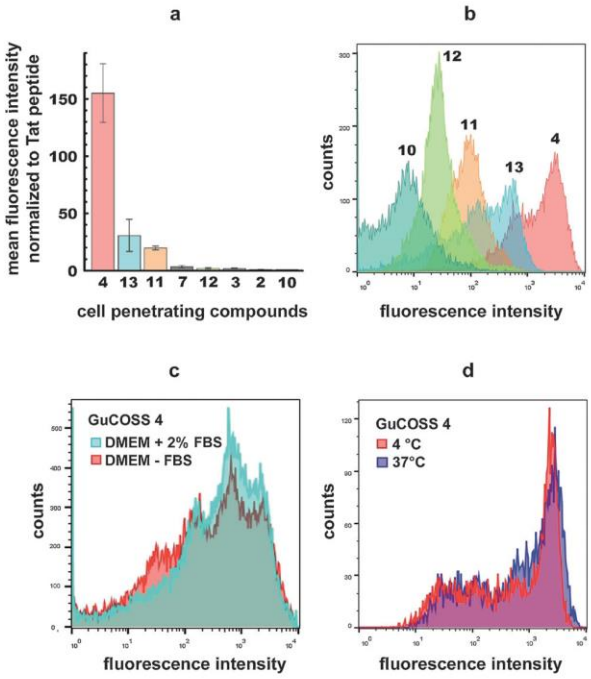

Figure 2. Flow-cytometric experiments using HeLa cells. a) mean fluorescence intensity of selected COSS derivatives and cell-penetrating peptides. b) representative histogram of TAMRA-GuCOSS (**4**) and cell-penetrating peptides (petrol-green: TAT (**10**); yellow-green: heptaargininе (**12**); orange: penetratin (**11**), light blue: decaarginine (**13**); red: TAMRA-GuCOSS (**4**). c) HeLa cells incubated with **4** in the presence and the absence of 2% FBS in DMEM. d) Cellular uptake of **4** in HeLa cells incubated in serum-free DMEM for 10 min with 20 μM **4** at 37 °C or 4 °C.

cence intensity was observed and 1 μM **4** was needed to reach full shift of the population after an incubation time of 10 min at 37 °C (Figure S7). In contrast to cell-penetrating peptides, no minimal internalization threshold within the investigated concentrations was observed.[13] As recent studies suggest that both the silsesquioxane core and guanidine groups promote clustering,[7,14] it could be supposed that high local concentration of **4** (as a result of its assembly on the cell surface) ensures cell penetration even at low concentrations. Our observations point to an energy-independent direct cell translocation, in accordance with the uptake mechanism of other polyguanidines.[13]

The uptake of cell-penetrating peptides is generally retarded in serum-containing media.[15] Impaired CPP-mediated permeation efficacy has been reported for polyarginines both in serum-containing media and in in vivo experiments, presumably owing to their aggregation with serum proteins. Therefore, we imaged **4** in the presence of 10% FBS in DMEM (Figure S8) and found that 40% of the mean fluorescence intensity was retained, compared to that for serum-free media.[3c,15a,16] This tolerance of serum proteins, combined with fast and effective cellular uptake, makes **4** a promising carrier for in vivo applications.

Since many cell-penetrating compounds were found to be toxic above a certain concentration, we investigated the toxicity of amino-GuCOSS (**8**) lacking a fluorescent label (Supporting Information 5.2) in HeLa cells using an XTT cell viability assay. Thereby the LC_{50} was determined to be 84 μM (Figure 3e), which is comparable to that of polyarginines (76 μM), TAT (86.6% viability at 50 μM), and penetratin (88.2% at 50 μM).[17] This low toxicity may be caused by biodegradation of the inorganic core under physiological conditions. Indeed, the pH-dependent degradation of polyhedral silsesquioxanes resulting in primary siloxanes is well established.[7]

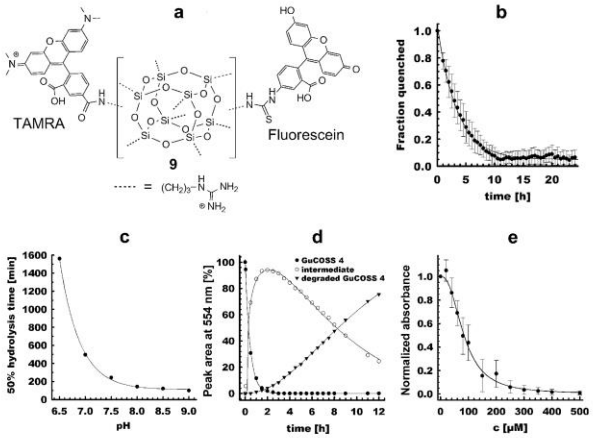

Figure 3. GuCOSS degradation studies. a) Guanidinylated COSS construct bearing the two fluorophores, fluorescein and TAMRA (Fluorescein-TAMRA-GuCOSS (**9**)). b) Decrease of the quenched fraction of fluorescein in the in vitro degradation studies in living HeLa cells. c) 50% hydrolysis of TAMRA-GuCOSS (**4**) as a function of the pH in PBS. d) Kinetics of the degradation of **4** at pH 7.0 in PBS analyzed by HPLC. e) XTT assay of the in vitro toxicity of guanidinylated COSS (**8**) bearing no fluorescent label.

For characterization of pH-dependent degradation of **4**, we monitored decomposition of the inorganic core by RP-HPLC. To that end, **4** was incubated in PBS at pH 6.5–9.0 (37 °C) and time-resolved HPLC traces were recorded within 12 h at 554 nm (absorption maximum of TAMRA). Hydrolysis intermediates and the degradation products were quantified by determination of the peak areas. Although hydroxyl-bearing intermediates were eluted earlier from the column, the completely hydrolyzed TAMRA-decorated siloxanes had longer retention times. Typical HPLC traces at pH 7.0 are shown at Figure S9, and respective half-life values at pH 6.5–9.0 in Figure 3c. Thereby, the $t_{1/2}$ at pH 7.4 (PBS) was determined to be 252 min. The degradation at neutral pH is shown in Figure 3d.

To assess the biodegradation of the GuCOSS-based carriers, we synthesized derivative **9** carrying two fluorescent markers, fluorescein and TAMRA (Figure 3a). As both dyes are attached to the same siloxane core in spatial proximity, the fluorescence of fluorescein is quenched upon Förster resonance energy transfer (FRET; Figure S10). As the inorganic core loses its integrity during breakdown, either fluorescein or TAMRA separates from the siloxane cage, and the fluores-

cence of fluorescein is restored. Along with excitation at 488 nm the increase of the emission at 520 nm was used to quantify the fraction of partially disassembled carriers. Based on the fluorescence recovery of fluorescein, a half-life of 186 min was found in human serum, indicating sufficient stability for in vivo applications (Figure S11). As HPLC analysis allowed the erosion process to be monitored up to the final degradation products, the half-life determined using this approach was significantly longer (252 min at pH 7.4). In former studies, the half-life of cell-penetrating peptides in the presence of serum was found to be in the range of minutes (e.g. $t_{1/2} = 5$ min for penetratin).[18] This fast decay is most likely caused by proteolysis. It is clear that the hybrid GuCOSS construct does not serve as a substrate for proteolytic enzymes. The enhanced half-life of derivative **9** in serum is an additional indication that the degradation of the COSS core is predominantly pH dependent.

To better understand how the degradation proceeds in living cells, we monitored the recovery of fluorescein fluorescence by live-cell confocal laser scanning microscopy upon internalization of construct **9** in HeLa cells (Figure 3b, Figure S12). The fluorescent markers were disconnected in half of the starting material within 149 min, and complete disassembly (reappearance of fluorescence) occurred in 11 h. The half-lives obtained in these experiments are on the same order of magnitude as those observed upon incubation in human serum ($t_{1/2} = 186$ min).

Applicability of GuCOSS as a molecular transporter was examined upon cellular delivery of a cytotoxic cargo doxorubicin (DOX, **14**)—a widely applied antitumor drug.[19] Being able to intercalate DNA, this agent induces apoptosis in cancer cells by activating the intrinsic death pathway.[20] Therefore, it is clear that the therapeutic effect of DOX could be exerted only if the drug gains access to the cell nucleus. However, because only passive diffusion ensures its penetration into tumor tissues, the efficiency of DOX is strongly compromised, which represents the major limitation of this highly potent compound.[21] In a model construct, we connected the GuCOSS delivery module to a DOX functional cargo via a disulfide yielding the conjugate **15** (Supporting Information 5.2). This bond is rapidly reduced in the reductive environment of cytosol, enabling drug release inside the cell.[22]

Cellular delivery was studied in HeLa cells. First, an incubation time-dependent cell assay with the free antibiotic was performed (Supporting Information 4.0, 5.1). Because of the slow uptake of free doxorubicin, the number of cancer cells killed correlated with the duration of incubation (Figure S13). The conjugate **15** as well as the controls (free doxorubicin (**14**) and untreated cells) were incubated at the same concentrations for 1 h (Supporting Information 3.0). Then the cells were washed with DMEM, and after 18 h an MTT assay was performed (Figure 4). The results clearly show that the hybrid construct **15** had an enhanced cytotoxic effect compared to the free drug **14**.

Although it is one of the cornerstones of cancer therapy, free doxorubicin causes irreversible cardiac damage.[23] Whereas its liposomal formulation[24] mitigates the toxic side effects,[23] the potency is unaltered compared to the conventional drug.[25] While the recently reported formulation based on liposomal coencapsulation of DOX with Listeriolysin O enables enhancement of nuclear targeting in certain carcinoma cell lines, it is supposed to be highly immunogenic.[26] Therefore, we believe that our delivery platform combining highly efficient cell penetration with small size, low toxicity, and biodegradability might provide clear benefits. Nevertheless, further validation by animal studies is required, which particularly addresses cardiotoxic effects in comparison to liposomal doxorubicin formulations. It may also be interesting to investigate whether the cellular uptake of other cytotoxins with particularly low cell-penetrating efficacy, such as for example, hygromycin,[27] can be enhanced upon COSS conjugation.

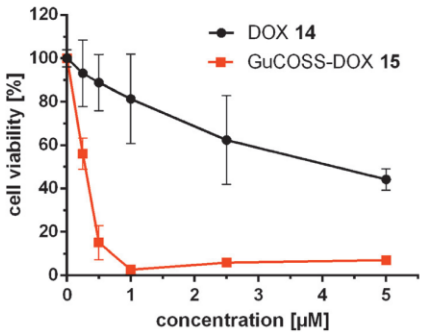

Figure 4. Cell viability assay (MTT) of free doxorubicin (DOX, **14**) and the doxorubicin-GuCOSS conjugate (**15**). Error bars indicate standard deviations from three independent measurements.

To summarize, we developed new-generation hybrid cell-penetrating compounds based on the cube-octameric silsesquioxane scaffold. Thus, the guanidinylated fluorescent COSS derivative was found to efficiently penetrate cells from all three domains of life with a 155-fold enhanced, compared to the cell-penetrating peptide TAT, cellular uptake in HeLa cells. The carrier has fast uptake kinetics and penetrates cells at double-digit nanomolar concentrations. It has low toxicity and decomposes under physiological conditions within 11 h. This novel molecular transporter retains its activity in the presence of serum, which makes it a promising candidate for in vivo delivery of drugs. Taking into consideration that these organic–inorganic hybrids are very small and compact, no or weak immune response could be assumed. We believe that our delivery platform may enrich the toolbox of low-toxic and highly efficient molecular systems needed for the development of future-oriented therapeutics.

Acknowledgements

We thank Dr. Anna-Lena Krause (Nationales Centrum für Tumorerkrankungen, DKFZ, Heidelberg, Germany) for assistance during flow cytometry interpretation, Thomas Pirzer for providing HeLa cells, and PD Dr. Arnulf Kletzin (Fachbereich Biologie, Technische Universität Darmstadt) for providing *sulfobacter* and *archaea*.

Keywords: cell penetration · cell-penetrating compound · COSS · drug delivery · silsesquioxanes

How to cite: *Angew. Chem. Int. Ed.* **2016**, *55*, 14842–14846
Angew. Chem. **2016**, *128*, 15063–15068

[1] L. Pauling, H. A. Itano, S. J. Singer, I. C. Wells, *Science* **1949**, *110*, 543–548.
[2] D. Derossi, M. H. Joliot, G. Chassaing, M. Prochiantz, *J. Biol. Chem.* **1994**, *269*, 10444–10450.
[3] a) A. Ho, S. R. Schwarze, S. J. Mermelstein, G. Waksman, S. F. Dowdy, *Cancer Res.* **2001**, *61*, 474–477; b) A. Nasrolahi Shirazi, R. Tiwari, B. S. Chhikara, D. Mandal, K. Parang, *Mol. Pharm.* **2013**, *10*, 488–499; c) P. A. Wender, D. J. Mitchell, K. Pattabiraman, E. T. Pelkey, L. Steinman, J. B. Rothbard, *Proc. Natl. Acad. Sci. USA* **2000**, *97*, 13003–13008; d) P. A. Wender, J. B. Rothbard, T. C. Jessop, E. L. Kreider, B. L. Wylie, *J. Am. Chem. Soc.* **2002**, *124*, 13382–13383.
[4] a) V. Bagnacani, V. Franceschi, M. Bassi, M. Lomazzi, G. Donofrio, F. Sansone, A. Casnati, R. Ungaro, *Nat. Commun.* **2013**, *4*, 1721; b) S. Bersani, S. Salmaso, F. Mastrotto, E. Ravazzolo, A. Semenzato, P. Caliceti, *Bioconjugate Chem.* **2012**, *23*, 1415–1425; c) Z. G. Chen, *Trends Mol. Med.* **2010**, *16*, 594–602; d) N. W. Luedtke, P. Carmichael, Y. Tor, *J. Am. Chem. Soc.* **2003**, *125*, 12374–12375; e) M. Okuyama, H. Laman, S. R. Kingsbury, C. Visintin, E. Leo, K. L. Eward, K. Stoeber, C. Boshoff, G. H. Williams, D. L. Selwood, *Nat. Methods* **2007**, *4*, 153–159; f) J. Valero, M. Van Gool, R. Perez-Fernandez, P. Castreno, J. Sanchez-Quesada, P. Prados, J. de Mendoza, *Org. Biomol. Chem.* **2012**, *10*, 5417–5430.
[5] a) Y. A. Fillon, J. P. Anderson, j. Chmielewski, *J. Am. Chem. Soc.* **2005**, *127*, 11798–11803; b) N. P. Gabrielson, H. Lu, L. Yin, D. Li, F. Wang, J. Cheng, *Angew. Chem. Int. Ed.* **2012**, *51*, 1143–1147; *Angew. Chem.* **2012**, *124*, 1169–1173; c) G. Lättig-Tünnemann, M. Prinz, D. Hoffmann, J. Behlke, C. Palm-Apergi, I. Morano, H. D. Herce, M. C. Cardoso, *Nat. Commun.* **2011**, *2*, 453; d) D. Mandal, A. Nasrolahi Shirazi, K. Parang, *Angew. Chem. Int. Ed.* **2011**, *50*, 9633–9637; *Angew. Chem.* **2011**, *123*, 9807–9811; e) A. Nasrolahi Shirazi, R. K. Tiwari, D. Oh, B. Sullivan, K. McCaffrey, D. Mandal, K. Parang, *Mol. Pharm.* **2013**, *10*, 3137–3151; f) H. Tang, L. Yin, K. H. Kim, J. Cheng, *Chem. Sci.* **2013**, *4*, 3839.
[6] K. K. Maiti, W. S. Lee, T. Takeuchi, C. Watkins, M. Fretz, D. C. Kim, S. Futaki, A. Jones, K. T. Kim, S. K. Chung, *Angew. Chem. Int. Ed.* **2007**, *46*, 5880–5884; *Angew. Chem.* **2007**, *119*, 5984–5988.
[7] S. Fabritz, S. Hörner, O. Avrutina, H. Kolmar, *Org. Biomol. Chem.* **2013**, *11*, 2224–2236.
[8] a) S. Fabritz, S. Hörner, D. Konning, M. Empting, M. Reinwarth, C. Dietz, B. Glotzbach, H. Frauendorf, H. Kolmar, O. Avrutina, *Org. Biomol. Chem.* **2012**, *10*, 6287–6293; b) D. Heyl, E. Rikowski, R. C. Hoffmann, J. J. Schneider, W. D. Fessner, *Chem. Eur. J.* **2010**, *16*, 5544–5548.
[9] C. McCusker, J. B. Carroll, V. M. Rotello, *Chem. Commun.* **2005**, 996–998.
[10] S. Hörner, S. Fabritz, H. D. Herce, O. Avrutina, C. Dietz, R. W. Stark, M. C. Cardoso, H. Kolmar, *Org. Biomol. Chem.* **2013**, *11*, 2258–2265.
[11] M. De Rosa, A. Gambacorta, A. Gliozzi, *Microbiol. Rev.* **1986**, *50*, 70–80.
[12] a) D. Derossi, S. Calvet, A. Trembleau, A. Brunissen, G. Chassaing, A. Prochiantz, *J. Biol. Chem.* **1996**, *271*, 18188–18193; b) S. Futaki, T. Suzuki, W. Ohashi, T. Yagami, S. Tanaka, K. Ueda, Y. Sugiura, *J. Biol. Chem.* **2001**, *276*, 5836–5840; c) E. Vivès, P. Brodin, B. Lebleu, *J. Biol. Chem.* **1997**, *272*, 16010–16017.
[13] F. Duchardt, M. Fotin-Mleczek, H. Schwarz, R. Fischer, R. Brock, *Traffic* **2007**, *8*, 848–866.
[14] M. Vazdar, E. Wernersson, M. Khabiri, L. Cwiklik, P. Jurkiewicz, M. Hof, E. Mann, S. Kolusheva, R. Jelinek, P. Jungwirth, *J. Phys. Chem. B* **2013**, *117*, 11530–11540.
[15] a) M. Kosuge, T. Takeuchi, I. Nakase, A. T. Jones, S. Futaki, *Bioconjugate Chem.* **2008**, *19*, 656–664; b) I. Nakase, Y. Konishi, M. Ueda, H. Saji, S. Futaki, *J. Controlled Release* **2012**, *159*, 181–188; c) K. Park, *J. Controlled Release* **2012**, *159*, 153.
[16] A. F. Saleh, A. Arzumanov, R. Abes, D. Owen, B. Lebleu, M. J. Gait, *Bioconjugate Chem.* **2010**, *21*, 1902–1911.
[17] S. W. Jones, R. Christison, K. Bundell, C. J. Voyce, S. M. Brockbank, P. Newham, M. A. Lindsay, *Br. J. Pharmacol.* **2005**, *145*, 1093–1102.
[18] M. Hällbrink, J. Oehlke, G. Papsdorf, M. Bienert, *Biochim. Biophys. Acta Biomembr.* **2004**, *1667*, 222–228.
[19] A. M. Meredith, C. R. Dass, *J. Pharm. Pharmacol.* **2016**, *68*, 729.
[20] a) Y. Sun, X. Yan, T. Yuan, J. Liang, Y. Fan, Z. Gu, X. Zhang, *Biomaterials* **2010**, *31*, 7124–7131; b) S. Wesselborg, I. H. Engels, E. Rossmann, M. Los, K. Schulze-Osthoff, *Blood* **1999**, *9*, 3053–3063.
[21] A. I. Minchinton, I. F. Tannock, *Nat. Rev. Cancer* **2006**, *6*, 583–592.
[22] G. Saito, J. A. swanson, K. D. Lee, *Adv. Drug Delivery Rev.* **2003**, *55*, 199–215.
[23] T. Safra, *Oncologist* **2003**, *8*, 17–24.
[24] A. L. B. Seynhaeve, B. M. Dicheva, S. Hoving, G. A. Koning, T. L. M. ten Hagen, *J. Controlled Release* **2013**, *172*, 330–340.
[25] a) L. Harris, G. Batist, R. Belt, D. Rovira, R. Navari, N. Azarnia, K. Welles, E. Winer, T. D.-S. Grp, *Cancer* **2002**, *94*, 25–36; b) E. Rivera, *Oncologist* **2003**, *8*, 3–9.
[26] a) J. A. Carrero, H. Vivanco-Cid, E. R. Unanue, *Plos One* **2012**, *7*, e32310; b) Z. F. Walls, H. Gong, R. J. Wilson, *Mol. Pharm.* **2016**, *13*, 1185–1190.
[27] J. C. Lacal, L. Carrasco, *Antimicrob. Agents Chemother.* **1983**, *24*, 273–275.

Received: June 22, 2016
Revised: September 27, 2016
Published online: October 24, 2016

6. Supporting Information

6.1. A Chemoenzymatic Approach to Protein Immobilization onto Crystalline Cellulose Nanoscaffolds

Supporting Information

69451 Weinheim, Germany

A Chemoenzymatic Approach to Protein Immobilization onto Crystalline Cellulose Nanoscaffolds**

Christina Uth, Stefan Zielonka, Sebastian Hörner, Nicolas Rasche, Andreas Plog, Hannes Orelma, Olga Avrutina, Kai Zhang, and Harald Kolmar**

anie_201404616_sm_miscellaneous_information.pdf

Supporting information

1. Materials and Methods

Microcrystalline cellulose (MCC) with granule size of 50 µm was purchased from Sigma-Aldrich. 2,2,6,6-Tetramethylpiperidine-1-oxyl (TEMPO) was obtained from Acros. Dialysis membrane from Spectrum Laboratories Inc. has an approximate molecular weight cut-off of 1000 Daltons.

All chemicals and solvents for the peptide synthesis, analysis, and isolation were used as supplied by Iris Biotech, Bachem, Novabiochem, Sigma-Aldrich, Roth, and Varian (Agilent). Deionized water was used in all experiments. All applied reagents, buffers and enzymes for protein expression and cloning were purchased either from Merck, Roth, Sigma Aldrich, Fermentas or Fluka and, if not mentioned otherwise, used without any further purifications.

1.1 Reversed-phase HPLC

Peptides were analyzed on an analytical RP-HPLC from Varian, model 920-LC using a Phenomenex Hypersil 5u BDS C18 LC column (150 x 4.6 mm, 5 µm, 130 Å), and isolated by semi-preparative RP-HPLC (Varian) using a Phenomenex Luna 5u C18 LC column (250 x 12.2 mm, 5 µm, 100 Å) as stationary phase. Both eluents A (water), and B (90 % aq. acetonitrile) contained 0.1 % aq. trifluoroacetic acid (TFA).

1.2 ESI-MS analysis

ESI mass spectra were collected by a Shimadzu LCMS-2020 equipped with a Phenomenex Jupiter 5u C4 LC column (50 x 1 mm, 5 µm, 300 Å) using an eluent system of 0.1 % aq. formic acid, LC-MS grade (eluent A) and acetonitrile containing 0.1 % aq. formic acid, LC-MS grade (eluent B).

1.3 Conductive titration

The ratio of the surface-exposed carboxylic to carbonyl groups of CNC was determined *via* electric conductivity titration. The content of carboxylic groups was evaluated using 3 ml of aq. CNC suspension where the pH value was adjusted to 2 with 0.1 M HCl. The solution was titrated using a 665 Dosimat (Metrohm) at the dosing rate of 0.01 ml/s, while the conductivity was recorded using an 865 Conductivity Module (Metrohm) with an interval of 2 s. (Fig. S1) In order to determine the content of aldehyde groups, the CNC suspension was oxidized with $NaClO_2$ at ambient temperature and pH 4-5. Then, the total carboxylic groups were titrated again. The difference between pre-oxidized and oxidized CNC was calculated, which is equal to the content of aldehyde groups.

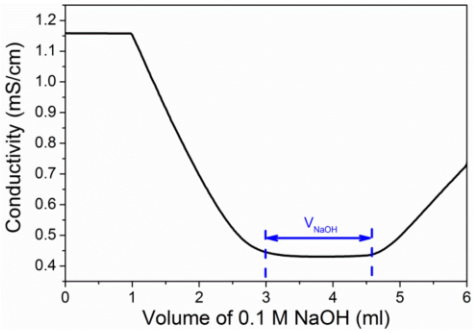

Figure S1. Conductive titration curve of aqueous CNC suspension for the determination of the carboxylic and aldehydic content.

1.4 Flow cytometric analysis

A MoFlo cell sorter (Beckman Coulter, analysis *via* Summit 4.3) was used to analyze properties of CNC-grafted proteins. Target staining was conducted using 15-fold molar excess fluorescein isothiocyanate (FITC) in dimethyl sulfoxide (DMSO) and 1.5 mg hen egg lysozyme.[1] After incubation for 30 min at ambient temperature excess of FITC was removed and the buffer exchanged using a protein desalting spin column (Thermo Scientific) according to the manufacturer's protocol. Quantitation of labeling success was performed spectrophotometrically on a Biospec-nano device (Shimadzu Europa GmbH).

1.5 Confocal Microscopy

Fluorescence micrographs were recorded at a Leica TCS SP5 II using 5 µL of the respective sample (Fig. S12).

1.6 Atomic force microscopy

Atomic force micrographs (AFM, Fig. 4) were obtained using a scanning-force microscope (MFP-3D, Asylum research). The samples were deposited from aqueous solutions on a silicon wafer, dried overnight, and the measurements were conducted with a tapping mode cantilever (Budget sensors, spring constant kc~48 N/m, res. frequency ~190 kHz) in tapping mode. The programs IGOR Pro 6.22A (WaveMetrics Inc.) and Gwyddion (Free Software Foundation, Inc.) were used to guide and analyze the AFM measurements, respectively. The peak-to-peak roughness of the samples was determined by calculating the difference between the peak maximum and minimum. The average value of 20 measured points is shown (Fig. 4).

1.7 Preparation of cellulose nanocrystals (CNC) [2]

5 g microcrystalline cellulose (MCC) were swollen in 50 ml water for 96 h prior to oxidation. Then, MCC was separated *via* centrifugation and re-dispersed in 250 mL water under vigorous stirring. Thereafter, 0.0781 g TEMPO and 0.5144 g NaBr were added to the cellulose suspension and the mixture was stirred for further 30 min. 10.89 mL aqueous (aq.) NaClO were progressively added to the mixture at pH 10. Subsequent to the addition of NaClO, the pH value was maintained at pH 10 by adding 1 M aq. NaOH. After 15 min ultrasonic treatment of the reaction mixture at ambient temperature, additional 10.89 mL aq. NaClO (14 wt. %) were progressively added to the mixture and the oxidation was repeated at pH 10. After the adjustment of the pH value to 7.5 using 1 M aq. HCl, the oxidized cellulose was isolated by centrifugation (15 min, 3800 g), re-dispersed in water and sonicated for 1 h at ambient temperature. Finally, the suspension was dialyzed until the conductivity reached ~1 µS/cm and its volume was adjusted to 200 mL.

1.8 Solid phase peptide synthesis (SPPS) of the peptidic motif

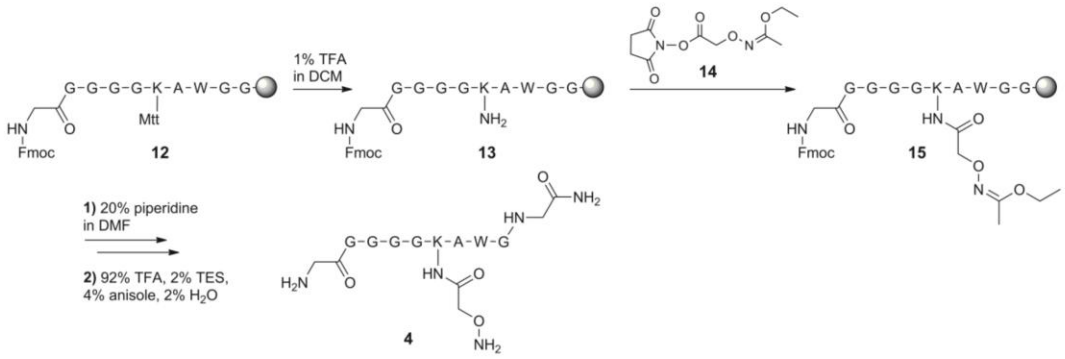

Figure S2. Synthesis of the peptidic motif **4**.

Synthesis of the peptidic motif **4** (Fig. S2) was carried out using standard Fmoc-SPPS on an AmphiSpheres 40 RAM resin (Agilent). Loading of RAM resin was performed manually as follows. After resin swelling and Fmoc deprotection, a solution of 0.29 g of Fmoc-Gly-OH (1 mmol; 4 equiv.) and 697 µL *N,N*-diisopropylethylamine (DIEA, 2 mmol, 8 equiv.) in a minimal amount of dimethylformamide (DMF) was added to the resin. The resulting mixture was shaken for 2 h at ambient temperature. The solution was removed by filtration and the loaded resin was washed five times with DMF.

Canonical amino acids were attached by double coupling using 4 equiv. of the corresponding amino acid, 3.97 equiv. of 2-(1H-benzotriazol-1-yl)-1,1,3,3-tetramethyluronoiumhexafluoro-phosphate (HBTU, 0.9925 mmol) and 8 equiv. of DIEA (2 mmol), or, in the case of Lys(Mtt), 3.97 equiv. of HATU (0.9925 mmol).

Introduction of the aminooxy moiety was performed on resin prior to the final Fmoc deprotection. The methyltrityl protecting group was removed with 1 % TFA in dichloromethane (DCM) and 1.1 equiv. (0.275 mmol, 97 mg) of the *N*-hydroxysuccinimide (NHS) activated aminooxy acetic acid **14** in 5 ml DCM was added and shaken for 3 h at ambient temperature. After the final Fmoc deprotection the peptide was cleaved from the resin using a mixture of TFA, anisole, triethylsilane (TES) and H_2O (92:4:2:2) resulting in **4**. The crude product was purified *via* preparative RP-HPLC and analyzed by analytical RP-HPLC and LC-MS (Fig. S3; S4).

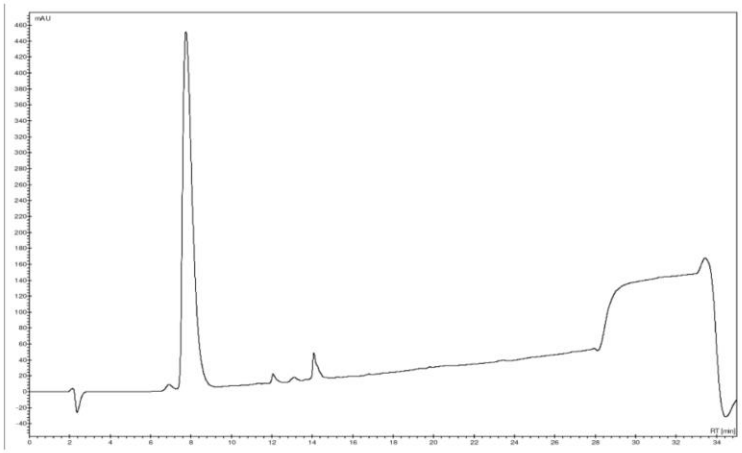

Figure S3. RP-HPLC analysis of **4**, gradient 10 to 60

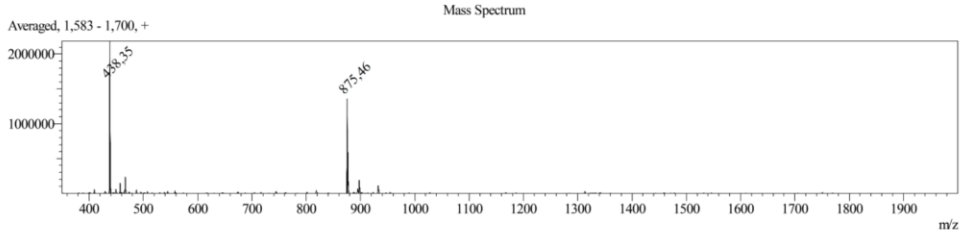

Figure S4. LC-MS analysis of **4**, calc. mass: 874.9 g/mol; meas. m/z: 875.46 $[M+H]^+$, 438.35 $[M+2H]^{2+}$.

Table S1. Elemental analysis of CNC and CNC-peptide conjugate **5**.

sample name	*weight [mg]*	*C/N ratio*	*content [%]*	*peak area*	*day factor*
sample (CU1)	2.851	41.34	N: 0.98 C: 40.5 H: 5.956	792 27393 13153	1.0072 0.9985 1.0244
reference (CU2)	1.78	0.0	N: 0.0 C: 40.22 H: 5.939	0 16874 8089	1.0072 0.9985 1.0244

2. Biological Materials and Methods

2.1 Culture media

dYT-medium (double yeast tryptone medium): 1 % (w/v) yeast extract, 1.6 % (w/v) tryptone/peptone from casein pancreatic digested, 0.5 % (w/v) NaCl

LB-medium (lysogeny broth): 0.5 % (w/v) yeast extract, 1 % (w/v) tryptone/peptone from casein pancreatic digested, 1 % (w/v) NaCl

Table S2. Oligonucleotide sequences for cloning.

Oligonucleotide	*sequence*
pET22b_Lys_vNAR_up	CGCGCGCCATGGATATGGCGCGCGTGGATCAGACC
pET22b_Lys_vNAR_lo	GCGCGCCTCGAGACCGGTTTCCGGCAGTGCGTTCACGGTCACCACGGTGCC
GOase_LPETG-XhoI-lo	GCGCGCCTCGAGGAATTCTTAACCACCGGTTTCCGGCAGCTGAGTAACGCGAATCGTCG
GOase_Eco_up	CGACGTGGAATTCCGTTCGAGG
tGFP Nco up	GCGCGCCCATGGAATCTGATGAA

2.2 Protein expression

E.coli BL21 (DE3) cells containing the respective plasmid were grown at 37 °C to an OD_{600} between 0.7 and 1 in dYT medium containing 100 mg/L ampicillin. Protein expression was induced with 1 mM isopropyl β-D-1 thiogalactopyranoside (IPTG) at 28 °C. After 16 h cells were harvested at 4 °C, 8182 g for 20 min.

2.2.1 Isolation of galactose oxidase from the periplasm of *E. coli* cells

After cell harvesting by centrifugation the pellet was suspended in 20-40 mL periplasm buffer (PPA) and 40 µL hen egg lysozyme in periplasm buffer (100 mg/mL in PPA buffer) were added. The suspension was incubated for 30 min on ice and afterwards sedimented with 21191 g for 15 min at 4 °C, sterilized using a 4.5 µm filter (Filtropur S) and the respective recombinant protein was isolated by metal chelate affinity chromatography (HisTrap, GE Healthcare), equilibrated in PBS, pH 7.4. Protein was eluted using a linear imidazole gradient (0 % - 100 % of 1 M imidazole over 30 min) and analyzed *via* SDS-PAGE (Fig. S7).
Lysozyme vNAR and tGFP were expressed and pelleted as described in section 2.2. Cells were re-suspended in 15 mL PBS and cell disruption was performed at a TS Series Benchtop cell disrupter (Constant Systems Ltd.) at 2.5 kbar. To isolate the soluble protein the cell lysate was centrifuged at 21191 g for 15 min at 4 °C. The supernatant was sterilized using a 4.5 µm filter (Filtropur S) and the respective recombinant protein was isolated by metal chelate affinity chromatography (HisTrap, GE Healthcare), equilibrated in PBS, pH 7.4. Protein was eluted using a linear imidazole gradient (0 % - 100 % of 1 M imidazole over 30 min). The pure protein was analyzed *via* SDS-PAGE (data not shown) and LC-MS (Fig. S5, S6).

2.2.2 evolved sortase A (eSrtA) [3]

E.coli BL21 (DE3) transformed with pET29b eSrtA expression plasmid were cultured at 37 °C in LB containing 50 µg/mL kanamycin until an OD_{600} between 0.6-1. Expression was induced with 0.5 mM IPTG for 3 h at 30 °C. Cells were harvested as described above. The pellet was suspended in 15 mL PBS and cell disruption was performed at a TS Series Benchtop cell disrupter (Constant Systems Ltd.) at 2.5 kbar. To isolate the soluble protein the cell lysate was centrifuged at 21191 g for 15 min at 4 °C. The supernatant was sterilized using a 4.5 µm filter (Filtropur S) and the respective recombinant protein was isolated by metal chelate affinity chromatography (HisTrap, GE Healthcare), equilibrated in PBS, pH 7.4. Protein was eluted using a linear imidazole gradient (0 % - 100 % of 1 M imidazole over 30 min). The pure protein was analyzed *via* SDS-PAGE (data not shown) and LC-MS (Fig. S7).

3. Analytical Data

3.1. tGFP

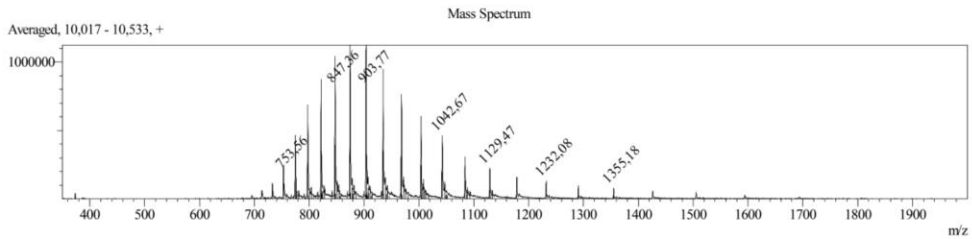

Figure S5. LC-MS analysis of tGFP, calc. mass: 27084.86 g/mol; meas. mass: 27083.52 g/mol, m/z: 847.36 $[M+32H]^{32+}$.

3.2. Lys vNAR

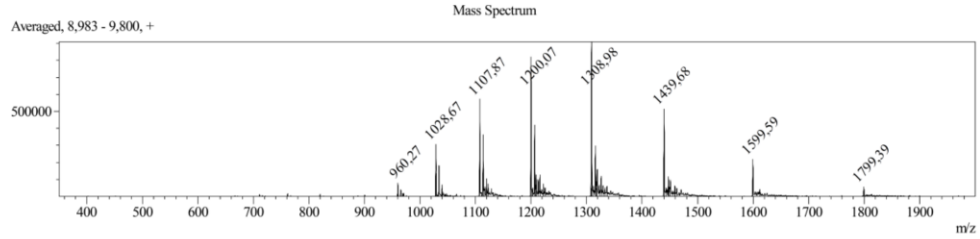

Figure S6. LC-MS analysis of Lys vNAR, calc. mass: 14390.87 g/mol; meas. mass: 14389.31 g/mol, m/z: 1107.87 $[M+13H]^{13+}$.

3.3. Sortase A mut 5

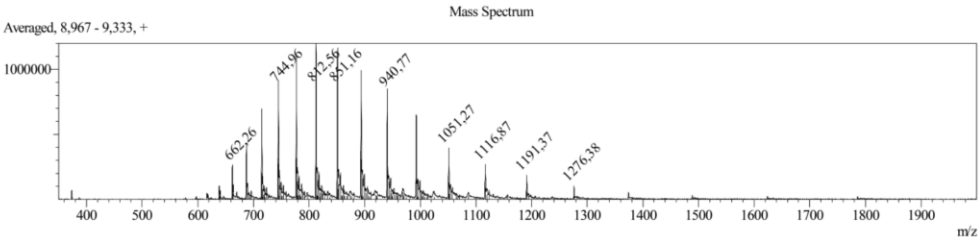

Figure S7. LC-MS analysis of sortase A mut 5, calc. mass: 17853.09 g/mol; meas. mass: 17854.32 g/mol, m/z: 812.56 $[M+22H]^{22+}$.

3.4. GOase

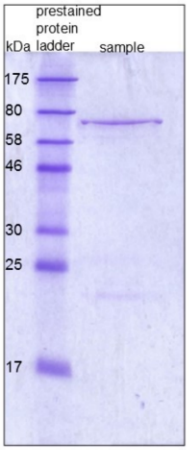

Figure S8. SDS-PAGE of the purified GOase. Prestained protein ladder (New England Biolabs) indicated in kDa.

3.2 Binding kinetics

The equilibrium dissociation constant the modified Lys vNAR **6** was determined on the Octet Red96 system (FortéBio). All assays were performed in kinetics buffer (PBS, pH 7.4, 0.1 % (w/v) bovine serum albumin (BSA), 0.02 % Tween-20) with Streptavidin dip and read biosensors. Sensors were loaded with biotinylated vNAR at approx. 10 µg/mL. Kinetic data sets were fitted using 1:1 Langmuir binding *via* the manufacturer's data analysis software with Savitzky-Golay filtering.

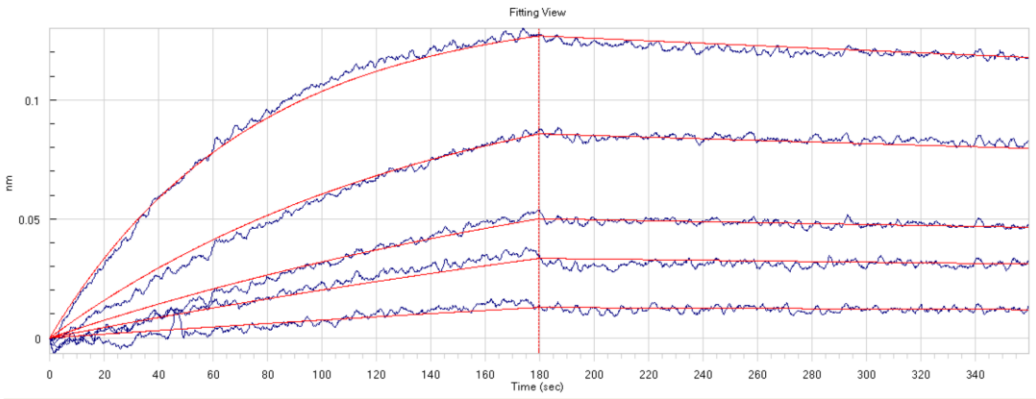

Figure S9. Biolayer interferometry: Fit for the determination of the binding kinetics with the Lys vNAR in concentrations 125 nM, 62.5 nM; 31.25 nM; 15.625 nM; 7.8125 nM top to bottom.

4. Sortase-mediated ligation

Sortase-mediated ligation was performed in 50 mM Tris, 0.15 M NaCl, 5 mM $CaCl_2$ (pH 7.5) using 0.03 equiv (0.1 mg, 5.6 nmol) sortase, 1 equiv. peptide modified CNC, 1 equiv. protein (Tab. S3). The reaction mixture was shaken at 28 °C for 12 h. After completion of the reaction CNCs were sedimented and washed three times with 1 mL Tris/NaCl buffer and four times with 1 mL PBS for further analysis.

Table S3. Sortase-mediated ligation: conditions and components.

	Sample	Negative control 1 (without Ca^{2+})	Negative control 2 (without peptide)	Negative control 3 (without sortase)
CNC-peptide	+	+	-	+
CNC	-	-	+	-
sortase	+	+	+	-
Ca^{2+}	+	-	+	+
EGTA	-	+	-	-
protein	+	+	+	+

5. Activity assay

Activity of galactose oxidase-CNC conjugates was determined by a colorimetric assay. Thus, a stock solution was prepared containing 0.5 mL 2,2'-azino-bis(3-ethylbenzothiazoline-6-

sulphonic acid) (ABTS) (10 mM in H_2O), 5 mL D-galactose (100 mM in H_2O), 50 µL horseradish peroxidase (23 mM) and 9 mL PBS. Each 100 µL of that solution were transferred into wells of a microtiter plate and 2 µL of the respective sample added. After 20 min incubation at ambient temperature the absorbance at $\lambda = 405$ nm was detected at an Elisa-reader (GENios™ Tecan Trading AG) Fig. S10.

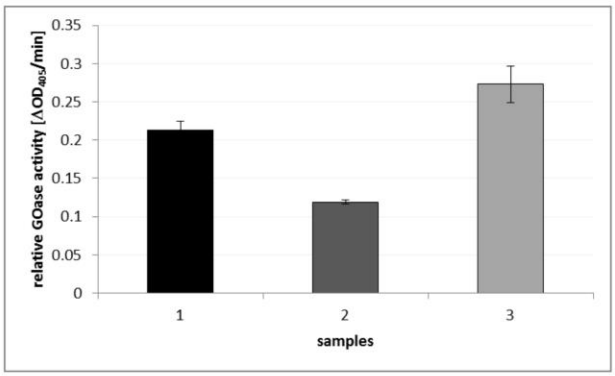

Figure S10. Relative enzyme activity of different samples:
1: conjugate **11** obtained by sortase-mediated ligation; 2: CNC particles with grafted GOase (NHS-mediated loading in equimolar ratio to the surface concentration of the recognition peptide; 3: CNC particles with grafted GOase (NHS in excess). Error bars were calculated from three independent measurements.

5.1 NHS activation of carboxylic groups

NHS activation of the carboxylic groups was conducted in PBS using 12.5 mg CNC, 4 mg *N*-hydroxysuccinimide (NHS) (2 equiv., 0.035 mmol) and 6.6 mg 1-ethyl-3-(3-dimethylaminopropyl)carbodiimid (EDC) (2 equiv., 0.035 mmol). The reaction mixture was shaken for 1 h at ambient temperature and washed three times with PBS to remove the excess of NHS/EDC. For the generation of equimolar amount of NHS activated carboxylic groups compared to the oximated peptide **4**, 25 mg cellulose was reacted with 0.15 mg NHS and 0.2 mg EDC in PBS for 1 h at ambient temperature and washed three times with PBS.

Figure S11. Comparison of protein immobilization using site-directed sortase-mediated coupling (right panel) and random NHS-mediated grafting *via* primary amines (left panel).

6. Flow cytometric analysis

A MoFlo cell sorter (Beckman Coulter, analysis *via* Summit 4.3) was used to analyze conjugation success of either 5FTSC, tGFP or Lys vNAR (Fig. S11 A-C) on CNC surface. Target staining of lysozyme with FITC was performed as described elsewhere.[1]

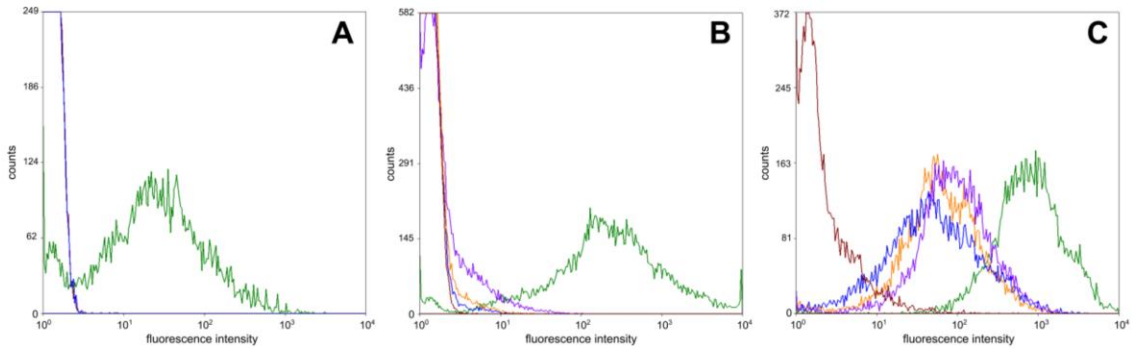

Figure S12. Flow-cytometric analysis of conjugates. **A**: fluorescently labelled CNC`s (red: reference CNC`s; blue: CNC`s with fluorescein-5-carboxylic acid; green: fluorescent CNC`s) **B**: CNC-tGFP conjugate (red: reference CNC`s; blue: without peptide; orange: without sortase; lilac: without $Ca^{2+}$ ; green: CNC-tGFP conjugate) **C**: CNC-Lys vNAR conjugate in complex with FITC labelled hen egg lysozyme (red: reference CNC`s; blue: without peptide; orange: without sortase; lilac: without Ca^{2+} ; green: CNC-Lys vNAR conjugate).

7. Fluorescence micrograph

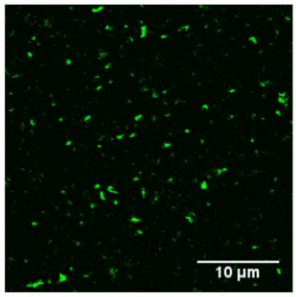

Figure S13. Fluorescence micrograph of CNC-tGFP conjugates **10**. Scale bar 10 µm indicated as white bar.

Literature

[1] G. T. Hermanson, *Bioconjugate techniques*, Academic Press, San Diego, **1996**.
[2] T. Saito, A. Isogai, *Biomacromolecules* **2004**, *5*, 1983-1989.
[3] I. Chen, B. M. Dorr, D. R. Liu, *Proc. Natl. Acad. Sci.* **2011**, *108*, 11399-11404.

6.2. Combination of inverse electron-demand Diels-Alder reaction with highly efficient oxime ligation expands the toolbox of site-selective peptide conjugations

Electronic Supplementary Material (ESI) for ChemComm.

Electronic Supplemental Information (ESI):

Combination of inverse electron-demand Diels-Alder reaction with highly efficient oxime ligation expands the toolbox of site-selective peptide conjugations

S. Hörner,‡ C. Uth,‡ O. Avrutina, H. Frauendorf, M. Wiessler, and H. Kolmar*

Content

1 Experimental

1.1 General

1.1.1 Reagents

All reagents were used as supplied by *Sigma Aldrich, Alfa Aesar,* or *Acros Organics* without further purification. Amino acids and resins for solid-phase peptide synthesis (SPPS) were purchased from *Novabiochem* (brand of *Merck KGaA*, Darmstadt, Germany), *CEM* (Kamp-Lintfort, Germany) or *Iris Biotech* (Marktredwitz, Germany).

1.1.2 Mass spectrometry

Electrospray ionization mass spectrometry (ESI-MS) spectra were obtained using a *Shimadzu LCMS-2020* mass spectrometer equipped with a *Phenomenex Jupiter 5u C4 LC* column (50x1 mm, 5 µm, 300 Å). The eluent system consisted of 0.1% (v/v) aq. formic acid (LC-MS grade, *Sigma-Aldrich* (St. Louis, USA)) (eluent A) and acetonitrile containing 0.1% (v/v) formic acid (LC-MS grade, *Karl Roth GmbH*, Karlsruhe, Germany)) (eluent B).

ESI-HRMS measurements were performed on a maXis Q-TOF mass spectrometer (Bruker Daltonik) equipped with an electrospray ion source. 2 µL solution of the dissolved analytes were injected (autoinjector G1313A, Agilent) and transferred into the ion source together with methanol (flow 0.2 mL/min) provided by a pump (G1311A, Agilent). Electrospray mass spectra were measured in the positive ion mode. Mass calibration using a mixture of calibrants (Agilent) was applied. Compound 31: ESI(+)-HRMS was carried on a FTICR mass spectrometer (APEX IV, Bruker Daltonik). Analyte solution was introduced into the electrospray ion source *via* a syringe pump. MALDI mass spectra were acquired applying a MALDI-TOF instrument Autoflex (Bruker). 2,5-dihydroxy benzoic acid (DHB) was used as a matrix.

1.1.3 Liquid chromatography

Analytical reversed-phase high performance liquid chromatography (RP-HPLC) was performed on a *Varian 920 LC* equipped with a *Phenomenex Luna Hypersil* 5u BDS C_{18} LC column (5 u, 130 Å, 150×4.60 mm, 5 µm) at a flow rate of 1 mL/min. For isolation of peptides by semi-preparative RP-HPLC a *Varian 940 LC* equipped with a preparative C_{18} column (*Phenomenex Luna* 5u C_{18} (250×20 mm; S-4 µm, 8 nm)) was used. At a flow rate of 18 mL/min, 5 min of isocratic flow (starting concentration of eluent B) was followed by 20 min of gradient flow. Eluent A: with 0.1% (v/v) aq. trifluoroacetic acid (TFA), eluent B: 90% (*v*/*v*) aq. MeCN with 0.1% (*v*/*v*) TFA. Absorption was measured by an UV/VIS detector at 220 nm and 280 nm or 220 nm and 534 nm.

1.2 Synthetic procedures:

1.2.1 Synthesis of compound 1

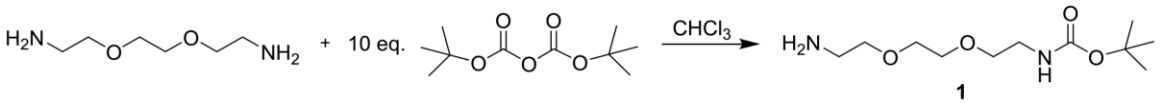

To a cooled solution (0°C) of 30.0 g (202.5 mmol) 2'2-(ethylenedioxy)bis(ethylamine) in 200 mL chloroform, a solution of 4.425 g (20.3 mmol) di-*tert.*-butyl dicarbonate in 200 mL chloroform was drop-wise added under inert atmosphere (N_2). After complete addition, the mixture was allowed to warm to ambient temperature and then stirred overnight. The organic solvent was removed and the colorless liquid was dissolved in 300 mL deionized water. It was extracted three times with each 100 mL methylene chloride. The combined organic phases were washed with 100 mL brine and dried over $MgSO_4$. The solvent was removed resulting in 4.74 g of turbid, colorless oil (yield: 94.1%).

^{1}H-NMR: (300 MHz, DMSO-d_6) δ: 1.37 (s, 9H), 2.63 (t, *J*=5.8 Hz, 2H), 3.05 (q, *J*=6.1 Hz, 2H), 3.35 (t, *J*=5.7 Hz, 2H), 3.38 (t, *J*=6.1 Hz, 2H), 3.49 (s, 4H).

1.2.2 Synthesis of compound 2

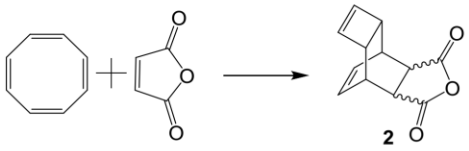

Reppe anhydride **2** was synthesized as described in reference **1**. 5 g (48 mmol) cyclooctatetraene and 4.708 g (48 mmol) maleic anhydride were converted in 1,2-dichlorobenzene. The crude product had a melting point of 162°C (lit. 165-168°C). It was purified by sublimation on high vacuum resulting in 6.123 g of colorless crystals with a melting point of 167°C (yield: 63%).

^{1}H-NMR (500 MHz, DMSO-d_6) δ: 2.81 (s, 2H), 3.04 (s, 2H), 3.25 (s, 2H), 5.89 (s, 2H), 5.97 (dd, *J*=4.6 Hz, 2H).

^{13}C-NMR (125 MHz, DMSO-d_6) δ: 36.42, 42.68, 43.71, 128.90, 138.10, 173.72.

1.2.3 Synthesis of compound 3

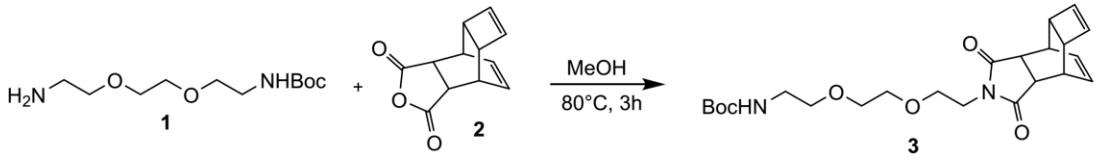

To obtain compound **3**, 0.870 g (1.1 eq., 3.54 mmol) Boc-PEG **1** were reacted with 0.651 g (1 eq., 3.22 mmol) Reppe anhydride **2** in 80 mL MeOH. The reaction mixture was heated for 3 h at 80°C under reflux. As the TLC analysis verified the completion of the reaction, the solution was cooled down and methanol was evaporated under reduced pressure. The crude product was dissolved in water and extracted twice with each 30 mL diethyl ether. The organic phase was dried over $MgSO_4$ and the solvent was removed. 1.1 g of compound **3** were obtained (yield: 82%).

^{1}H-NMR (300 MHz, $CDCl_3$) δ: 1.376 (s, 9H), 2.715 (s, 2H), 2.744 (s, 2H), 3.092 (m, 2H), 3.242 (t, *J*=5.6 Hz, 2H), 3.443 (m, 2H), 3.489 (m, 2H), 3.549 (m, 2H), 5.804 (m, 4H), 5.818 (s, 2H).

ESI-MS calc. for $C_{23}H_{32}N_2O_6$ 432.23; meas.: 433.4 $[M+H]^+$.

1.2.4 Synthesis of compound 4

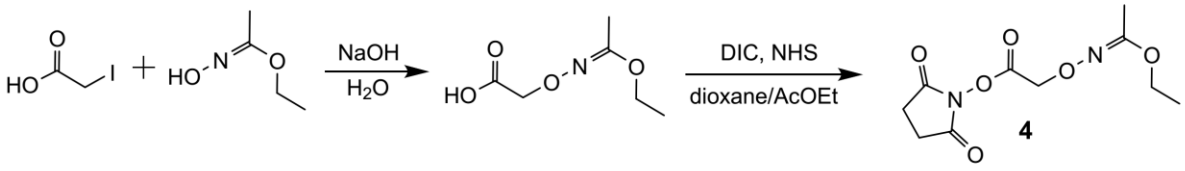

Synthesis of compound **4** was performed as described in reference **2**. 15 g (80.7 mmol) iodoacetic acid were dissolved in 30 mL deionized water and 5 mL aq. NaOH (40% (*w*/*w*)) were slowly added at 0°C. The solution was allowed to warm to ambient temperature. 9.56 g (92.8 mmol) ethyl-acetohydroxamate were added drop-wise to the stirring solution followed by the addition of 7.5 mL aq. NaOH (40% (*w*/*w*)) and 20 mL deionized water. The mixture was heated to 80°C for four hours. During this time, the pH was retained above pH 12 using aq. NaOH (40% (*w*/*w*)). The yellow solution was cooled down to ambient temperature and 100 mL deionized water were added. The solution was washed twice with each 50 mL methylene chloride. The pH of the solution was adjusted to pH 2.0 using 1 M aq. hydrochloric acid. The solution was extracted four times with each 50 mL methylene chloride. Between the extraction steps, the pH was adjusted to pH 2.0 using 1 M aq. hydrochloric acid. The combined organic phases were washed with 50 mL brine and dried over $CaSO_4$. Evaporation of the solvent resulted in 6.98 g colorless oil (yield: 53.8%). This compound is the precursor for compound **4**.

^{1}H-NMR (300 MHz, DMSO-d_6) δ: 1.26 (t, *J*=6.8 Hz, 3H), 2.01 (s, 3H), 4.00 (q, *J*=7.0 Hz, 2H), 4.49 (s, 2H).

^{13}C-NMR (75 MHz, DMSO-d_6) δ: 13.95, 14.21, 62.68, 70.11, 164.73, 175.45.

The colorless oil (6.98 g, 43.2 mmol) and 4.973 g (43.2 mmol) *N*-hydroxysuccinimide were dissolved in a mixture containing 100 mL dioxane and 120 mL AcOEt. The solution was cooled to 0°C and 6.69 mL (5.452 g, 43.2 mmol) *N*,*N*′-diisopropylcarbodiimide (DIC) were added drop-wise. After complete addition the cooled mixture was stirred for additional 30 min and was afterwards allowed to warm to ambient temperature and stirred overnight. The white precipitate was separated by filtration and the solvent was reduced to a volume of 50 mL *in vacuo*. The colorless precipitate was removed by filtration and the remaining solvent was removed. The colorless oil was dissolved in 200 mL chloroform and washed three times with each 40 mL aq. $NaHCO_3$ (5% (*w*/*w*)) and three times with each 40 mL brine. The organic phase was dried over $MgSO_4$. After removing the solvent a colorless oil containing a white precipitate was obtained. The precipitate was removed by filtration using a syringe equipped with a Teflon filter. 8.421 g colorless oil were obtained which crystallized quickly upon freezing at -20°C (yield: 75.5%). Compound **4** should be stored sealed below -20°C.

^{1}H-NMR (300 MHz, DMSO-d_6) δ: 1.26 (t, *J*=7.0 Hz, 3H), 2.01 (s, 3H), 2.84 (s, 4H), 4.02 (q, *J*=7.1 Hz, 2H), 4.78 (s, 2H).

^{13}C-NMR (75 MHz, DMSO-d_6) δ: 13.89, 14.23, 25.57, 62.76, 68.51, 164.77, 165.70, 168.74.

ESI-MS calc. for $C_{10}H_{14}N_2O_6$ m/z: 258.09 meas. 259.05 $[M+H]^+$.

1.2.5 Synthesis of compound 5

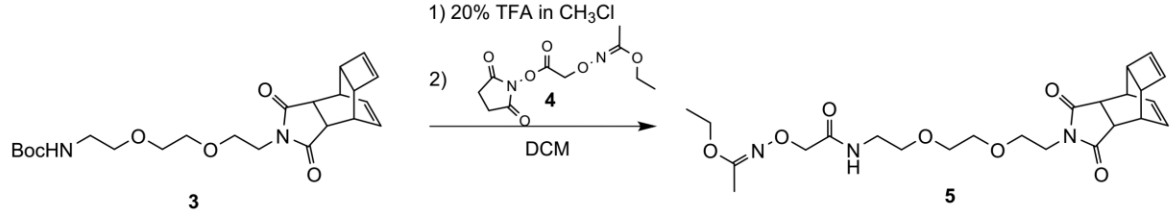

The deprotection of the Boc group was conducted in 20% TFA in chloroform for 1 h at ambient temperature. As LC-MS analysis confirmed the complete Boc elimination, TFA was removed under reduced pressure. 0.8 g (1.0 eq., 1.85 mmol) of the deprotected Reppe-PEG **3** were reacted with 1.01 g (2.0 eq., 3.7 mmol) NHS activated aminooxy building block **4** in 30 mL dichloromethane for 16 h at ambient temperature. After complete reaction dichloromethane was removed under reduced pressure and the crude product was dissolved in deionized water. The aqueous solution was extracted thrice with chloroform. The organic phase was dried over $MgSO_4$ and the solvent evaporated *in vacuo*. Final purification was done by flash column chromatography, applying an isocratic DCM:MeOH (9.5:0.5) mixture giving 0.167 g light yellow oil (yield: 19%).

^{1}H-NMR (300 MHz, $CDCl_3$) δ: 1.196 (t, *J*=7.1 Hz, 3H), 1.918 (s, 3H), 2.713 (s, 2H), 2.745 (s, 2H), 3.087 (s, 2H), 3.484 (m, 12H), 3.912 (q, *J*=7.0 Hz, 2H), 4.299 (s, 2H), 5.799 (q, *J*=4.6 Hz 2 H), 5.819 (s, 2 H).

ESI-MS calc. for $C_{24}H_{33}N_3O_7$ m/z: 475.24 meas. 476.45 $[M+H]^+$.

1.2.6 Synthesis of compound 6

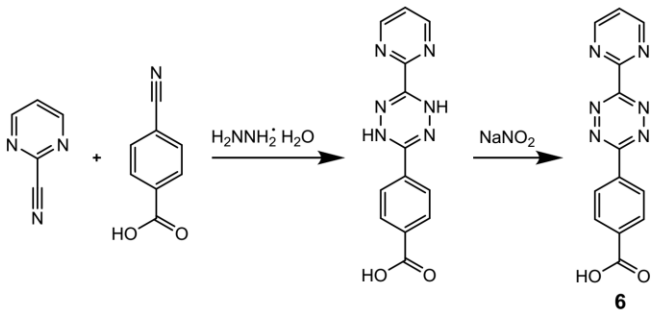

Compound **6** was synthesized according to reference **3**. 5 g (47.57 mmol) 2-pyrimidine-carbonitrile and 7 g (47.57 mmol) 4-cyanobenzoic acid were employed as described in reference **3**. 2.915 g of a yellow solid were obtained (yield: 21.7%). This substance is the precursor for compound **6**.

^{1}H-NMR (300 MHz, DMSO-d_6) δ: 7.61 (t, *J*=4.9 Hz, 1H), 7.93 (d, *J*=9.6 Hz, 2H), 8.00 (d, *J*=8.4 Hz, 2H), 8.83 (s, 1H), 8.92 (d, *J*=4.8 Hz, 2H), 9.52 (s, 1H).

^{13}C-NMR (75 MHz, DMSO-d_6) δ: 122.09, 126.27, 129.41, 132.20, 133.65, 145.62, 146.64, 155.89, 157.67, 166.72.

2.8 g (9.9 mmol) of the yellow solid were oxidized as described in reference **3**. 2.37 g of purple solid **6** were obtained (yield: 85.5%).

^{1}H-NMR (300 MHz, DMSO-d_6) δ: 7.83 (t, *J*=4.4 Hz, 1H), 8.24 (d, *J*=8.5 Hz, 2H), 8.68 (d, *J*=8.5 Hz, 2H), 9.17 (d, *J*=4.8 Hz, 2H)

^{13}C-NMR (75 MHz, DMSO-d_6) δ: 123.00, 128.31, 130.23, 134.63, 135.25, 158.50, 159.01, 162.89, 163.16, 166.68.

1.2.7 Synthesis of compound 7

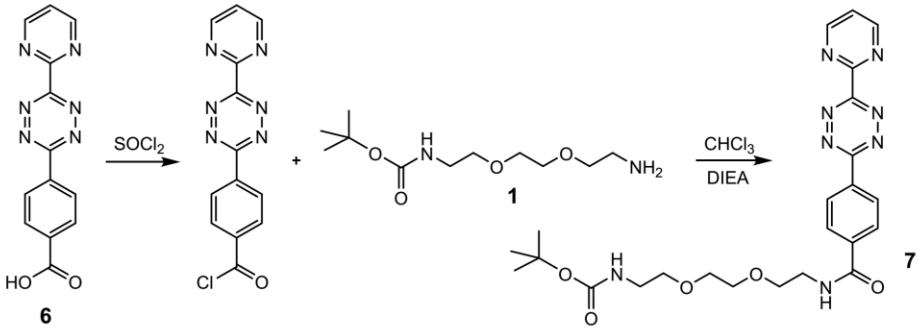

0.62 g (2.08 mmol) of compound **6** were suspended in 10 mL thionyl chloride and 10 drops of DMF were added. The setup was equipped with a dry pipe filled with $MgSO_4$. The mixture was stirred for three hours at 90°C. Afterwards the mixture was allowed to cool to ambient temperature and the excess of thionyl chloride was removed *in vacuo*.

The residue was dissolved in 100 mL chloroform and 1.445 mL (1.072 g, 8.3 mmol) *N*,*N*'-diisopropylethylamine (DIEA) were added. The mixture was cooled to 0°C. 1.031 g

(4.16 mmol) of compound **1** were dissolved in 10 mL chloroform and the solution was added drop-wise. The setup was equipped with a dry pipe filled with $MgSO_4$ and the mixture was stirred overnight at ambient temperature. The reaction mixture was washed five times with each 30 mL deionized water and the organic phase was dried over $MgSO_4$. After removing the solvent the purple residue was purified by flash column chromatography using the solvent mixture EtOH:DCM 1:9 (*v*:*v*) (R_f=0.44). 0.452 g purple solid were obtained (yield: 42.6%).

^{1}H-NMR (500 MHz, $CDCl_3$) δ: 1.35 (s, 9H), 3.25 (d, *J*=4.2 Hz, 2H), 3.50 (s, 2H), 3.59 (s, 2H), 3.60 (s, 2H), 3.66 (s, 4H), 4.94 (s, 1H), 6.94 (s, 1H), 7.54 (t, *J*=4.9 Hz, 1H), 7.99 (d, *J*=9.4 Hz, 2H), 8.73 (d, *J*=5.0 Hz, 2H), 9.07 (d, *J*=4.8 Hz, 2H).

^{13}C-NMR (125 MHz, $CDCl_3$) δ: 28.40, 39.97, 40.28, 70.34, 122.58, 128.05, 128.92, 133.88, 138.79, 158.45, 159.46, 163.18, 164.04, 166.51.

ESI-MS calc. for $C_{24}H_{30}N_8O_5$ m/z: 510.24 meas. 511.45 $[M+H]^+$.

1.2.8 Synthesis of compound 8

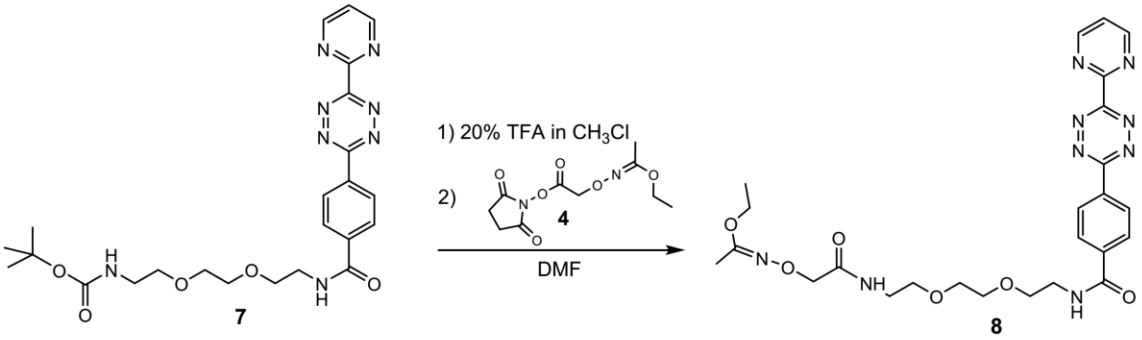

0.452 g (0.885 mmol) of compound **7** were dissolved in 5 mL 20% TFA (*v*:*v*) in chloroform. After two hours at ambient temperature, complete deprotection of compound **7** was confirmed by thin-layer chromatography (TLC). The solvent was removed and a purple oil containing residual TFA was obtained. To remove remaining TFA, the oil was dissolved in a mixture of methanol and cyclohexane and the solvent was removed *in vacuo*. After several steps, the remaining oil was dissolved in water and dried by lyophilization. The purple solid was dissolved in 60 mL DMF and 0.462 mL (0.343 g, 2.66 mmol) DIEA were added. 0.457 g (1.77 mmol) of compound **4** were dissolved in 10 mL DMF and were added drop-wise to the mixture. After complete addition, the mixture was stirred for additional three hours at ambient temperature. The solvent was removed in high vacuum and the excess of DIEA was removed thoroughly. The remaining purple oil was dissolved in 70 mL deionized water and the aqueous phase was extracted twice with each 30 mL chloroform. The solvent was removed and 0.584 g of a purple solid were obtained which was purified by flash column chromatography using the solvent mixture DCM:MeOH (9.5:1 (*v*:*v*)) (R_f=0.59). 0.302 g of yellow solid were obtained (yield: 61.2%).

^{1}H-NMR (500 MHz, $CDCl_3$) δ: 1.18 (t, *J*=7.2 Hz, 3H), 1.90 (s, 3H), 3.44 (q, *J*=5.0 Hz, 2H), 3.53 (t, *J*=5.0 Hz, 2H), 3.59 (m, 4H), 3.65 (m, 4H), 3.89 (q, *J*=7.2 Hz, 2H), 4.28 (s, 2H), 6.64 (s, 1H), 6.99 (s, 1H), 7.54 (t, *J*=4.8 Hz, 1H), 8.00 (d, *J*=8.5 Hz, 2H), 8.74 (d, *J*=8.5 Hz, 2H), 9.08 (d, *J*=4.8 Hz, 2H)

^{13}C-NMR (125 MHz, $CDCl_3$) δ: 13.85, 14.28, 38.59, 39.97, 62.69, 69.80, 69.91, 70.24, 70.36, 72.85, 122.60, 128.07, 128.91, 133.88, 138.74, 158.45, 159.44, 163.19, 164.02, 166.51, 170.50.

RP-HPLC, 10→100% B, t_R=12.62 min.

ESI-MS calc. for $C_{25}H_{31}N_9O_6$ m/z: 553.25 meas. 554.46 $[M+H]^+$.

Deprotection of compound **8** towards **8a**:

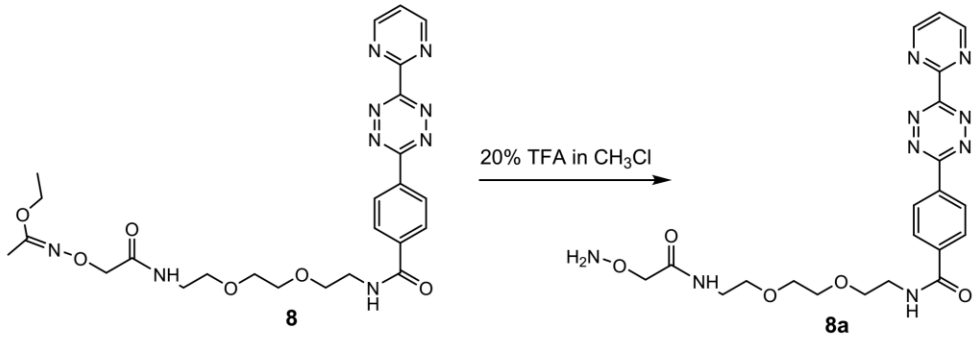

For deprotection of compound **8** it was dissolved in 20% (*v*:*v*) TFA in chloroform and stirred for 120 min at ambient temperature (the deprotected compound forms a second phase). The solvent was removed and residual TFA removed by dissolving the purple oil in water followed by lyophilization.

RP-HPLC, 10→100% B, t_R=9.11 min.

ESI-MS calc. for $C_{21}H_{25}N_9O_5$ m/z: 483.20 meas. 484.45 $[M+H]^+$.

1.2.9 Microwave-assisted solid-phase peptide synthesis (SPPS) of peptides 9-14

Microwave-assisted Fmoc-SPPS was performed on a CEM *liberty*® peptide synthesizer equipped with a CEM *discover*® SPS microwave (CEM GmbH) using DMF as solvent. As solid supports 2-chlorotrityl resin from Iris Biotech GmbH (peptides **9**, **10**, **12**, and **13**) and AmphiSphere™ 40 RAM resin from Varian Inc. (peptides **11** and **14**) were used. Triple coupling of the amino acids and double deprotection was performed upon microwave assistance. For all amino acids except arginine, coupling was performed at 30 W and 50°C for 15 min. Coupling of arginine was performed at ambient temperature for 60 min. Deprotection was performed at 30 W at 50°C for 5 min). Each amino acid was attached using 4 eq. of the respective Fmoc-protected amino acid, 3.9 eq. of *O*-(benzotriazol-1-yl)-*N,N,N′,N′*-tetramethyluronium hexafluorophosphate (HBTU) (*Iris Biotech* GmbH), and 8 eq. base (DIEA for all amino acids except cysteine; for coupling of Fmoc-S-trityl-L-cysteine, collidine (*Sigma-Aldrich*) was used).

1.2.10 Peptide cleavage and workup

All peptides were cleaved from the resin using 92% (*v*:*v*) trifluoroacetic acid (TFA), 2% (*v*:*v*) H_2O, 4% (*v*:*v*) triethylsilane (TES), and 2% (*v*:*v*) anisole. In case of cysteine-containing

peptides, a spatula tip of dithiothreitol (DTT) was added to the cleavage cocktail. After shaking 2 h at room temperature, the solution was filtered and injected into ice-cold diethyl ether. The mixture was cooled down to -20°C for one hour and the precipitate was separated by centrifugation. The supernatant was discharged and the precipitate resuspended in ice-cold diethyl ether. The procedure was repeated additionally two times and the precipitate was dried in a desiccator. The obtained solid was dissolved in 10% (*v*:*v*) aqueous MeCN and the solvent was removed by lyophilization resulting in a fluffy consistency of the solid.

1.2.11 Oxidation of *N*-terminal serine residues

Cysteine-free crude products were oxidized using 10 eq. of sodium periodate in PBS buffer for 10 min. The reaction product was isolated by RP-HPLC using a Varian 940-LC equipped with a YMC Europe GmbH C_{18} column (250 × 20mm; S- 4 µm, 8 nm). Thereby, aldehyde-bearing peptides **9**, **12**, and **13** were obtained. For the synthesis of aldehyde-bearing folded peptides **10**, **11** and **14**, oxidative folding was followed by the above-described periodate oxidation procedure and by RP-HPLC purification.[4,5] The structures of all synthesized peptides are given in scheme ESI-2.

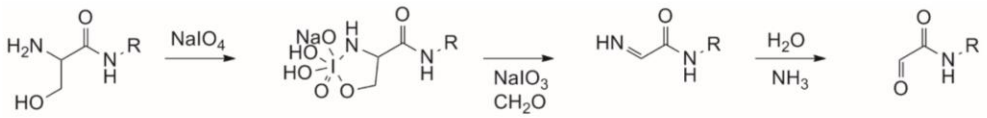

Scheme ESI-1: *Mechanism of periodate oxidation of N-terminal serine residues.*

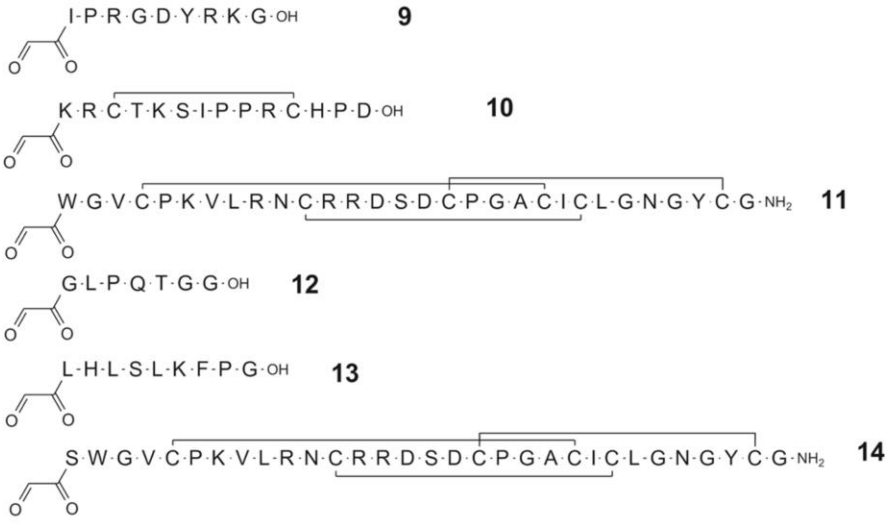

Scheme ESI-2: *Bioactive peptides **9-14** equipped with aldehyde functionality.*

Table ESI-1: *Analytical data of compounds **9-14**.*

Compound	HPLC gradient	t_R [min]	Formula and calculated molar mass	ESI-MS measured	Yield
9	10→100 B	13.22	$C_{48}H_{76}N_{16}O_{15}$ 1116.57	1117.8 $[M+H]^+$, 559.5 $[M+2H]^{2+}$, 373.2 $[M+3H]^{3+}$.	43%

10	10→100 B	11.54	$C_{70}H_{114}N_{24}O_{21}S_2$ 1690.80	846.9 $[M+2H]^{2+}$, 571.0 $[M+3H+H_2O]^{3+}$, 428.5 $[M+4H+H_2O]^{4+}$.	12.5%
11	10→100 B	14.27	$C_{134}H_{206}N_{44}O_{40}S_6$ 3263.38	1642.89 $[M+2H+H_2O]^{2+}$, 1095.57 $[M+3H+H_2O]^{3+}$, 821.86 $[M+4H+H_2O]^{4+}$.	16.3%
12	10→100 B	10.76	$C_{28}H_{45}N_9O_{11}$ 683.32	684.4 $[M+H]^{+}$, 702.4 $[M+H+H_2O]^{+}$.	32%
13	10→100 B	15.06	$C_{51}H_{78}N_{12}O_{13}$ 1066.58	1085.87 $[M+H+H_2O]^{+}$, 543.55 $[M+2H+H_2O]^{2+}$.	23.8%
14	10→100 B	13.56	$C_{137}H_{211}N_{45}O_{42}S_6$ 3350.41	1686.39 $[M+2H+H_2O]^{2+}$, 1124.67 $[M+3H+H_2O]^{3+}$, 843.76 $[M+4H+H_2O]^{4+}$.	18.1%

1.2.12 General procedure for oxime ligation of inverse electron-demand Diels-Alder building blocks 5 and 8 to peptides 9-14

Each 1 eq. of the aldehyde-bearing peptides **9-14** and varying equivalents of the aminooxy-bearing inverse electron-demand Diels-Alder building blocks **5** and **8** were mixed in 50% (*v*:*v*) aq. TFA and the mixture was shaken overnight at ambient temperature. The TFA was removed under reduced pressure and the aqueous solution was purified by semi-preparative HPLC. Reaction details are listed in table ESI-1 and table ESI-2. The structures of peptides **15-20** equipped with inverse electron-demand Diels-Alder functional groups are shown in scheme ESI-3.

Table ESI-2: *reaction details of the synthesis of bioactive peptides* ***15-17*** *equipped with inverse electron-demand Diels-Alder functionality.*

Synthesis of:	Peptide no.	# mg peptide	# mmol peptide	# equiv. of **8**	# mg of **8**	# mmol of **8**	Yield [mg]	Yield [%]
15	9	2.0	0.0018	5.0	5.0	0.0090	1.4	49.4
16	10	10.0	0.0059	5.0	16.4	0.0030	1.7	13.3
17	11	13.0	0.0040	5.0	10.9	0.0198	2.0	13.6

Table ESI-3: *reaction details of the synthesis of bioactive peptides* ***18-20*** *equipped with inverse-electron-demand Diels-Alder functionality.*

Synthesis of	Peptide no.	# mg peptide	# mmol peptide	# equiv. of **5**	# mg of **5**	# mmol of **5**	Yield [mg]	Yield [%]
18	12	19.0	0.0278	1.2	15.4	0.0334	3.0	10.1
19	13	10.0	0.0092	1.2	5.1	0.0110	1.4	10.3
20	14	8.0	0.0024	1.5	1.7	0.0036	0.8	8.9

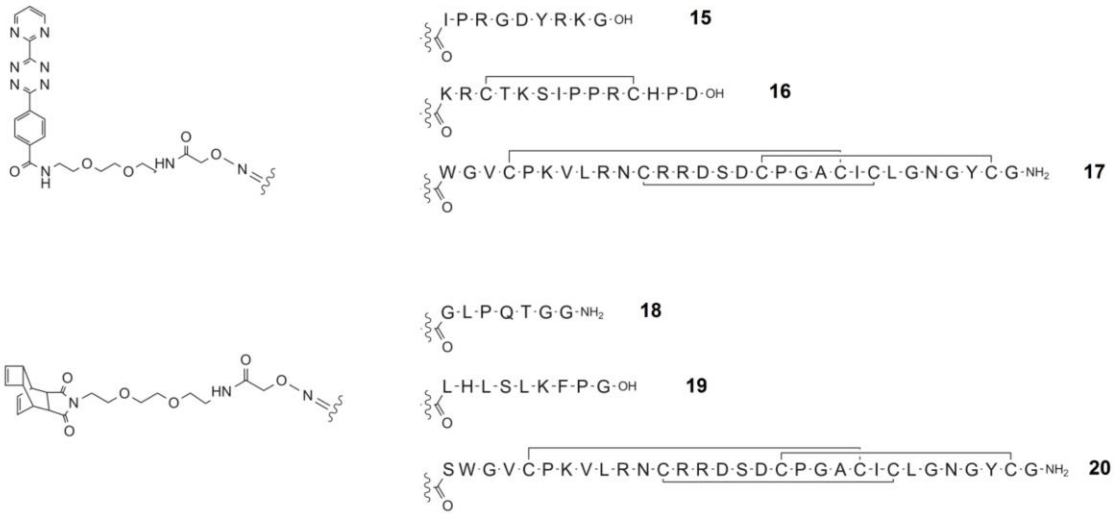

Scheme ESI-3: *Inverse electron-demand Diels-Alder building blocks grafted to diverse bioactive peptides.*

Table ESI-4: *Analytical data of compounds **15**-**20**.*

Compound	HPLC gradient	t_R [min]	Formula and mass calculated	MS type	MS measured
15	10→100 B	12.98	$C_{69}H_{99}N_{25}O_{19}$ 1581.7549	ESI-HR-MS	791.8851 $[M+2H]^{2+}$, 528.2598 $[M+3H]^{3+}$.
16	10→100 B	12.20	$C_{91}H_{137}N_{33}O_{25}S_2$ 2155.9905	ESI-HR-MS	1079.0016 $[M+2H]^{2+}$, 719.6713 $[M+3H]^{3+}$ 540.0067 $[M+4H]^{4+}$.
17	10→100 B	14.67	$C_{155}H_{229}N_{53}O_{44}S_6$ 3728.5635	ESI-HR-MS	1243.8574 $[M+3H]^{3+}$, 933.1459 $[M+4H]^{4+}$.
18	10→100 B	14.78	$C_{48}H_{70}N_{12}O_{16}$ 1070.5033	ESI-HR-MS	1071.5077 $[M+H]^{+}$, 1093.4910 $[M+Na]^{+}$, 536.2598 $[M+2H]^{2+}$, 547.2502 $[M+H+Na]^{2+}$.
19	10→100 B	16.72	$C_{71}H_{103}N_{15}O_{18}$ 1453.7606	ESI-HR-MS	1454.7668 $[M+H]^{+}$, 727.8883 $[M+2H]^{2+}$.
20	10→100 B	15.07	$C_{157}H_{236}N_{48}O_{47}S_6$ 3737.5877	ESI-HR-MS	1246.8713 $[M+3H]^{3+}$, 935.4055 $[M+4H]^{4+}$.

1.2.13 Synthesis of compound 30

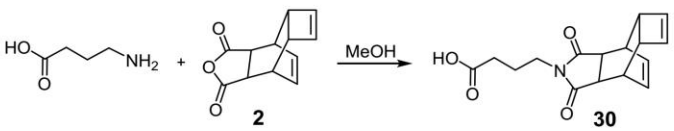

0.51 g (4.94 mmol) 4-aminobutyric acid and 0.5 g (2.47 mmol) of compound **2** were suspended in 10 mL methanol. The mixture was stirred for two hours at 100°C. After cooling down to ambient temperature, the solvent was removed *in vacuo*. The colorless solid was

purified by flash column chromatography by using a solvent mixture of toluene and methanol in a ratio of 9:1 (*v*:*v*) (R_f=0.43). 472.1 mg of a colorless solid were obtained (yield: 66.6%).

^{1}H-NMR (300 MHz, DMSO-d_6) δ: 1.60 (q, *J*=7.1 Hz, 2H), 2.13 (t, *J*=7.5 Hz, 2H), 2.80 (s, 2H), 2.85 (s, 2H), 2.98 (s, 2H), 3.31 (t, *J*=6.7 Hz, 2H), 5.80 (d, *J* =4.5 Hz, 2H), 5.88 (d, *J* =4.5 Hz, 2H).

^{13}C-NMR (75 MHz, DMSO-d_6) δ: 22.61, 30.80, 36.21, 37.06, 42.62, 43.58, 128.03, 137.93, 173.73, 178.50.

1.2.14 Synthesis of compound 31

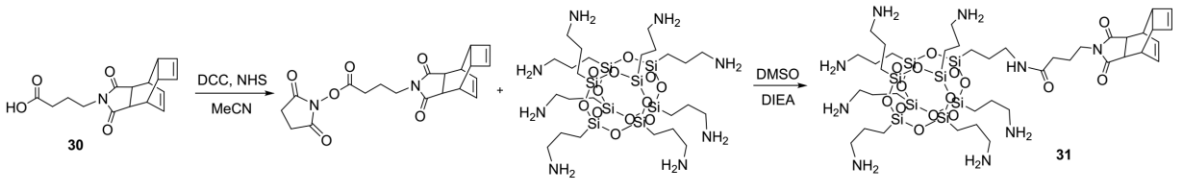

0.1 g (0.348 mmol) of compound **30** were dissolved in 5 mL dry acetonitrile and the solution was cooled to 0°C. 0.121 mL (0.09 g, 0.696 mmol) DIEA were added to the cooled solution. 0.093 g (0.452 mmol) dicyclohexylcarbodiimide (DCC) and 0.06 g (0.522 mmol) *N*-hydroxysuccinimide (NHS) were dissolved in 3 mL acetonitrile and were added drop-wise to the cooled solution. After complete addition, the mixture was stirred for one hour on ice and afterwards stirred at ambient temperature overnight. The colorless precipitate was separated by filtration. The solvent was removed *in vacuo* and the colorless solid dissolved in 40 mL dry DMSO. 1.225 g (1.044 mmol) of octammonium POSS (Hybrid Plastics) were dissolved in 10 mL dry DMSO. To this vigorously stirred solution, activated compound **30** was added drop-wise at ambient temperature and after complete addition, the mixture was stirred overnight. The solvent was removed by lyophilization and the colorless oil was purified by semi-preparative RP-HPLC (gradient: 10→100). The solvent was removed by lyophilization and 0.113 g of a white solid were obtained (yield: 28.3%).

RP-HPLC, 10→100% B, t_R=12.64 min.

ESI-HR-MS calc. for $C_{40}H_{79}N_9O_{15}Si_8$ 1149.3850 meas. 575.7000 $[M+3H]^{3+}$, 384.1356 $[M+4H]^{4+}$.

1.2.15 General procedure for inverse electron-demand Diels-Alder reactions of peptides 15-20

Inverse electron-demand Diels-Alder functional groups grafted peptides **15** to **20** were dissolved in 10% aq. acetonitrile containing 0.1% TFA at a concentration of 10 mg/mL (*w*:*v*). Equimolar amounts were mixed according to table ESI-5 and were shaken at ambient temperature overnight. The reaction is schematically shown in scheme ESI-4. The reaction mixtures were analyzed by RP-HPLC and the turnover was determined by comparing the area of the absorption at 220 nm corresponding to the peptides **15** to **20** before and after the reaction. The HPLC-traces of the reactions are shown in figure ESI-1 and ESI-2. The

reaction products of the Diels-Alder reaction with inverse electron-demand (DAR_{inv}) reactions are shown in scheme ESI-5.

		Peptides		
		15	**16**	**17**
Peptides	**18**	**21**	**24**	**27**
	19	**22**	**25**	**28**
	20	**23**	**26**	**29**

Table ESI-5: *Overview of the DAR_{inv} building block bearing bioactive peptides **15-20** and the formed reaction products **21-29**.*

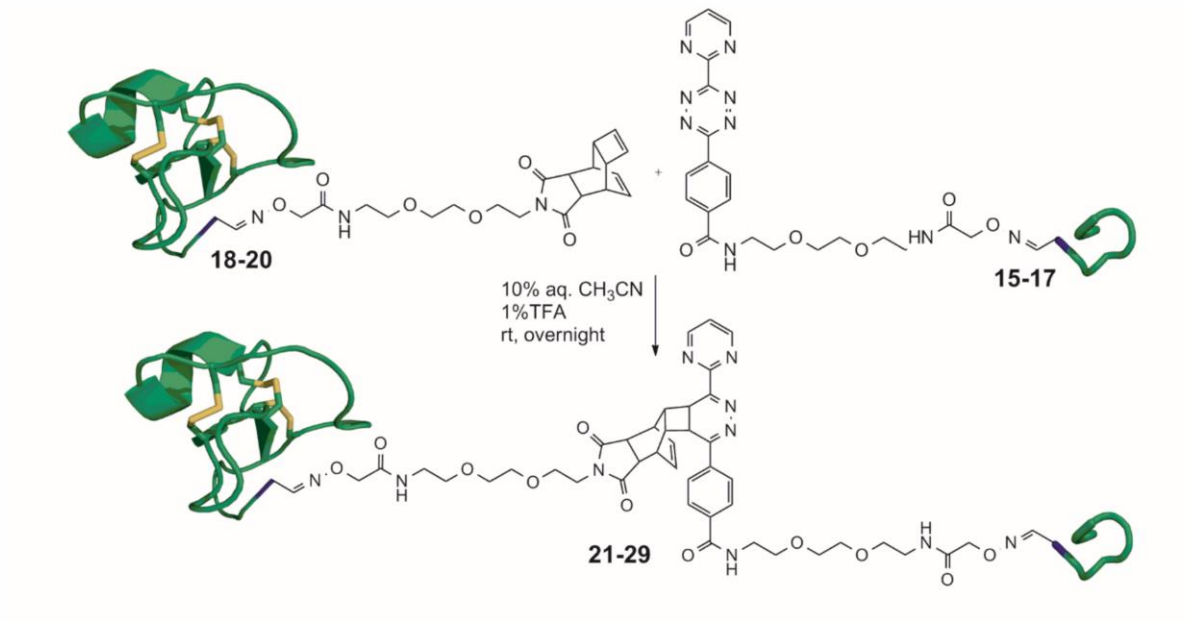

Scheme ESI-4: *DAR_{inv} reaction for the synthesis of heterodimers of bioactive peptides.*

In the frame of our proof-of-concept study, the products **21-29** were HPLC purified in the amounts required to perform the HR-MS analysis. As we did not plan further activity assays, the fractions from the analytical purification runs were collected and analyzed. Therefore no isolated yields but HPLC conversions are given (**Fig. 4B**).

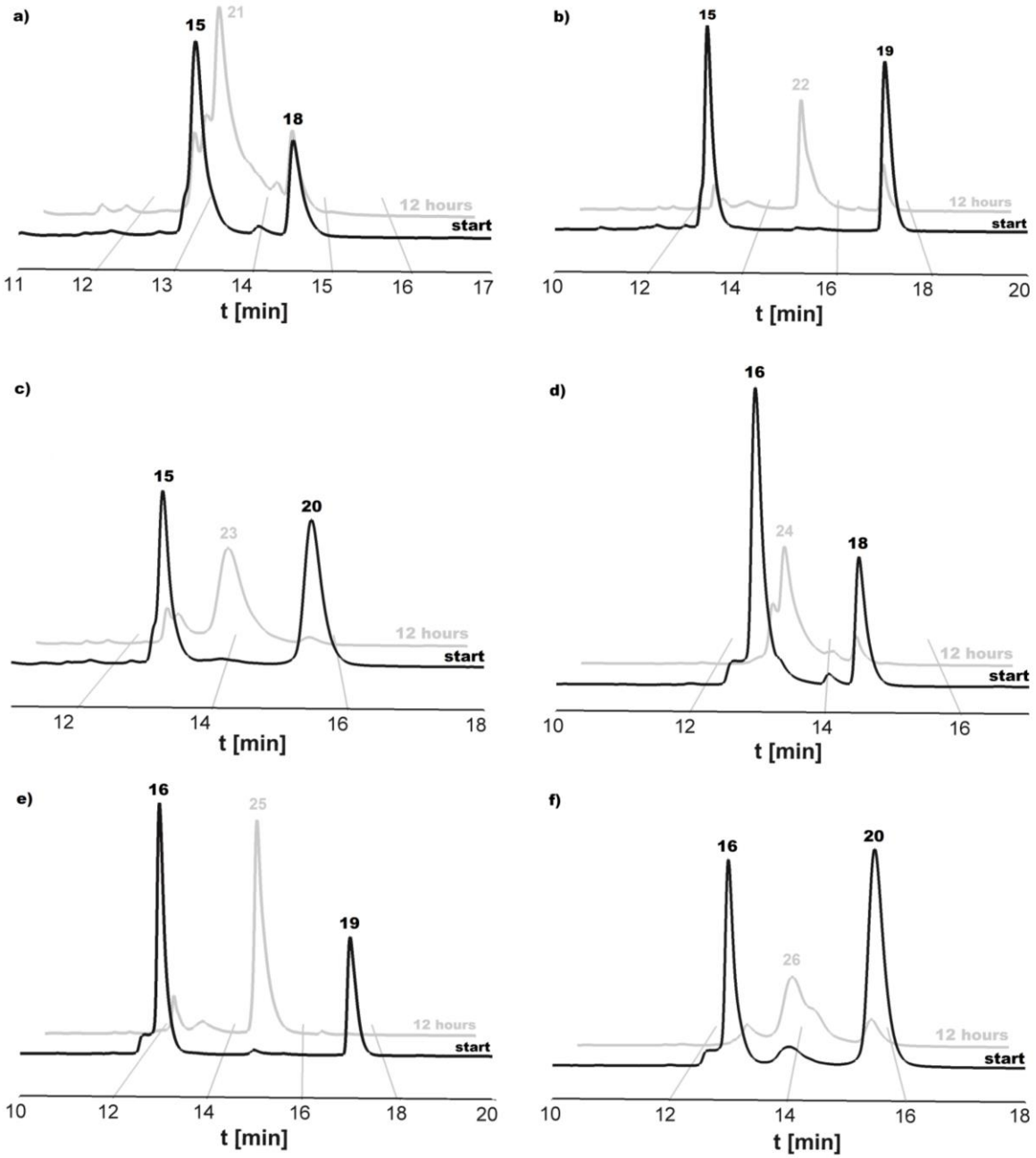

Figure ESI-1: *HPLC traces of DAR_{inv} reactions for generation of heterodimers comprising different bioactive peptides. The reaction mixtures were investigated at the beginning and after a reaction time of 12 hours. Absorbance at 220 nm. Reaction of: a)* ***15*** *and* ***18****; b)* ***15*** *and* ***19****; c)* ***15*** *and* ***20****; d)* ***16*** *and* ***18****; e)* ***16*** *and* ***19****; f)* ***16*** *and* ***20****.*

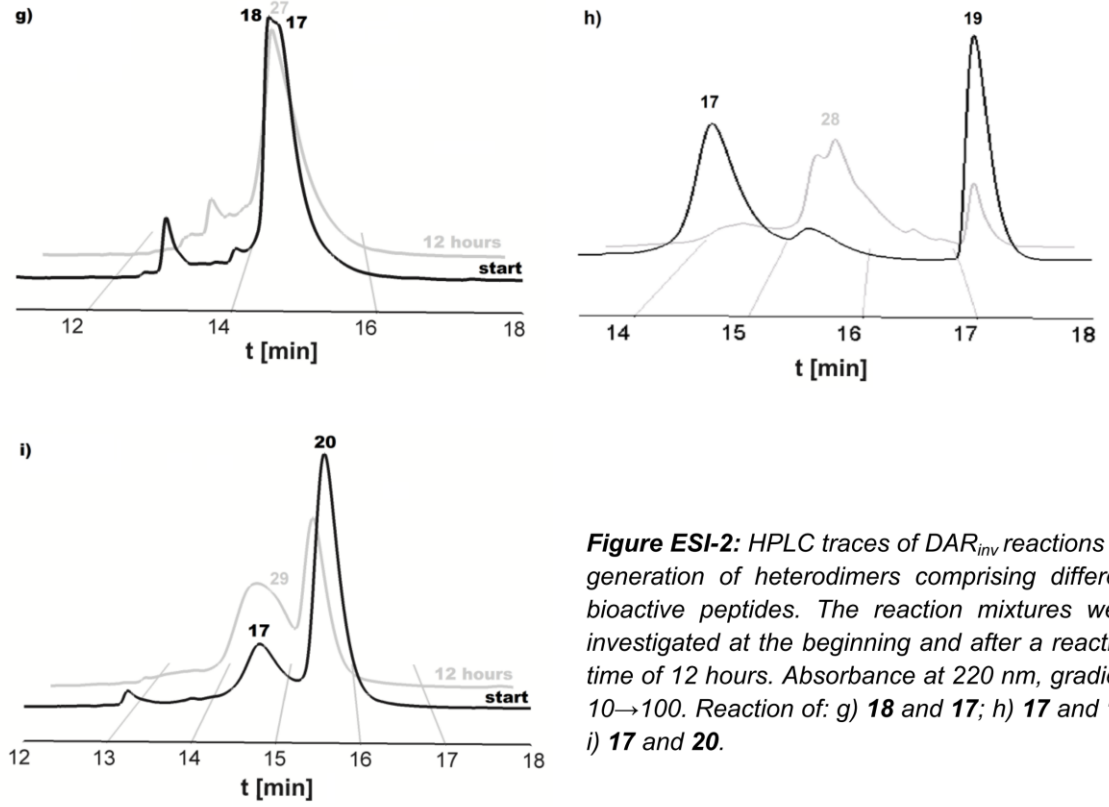

Figure ESI-2: *HPLC traces of DAR_{inv} reactions for generation of heterodimers comprising different bioactive peptides. The reaction mixtures were investigated at the beginning and after a reaction time of 12 hours. Absorbance at 220 nm, gradient 10→100. Reaction of: g)* ***18*** *and* ***17****; h)* ***17*** *and* ***19****; i)* ***17*** *and* ***20****.*

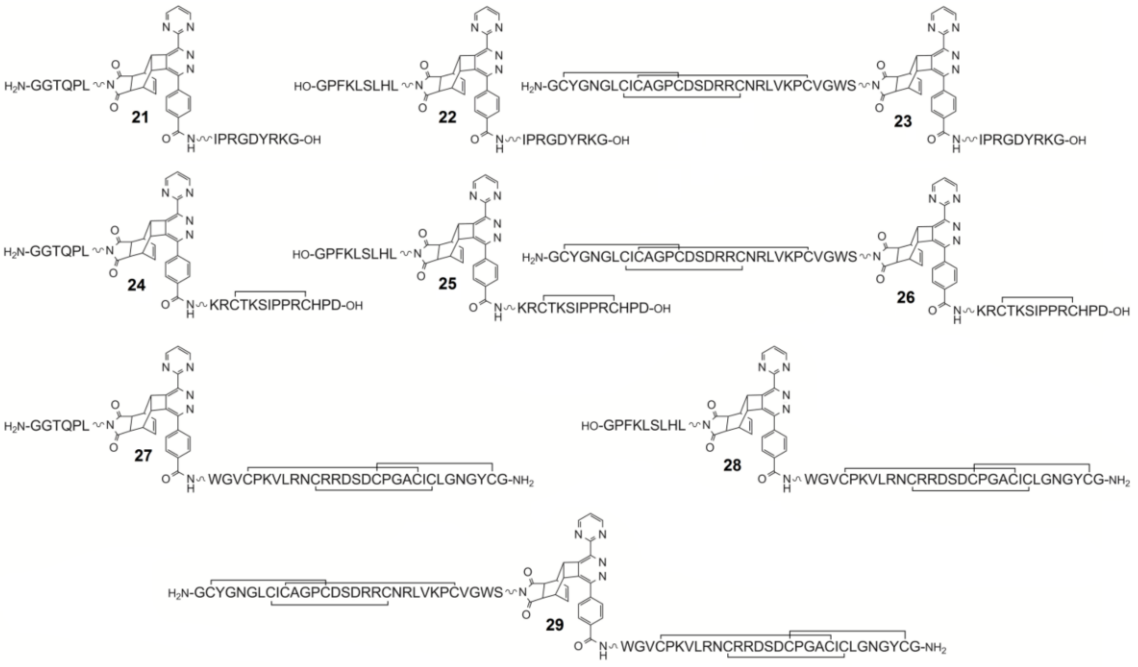

Scheme ESI-5*: Structures of DAR_{inv} conjugates* ***21****-****29****.*

Table ESI-6: *Mass spectrometric data of DAR_{inv} conjugates **21**-**29** and **32**.*

compound	Formula and calculated molar mass	MS method	MS measured
21	$C_{117}H_{167}N_{35}O_{35}$ 2622.2364	HR ESI	875.0857 $[M+3H]^{3+}$, 656.5662 $[M+3H]^{3+}$.
22	$C_{140}H_{200}N_{38}O_{37}$ 3005.4937	HR ESI	1002.8383 $[M+3H]^{3+}$, 752.3804 $[M+4H]^{4+}$, 602.1064 $[M+5H]^{5+}$.
23	$C_{226}H_{333}N_{71}O_{66}S_6$ 5289.3208	HR ESI	1058.8703 $[M+5H]^{5+}$, 882.5639 $[M+6H]^{6+}$.
24	$C_{139}H_{205}N_{43}O_{41}S_2$ 3196.4720	HR ESI	800.1251 $[M+4H]^{4+}$, 640.2998 $[M+5H]^{5+}$.
25	$C_{162}H_{238}N_{46}O_{43}S_2$ 3579.7292	HR ESI	1194.2505 $[M+3H]^{3+}$, 895.9390 $[M+4H]^{4+}$, 716.9526 $[M+5H]^{5+}$, 597.6290 $[M+6H]^{6+}$, 512.3984 $[M+7H]^{7+}$.
26	$C_{248}H_{371}N_{79}O_{72}S_8$ 5863.5564	HR ESI	978.2661 $[M+6H]^{6+}$, 838.6411 $[M+7H]^{7+}$, 733.9730 $[M+8H]^{8+}$.
27	$C_{203}H_{299}N_{63}O_{60}S_6$ 4771.0606	MALDI	4775.3 $[M+H]^{+}$.
28	$C_{226}H_{332}N_{66}O_{62}S_6$ 5154.3179	HR ESI	1031.6788 $[M+5H]^{5+}$, 860.0650 $[M+6H]^{6+}$.
29	$C_{312}H_{463}N_{99}O_{91}S_{12}$ 7436.1294	MALDI	7482.0 $[M+K]^{+}$.
32	$C_{131}H_{214}N_{40}O_{40}S_2Si_8$ 3275.3537	HR ESI	819.8464 $[M+4H]^{4+}$, 656.0783 $[M+5H]^{5+}$, 546.8998 $[M+6H]^{6+}$.

1.2.16 Inverse electron-demand Diels-Alder reaction for the synthesis of compound 32

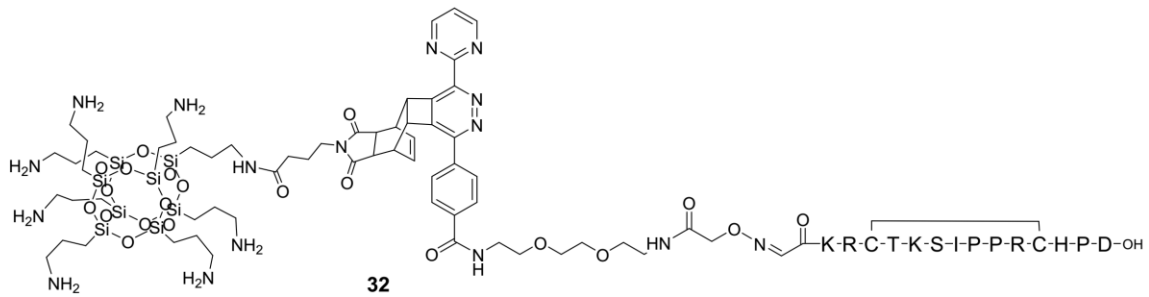

32

Compound **32** was synthesized using 1.0 mg of **31** (1 eq., 0.87 µmol) and 2.3 mg of **16** (1.2 eq., 1.044 µmol). Both compounds were dissolved in dry DMSO and reacted overnight at ambient temperature. The reaction completion was confirmed via LC-MS.

ESI-HR-MS calc. for $C_{131}H_{214}N_{40}O_{40}S_2Si_8$ 3275.3537 meas. 819.8464 $[M+4H]^{4+}$, 656.0783 $[M+5H]^{5+}$, 546.8998 $[M+6H]^{6+}$.

1.2 Analytical data

1.2.1 Compound 1

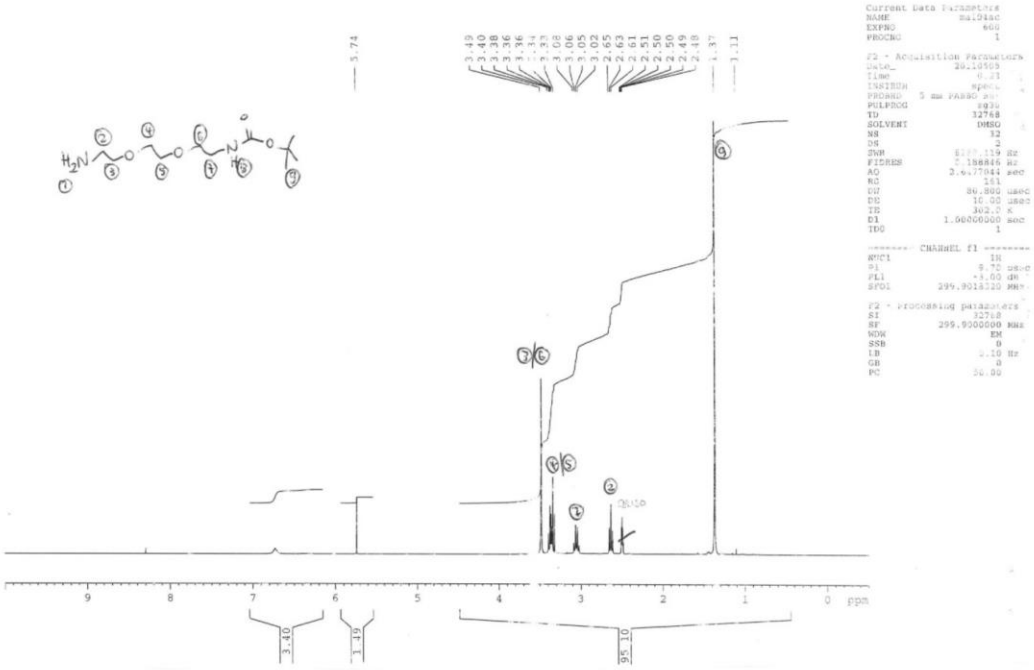

***Figure ESI-3**: [1]H-NMR spectrum of compound **1**.*

1.2.2 Compound 2

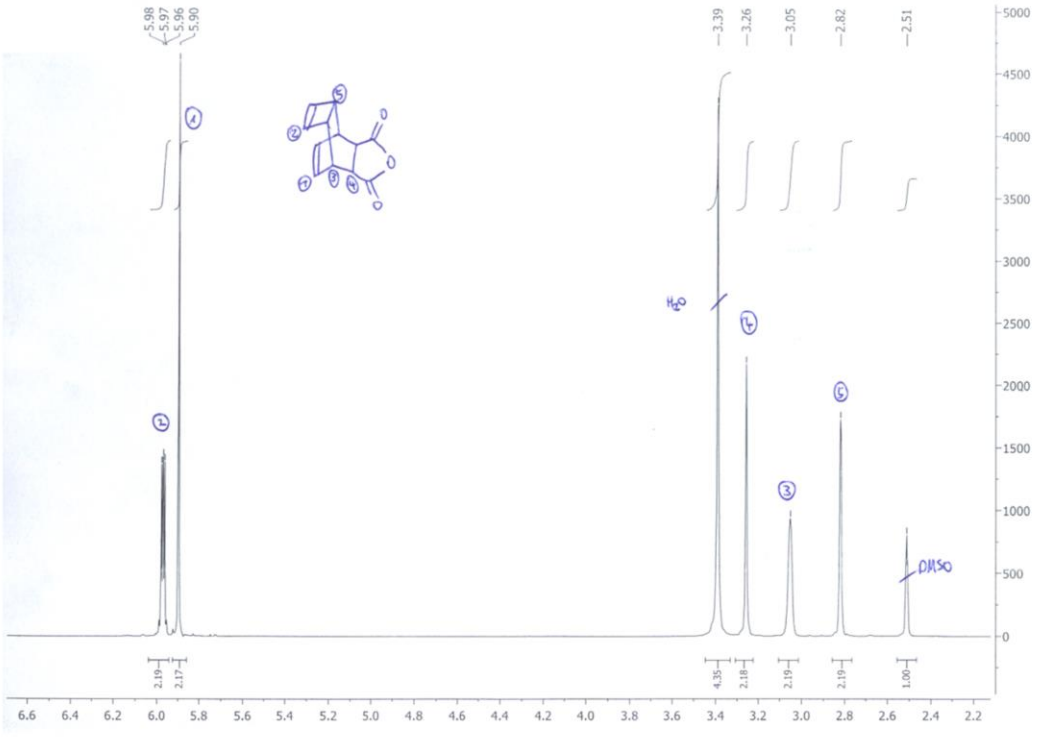

***Figure ESI-4:** [1]H-NMR spectrum of compound **2**.*

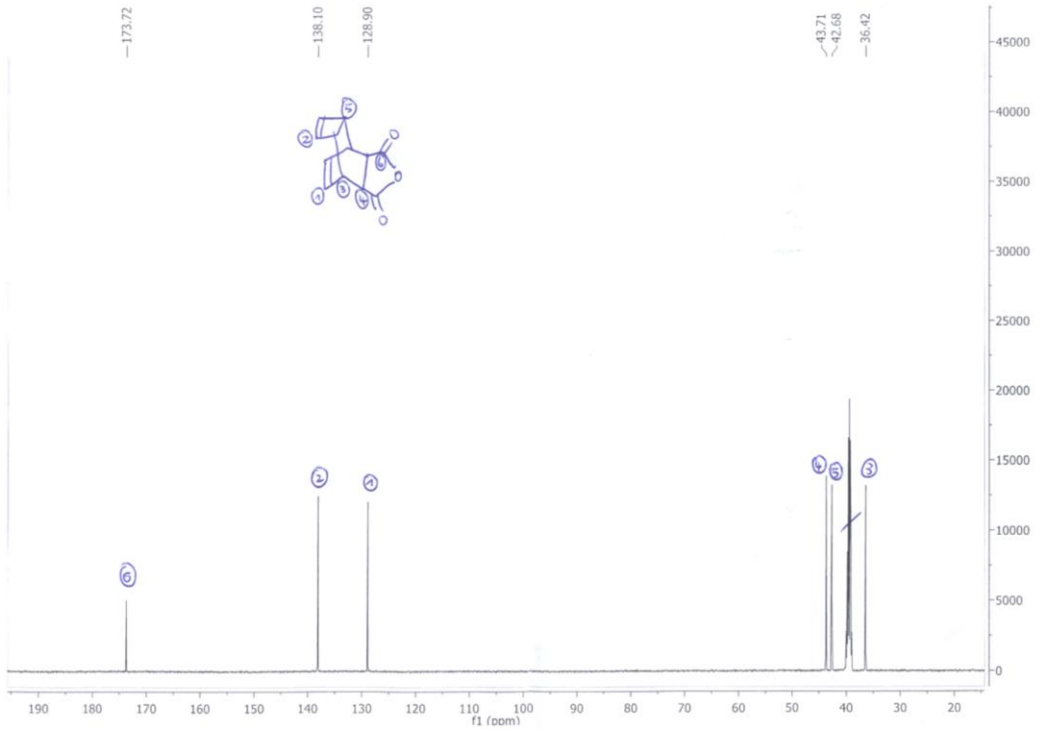

Figure ESI-5: *^{13}C-NMR spectrum of compound **2**.*

1.2.3 Compound 3

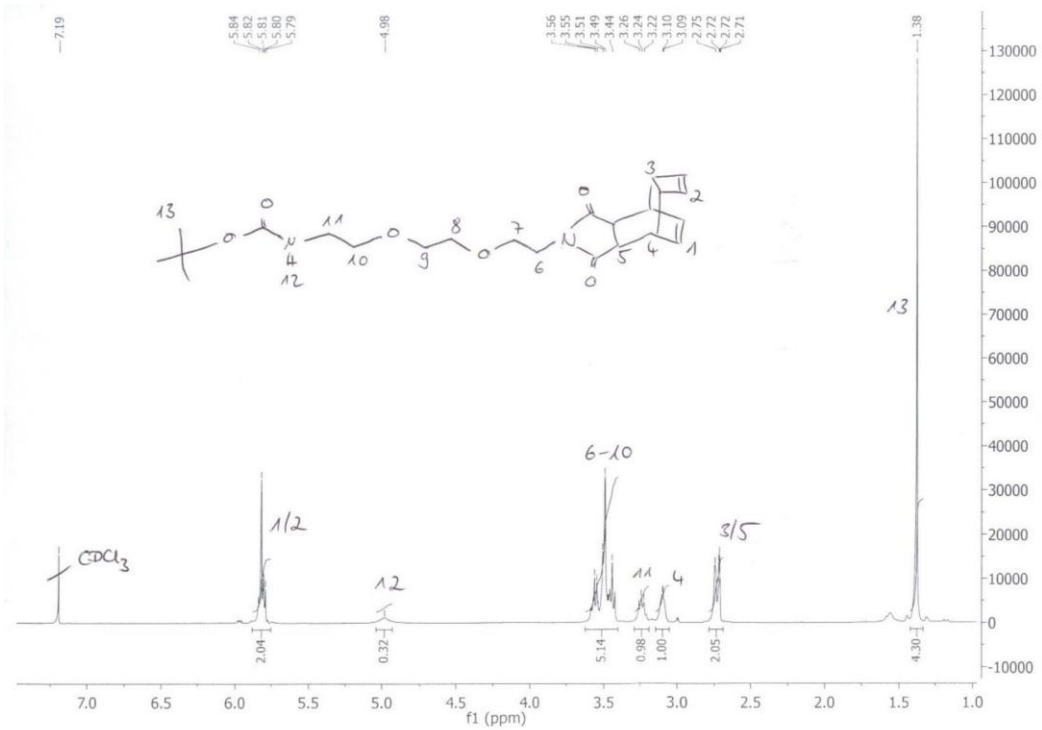

Figure ESI-6*: ^{1}H-NMR spectrum of compound **3**.*

1.2.4 Compound 4

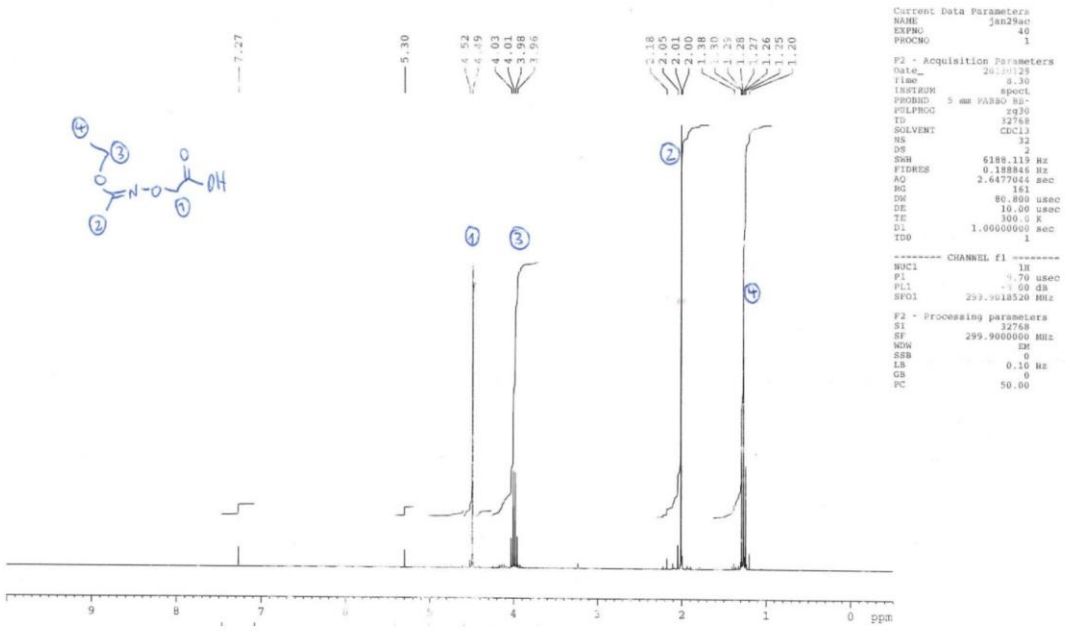

Figure ESI-7: *^{1}H-NMR spectrum of the precursor compound **4**.*

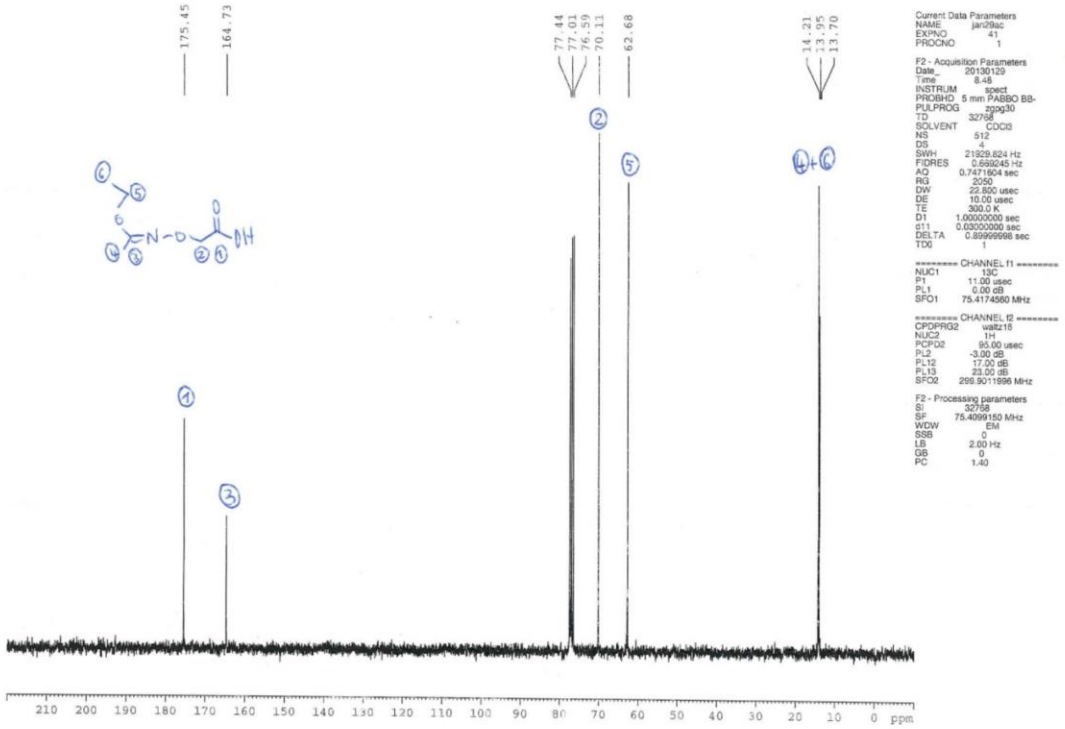

Figure ESI-8: *^{13}C-NMR spectrum of the precursor of compound **4**.*

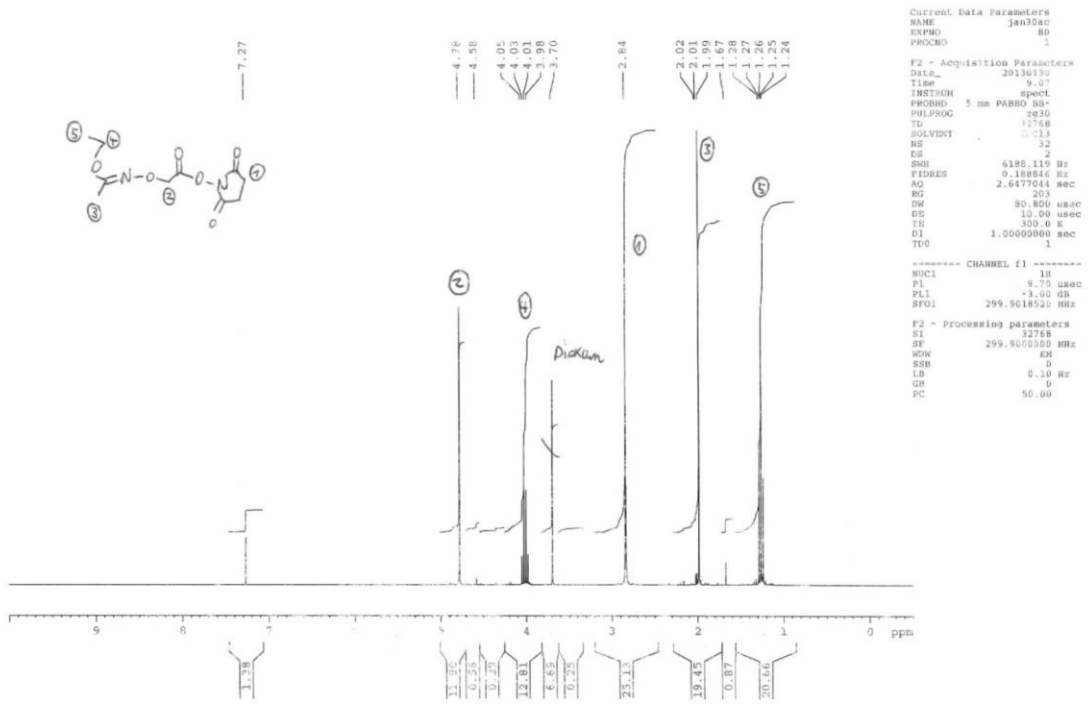

Figure ESI-9: *^{1}H-NMR spectrum of compound **4**.*

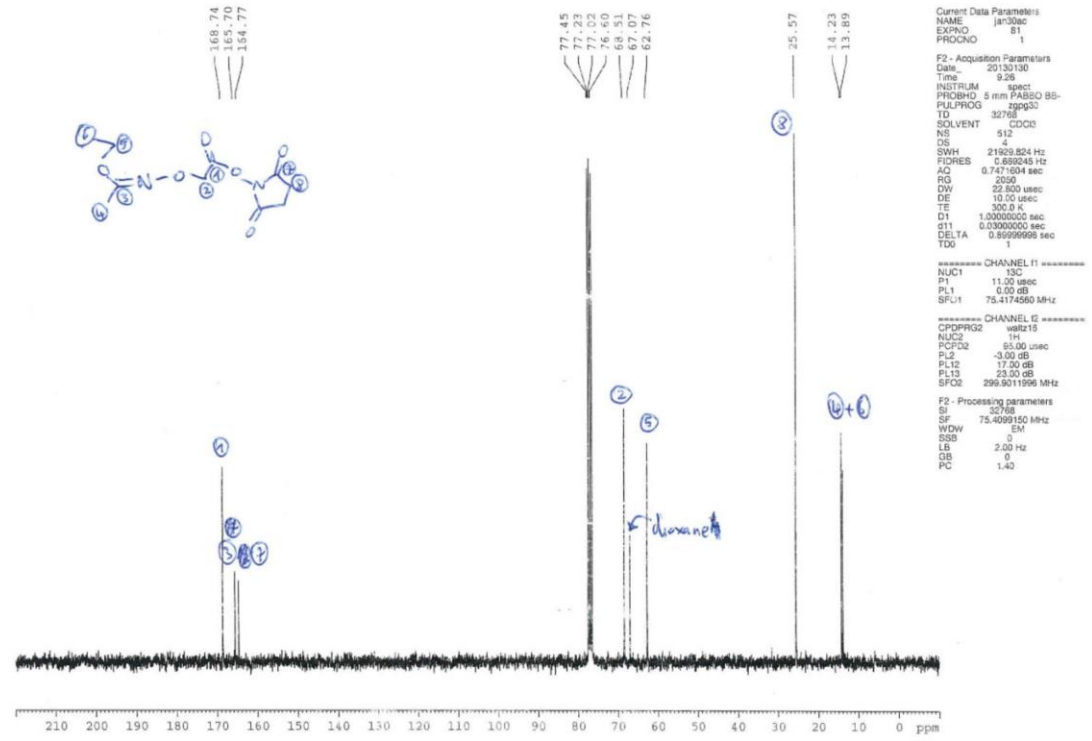

Figure ESI-10: *^{13}C-NMR spectrum of compound **4**.*

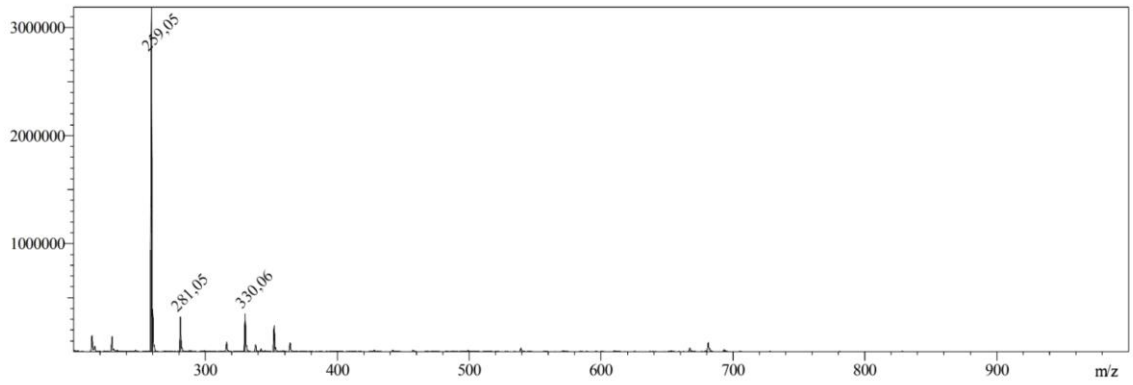

Figure ESI-11: *ESI-MS spectrum of compound **4**; calc. for $C_{10}H_{14}N_2O_6$ M: 258.09 m/z meas.: 259.05 $[M+H]^+$.*

1.2.5 Compound 5

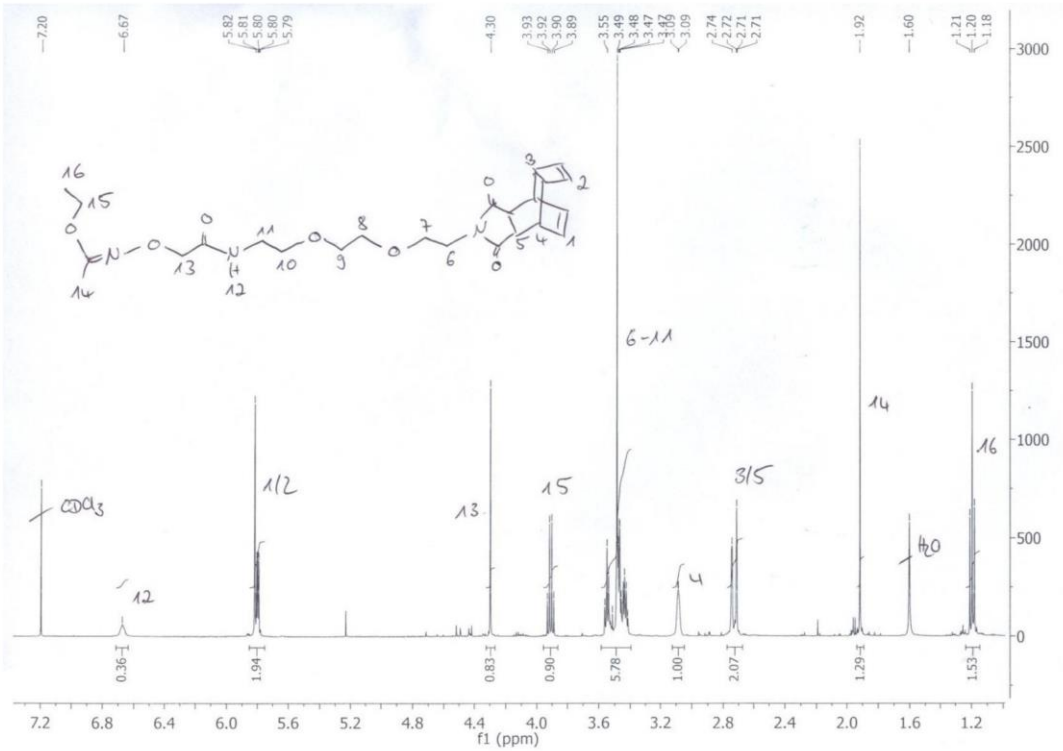

Figure ESI-12: *^{1}H-NMR spectrum of compound **5**.*

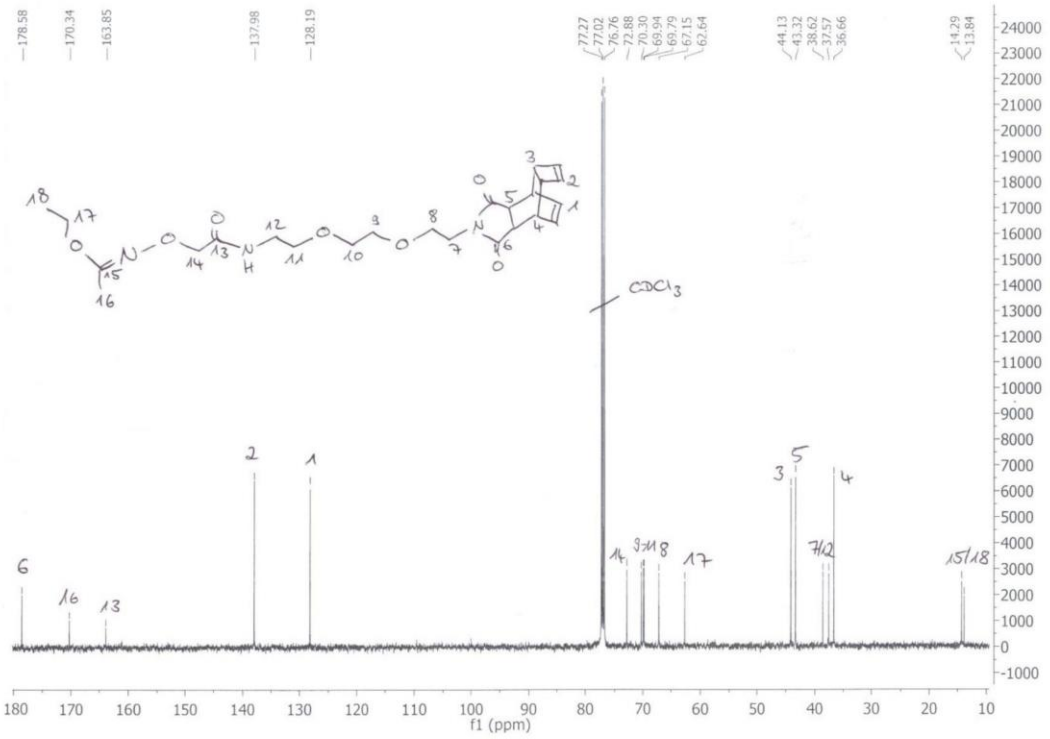

Figure ESI-13: *^{13}C-NMR spectrum of compound **5**.*

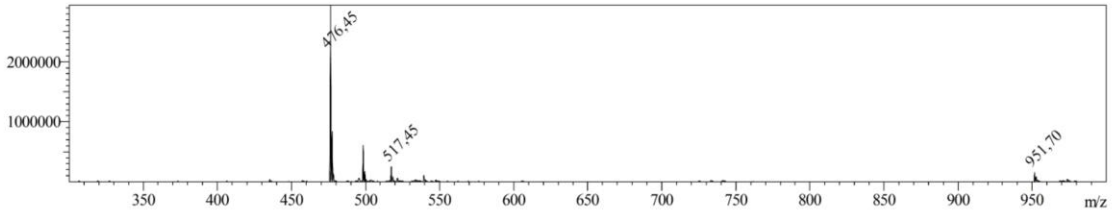

Figure ESI-14: *ESI-MS spectrum of compound **5**; calc. for $C_{24}H_{33}N_3O_7$ M: 475.24, m/z meas.: 476.45 $[M+H]^+$.*

1.2.6 Compound 6

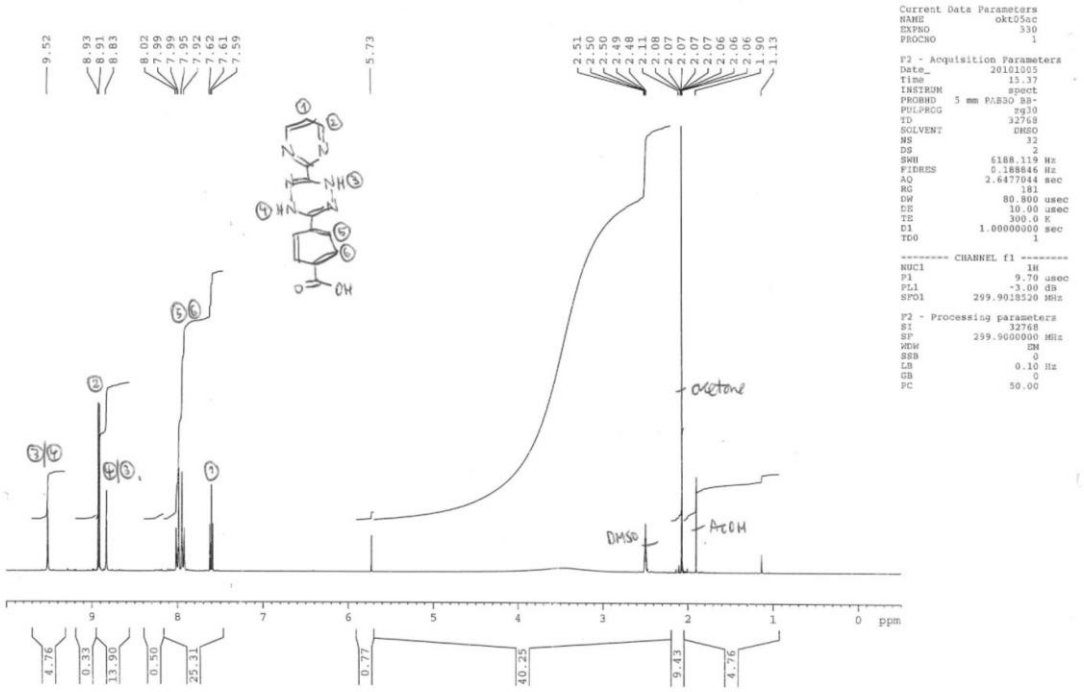

Figure ESI-15: *[1]H-NMR spectrum of the precursor of compound* ***6****.*

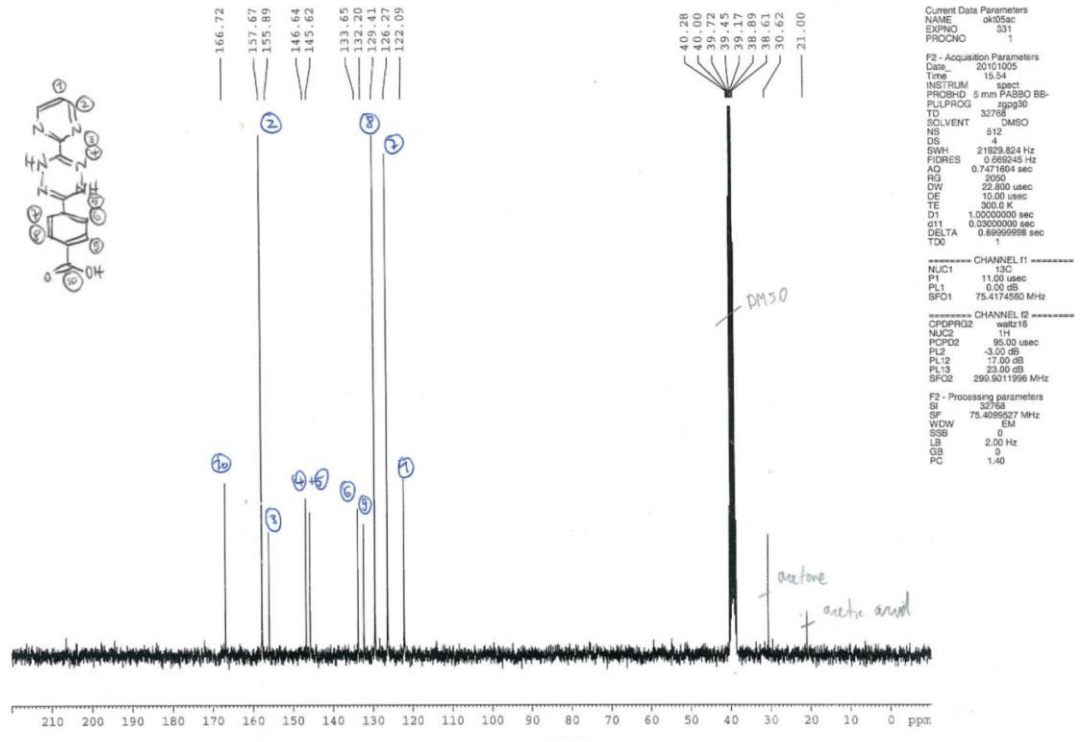

Figure ESI-16: *[13]C-NMR spectrum of the precursor of compound* ***6****.*

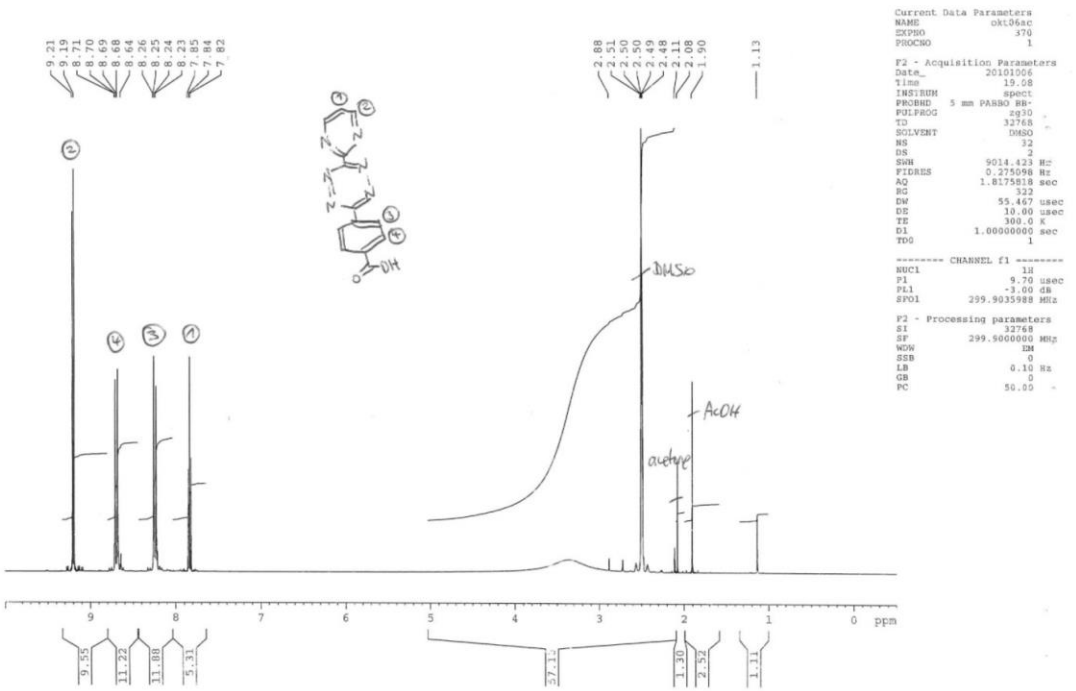

Figure ESI-17: *^{1}H-NMR spectrum of compound* ***6****.*

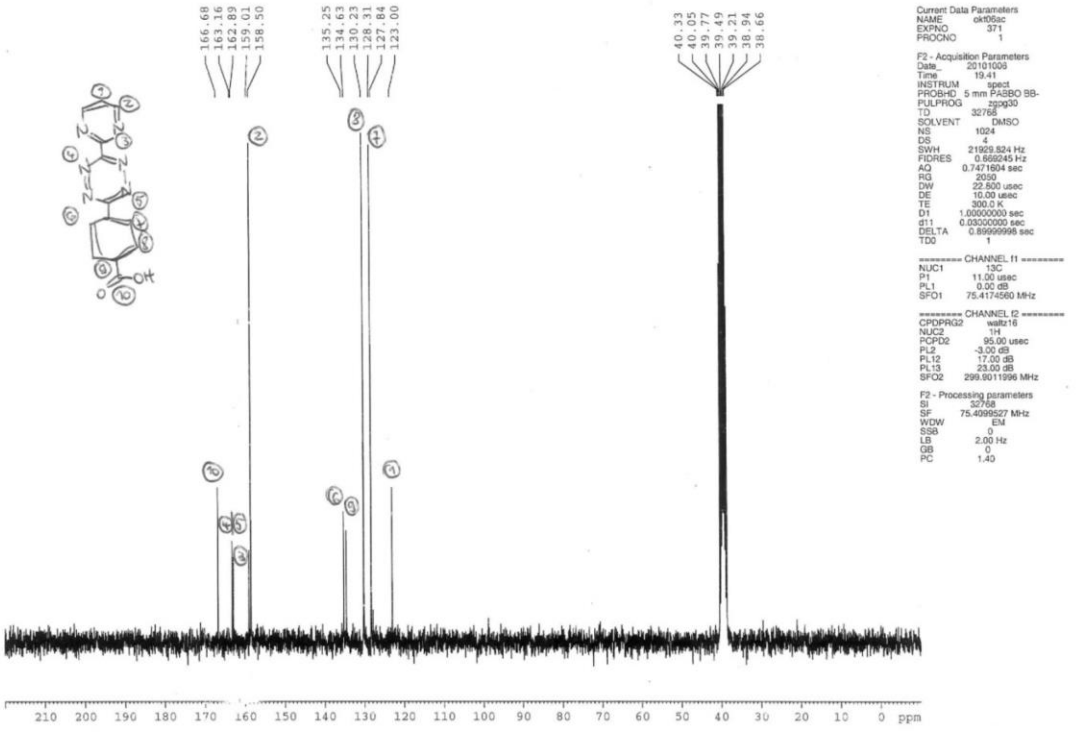

Figure ESI-18: *^{13}C-NMR spectrum of compound* ***6****.*

1.2.7 Compound 7

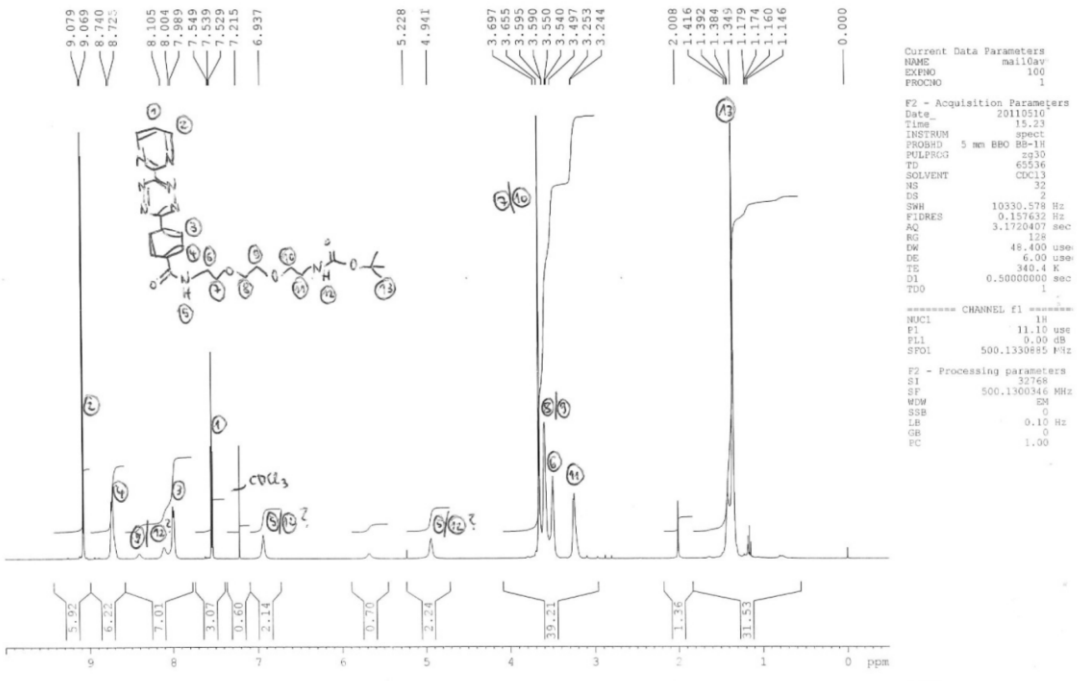

Figure ESI-19: *^{1}H-NMR spectrum of compound* ***7****.*

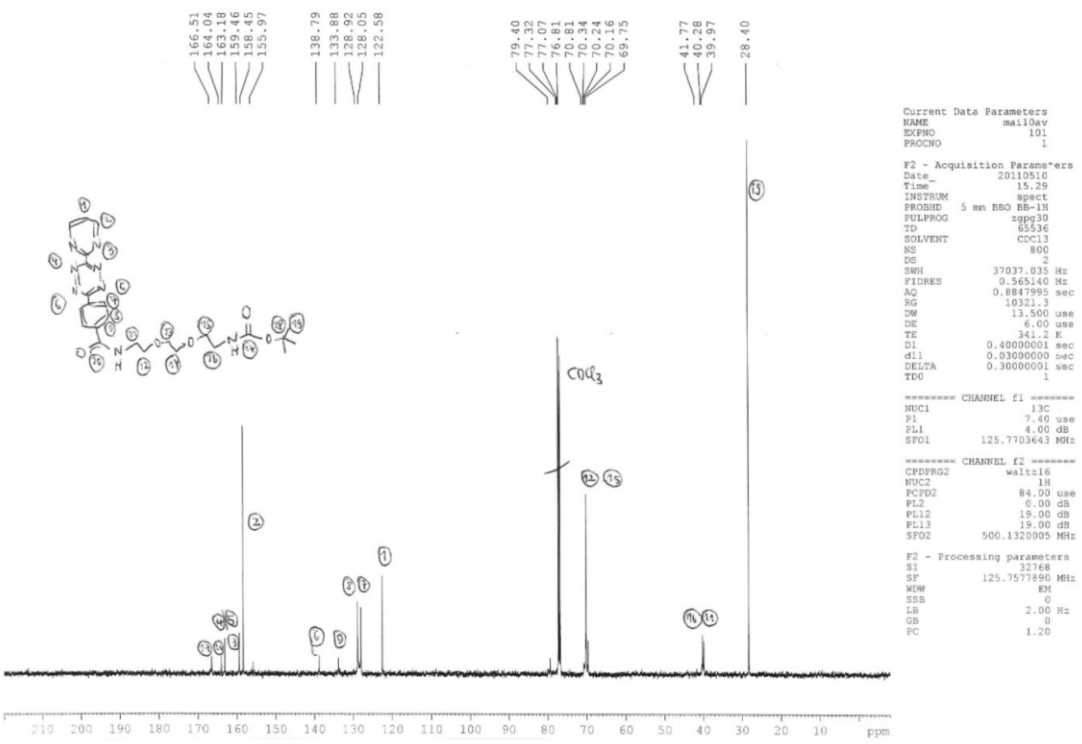

Figure ESI-20: *^{13}C-NMR spectrum of compound* ***7****.*

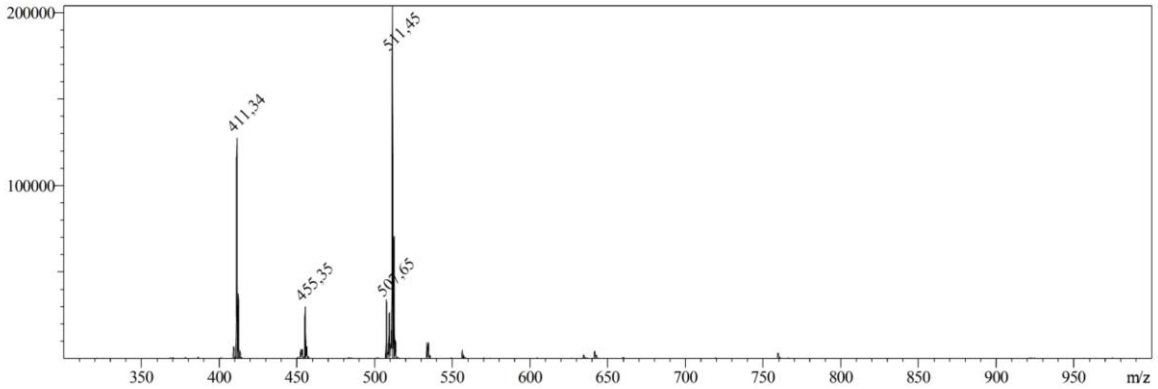

Figure ESI-21: *ESI-MS spectrum of compound* ***7****; calc. for* $C_{24}H_{30}N_8O_5$ *M: 510.24, m/z meas.: 511.45* $[M+H]^+$.

1.2.8 Compound 8

Figure ESI-22: *[1]H-NMR spectrum of compound* ***8****.*

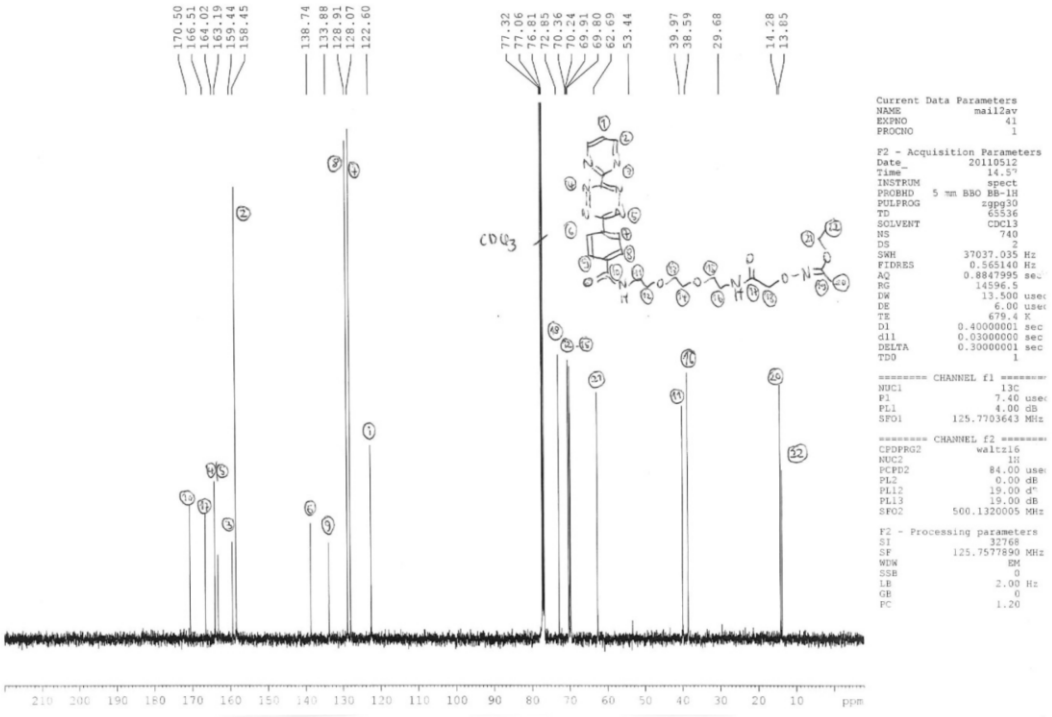

Figure ESI-23: *^{13}C-NMR spectrum of compound **8**.*

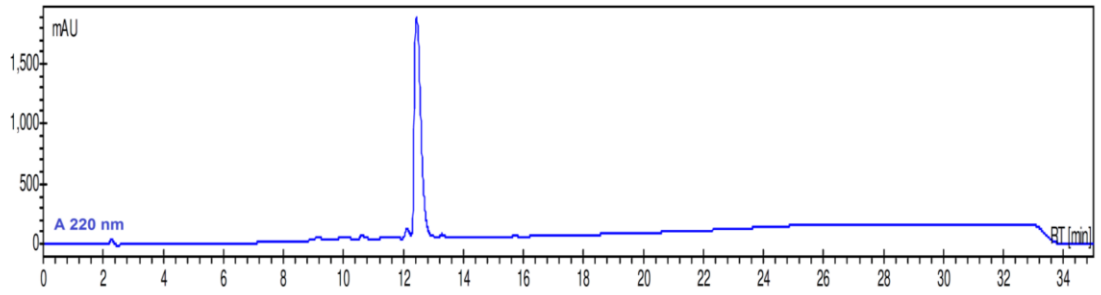

Figure ESI-24: *HPLC trace of compound **8**. Absorbance at 220 nm; gradient 10→100 B; t_R=12.62 min.*

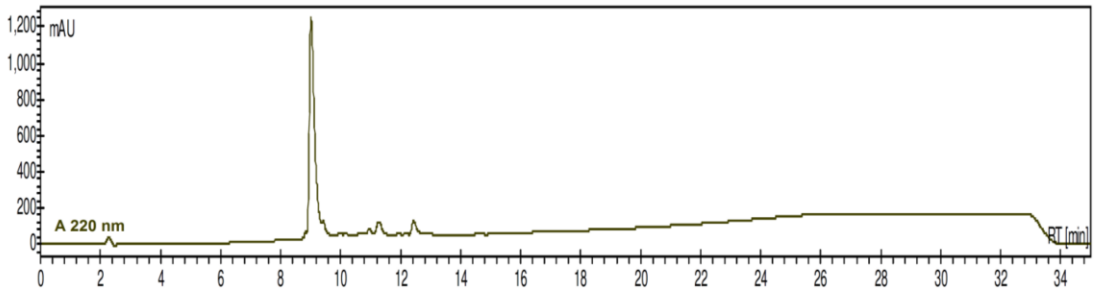

Figure ESI-25: *HPLC trace of compound **8a**. Absorbance at 220 nm; gradient 10→100 B; t_R=9.11 min.*

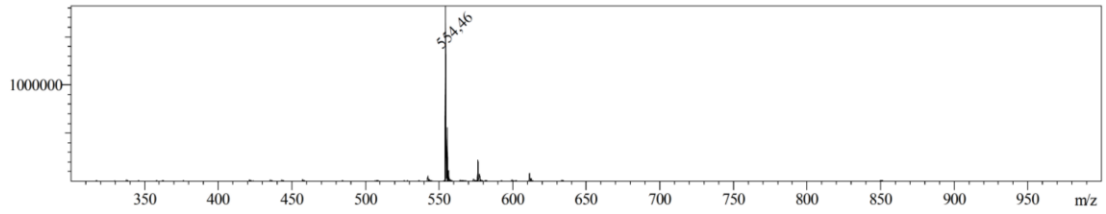

Figure ESI-26: *ESI-MS spectrum of compound* ***8****; calc. for* $C_{25}H_{31}N_9O_6$ *M: 553.25, m/z meas.: 554.46* $[M+H]^+$.

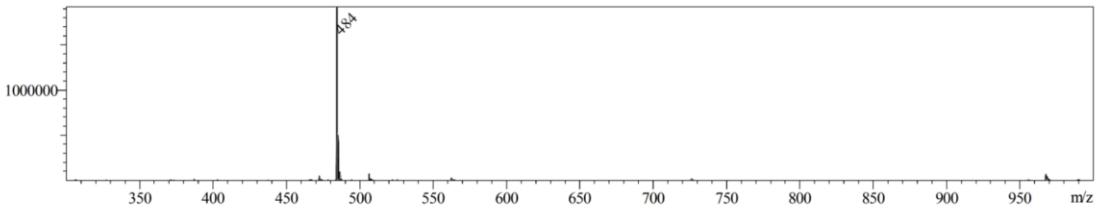

Figure ESI-27: *ESI-MS spectrum of compound* ***8a****; calc. for* $C_{21}H_{25}N_9O_5$ *M: 483.20, m/z meas.: 484.45* $[M+H]^+$.

1.2.9 Compound 9

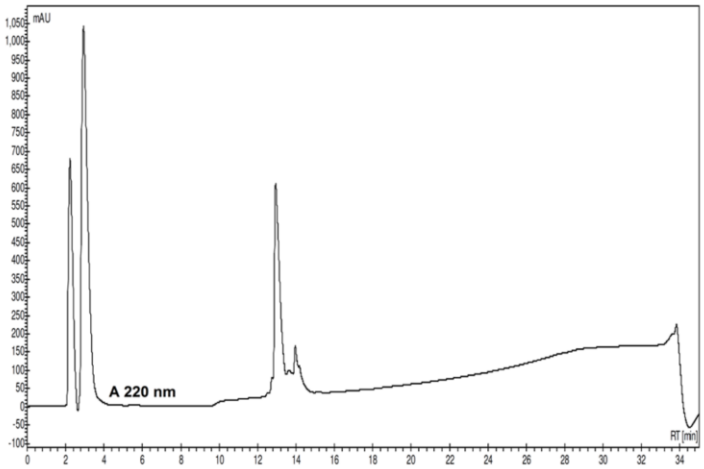

Figure ESI-28: *HPLC trace of compound* ***9****. Absorbance at 220 nm; gradient 10→100 B;* t_R*=13.22 min.*

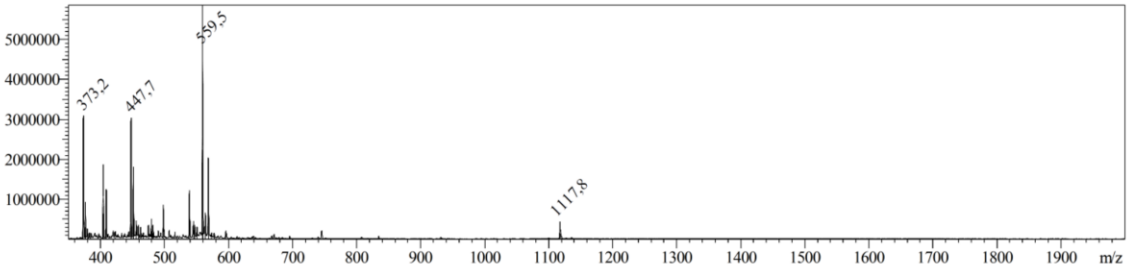

Figure ESI-29: *ESI-MS spectrum of compound* ***9****; calc. for* $C_{48}H_{76}N_{16}O_{15}$ *M: 1116.57, m/z meas.: 1117.8* $[M+H]^+$*, 559.62 meas. 559.5* $[M+2H]^{2+}$*, 373.41 meas. 373.2* $[M+3H]^{3+}$.

1.2.10 Compound 10

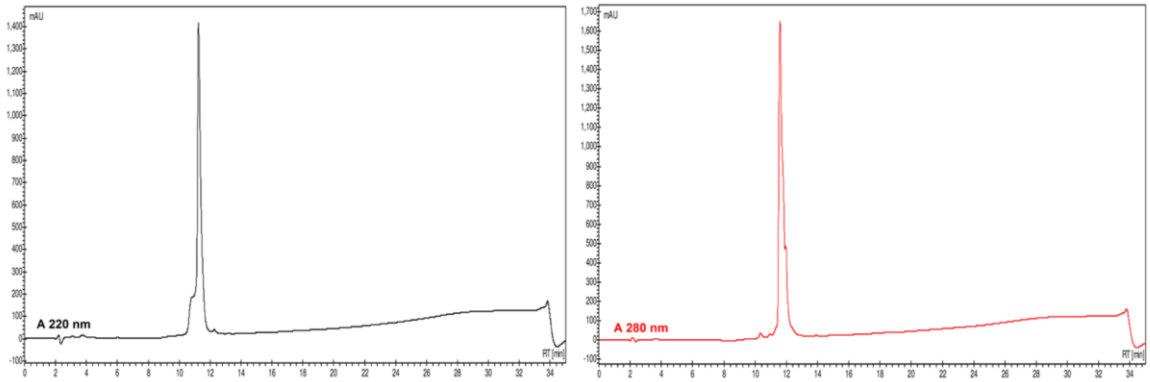

Figure ESI-30: *HPLC trace of compound* ***10****. Left: absorbance at 220 nm; right: absorbance at 220 nm; gradient 10→100 B;* t_R*=11.54 min.*

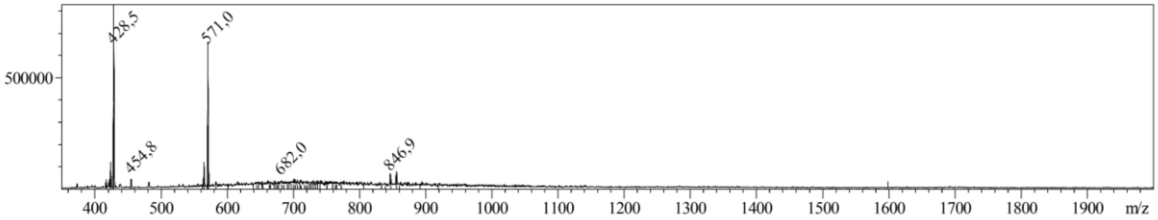

Figure ESI-31: *ESI-MS spectrum of compound* ***10****; calc. for* $C_{70}H_{114}N_{24}O_{21}S_2$ *M: 846.98, m/z meas.: 846.9* $[M+2H]^{2+}$*, calc. 564.98 meas. 571.0* $[M+3H+H_2O]^{3+}$*, calc. 423.99 meas. 428.5* $[M+4H+H_2O]^{4+}$*.*

1.2.11 Compound 11

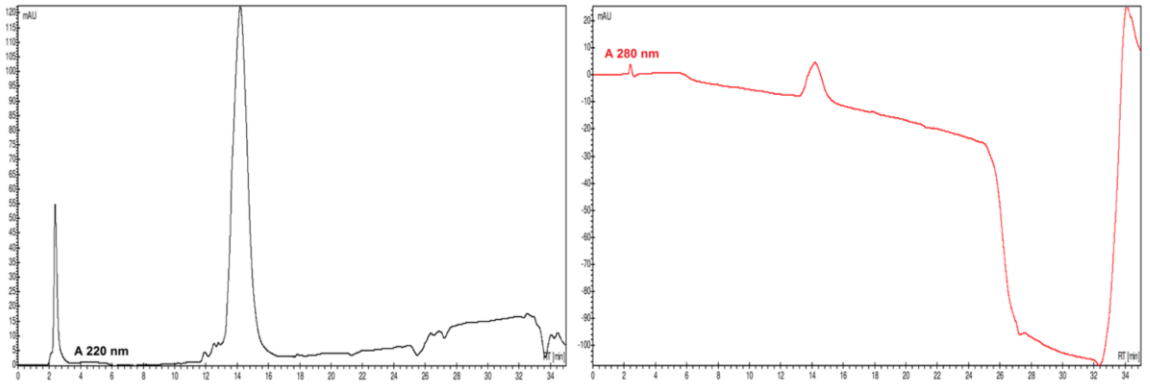

Figure ESI-32: *HPLC trace of compound* ***11****. Left: absorbance at 220 nm; right: absorbance at 280 nm; gradient 10→100 B;* t_R*=14.27 min.*

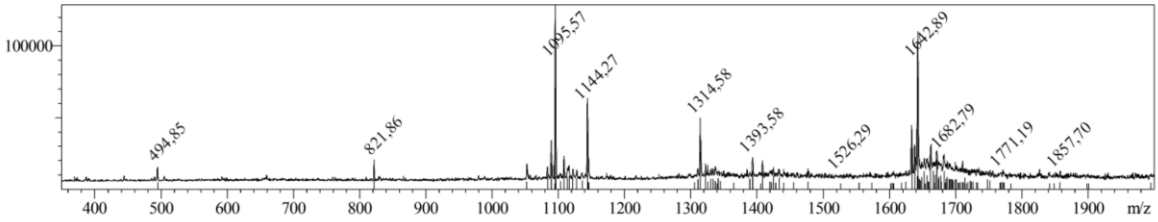

Figure ESI-33: *ESI-MS spectrum of compound* ***11****; calc. for* $C_{134}H_{206}N_{44}O_{40}S_6$ *M: 1633.88, m/z meas.: 1642.89* $[M+2H+H_2O]^{2+}$*, calc. 1095.59 meas. 1095.57* $[M+3H+H_2O]^{3+}$*, calc. 821.95 meas. 821.86* $[M+4H+H_2O]^{4+}$*.*

1.2.12 Compound 12

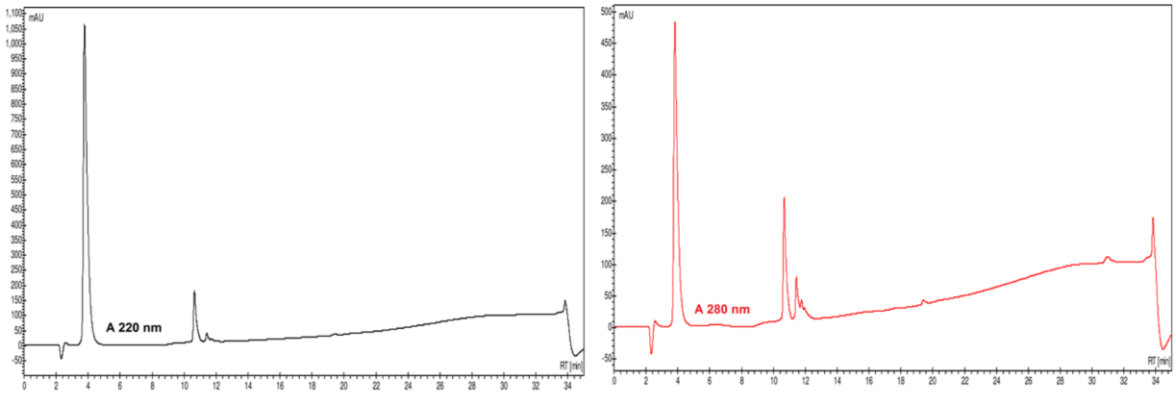

Figure ESI-34: *HPLC trace of compound* ***12****. Left: absorbance at 220 nm; right: absorbance at 280 nm; gradient 10→100 B;* t_R*=10.76 min.*

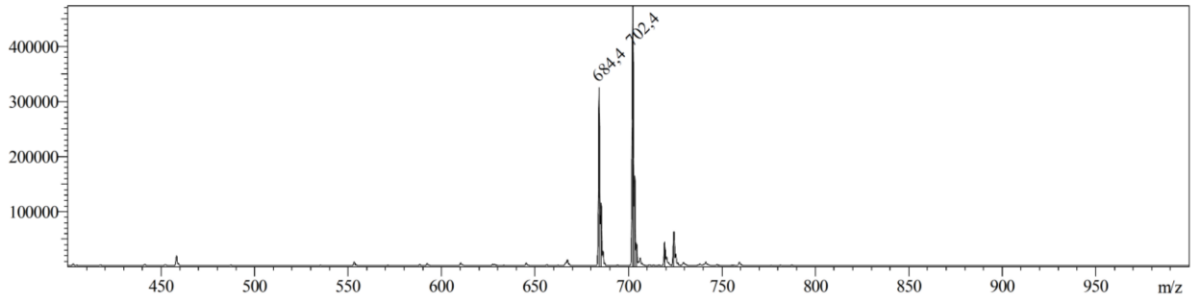

Figure ESI-35: *ESI-MS spectrum of compound* ***12****; calc. for* $C_{28}H_{45}N_9O_{11}$ *M: 683.32, m/z meas.: 684.4* $[M+H]^+$*, 702.4* $[M+H+H_2O]^+$*.*

1.2.13 Compound 13

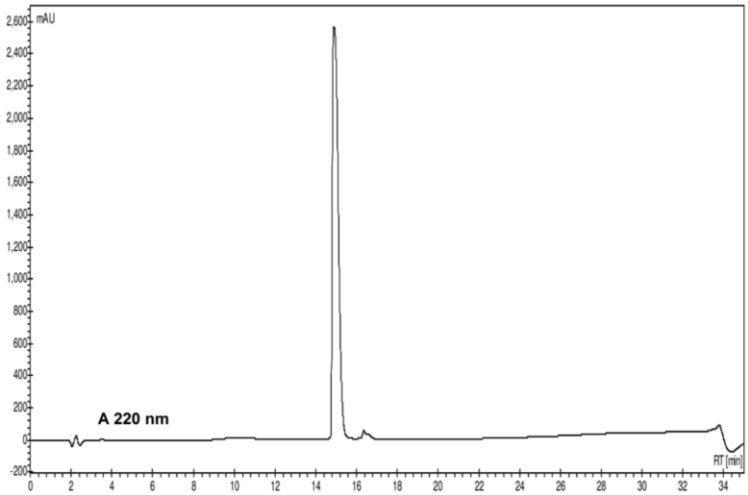

Figure ESI-36: *HPLC trace of compound* ***13****. Absorbance at 220 nm; gradient 10→100 B;* t_R*=15.06 min.*

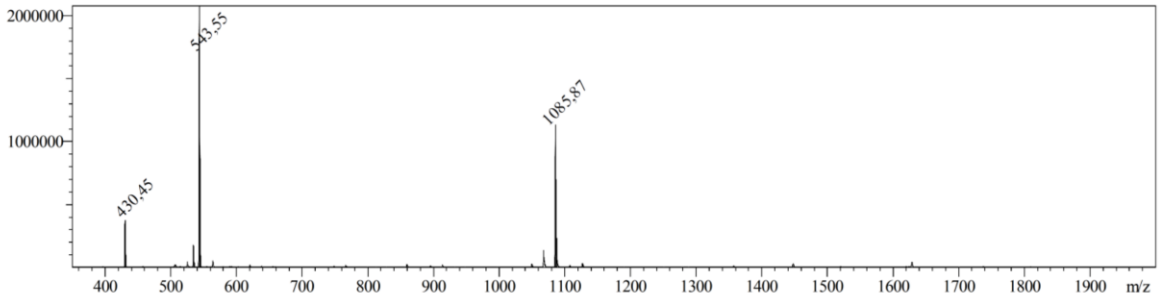

Figure ESI-37: *ESI-MS spectrum of compound* ***13****; calc. for* $C_{51}H_{78}N_{12}O_{13}$ *M: 1067.26, m/z meas.: 1085.87* $[M+H+H_2O]^+$*, 534.63 meas. 543.55* $[M+2H+H_2O]^{2+}$*.*

1.2.14 Compound 14

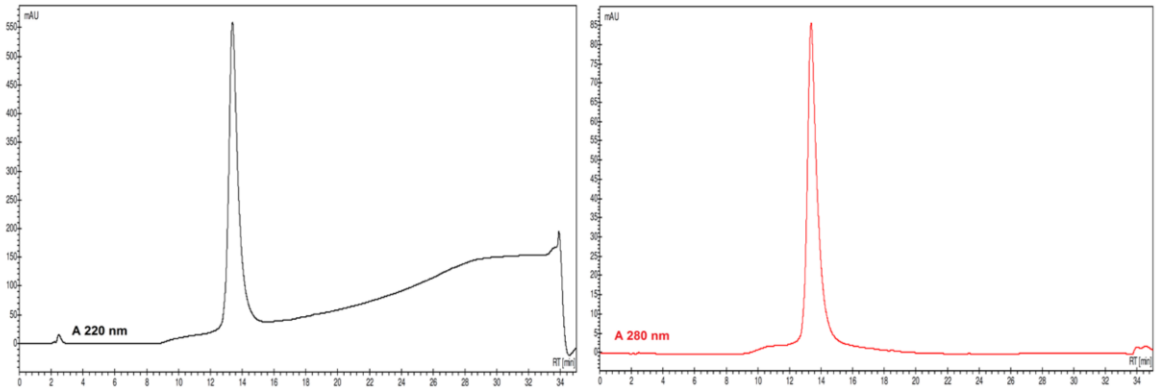

Figure ESI-38: *HPLC trace of compound* ***14****. Left: absorbance at 220 nm; right: absorbance at 280 nm; gradient 10→100 B;* t_R*=13.56 min.*

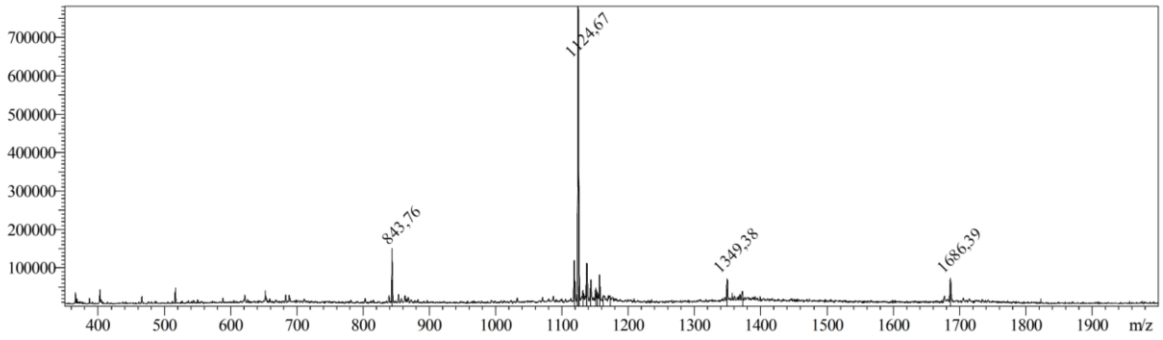

Figure ESI-39: *ESI-MS spectrum of compound* ***14****; calc. for* $C_{137}H_{211}N_{45}O_{42}S_6$ *M: 1677.42, m/z meas.: 1686.39* $[M+2H+H_2O]^{2+}$*, 1118.61 meas.1124.67* $[M+3H+H_2O]^{3+}$*, 839.21 meas.843.76* $[M+4H+H_2O]^{4+}$*.*

1.2.15 Compound 15

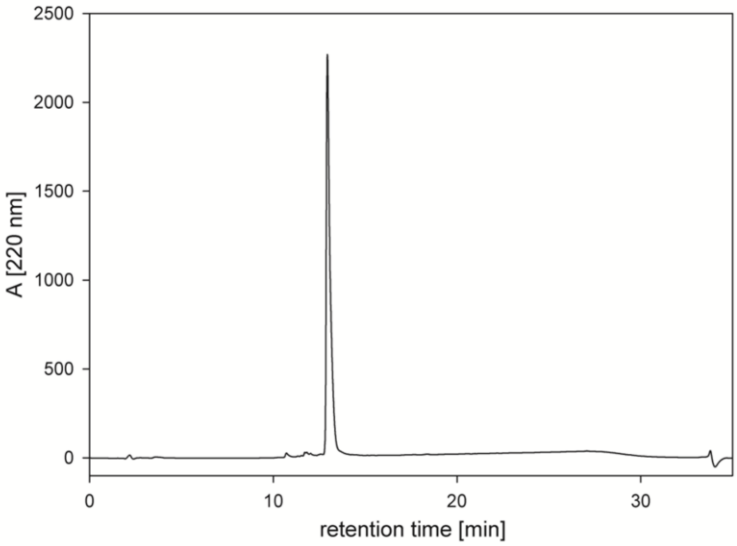

Figure ESI-40: *HPLC trace of compound **15**. Absorbance at 220 nm; gradient 10→100 B; t_R=12.98 min.*

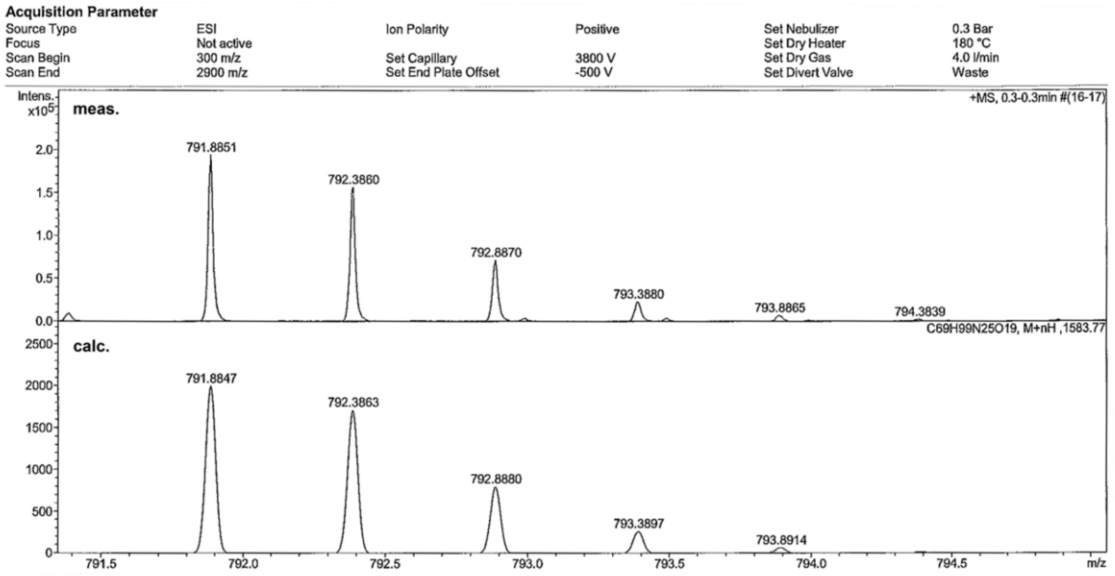

Figure ESI-41: *Section of HR ESI-MS spectrum of compound **15**. Upper panel: measured isotopic pattern $[M+2H]^{2+}$. Lower panel: simulated isotopic pattern $[M+2H]^{2+}$.*

1.2.16 Compound 16

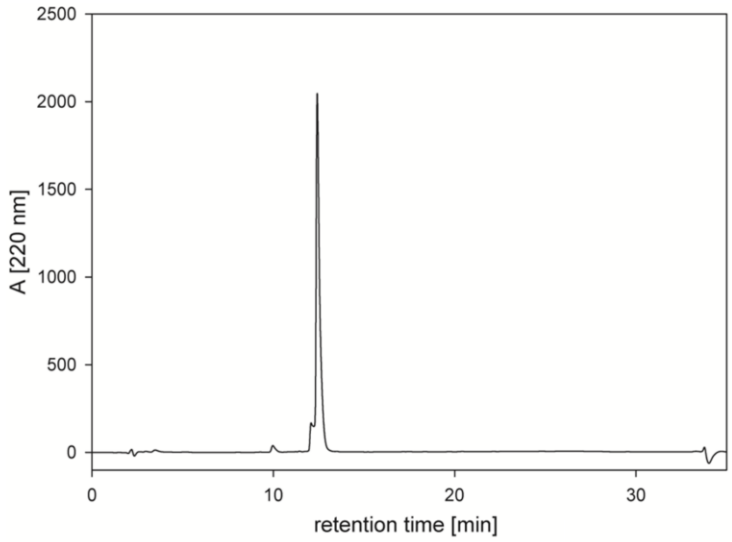

Figure ESI-42: *HPLC trace of compound* ***16****. Absorbance at 220 nm; gradient 10→100 B;* t_R*=12.20 min.*

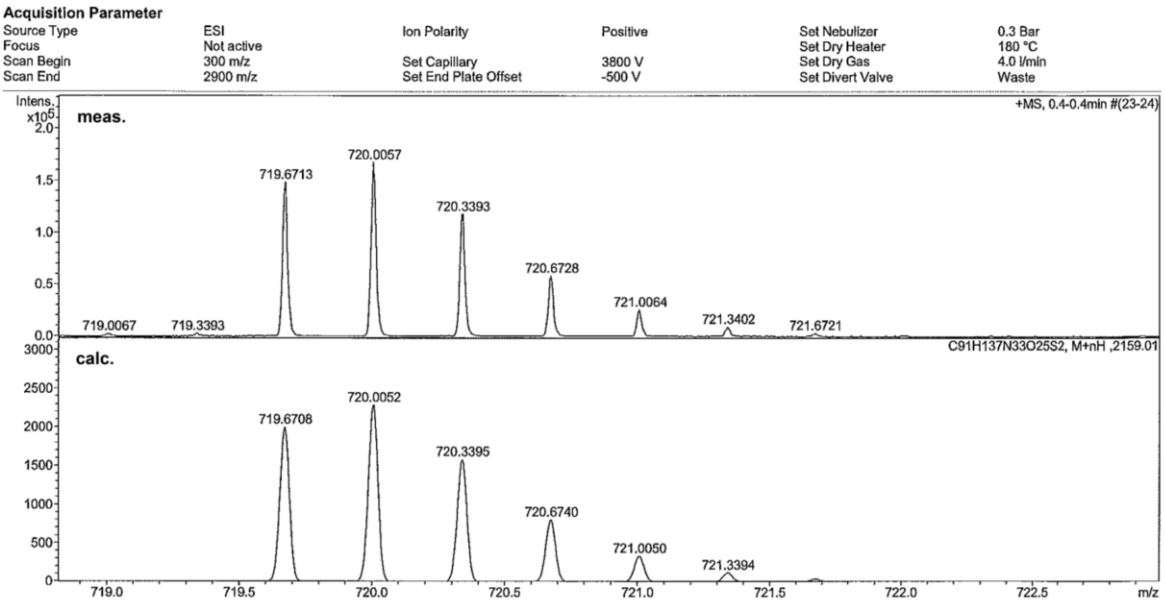

Figure ESI-43: *Section of HR ESI-MS spectrum of compound* ***16****. Upper panel: measured isotopic pattern* $[M+3H]^{3+}$*. Lower panel: simulated isotopic pattern* $[M+3H]^{3+}$*.*

1.2.17 Compound 17

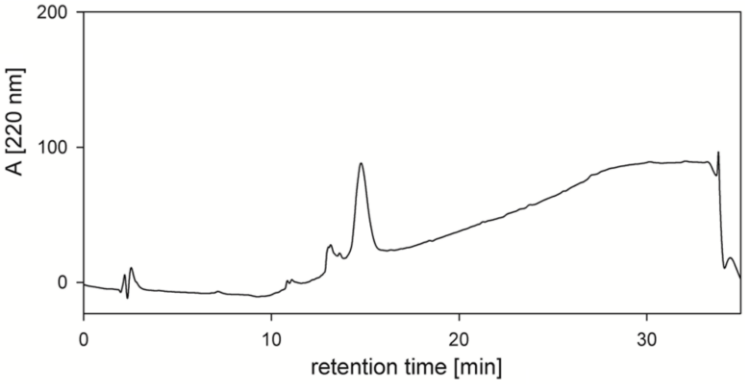

Figure ESI-44: *HPLC trace of compound* ***17****. Absorbance at 220 nm; gradient 10→100 B;* t_R*=14.67 min.*

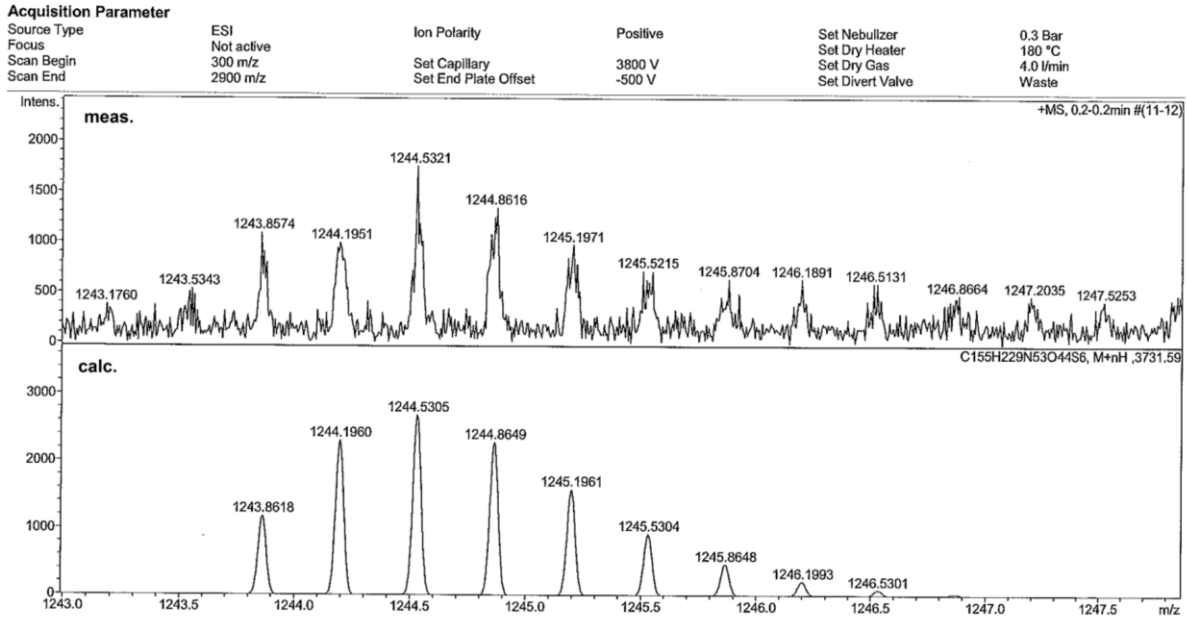

Figure ESI-45: *Section of HR ESI-MS spectrum of compound* ***17****. Upper panel: measured isotopic pattern* $[M+3H]^{3+}$*. Lower panel: simulated isotopic pattern* $[M+3H]^{3+}$*.*

1.2.18 Compound 18

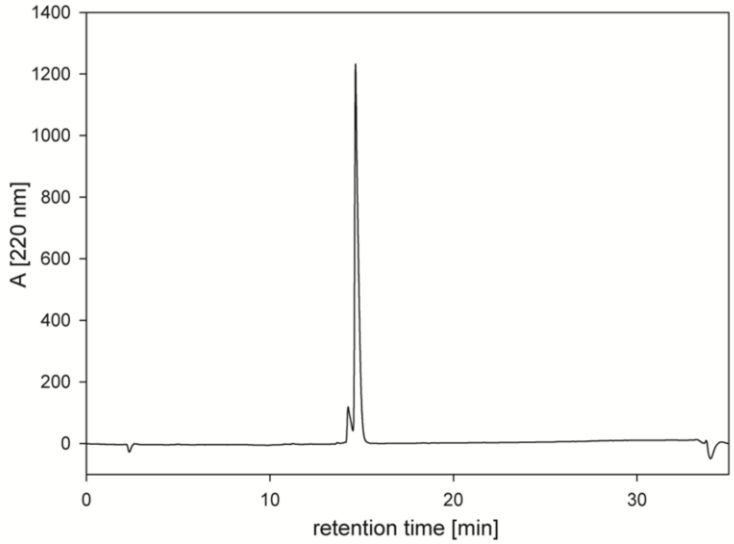

Figure ESI-46: *HPLC trace of compound* ***18****. Absorbance at 220 nm; gradient 10→100 B;* t_R*=14.78 min.*

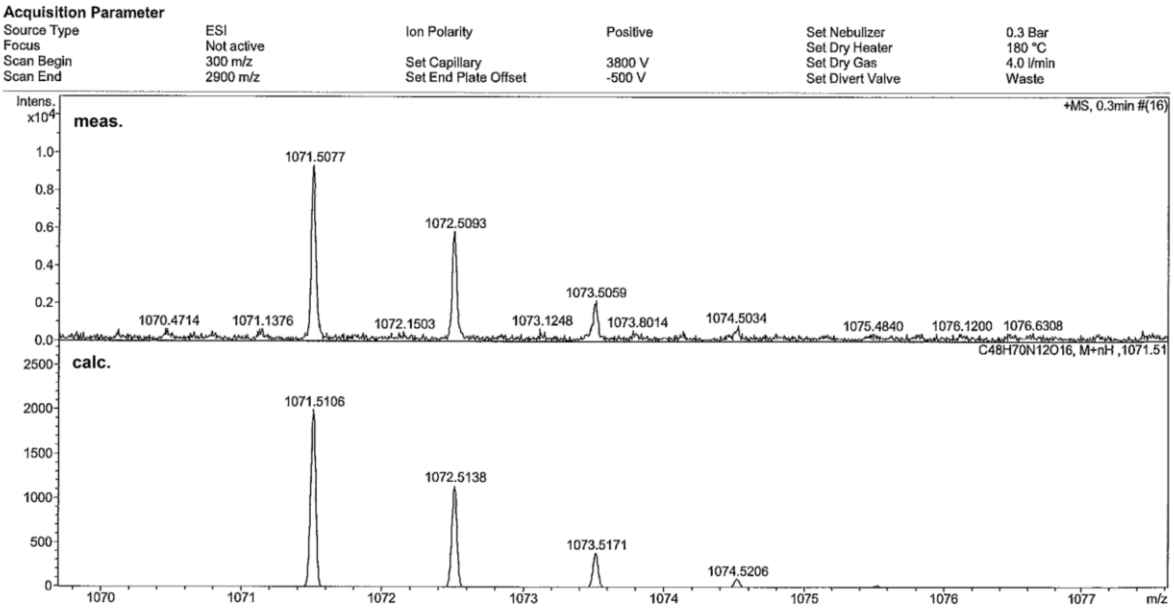

Figure ESI-47: *Section of HR ESI-MS spectrum of compound* ***18****. Upper panel: measured isotopic pattern* $[M+H]^+$*. Lower panel: simulated isotopic pattern* $[M+H]^+$*.*

1.2.19 Compound 19

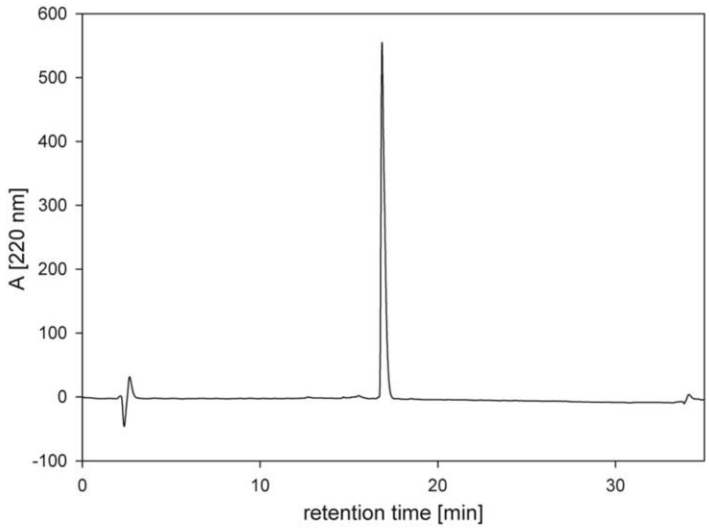

Figure ESI-48: *HPLC trace of compound* ***19****. Absorbance at 220 nm; gradient 10→100 B;* t_R*=16.72 min.*

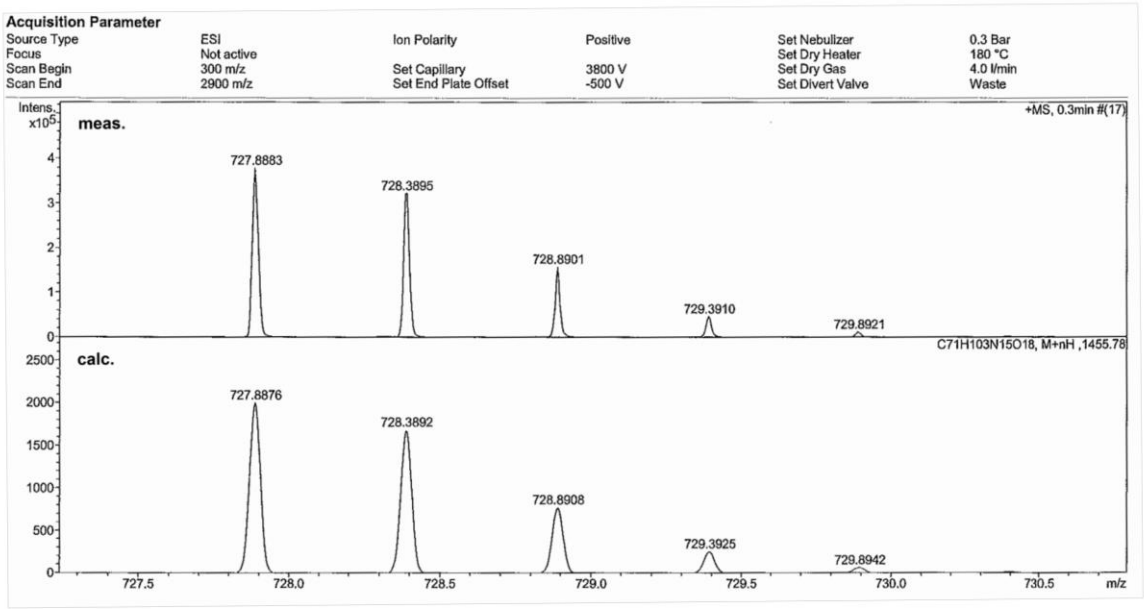

Figure ESI-49: *Section of HR ESI-MS spectrum of compound* ***19****. Upper panel: measured isotopic pattern* $[M+2H]^{2+}$*. Lower panel: simulated isotopic pattern* $[M+2H]^{2+}$*.*

1.2.20 Compound 20

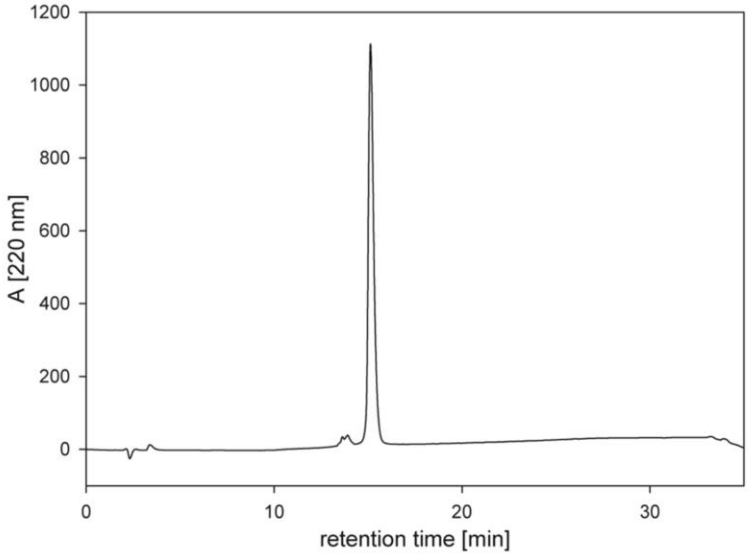

Figure ESI-50: *HPLC trace of compound* ***20****. Absorbance at 220 nm; gradient 10→100 B;* t_R*=15.07 min.*

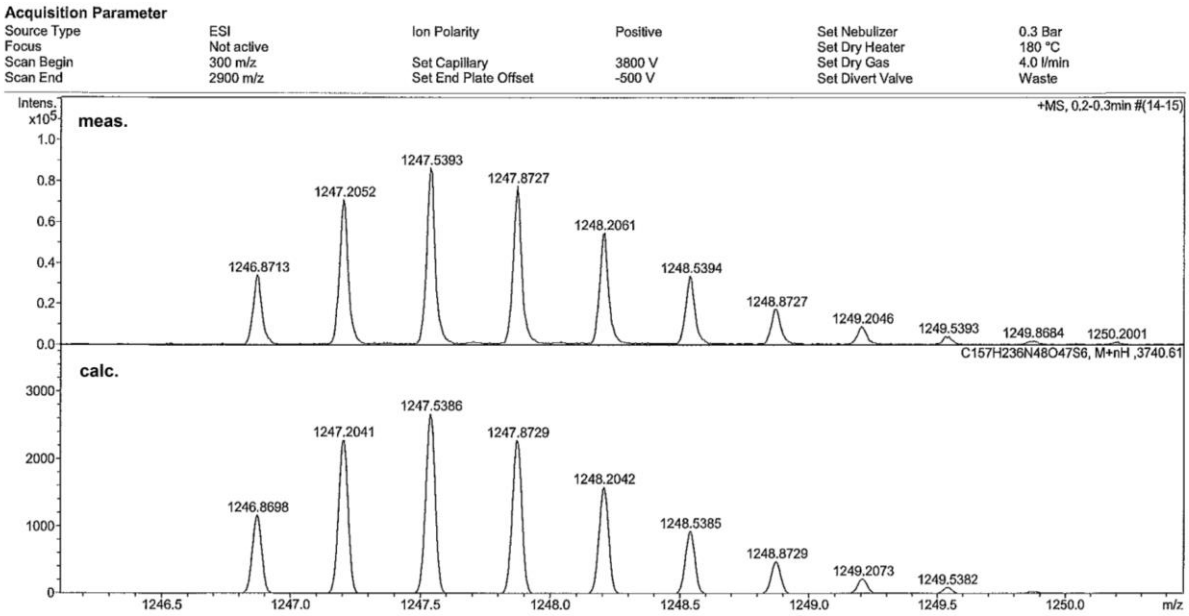

Figure ESI-51: *Section of HR ESI-MS spectrum of compound* ***20****. Upper panel: measured isotopic pattern* $[M+3H]^{3+}$*. Lower panel: simulated isotopic pattern* $[M+3H]^{3+}$*.*

1.2.21 Compound 21

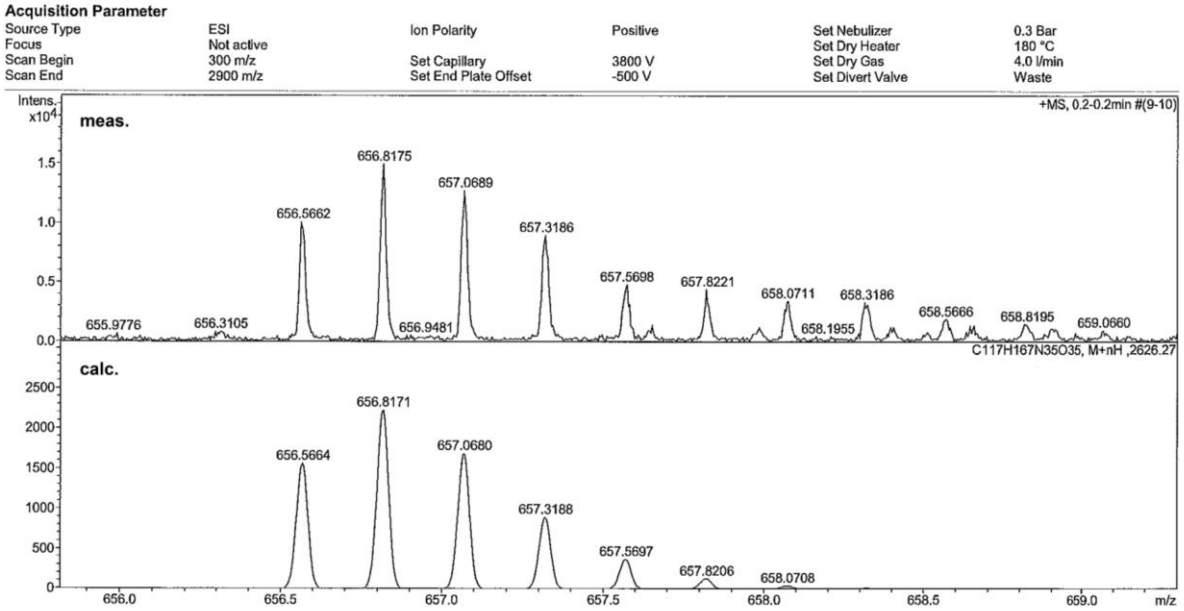

Figure ESI-52: *Fragment of HR ESI-MS spectrum of compound* ***21****. Upper panel: measured isotopic pattern* $[M+4H]^{4+}$*. Lower panel: simulated isotopic pattern* $[M+4H]^{4+}$*.*

1.2.22 Compound 22

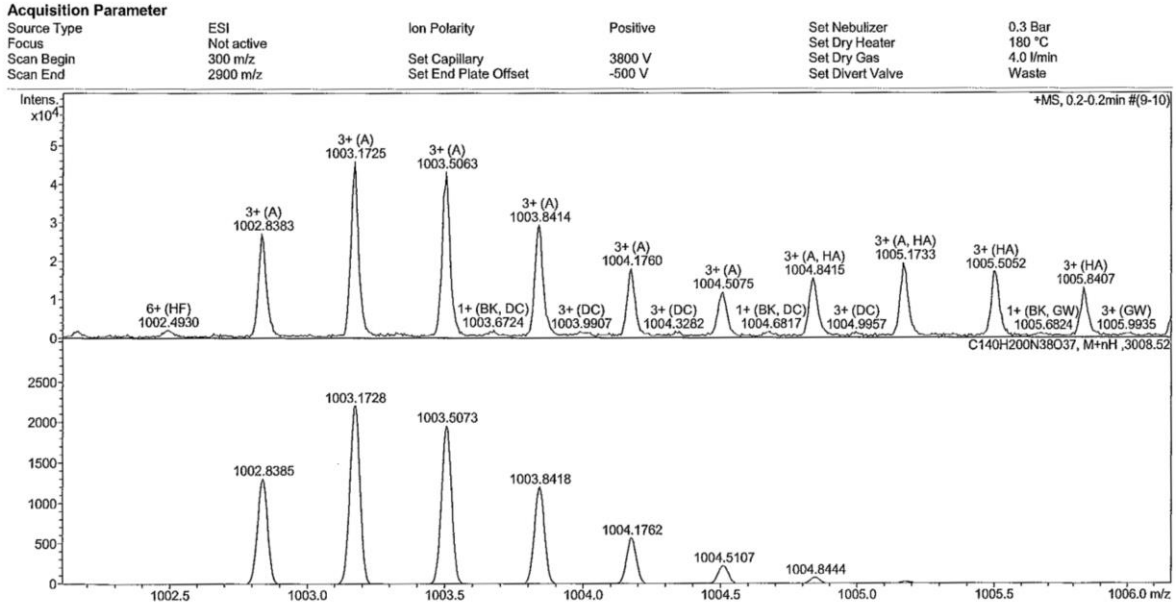

Figure ESI-53: *Section of HR ESI-MS spectrum of compound* ***22****. Upper panel: measured isotopic pattern* $[M+3H]^{3+}$*. Lower panel: simulated isotopic pattern* $[M+3H]^{3+}$*.*

1.2.23 Compound 23

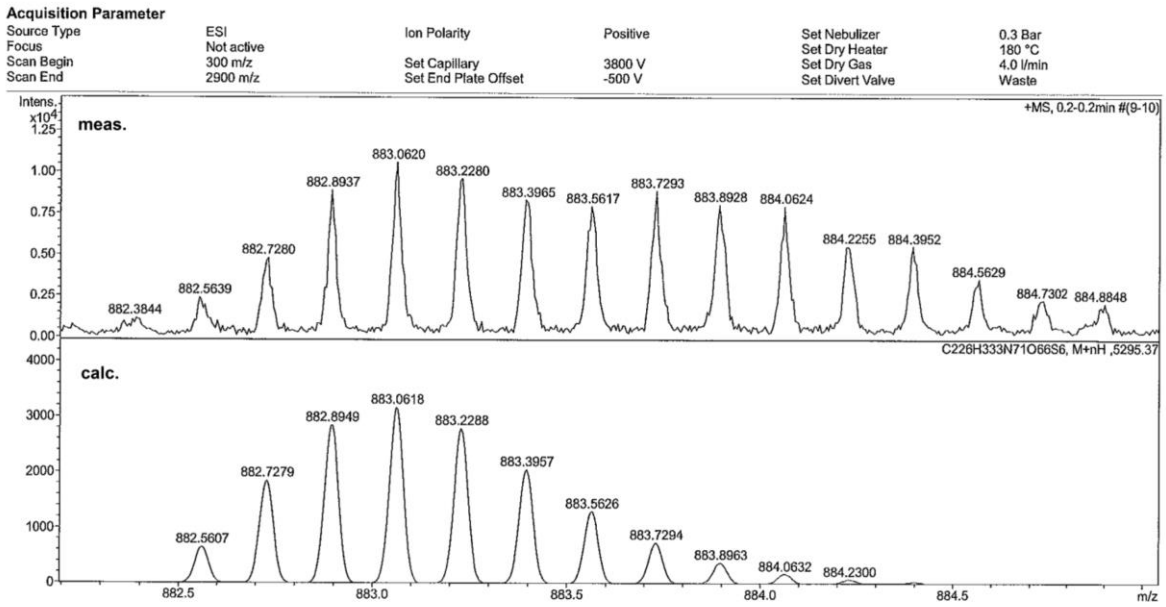

Figure ESI-54: *Section of HR ESI-MS spectrum of compound* ***23****. Upper panel: measured isotopic pattern* $[M+6H]^{6+}$*. Lower panel: simulated isotopic pattern* $[M+6H]^{6+}$*.*

1.2.24 Compound 24

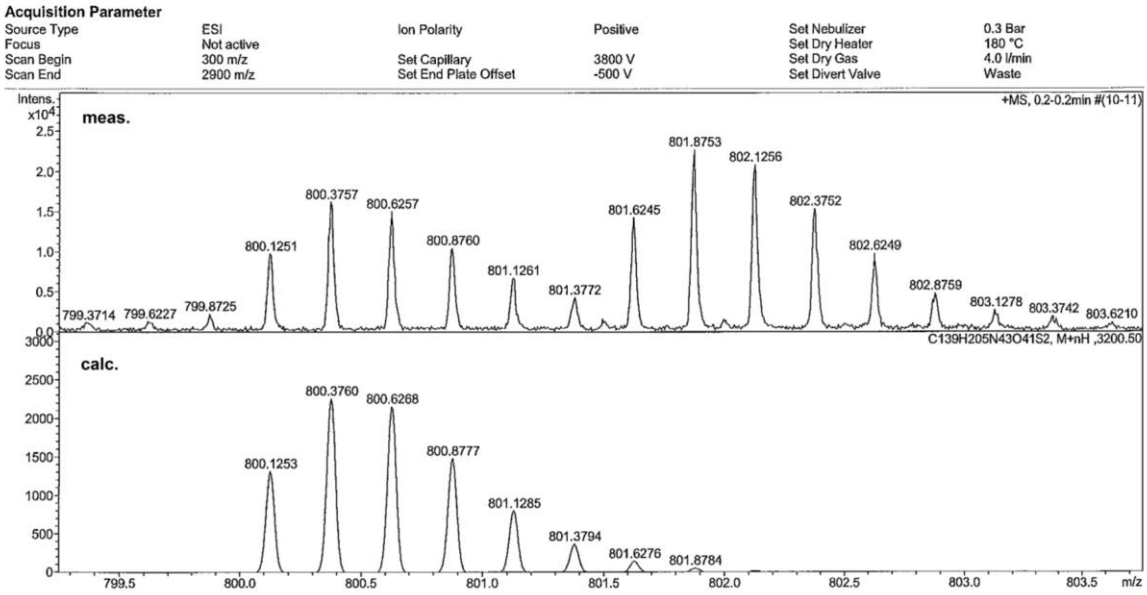

Figure ESI-55: *Section of HR ESI-MS spectrum of compound* ***24****. Upper panel: measured isotopic pattern* $[M+4H]^{4+}$*. Lower panel: simulated isotopic pattern* $[M+4H]^{4+}$*.*

1.2.25 Compound 25

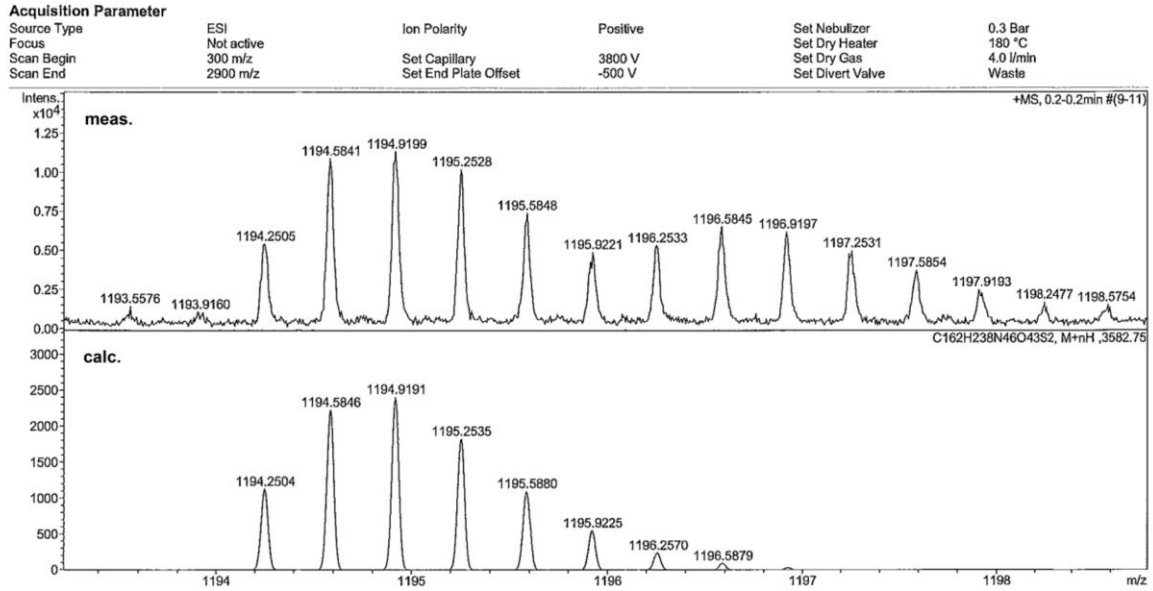

Figure ESI-56: *Section of HR ESI-MS spectrum of compound* ***25****. Upper panel: measured isotopic pattern* $[M+3H]^{3+}$*. Lower panel: simulated isotopic pattern* $[M+3H]^{3+}$*.*

1.2.26 Compound 26

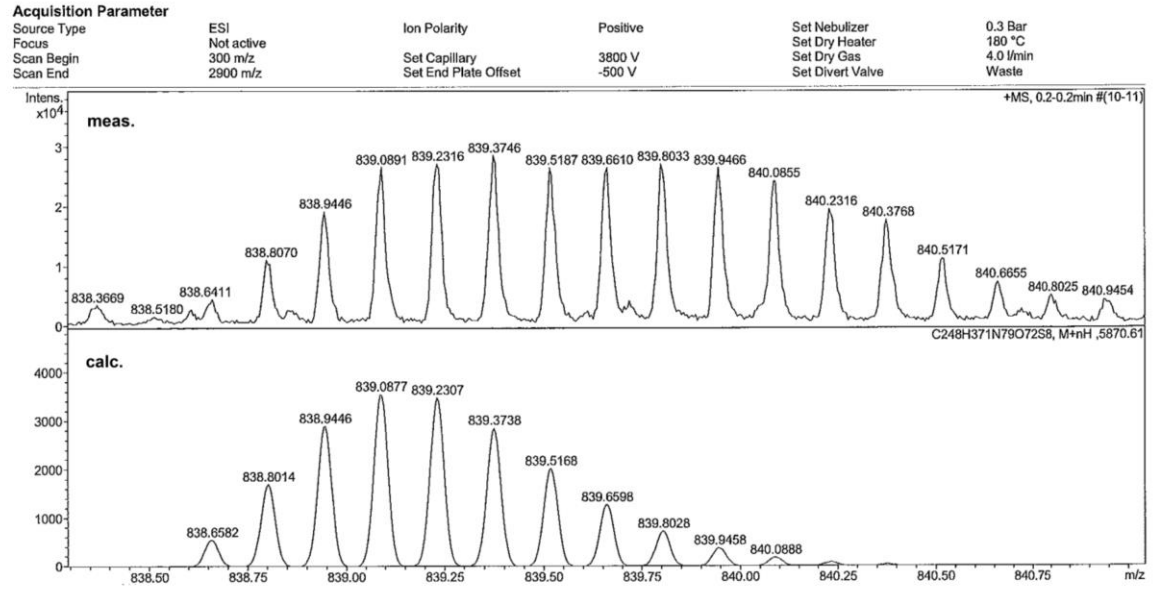

Figure ESI-57: *Section of HR ESI-MS spectrum of compound* ***26****. Upper panel: measured isotopic pattern* $[M+7H]^{7+}$*. Lower panel: simulated isotopic pattern* $[M+7H]^{7+}$*.*

1.2.27 Compound 27

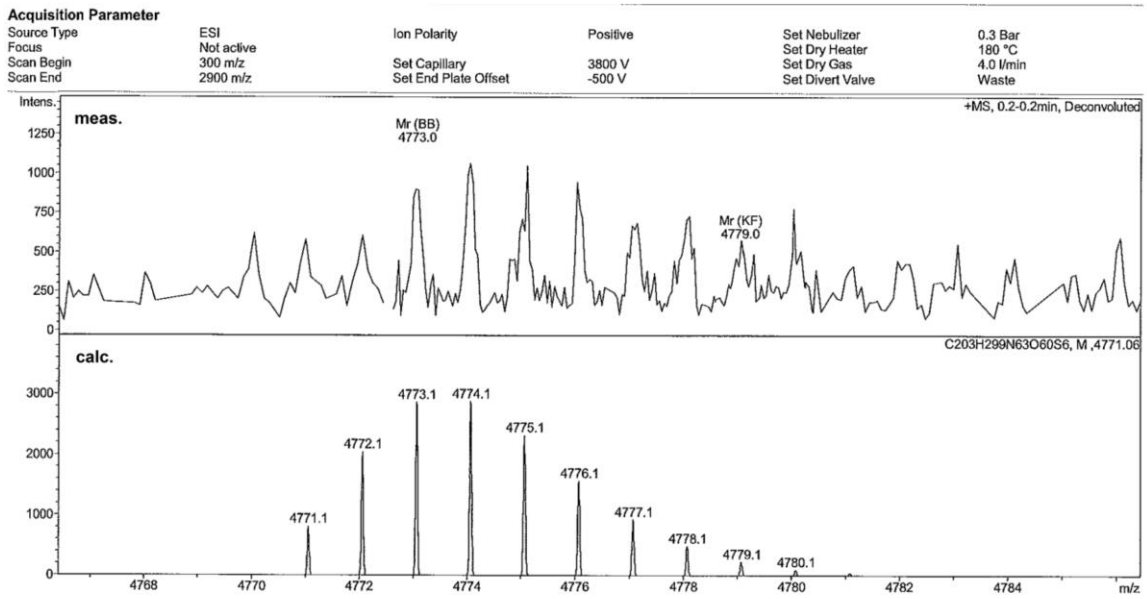

Figure ESI-58: *Section of deconvoluted HR ESI-MS spectrum of compound* ***27****. Upper panel: deconvoluted isotopic pattern measured. Lower panel: calculated isotopic pattern.*

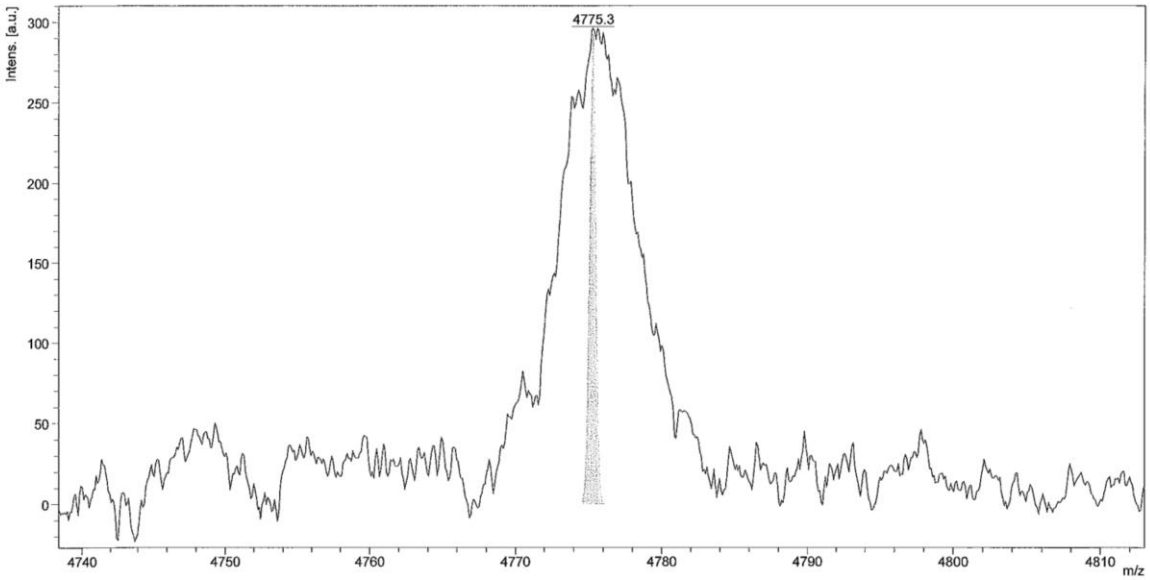

Figure ESI-59: *Fragment of a MALDI-MS spectrum of compound* ***27****.Calc. for* $C_{203}H_{299}N_{63}O_{60}S_6$ *4774.4 meas. 4775.3* $[M+H]^+$.

1.2.28 Compound 28

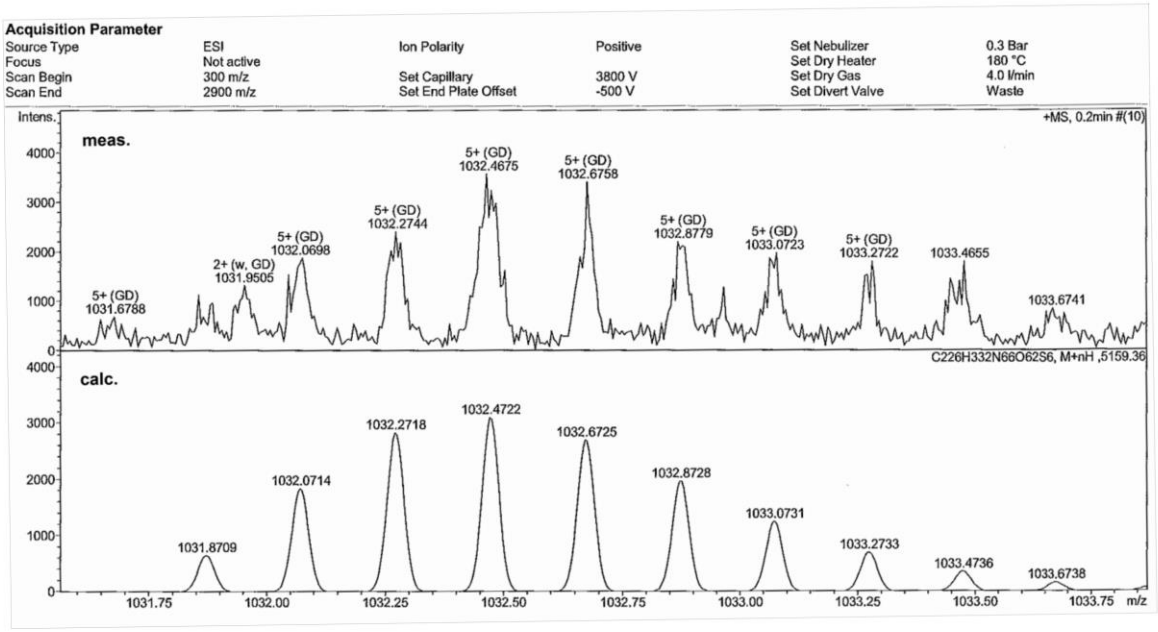

Figure ESI-60: *Section of HR ESI-MS spectrum of compound* ***28****. Upper panel: measured isotopic pattern* $[M+5H]^{5+}$*. Lower panel: simulated isotopic pattern* $[M+5H]^{5+}$*.*

1.2.29 Compound 29 possessed extremely poor ionization upon mass-spectrometric analysis, combined with strong aggregation tendency. Therefore, although mass peaks corresponding to $[M+K^{+}+H^{+}]$ species were found in MALDI-MS spectrum, it was not used for characterization, and analysis relied on chromatographic methods (see Fig. ESI-2).

1.2.30 Compound 30

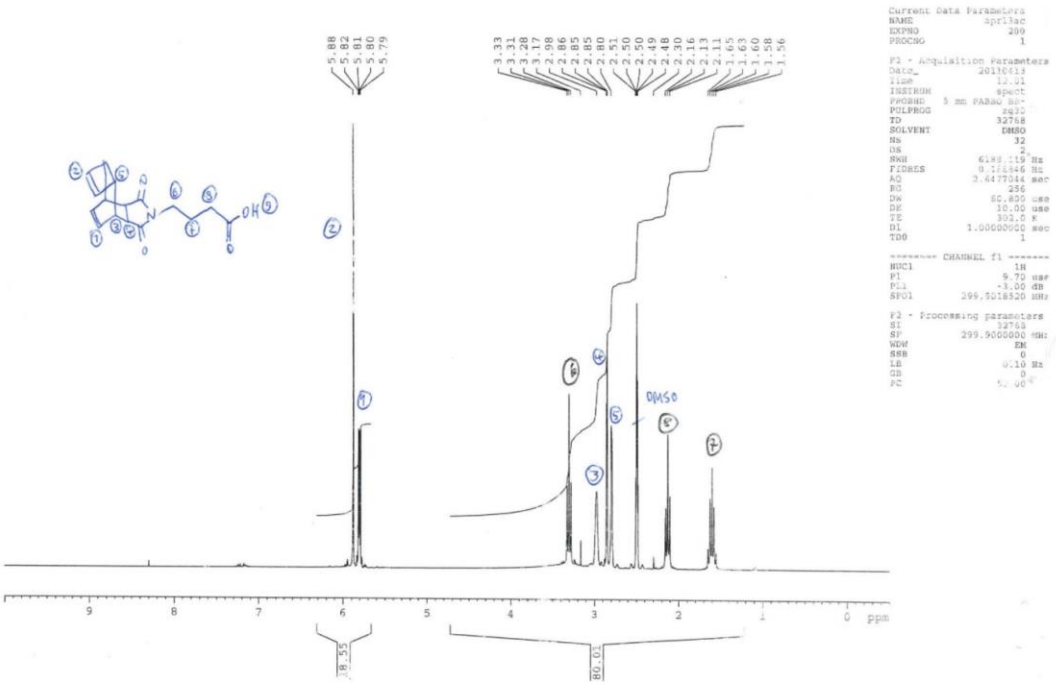

Figure ESI-62: *^{1}H-NMR spectrum of compound* ***30****.*

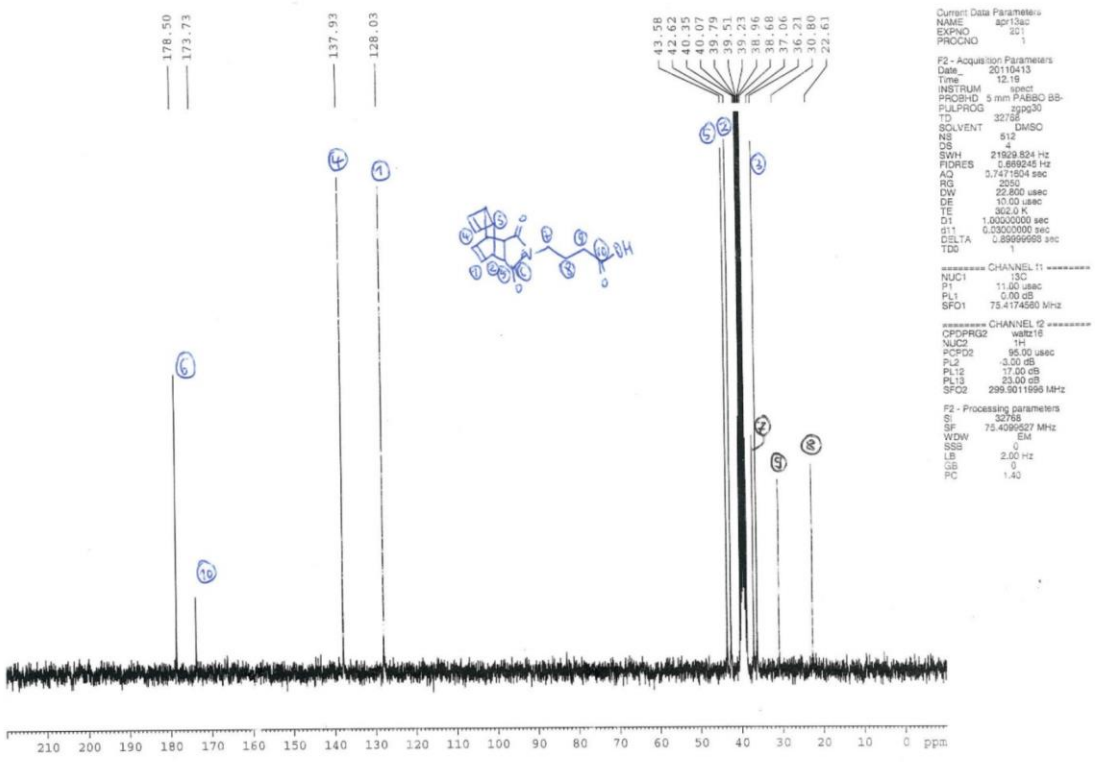

Figure ESI-63: *^{13}C-NMR spectrum of compound **30**.*

1.2.31 Compound 31

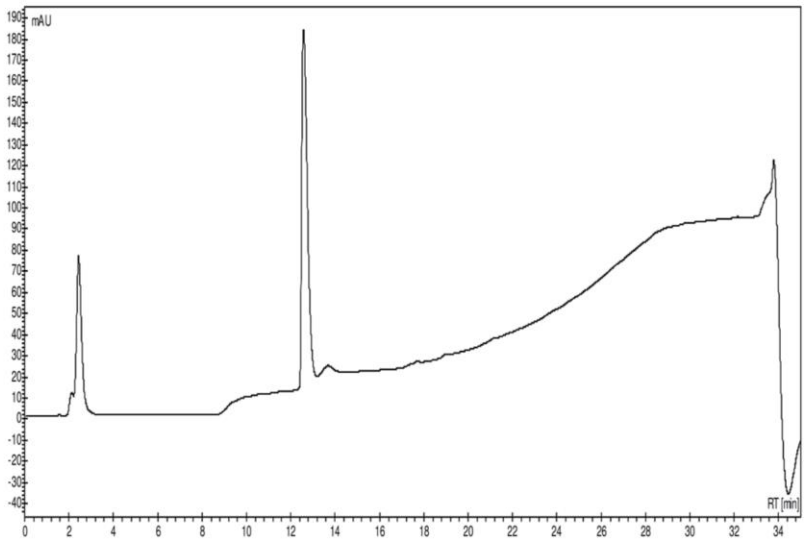

Figure ESI-64: *HPLC trace of compound **31**. Absorbance at 220 nm; gradient 10→100 B; t_R=12.27 min.*

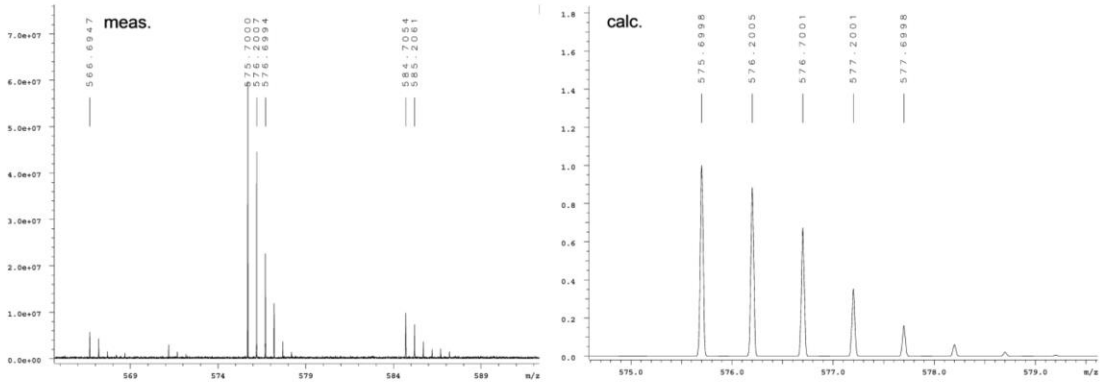

Figure ESI-65: *Section of ESI-HR-MS spectrum of compound* ***31****. Left: measured isotopic pattern* $[M+3H]^{3+}$*; right: calculated isotopic pattern* $[M+3H]^{3+}$*.*

1.2.32 Compound 32

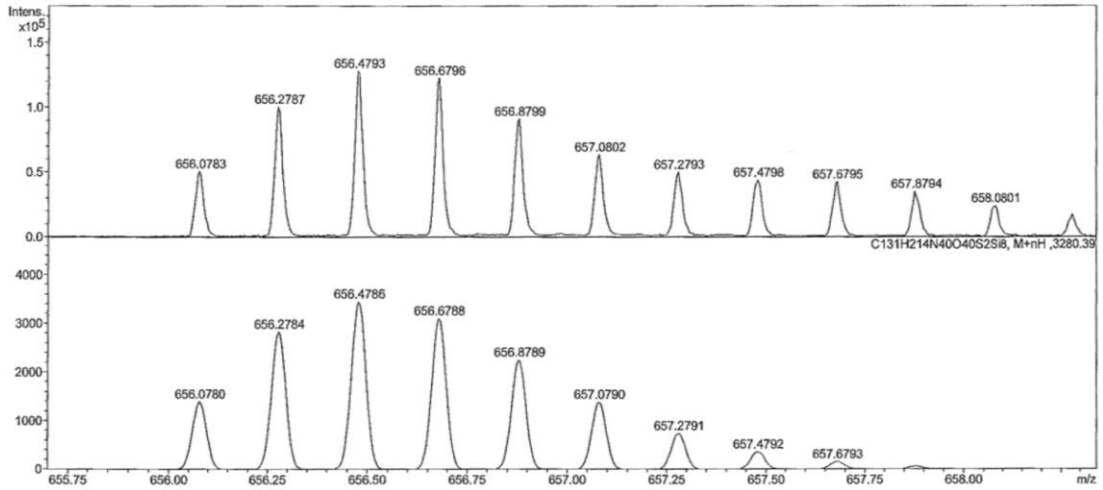

Figure ESI-66: *Section of HR ESI-MS spectrum of compound* ***32****. Upper panel: measured isotopic pattern* $[M+5H]^{5+}$*. Lower panel: simulated isotopic pattern* $[M+5H]^{5+}$*.*

2 References

[1] W. Reppe, *Justus Liebigs Ann. Chem.,* **1948**, *560*, 1-92. (page 66)

[2] V. Dulery, O. Renaudet, P. Dumy, Tetrahedron, **2007**, *63*, 11952–11958.

[3] R. Pipkorn, W. Waldeck, B. Didinger, M. Koch, G. Mueller, M. Wiessler, K. J. Braun, *J. Pept. Sci.,* **2009**, *15*, 235−241.

[4] H. Fittler, O. Avrutina, B. Glotzbach, M. Empting, H. Kolmar, *Org. Biomol. Chem.*, **2013**, *11*, 1848–1857.

[5] M. Reinwarth, B. Glotzbach, M. Tomaszowski, S. Fabritz, O. Avrutina, H. Kolmar, *ChemBioChem*, **2013**, *14*, 137–146.

6.3. Nanoscale biodegradable organic-inorganic hybrids for efficient cell penetration and drug delivery

Supporting Information

Nanoscale Biodegradable Organic–Inorganic Hybrids for Efficient Cell Penetration and Drug Delivery

*Sebastian Hörner[+], Sascha Knauer[+], Christina Uth[+], Marina Jöst, Volker Schmidts, Holm Frauendorf, Christina Marie Thiele, Olga Avrutina, and Harald Kolmar**

ange_201606065_sm_miscellaneous_information.pdf

Supporting Information (SI)

Content

1. Live-cell laser scanning confocal microscopy and fluorescence microscopy studies

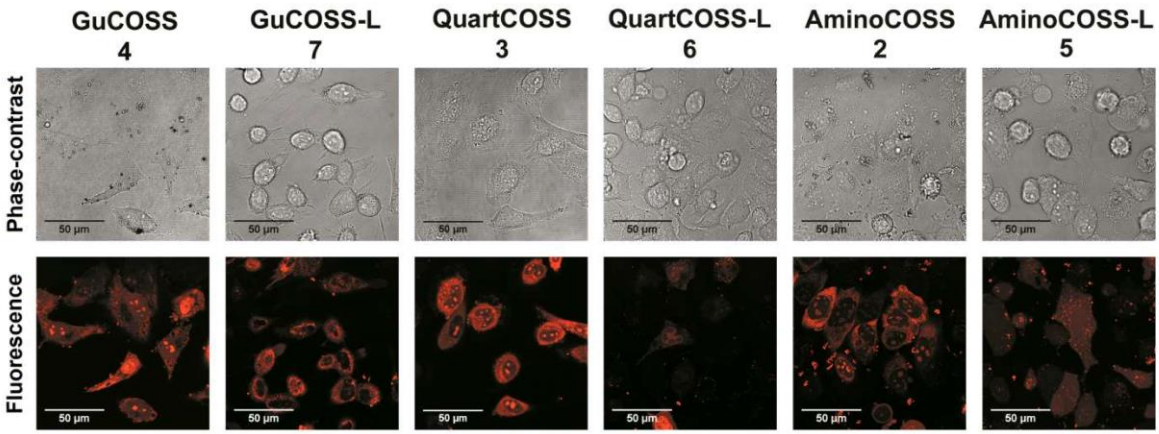

Figure S1: *Live-cell laser scanning confocal microscopy imaging of cellular uptake of TAMRA-labeled COSS derivatives 2-7. Cells were incubated with 20 µM of the respective COSS derivative in DMEM media lacking fetal bovine serum (FBS) for 30 min at 37°C. After incubation, the cells were washed thrice with PBS and investigated in DMEM media containing 2 vol% FBS. Controls with cells similarly treated in the absence of the respective COSS derivative showed no fluorescence (not shown).*

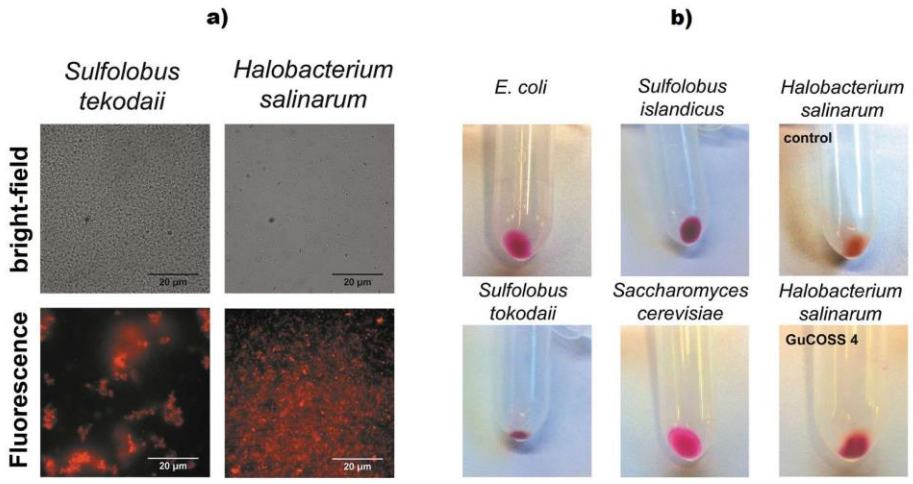

Figure S2: *Fluorescence microscopy imaging of cells incubated with TAMRA-labeled GuCOSS **4** at a concentration of 20 µM for 30 min: a) Sulfolobus tekodaii incubated at 80°C and Halobacterium salinarum incubated at ambient temperature. Controls with cells similarly treated in the absence of the respective COSS derivative showed no fluorescence. b) Pellets of cells incubated with GuCOSS **4** at a concentration of 20 µM for 30 min; E. coli incubated at 37°C; Sulfolobus islandicus incubated at 80°C; Sulfolobus tokodaii incubated at 80°C; Saccharomyces cerevisiae incubated at ambient temperature; Halobacterium salinarium incubated at ambient temperature. Due to background color of Halobacterium salinarium untreated cells are shown.*

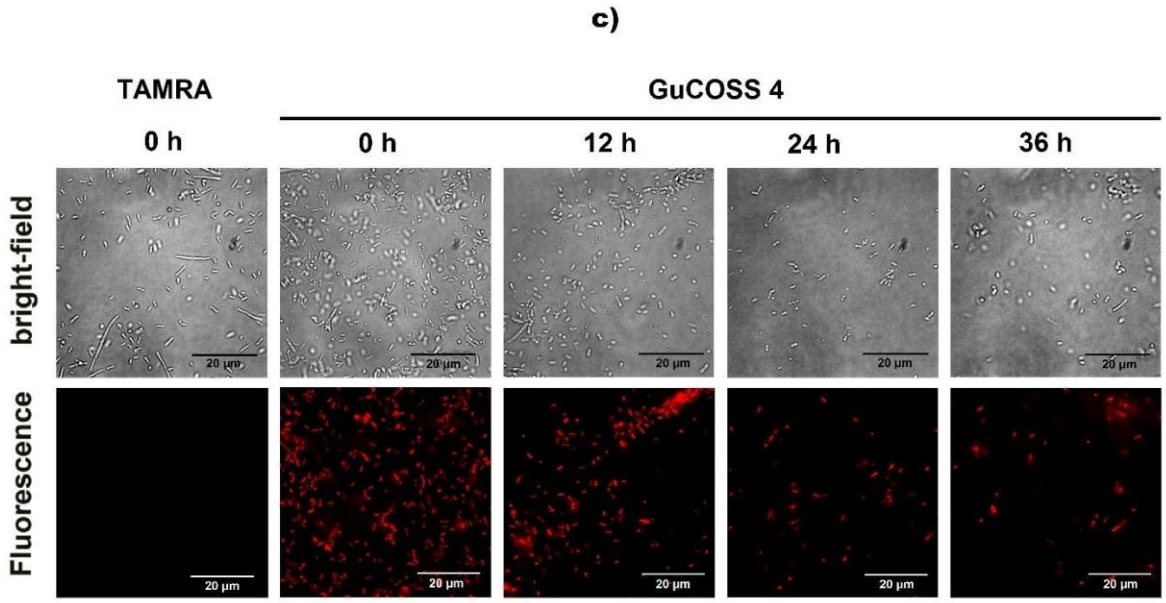

Figure S2: *c) Incubation of E.coli with GuCOSS **4** and 5-carboxytetramethylrhodamine (TAMRA) at a concentration of each 20 µM for 30 min at 37 °C. No fluorescence was observed when E. coli were incubated with solitaire TAMRA (same exposure time as for GuCOSS **4** was used). Fluorescence of E. coli incubated with GuCOSS **4** was still detectable after an incubation time of 36 h in PBS at pH 7.4, 37 °C.*

Discussion on figure S 2c:

As GuCOSS **4** could be of interest for the delivery of antibiotics, we investigated its ability to penetrate *E. coli* in detail. To that end, we incubated bacteria with 5-carboxytetramethylrhodamine (TAMRA) or TAMRA-labelled GuCOSS **4**. After incubation with **4** strong fluorescence was observed in microscopy experiments, whereas after incubation with solitaire dye no fluorescence signal was detected, suggesting that TAMRA was not associated with the cell membrane of *E. coli*. To exclude the possibility that the recorded fluorescence was attributed to the accumulation of **4** on the cell membrane *via* its GuCOSS part, we examined stained bacteria under COSS degradation-promoting conditions. Indeed, we found that bacterial cells treated with **4** retained their fluorescence after incubation in PBS (pH 7.4) for 36 hours (Figure S 2c). As it is known that the COSS carrier degrades at pH 7.4 within 18 h (Figure 3c-d, Figure S9), this observation clearly indicates that the TAMRA fluorophore is trapped inside the bacteria.

2. Flow-cytometric studies

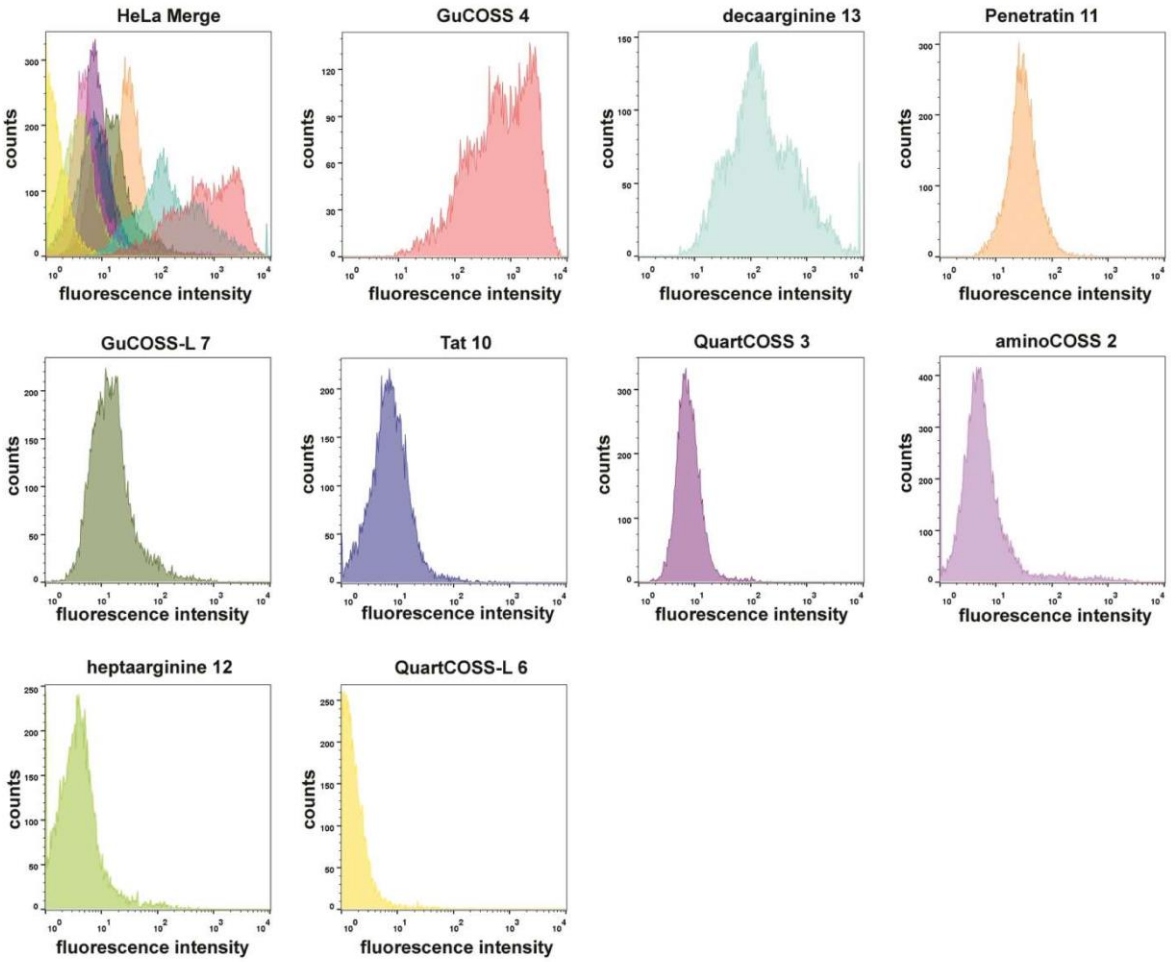

Figure S3 a: *First of three independent flow-cytometric studies of the cellular uptake of highly efficient COSS derivatives (**2**, **3**, **4**, **6**, and **7**) and cell-penetrating peptides **10-13** in HeLa cells. Cells were incubated with 20 µM of the respective compound in DMEM lacking fetal bovine serum (FBS) for 10 min at 37°C. After incubation, the cells were washed thrice with PBS both before and after trypsinization for 10 min at ambient temperature. Afterwards cells were kept on ice. Experiments with HeLa cells were performed in triplicates, each comprising 10000 events; average values are shown.*

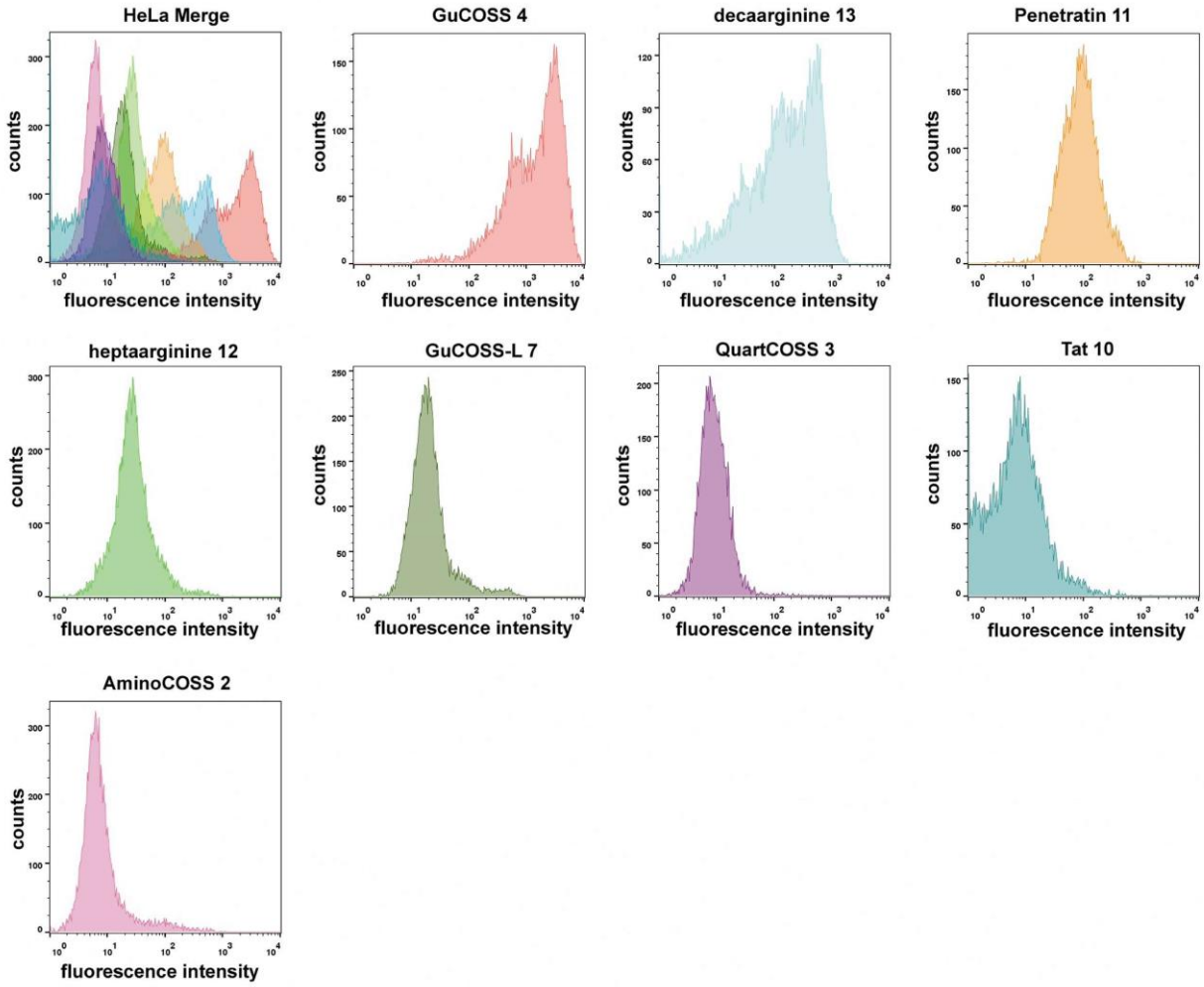

Figure S3 b: *Second of three independent flow-cytometric studies of the cellular uptake of highly efficient COSS derivatives (**2**, **3**, **4**, and **7**) and cell-penetrating peptides **10-13** in HeLa cells. Cells were incubated with 20 µM of the respective compound in DMEM lacking fetal bovine serum (FBS) for 10 min at 37°C. After incubation, the cells were washed thrice with PBS both before and after trypsinization for 10 min at ambient temperature. Afterwards cells were kept on ice. Experiments with HeLa cells were performed in triplicates, each comprising 10000 events; average values are shown.*

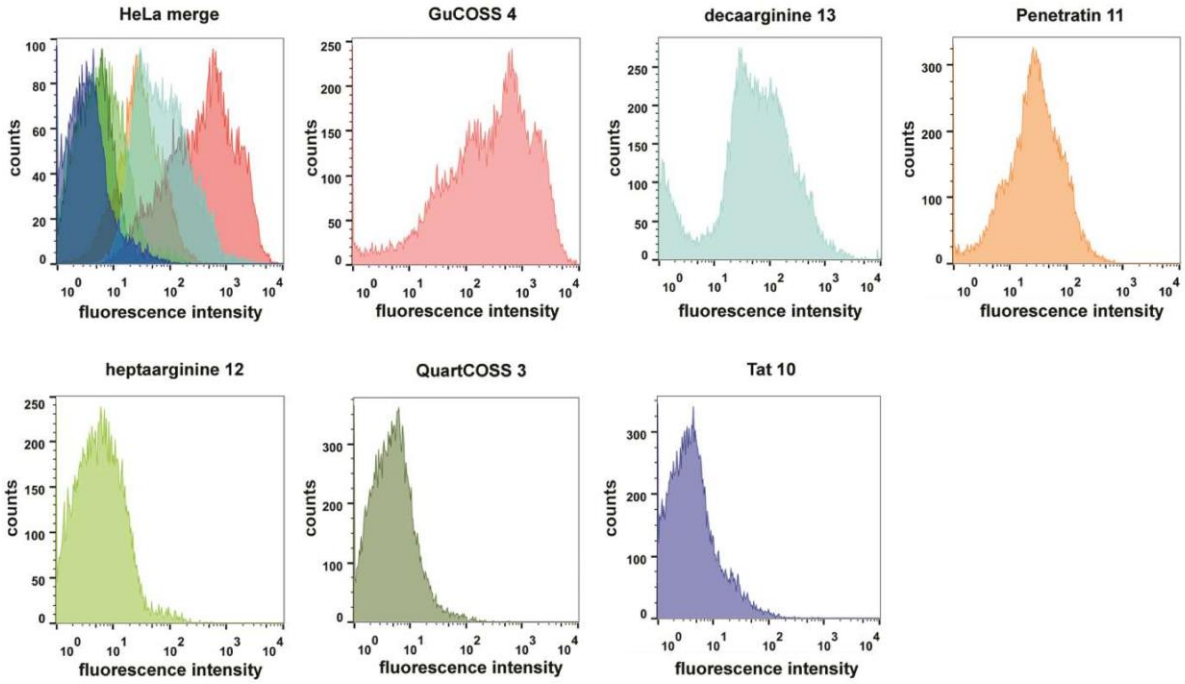

Figure S3 c: *Third of three independent flow-cytometric studies of the cellular uptake of highly efficient COSS derivatives (**3** and **4**) and cell-penetrating peptides **10-13** in HeLa cells. Cells were incubated with 20 µM of the respective compound in DMEM lacking fetal bovine serum (FBS) for 10 min at 37°C. After incubation, the cells were washed thrice with PBS both before and after trypsinization for 10 min at ambient temperature. Afterwards cells were kept on ice. Experiments with HeLa cells were performed in triplicates, each comprising 10000 events; average values are shown.*

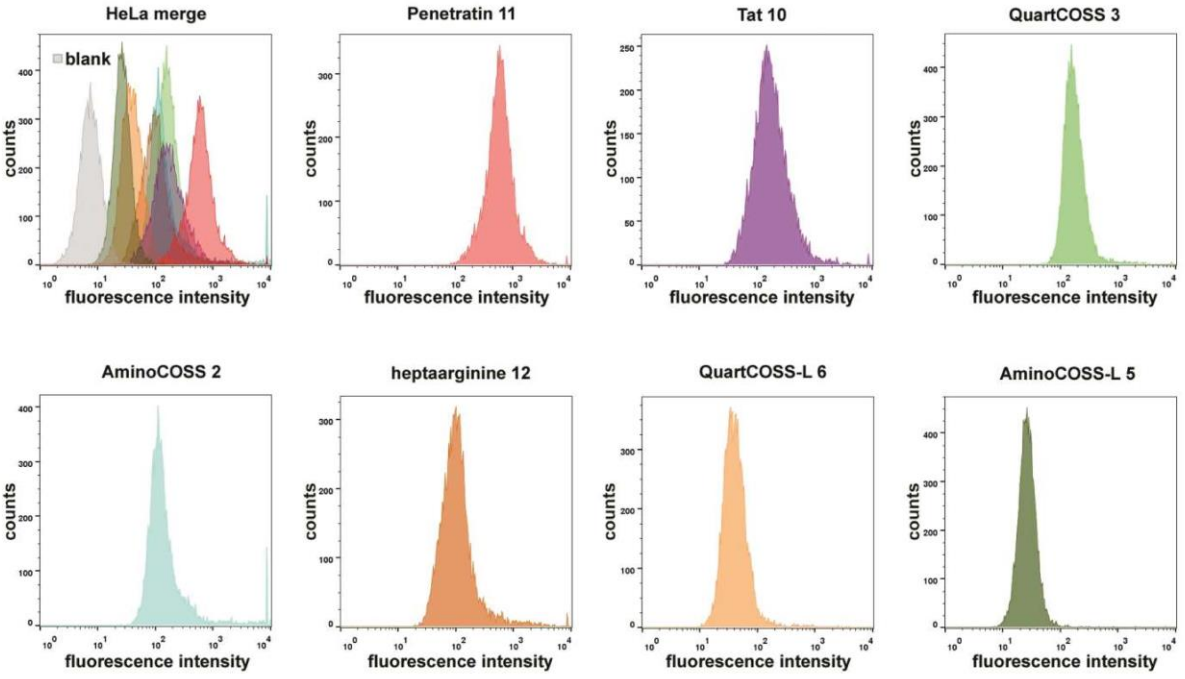

Figure S3 d: *First of three independent flow-cytometric studies of the cellular uptake of COSS derivatives (**2**, **3**, **5**, and **6**) and cell-penetrating peptides **10-12** in HeLa cells. Cells were incubated with 20 µM of the respective compound in DMEM lacking fetal bovine serum (FBS) for 10 min at 37°C. After incubation, the cells were washed thrice with PBS both before and after trypsinization for 10 min at ambient temperature. Afterwards cells were kept on ice. Experiments with HeLa cells were performed in triplicates, each comprising 10000 events; average values are shown.*

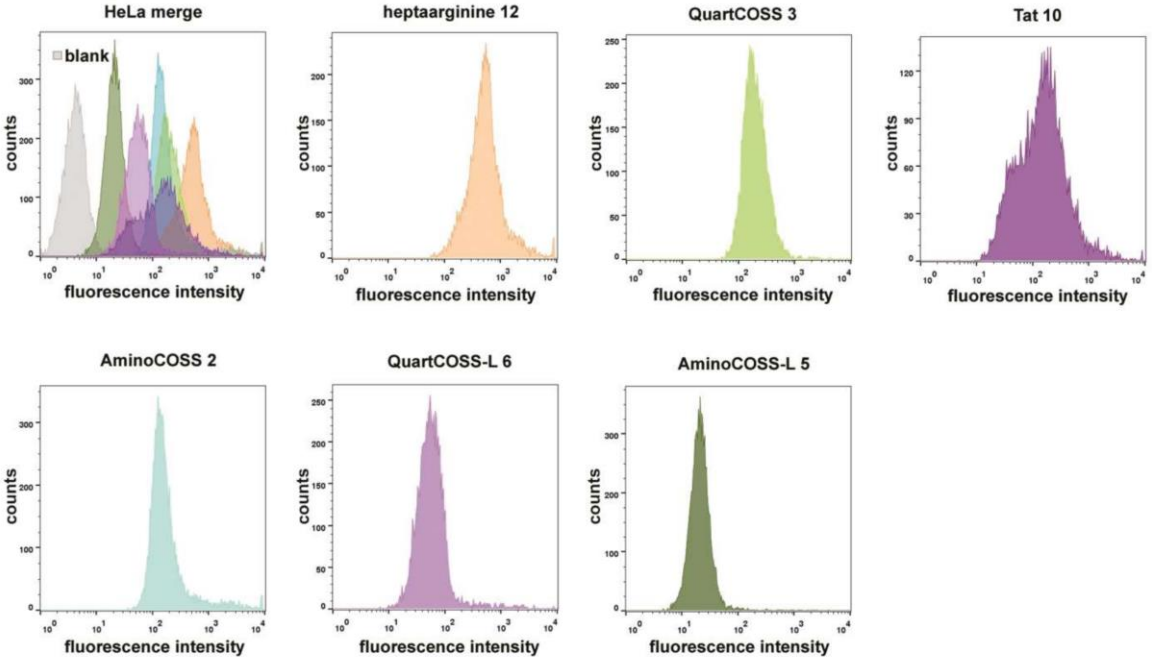

Figure S3 e: *Second of three independent flow-cytometric studies of the cellular uptake of COSS derivatives (**2**, **3**, **5**, and **6**) and cell-penetrating peptides **10** and **12** in HeLa cells. Cells were incubated with 20 µM of the respective compound in DMEM lacking fetal bovine serum (FBS) for 10 min at 37°C. After incubation, the cells were washed thrice with PBS both before and after trypsinization for 10 min at ambient temperature. Afterwards cells were kept on ice. Experiments with HeLa cells were performed in triplicates, each comprising 10000 events; average values are shown.*

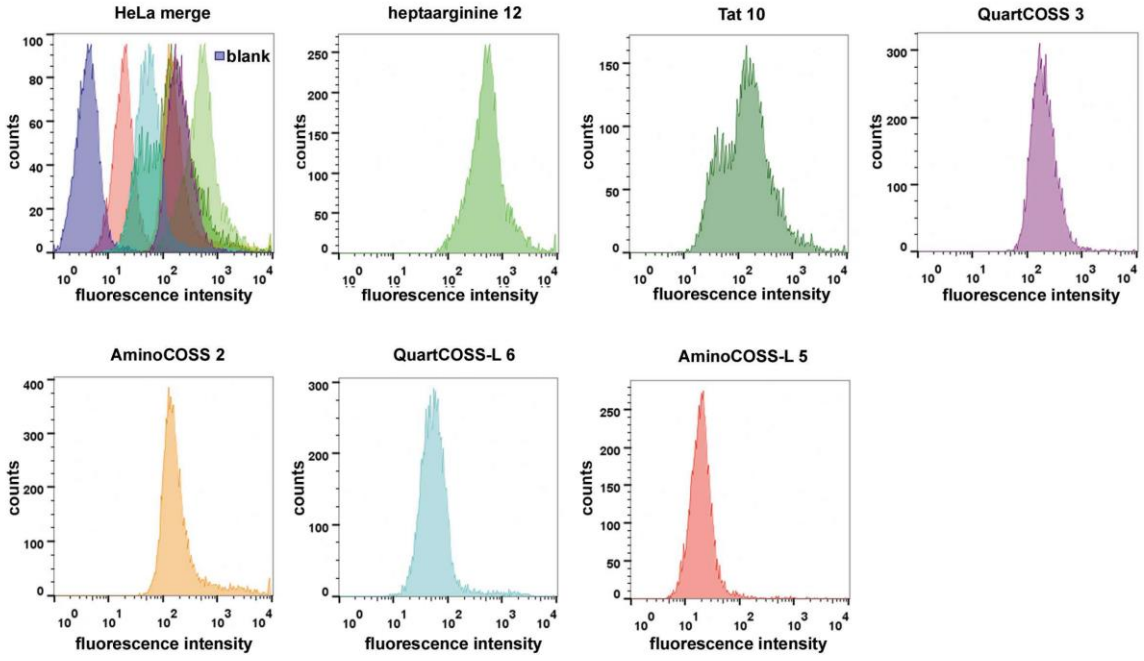

Figure S3 f: *Third of three independent flow-cytometric studies of the cellular uptake of COSS derivatives (**2**, **3**, **5**, and **6**) and cell-penetrating peptides **10** and **12** in HeLa cells. Cells were incubated with 20 µM of the respective compound in DMEM lacking fetal bovine serum (FBS) for 10 min at 37°C. After incubation, the cells were washed thrice with PBS both before and after trypsinization for 10 min at ambient temperature. Afterwards cells were kept on ice. Experiments with HeLa cells were performed in triplicates, each comprising 10000 events; average values are shown.*

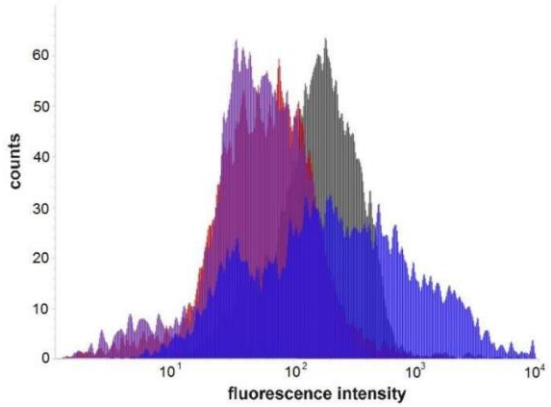

Figure S3 g: *Flow-cytometric studies of the cellular uptake of COSS derivative **4** and cell-penetrating peptides **10, 11** and **12** in HeLa cells. Cells were incubated with 20 µM of the respective compound in DMEM lacking fetal bovine serum (FBS) for 60 min at 37°C. After incubation, the cells were washed thrice with PBS both before and after trypsinization for 10 min at ambient temperature. Afterwards cells were kept on ice. Experiments with HeLa cells were performed in triplicates, each comprising 10000 events; average values are shown. Violet: **12**, red: **10**, grey: **11**, blue:**4**.*

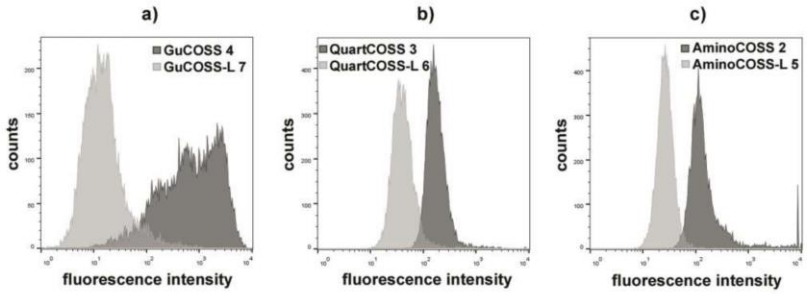

Figure S4: *Direct comparison of cellular uptake of COSS derivatives equipped with similar functional groups and varying in the linker length (in HeLa cells). a) GuCOSS **4** and GuCOSS-L **7** bearing an elongated linker; b) QuartCOSS **3** and QuartCOSS-L **6** bearing an elongated linker; c) AminoCOSS **2** and AminoCOSS-L **5** bearing an elongated linker. Cells were incubated with 20 µM of the respective compound in DMEM lacking fetal bovine serum (FBS) for 10 min at 37°C. After incubation, the cells were washed thrice with PBS both before and after trypsinization for 10 min at ambient temperature. Afterwards cells were kept on ice. Experiments with HeLa cells were performed in triplicates, each comprising 10000 events; average values are shown. In general, shorter linkers (compounds **2**-**4**) led to enhanced cellular uptake whereas cellular uptake of linker-bearing derivatives **5**-**7** was reduced when compared to the directly modified derivative.*

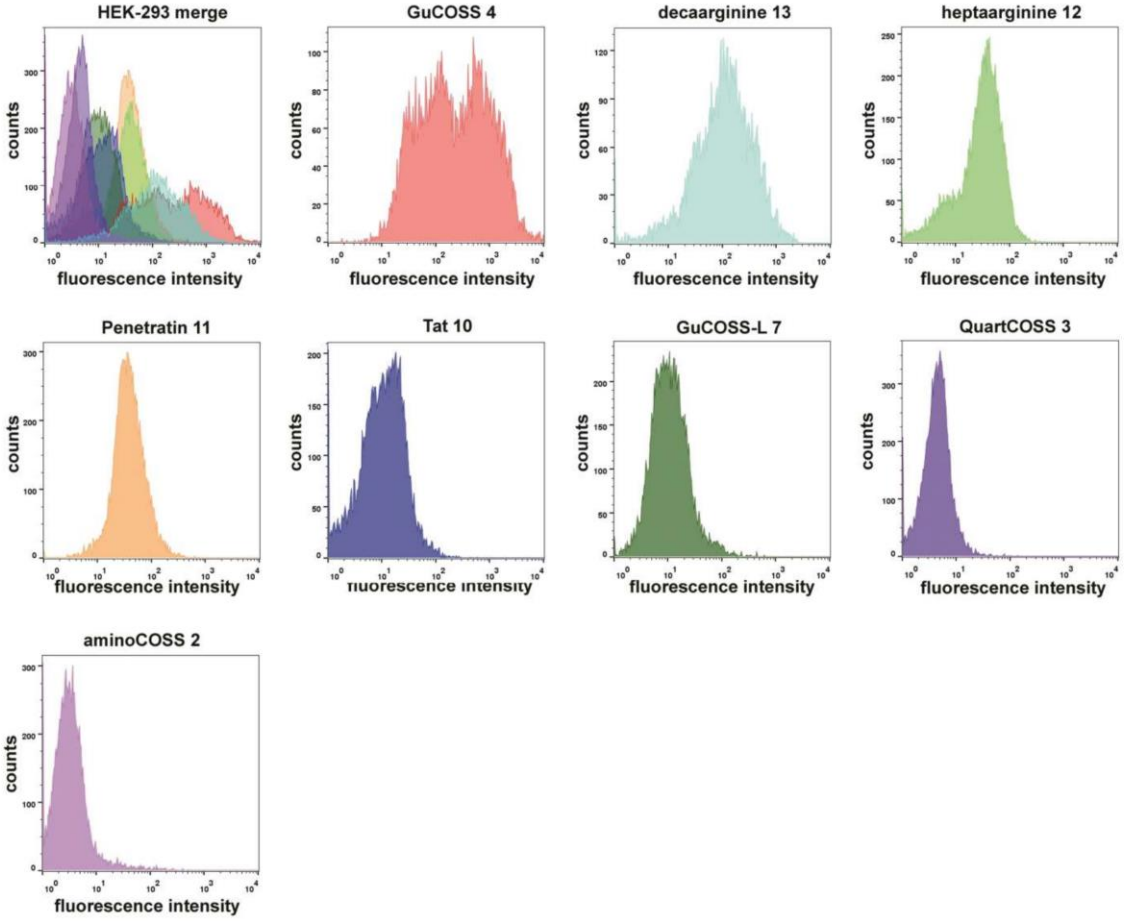

Figure S5 a: *Flow-cytometric studies of the cellular uptake of COSS derivatives (**2**, **3**, **4**, and **7**) and cell-penetrating peptides **10-13** in HEK-293 cells. Cells were incubated with 20 µM of the respective compound in DMEM lacking fetal bovine serum (FBS) for 10 min at 37°C. After incubation, the cells were washed thrice with PBS both before and after trypsinization for 10 min at ambient temperature. Afterwards cells were kept on ice. Experiments with HEK-293 cells were performed in triplicates, each comprising 10000 events; average values are shown.*

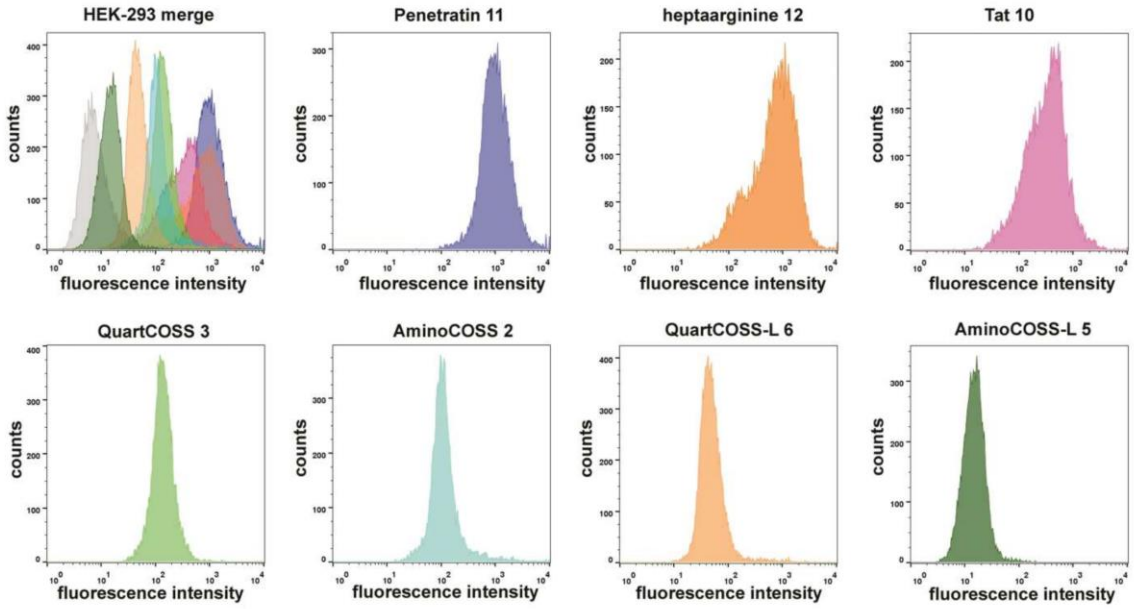

Figure S5 b: *Flow-cytometric studies of the cellular uptake of COSS derivatives (**2**, **3**, **5**, and **6**) and cell-penetrating peptides **10-12** in HEK-293 cells. Cells were incubated with 20 µM of the respective compound in DMEM lacking fetal bovine serum (FBS) for 10 min at 37°C. After incubation, the cells were washed thrice with PBS both before and after trypsinization for 10 min at ambient temperature. Afterwards cells were kept on ice. Experiments with HEK-293 cells were performed in triplicates, each comprising 10000 events; average values are shown.*

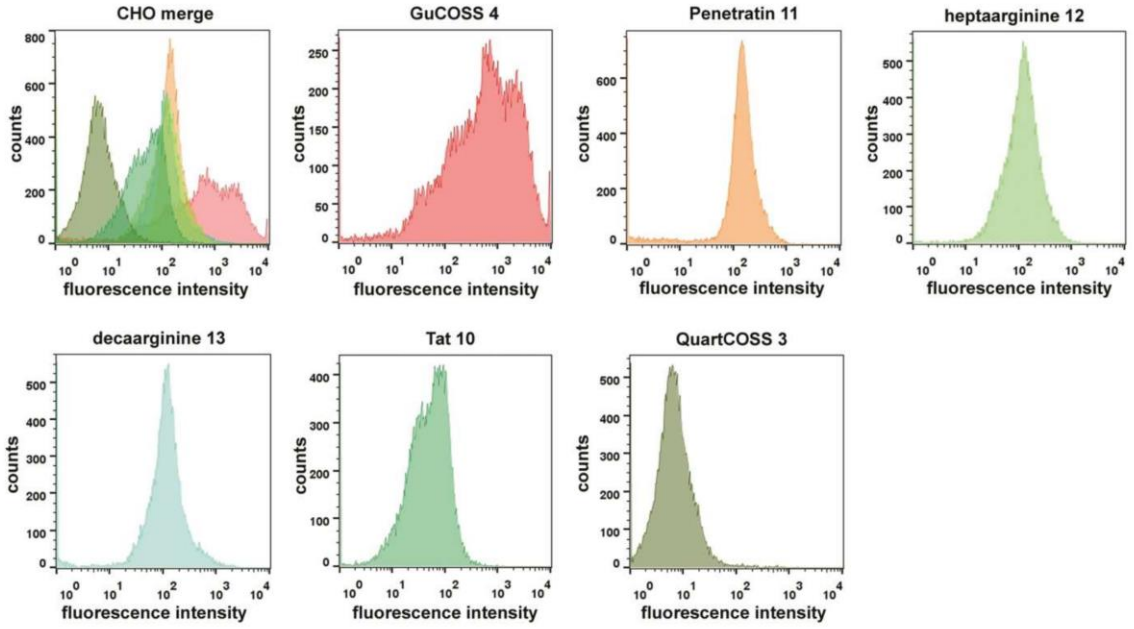

Figure S5 c: *Flow-cytometric studies of the cellular uptake of COSS derivatives (**3** and **4**) and cell-penetrating peptides **10-13** in CHO cells. Cells were incubated with 20 µM of the respective compound in DMEM lacking fetal bovine serum (FBS) for 10 min at 37°C. After incubation, the cells were washed thrice with PBS both before and after trypsinization for 10 min at ambient temperature. Afterwards cells were kept on ice. Experiments with CHO cells were performed in triplicates, each comprising 10000 events; average values are shown.*

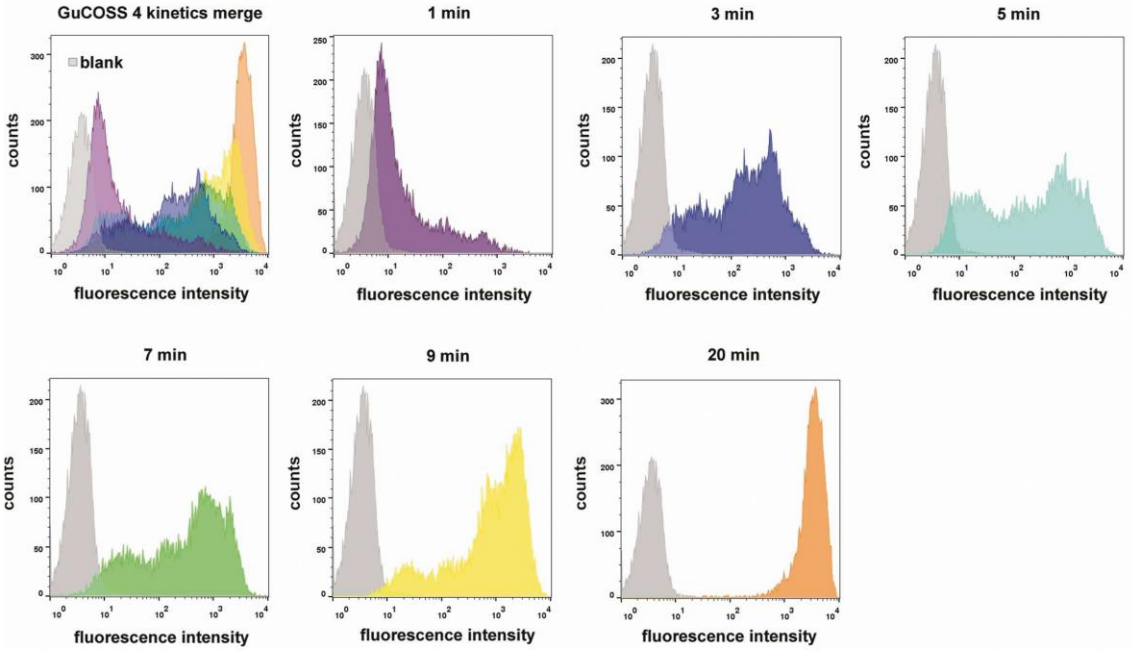

Figure S6: *Time-resolved flow-cytometric studies of the cellular uptake of GuCOSS **4** in HeLa cells. Cells were incubated for indicated times with 20 µM of compound **4** in DMEM lacking fetal bovine serum (FBS) at 37°C. After incubation, the cells were washed thrice with PBS both before and after trypsinization for 10 min at ambient temperature. Afterwards cells were kept on ice. Experiments with HeLa cells were performed in triplicates, each comprising 10000 events; average values are shown.*

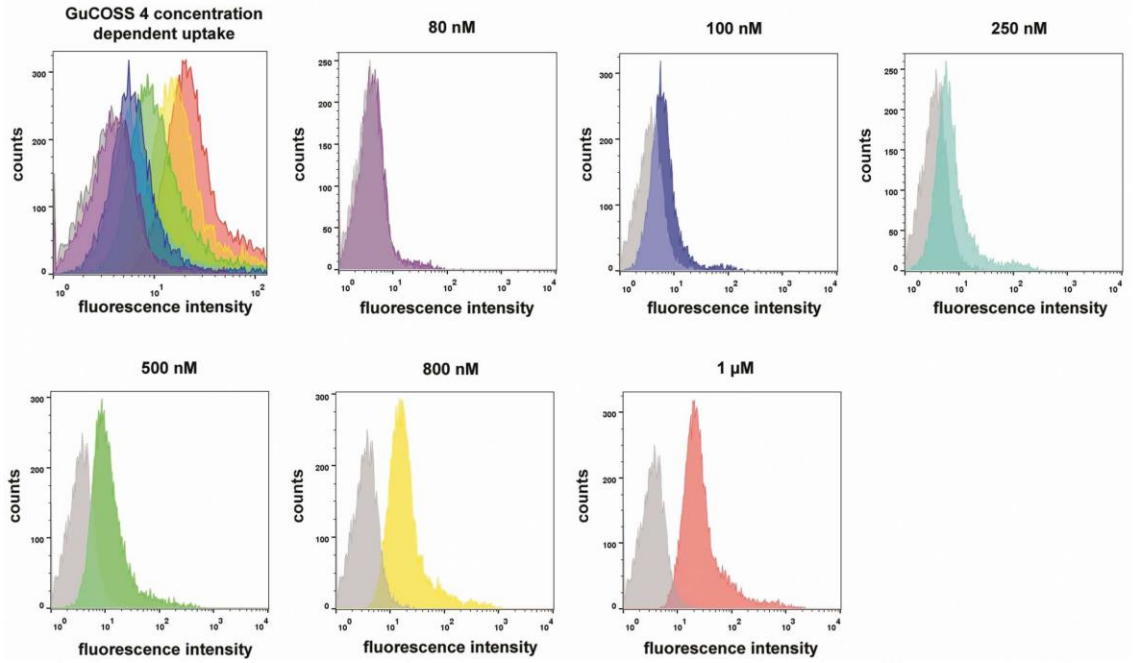

Figure S7: *Flow-cytometric studies of the cellular uptake of GuCOSS **4** in HeLa cells. Cells were incubated with compound **4** (at the indicated concentration) in DMEM lacking fetal bovine serum (FBS) for 10 min at 37°C. After incubation, the cells were washed thrice with PBS both before and after trypsinization for 10 min at ambient temperature. Afterwards cells were kept on ice. Experiments with HeLa cells were performed in triplicates, each comprising 10000 events; average values are shown.*

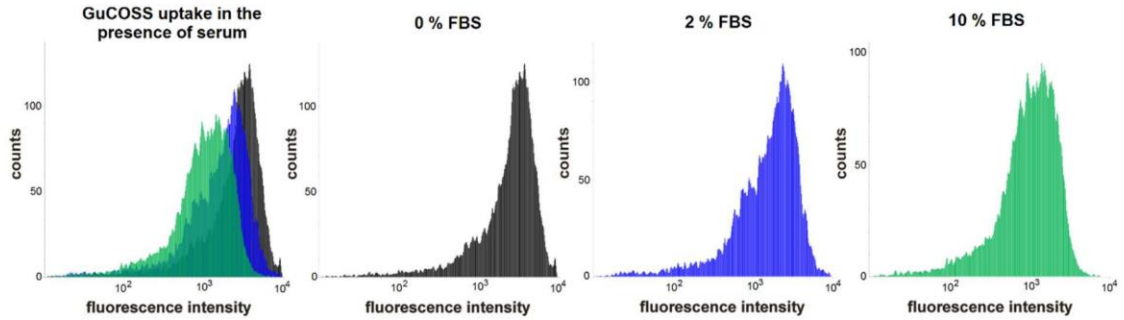

Figure S8: *Flow-cytometric studies of the cellular uptake of GuCOSS* ***4*** *in HeLa cells. Cells were incubated with compound* ***4*** *(20 µM) either in DMEM lacking fetal bovine serum (FBS) or in DMEM containing 2% or 10% FBS at 37°C for 10 min. After incubation, the cells were washed thrice with PBS both before and after trypsinization for 10 min at ambient temperature. Afterwards cells were kept on ice. Experiments with HeLa cells were performed in triplicates, each comprising 10000 events; average values are shown. Upon incubation with 2 % or 10 % FBS, mean fluorescence decreased to 72 % and 40 % of the intensity measured with DMEM lacking FBS (mean fluorescence data from three independent experiments; data not shown).*

3. Degradation studies

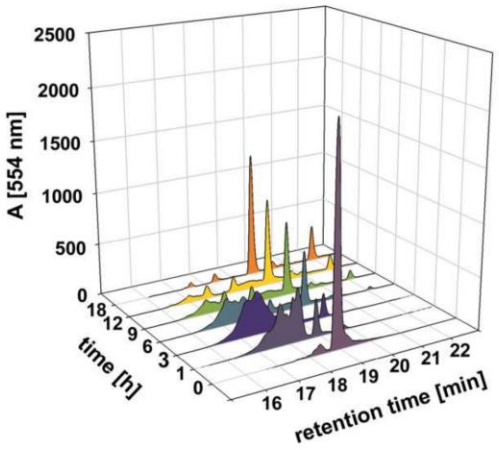

Figure S9: *Exemplary HPLC traces showing the time-resolved monitoring of the hydrolysis of GuCOSS* ***4****. To that end, compound* ***4*** *was investigated at a concentration of 50 µM in PBS at pH 7.0. Hydrolysis intermediates and the degradation products were identified and quantitatively analyzed by the change of the retention time and by determination of the peak area at 554 nm, which corresponds to the absorption maximum of TAMRA. Although hydroxyl-bearing hydrolysis intermediates of* ***4*** *are eluted earlier from the RP-HPLC column, the completely hydrolyzed TAMRA-bearing siloxanes have enhanced retention times.*

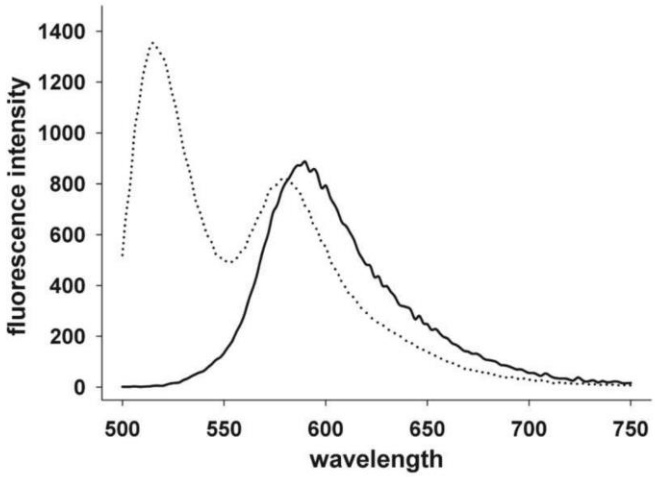

Figure S10: *Fluorescence emission spectra of intact and disassembled COSS derivative* ***9*** *bearing fluorescein and TAMRA. Samples of COSS derivative* ***9*** *(20 µM) were incubated for 30 min in 0.2 M HCl (solid line) and in 0.2 M NaOH (dotted line). Both samples were excited at 488 nm and fluorescence emission spectra were recorded using a Tecan infinite M1000 microplate reader. At acidic pH, the inorganic core of compound* ***9*** *is intact and the fluorescence of fluorescein is efficiently quenched by Förster resonance energy transfer due to the spatial proximity of TAMRA. Therefore, only the emission of TAMRA can be measured (580 nm; solid line). Upon hydrolytic disassembly of the inorganic core under aqueous basic conditions, the fluorescence of fluorescein is restored (520 nm; dotted line).*

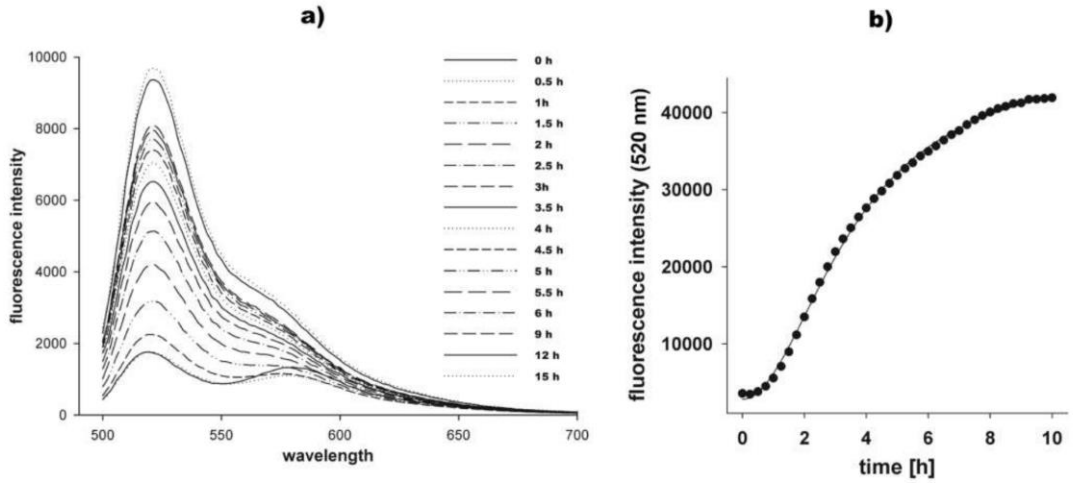

Figure S11: *Degradation studies of COSS derivative* ***9*** *in human blood serum at 37°C. COSS derivative* ***9*** *was incubated at a concentration of 20 µM in triplicates in 200 µL human serum (Sigma-Aldrich). The samples were excited at 488 nm and the fluorescence intensity at 520 nm was quantified for 15 h using a Tecan infinite M1000 microplate reader. a) Emission spectra of COSS derivative* ***9*** *(excitation at 488 nm). The recovery of the fluorescence of fluorescein was monitored by the increase of the emission at 520 nm. b) Fluorescence recovery of fluorescein measured at 520 nm. 50% fluorescence recovery was reached after 186 min.*

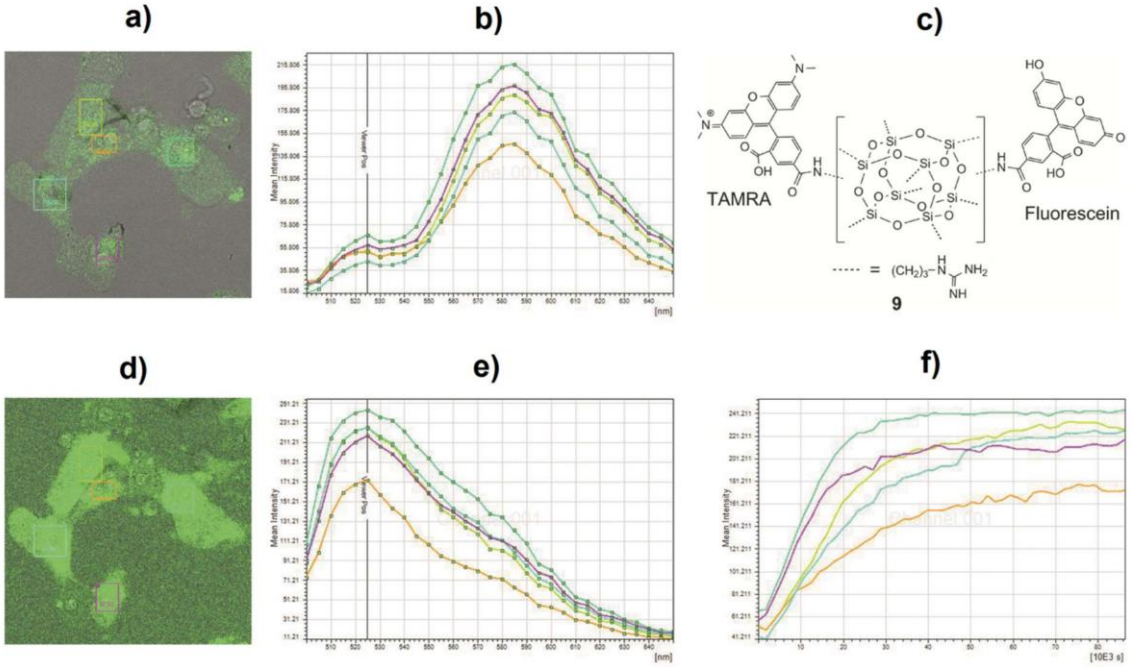

Figure S12: *Degradation studies of COSS derivative* ***9*** *in HeLa cells using live-cell laser scanning confocal microscopy. Cells were incubated with compound* ***9*** *(25 µM) in DMEM lacking FBS at 37°C for 20 min. After incubation, the cells were washed thrice with PBS and investigated in DMEM with 2 vol% FBS at 37°C and 5% CO_2 for 24 h. Every 30 min, excitation at 488 nm was performed and an emission spectrum was recorded. a) Fluorescence of fluorescein after an incubation time of 30 min. Colored windows indicate the selected areas for the emission scans. b) Emission scans after an incubation time of 30 min. The fluorescence of fluorescein is efficiently quenched (520 nm) and the emission of TAMRA (580 nm) is dominating. c) Structure of guanidine-bearing COSS derivative* ***9*** *comprising two fluorescent markers, fluorescein and TAMRA. d) Fluorescence of fluorescein after 24 h. e) Emission scans after 24 h. The fluorescence of fluorescein (520 nm) is restored and the emission of TAMRA (580 nm) is reduced. f) Time-resolved recovery of the fluorescence of fluorescein at 520 nm.*

4. Cellular delivery of a cytotoxic drug

Time-dependent delivery of free doxorubicin

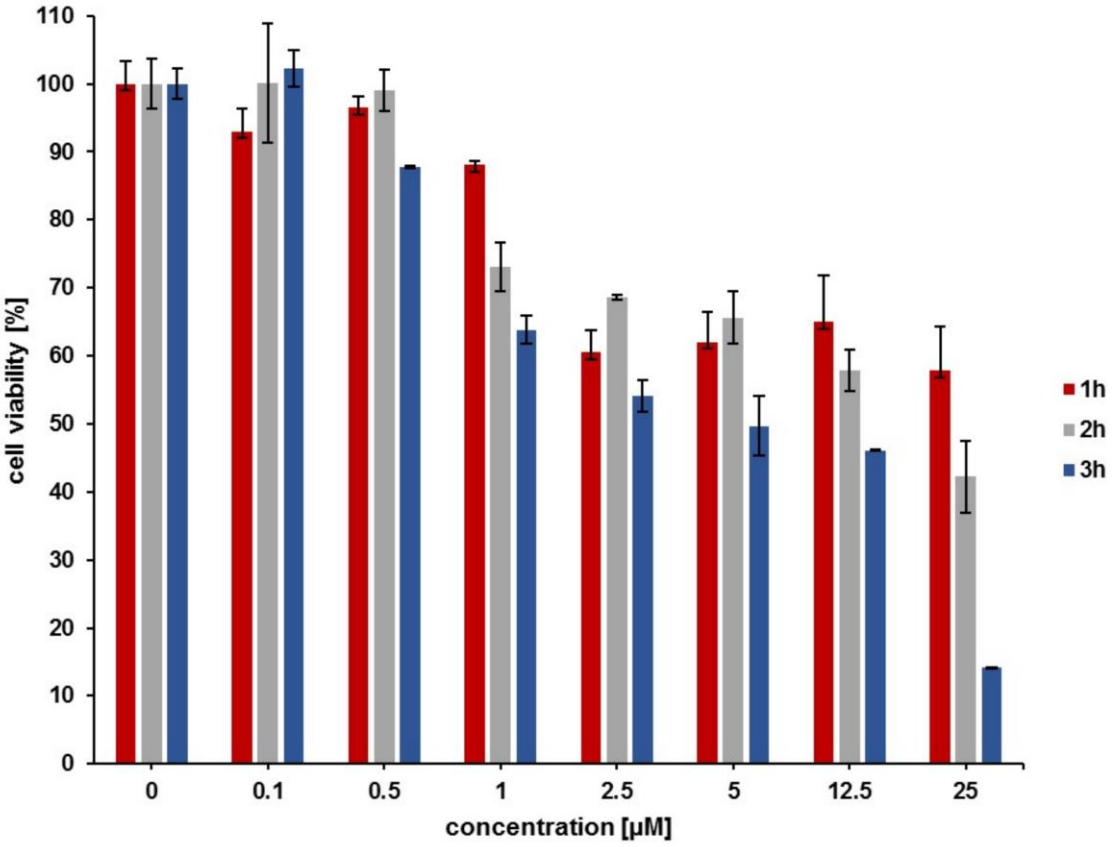

Figure S13: *Time-dependent cytotoxicity of free doxorubicin in HeLa cells. Serial dilutions of doxorubicin* ***14*** *in PBS (pH 5.5) were prepared and the resulting solutions were incubated in duplicates for 1 h, 2 h and 3 h with HeLa cells. After 18 h a MTT assay was performed. Upon co-incubation of unconjugated GuCOSS derivatives* ***8*** *or* ***28*** *and doxorubicin* ***14*** *at 1 µM, a concentration where the covalent GuCOSS-DOX conjugate showed a strong cytotoxic effect, no effect on cell viability was observed (data not shown)*

5. Experimental details

5.1 Cell culture assays

Cell culture

Human cervical cancer (HeLa), Chinese hamster ovary (CHO) and human embryonic kidney (HEK293) cells were maintained in Dulbecco`s modified eagle`s medium (DMEM, *Sigma-Aldrich*), supplemented with 2 mM L-glutamine, 10% (*v*/*v*) fetal bovine serum (FBS, *Sigma-Aldrich*) and penicillin (100 U/mL), streptomycin (100 µg/mL). *Sulfolobus islandicus*, and *Sulfolobus tokodaii* were cultured in 0.2% bacto-trypton (Difco) media as reported by Grogan *et al* and Brock *et al*.[1] *Halobacterium salinarum* were cultured in peptone (oxoid No. 37) media

as reported by Hechtler *et al*.[2] *E. coli* cells were cultured in dYT media and *Saccharomyces cerevisiae* were cultured in YPD media.

Live-cell confocal laser scanning microscopy

HeLa cells were grown to 70% confluence on *Lab Tek®II Chambered Coverglass System Nunc ThermoScientific 8 Chamber* (brand of *Merck KGaA*, Darmstadt, Germany). Cells were washed with Dulbecco's modified eagle medium without serum and then incubated with 20 µM of the labeled compounds in DMEM media lacking FBS at 37°C for 30 min. Afterwards the cells were washed thrice with PBS and investigated in DMEM supplemented with 2 mM L-glutamine, 10% (*v*/*v*) FBS (*Sigma-Aldrich*), and penicillin (100 U/mL), streptomycin (100 µg/mL) at 37°C and 5% CO_2. With a *Leica TCS SP5 II* TAMRA-labeled compounds were excited at 561 nm and detected at 580-650 nm. Exposure time settings were adjusted in the software to achieve the optimal quality of images. For controls lacking the COSS derivative, the same exposure time was used.

Fluorescence microscopy

Cells were incubated with 20 µM of GuCOSS **4** for 30 min in different buffers (*Saccharomyces cerevisiae, E. coli (BMH 71-18), Sulfolobus islandicus*, and *Sulfolobus tokodaii in PBS; Halobacterium salinarum in 3 M NaCl)* at different temperature (*Saccharomyces cerevisiae, and Halobacterium salinarum:* ambient temperature*; Sulfolobus islandicus*, and *Sulfolobus tokodaii*: 80°C; *E. coli*: 37°C). Cells were centrifuged for 3 min at 2500 rpm. The cell pellet was resuspended and centrifuged for 3 min at 2500 rpm; this procedure was repeated. The cells were investigated *on Millicell EZ SLIDE 4-well glass* (brand of *Merck KGaA*, Darmstadt, Germany). Microscopy images were acquired with *Zeiss Observer Z.1 microscope* (*Carl Zeiss AG*, Oberkochen, Germany) using an *EC Plan-Neofluar 63x/1.25 Oil objective* (*Carl Zeiss AG*, Oberkochen, Germany). The TAMRA moiety was excited at 543 nm and emission was detected at 565–615 nm. Exposure time settings were adjusted in the *Zeiss AxioVision SE64 Rel. 4.9* software to achieve the optimal quality of images. For controls lacking the COSS derivative, the same exposure time was used.

Flow-cytometric analysis

Cell-lines were subcultured overnight in 24-well plates to 70% confluence (*Costar*, *24-well cell culture cluster, Corning Incorporation*). Cells were grown on *CELLSTAR* 6-well slides (*Greiner Bio-One GmbH*, Frickenhausen, Germany). Cells were washed once with serum-free DMEM and then incubated with the labeled compounds at a concentration of 20 µM in DMEM lacking FBS for 10 min at 37°C. Afterwards the cells were washed thrice with PBS and trypsinized for 10 min at ambient temperature (0.05% trypsin/0.02% EDTA in PBS). Trypsinization was

terminated by adding 400 µL growth medium with 2 vol% FBS per well. Afterwards the cells were centrifuged for 3 min at 2500 rpm. The cell pellet was resuspended in PBS and centrifuged for 3 min at 2500 rpm. This procedure was repeated one more time. The cells have been resuspended in PBS and hold on ice until they were analyzed in a *BD Influx* cell sorter (*Becton, Dickinson and Company*, Franklin Lakes, USA), excited with a *BD Influx Yellow-Green Laser* (561 nm) (*Becton, Dickinson and Company*, Franklin Lakes, USA), emission detected between 573-613 nm (593/40 Filter). 10000 events were analyzed in each experiment.

Doxorubicin delivery

Cellular delivery of doxorubicin **14** (DOX) was studied in HeLa cells. First, an incubation time-dependent cell assay with the free antibiotic was conducted. To this end, the medium was exchanged with high glucose DMEM without L-methionine, L-cystine and L-glutamine. Free Doxorubicin was dissolved in phosphate buffered saline (PBS, pH 5.5), incubated at 37°C at different concentrations for 1 h, 2 h and 3 h with 1×10^4 HeLa cells/well (48-well plates, *Sigma Aldrich*) and subsequently washed with DMEM. After 18 h a cell proliferation assay (*CellTiter 96® Aqueous One Solution Cell Proliferation Assay, Promega Corporation*) was carried out (**figure S9**). For the investigation of the doxorubicin delivery *via* GuCOSS, the conjugate **15** as well as the controls were dissolved in PBS (pH 5.5), incubated at the different concentrations for 1 h at 37°C, in triplicates. To preserve the disulfide bond, the medium was exchanged with high glucose DMEM without L-methionine, L-cystine and L-glutamine prior to the incubation. After incubation, the cells were washed with DMEM and after 18 h a MTT assay was performed (**figure 3**).

Cell toxicity test: XTT assay

Cell proliferation assay XTT was purchased from *Applichem* and performed according to the manufacturer's instructions. 5,000 HeLa-cells per well were seeded in triplicates into 96-well plates the day before the experiment (Cellstar, 96-Well Cell Culture Plate, Greiner Bio-one) and used at 70% confluency. Cells were washed with serum-free DMEM and incubated for one h at 37°C and 5% CO_2 with different concentrations with COSS derivative **8** (0 µM; 20 µM; 40 µM; 60 µM; 80 µM; 100 µM; 150 µM; 200 µM; 250 µM; 300 µM; 400 µM; 500 µM) in DMEM lacking FBS. Additionally, cells were incubated with 50% (v/v) DMSO in DMEM lacking FBS (positive control). Cells were cultured 12 h at 37°C and 5% CO_2 in DMEM media supplemented with 2 mM L-glutamine, 10% (*v*/*v*) fetal bovine serum (FBS, Sigma-Aldrich) and penicillin (100 U/mL), streptomycin (100 µg/mL). The media was exchanged to DMEM lacking FBS and 0.3 mg/mL of 2,3-bis(2-methoxy-4-nitro-5-sulfophenyl)-5-((phenylamino)-carbonyl)-2H-

tetrazolium-hydroxide (XTT) (*AppliChem*, brand of *Illinois Tool Works Inc.*, Glenview, USA) in DMEM media including 25 mM HEPES (Life technologies) were added. After an incubation time of 4 h, the XTT enzymatic reduction was measured by measuring the absorbance at 450 nm, with a reference wavelength of 630 nm in a *Tecan Infinite M1000* (*Tecan Group AG*, Männedorf, Switzerland) microplate reader. Each measurement was conducted in triplicate and the toxicity was determined in three independent experiments.

Cell toxicity test: MTT assay

Cell proliferation assay *CellTiter 96® AQ_{ueous} One Solution* was purchased from *Promega Corporation* and performed according to the manufacturer's instructions. 1×10^4 HeLa cells/well were seeded into 48-well plates (48-well cell culture plate, *Sigma Aldrich*). After 24 h culturing, the cells were washed with serum-free high glucose DMEM lacking L-methionine, L-cystine and L-glutamine (*D0422, Sigma Aldrich*) and incubated with 150 µL medium and 50 µL of the respective probe. After the corresponding incubation period the cells were washed with DMEM. After 18 h 40 µL of the MTT solution was added and the absorbance at 485 nm was measured in a *Tecan Infinite M1000* (*Tecan Group AG*, Männedorf, Switzerland) microplate reader. Each measurement was conducted in triplicate or duplicate and the toxicity was determined in two independent experiments.

5.2 Synthetic procedures

Solvents

Solvents were obtained from *Carl Roth GmbH* (Karlsruhe, Germany), *Acros* (Taufkirchen, Germany), *Fluka* (Buchs, Switzerland) or *Sigma-Aldrich* (St. Louis, USA) and had the following quality: acetone: synthesis grade; dimethyl sulfoxide (DMSO): spectroscopic grade; acetonitrile (MeCN): HPLC grade. Millipore quality water was used for the HPLC analysis. Some solvents were dried und purified using the following procedures:

MeCN: 1 g/L sodium hydride dispersion was added to the solvent. After being heated to reflux for 1 h, the solvent was distilled. 2 g/L P_2O_5 were added and the mixture was heated to reflux for 1 h. It was subsequently distilled and stored in the dark under argon atmosphere over activated 4 Å molecular sieve.

DMSO: The solvent was pre-dried by stirring over 25 g/L calcium hydride at ambient temperature for one day. Afterwards it was distilled and stored in the dark under argon atmosphere over activated 4 Å molecular sieve.

N,N-diisopropylethylamine (DIEA): The solvent was refluxed over 50 g/L potassium hydroxide for 1 h. After cooling to ambient temperature, it was decanted and 50 g/L fresh potassium hydroxide was added. The solvent was refluxed for 1 h and afterwards decanted. After distillation, the obtained solvent was refluxed for 3 h over calcium hydride, distilled and stored in the dark under argon atmosphere over activated 4 Å molecular sieve.

Reagents

All reagents were used as supplied by *Sigma Aldrich* or *Acros Organics* without further purification or drying. Amino acids and resins were purchased from *Novabiochem* (brand of *Merck KGaA*, Darmstadt, Germany), *CEM* (Kamp-Lintfort, Germany) or *Iris Biotech* (Marktredwitz, Germany).

Microwave-assisted solid-phase peptide synthesis (SPPS)

Microwave-assisted SPPS was performed using a *CEM Liberty*® peptide synthesizer equipped with a *CEM Discover*® SPS microwave.

Manual SPPS

Coupling of Fmoc-protected amino acids was performed as triple coupling. 4 eq. of the respective amino acid, 3.9 eq. of the activator *O*-benzotriazole-*N,N,N′,N′*-tetramethyl-uronium-hexafluoro-phosphate (HBTU) and 8 eq. DIEA, were diluted in a minimal amount of *N,N*-dimethylformamide (DMF) and pre-activated for 10 min. Coupling was performed at ambient temperature for 1 h. *N*-Terminal deprotection of amino acids was performed as double deprotection step with 20% piperidine in DMF for 5 and 15 min at ambient temperature. Afterwards the resin was washed thrice with DMF and dichloromethane (DCM).

Peptide cleavage and work-up

All peptides were cleaved from the resin using 92 vol% trifluoroacetic acid (TFA), 2 vol% H_2O, 4 vol% triethylsilane (TES), 2 vol% anisole and a spatula tip of dithiothreitol (DTT). After 1-2 h of shaking at ambient temperature the solution was filtered and poured into ice-cold MTBE. The mixture was cooled to -20°C for at least 30 min and centrifuged for 15 min at 4000 rpm at 4°C. The supernatant was discharged and the precipitate was washed by MTBE twice and dried in a desiccator. The peptide was dissolved in a mixture of MeCN and water and the solvent mixture was removed by lyophilization.

Mass spectrometry

Electrospray ionization mass spectrometry (ESI-MS) spectra were obtained using a *Shimadzu LCMS-2020* mass spectrometer equipped with a *Phenomenex Jupiter 5u C4 LC* column (50x1 mm, 5 µm, 300 Å). Eluent system consisted of eluent A comprising 0.1 vol% aq. formic acid, LC-MS grade (*Sigma-Aldrich*, St. Louis, USA) and eluent B comprising 100% acetonitrile with 0.1 vol% formic acid, LC-MS grade (*Carl Roth GmbH*, Karlsruhe, Germany). High-resolution ESI-MS were performed using a *maXis Q-TOF* (*Bruker*) or an *APEX IV FTICR-MS* (*Bruker*).

Liquid chromatography

Analytical reversed-phase high-performance liquid chromatography (RP-HPLC) was performed on a *Varian 920 LC* equipped with a *Phenomenex Luna Hypersil 5u BDS C_{18} LC* column (5 u, 130 Å, 150×4.60 mm, 5 µm) at a flow rate of 1 mL/min. For isolation of peptides a semi-preparative RP-HPLC *Varian 940 LC* equipped with a preparative C_{18} column (*Phenomenex Luna 5u C_{18}* (250×20 mm; S-4 µm, 8 nm)) was used at a flow rate of 18 mL/min. Eluent A: 0.1 vol% aq. trifluoroacetic acid (TFA), eluent B: 90 vol% aq. MeCN with 0.1 vol% TFA. 5 min of isocratic flow (starting concentration of eluent B) was followed by 20 min of gradient flow. Absorption was measured by UV/VIS detector at 220 nm and 280 nm or 220 nm and 534 nm

NMR

NMR spectra were recorded with a *Bruker DRX 500 MHz NMR spectrometer* (*Bruker Biospin*, Karlsruhe) equipped with a 5mm TBI probe (^{1}H, ^{2}H, ^{31}P, BB, z-gradient) and a *Bruker AV III HD 400 MHz spectrometer* equipped with a 5mm BBFO smart probe. Unless noted otherwise, the sample temperature was held constant at 300 K using a *BCU-Xtreme chiller*. All samples were dissolved in deuterated DMSO-d_6 purchased from *Euriso Top* (Gif-Sur-Yvette, France). Samples were prepared inside PTFE tube liners to improve the signal to noise ratio of the dilute solutions.

Experiments (1D: ^{1}H, ^{13}C, ^{29}Si, 2D: ^{1}H-^{13}C HSQC, ^{1}H-^{1}H COSY and ^{1}H-^{29}Si HMBC) were performed using standard pulse sequences from the Bruker library and default settings. ^{29}Si 1D spectra were acquired with inverse gated decoupling of protons, 32k FID data points, and a relaxation delay of 30s and a spectral offset of -50ppm. Some spectra acquired on the older hardware showed a spike at the carrier frequency of the experiment, presumably due to a DC offset caused by the amplifiers. Acquisition was performed under *XWinNMR 3.5* on older hardware and *TopSpin 3.2pl5* on the newer hardware. Processing was performed with *MestreNova 10.0.1*. For ^{29}Si 1D spectra the FID was apodized by exponential multiplication with a broadening factor of 0.2 – 2 Hz, followed by zero-filling to 128k data points (incl. linear

prediction), manual phase correction, and automatic baseline correction (Whittaker smoothing, 5 Hz filter). For ^{1}H 1D spectra the FID was apodized by exponential multiplication with a broadening factor of 0.3 Hz, followed by zero-filling to 128k data points (incl. linear predition), manual phase correction and automatic baseline correction (Whittaker smoothing, 8 -15 Hz filter).

As a first step of structural characterization, ^{1}H and ^{29}Si spectra were analyzed. Quantitative analysis of the ^{1}H spectra was performed with the multiplet analysis tool in *MestreNova 10.0.1*, giving the line-shape fitted numerical integrals even in overlapping spectral regions. In several spectra the integrals of labile amine protons are difficult to quantify due to an undetermined protonation state. Similarly, a strong residual water signal around 3.50 ppm leads to perturbed integrals in some spectra. The chemical shift of the Si-nuclei in the cage-like siloxane core was used as an indicator for stability. Within an intact structure where all Si-nuclei are connected to three other Si-nuclei *via* oxygen atoms (denoted as T_8 structure), the chemical shifts of the four non-isochronous Si-sites are expected around -65 ppm. Hydrolysis (or other decomposition) products would be expected around -40 ppm. The spectra confirmed the integrity of the cage-like T_8 core and the unsymmetrical substitution pattern allowed for full assignment of all non-isochronous resonances in favorable cases, where resonance overlap is minimal.

COSS derivative 2 (TAMRA-aminoCOSS)

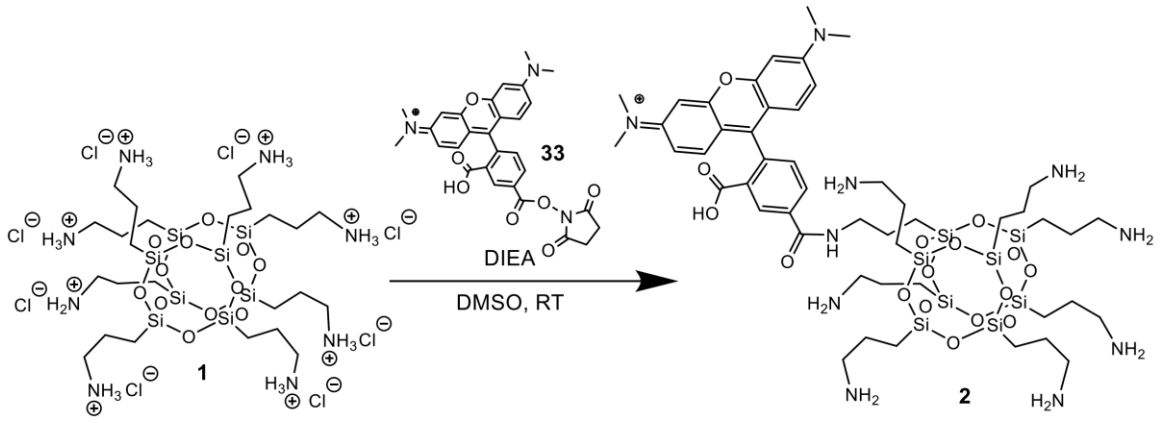

100 mg (85.2 µmol, 6.4 eq.) of octaammonium COSS hydrochloride **1** (purchased from *Hybrid Plastics* Inc., USA) were dissolved in 0.5 mL dry DMSO and vigorously stirred. The solution comprising 7 mg (13.2 µmol, 1 eq.) of TAMRA-NHS ester **33** (*Thermo Fischer Scientific*) and 13.8 µL (79.5 µmol, 6 eq.) of dry DIEA in 8 mL dry DMSO was added slowly using a peristaltic pump (flow: 0.05 mL/min). The resulting mixture was stirred for additional 2 h at room temperature and the solvent was removed by lyophilization. The purple residue was suspended in dry acetonitrile and the insoluble part was washed twice with dry acetonitrile.

The precipitate was dissolved in 10 vol% aq. MeCN with 0.1 vol% TFA and purified by semi-preparative RP-HPLC (gradient 10to40% B). After lyophilization, 13 mg of a purple solid **2** were obtained (76.3%).

RP-HPLC, 10→40% B, t_R= 19.35 min.

HR-MS calc. for $C_{49}H_{84}N_{10}O_{16}Si_8$ m/z: 431.8146 meas. 431.8134 $[M+3H]^{3+}$.

^{1}H NMR (500 MHz, DMSO-d_6) δ: 9.00 (t, *J* = 5.6 Hz, 1H), 8.65 (s, 1H), 8.30 (d, *J* = 8.0 Hz, 1H), 8.01 (s, 29H), 7.54 (d, *J* = 8.1 Hz, 1H), 7.15 – 6.75 (m, 6H), 3.38 – 3.29 (m, 2H), 3.23 (s, 12H), 2.94 – 2.60 (m, 20H, expected 14H), 1.88 – 1.41 (m, 23H, expected 16H), 0.96 – 0.32 (m, 23H, expected 16H).

The integral mismatch between the TAMRA and C_3-NH_2 side chains might indicate an incomplete reaction.

^{29}Si NMR (99 MHz, DMSO-d_6) δ: -65.94, -66.62, -66.67.

COSS derivative 3 (TAMRA-quartCOSS)

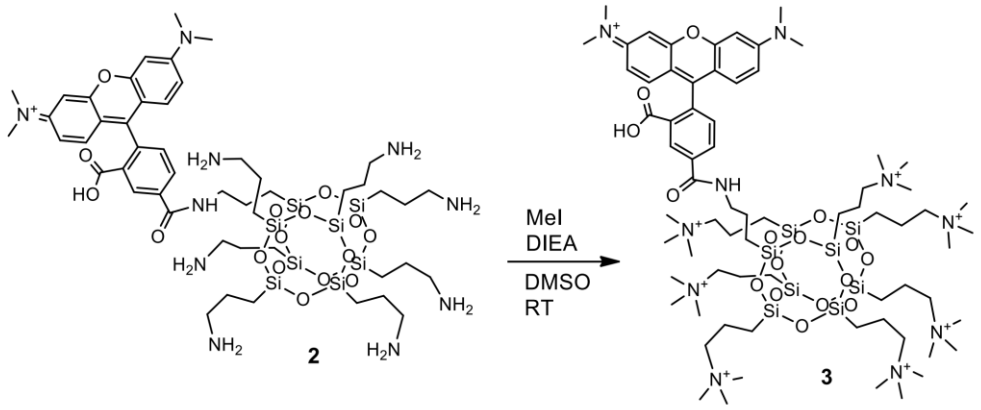

A mixture of 25 mg (19.3 µmol, 1 eq.) of TAMRA-aminoCOSS **2**, 84 µL (482.8 µmol, 25 eq.) dry DIEA and 42 µL (674.7 µmol, 35 eq.) methyl iodide are dissolved in 5 mL dry DMSO. After being stirred for 5 days the solvent was removed using a rotary evaporator. The purple residue was dissolved in 10 vol% aq. MeCN with 0.1 vol% TFA and purified by semi-preparative RP-HPLC (gradient 10to40% B). After lyophilization, 14.9 mg of a purple solid **3** were obtained (48.8%).

RP-HPLC, 10→40% B, t_R=19.81 min.

^{1}H NMR (500 MHz, DMSO-d_6) δ: 9.32 – 9.11 (m, 1H), 8.71 (s, 1H), 8.37 (d, *J* = 8.1 Hz, 1H), 7.63 (d, *J* = 8.0 Hz, 1H), 7.13 – 7.02 (m, 2H), 7.04 – 6.92 (m, 4H), 3.47 – 3.18 (m, 28H), 3.08 (s, 63H), 1.96 – 1.52 (m, 16H), 0.91 – 0.74 (m, 2H), 0.74 – 0.48 (m, 14H).

^{29}Si NMR (99 MHz, DMSO-d_6) δ: -65.89, -67.26, -67.32, -67.39.

COSS derivative 4 (TAMRA-GuCOSS)

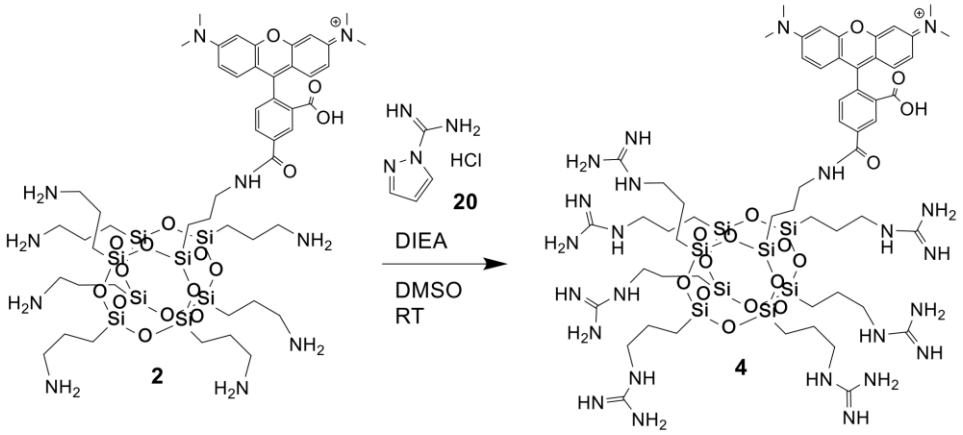

19.2 mg of TAMRA-aminoCOSS **2** (1 eq., 14.8 µmol), 45.6 mg of 1*H*-pyrazole-1-carboxamidine hydrochloride (21 eq., 311.4 µmol) and 126 µL of DIEA (50 eq., 741 µmol) were dissolved in 5 mL dry DMSO and stirred at room temperature for 4 days. The mixture was freeze-dried. The oily residue was suspended in dry acetonitrile and the insoluble part was washed twice with dry acetonitrile. The purple solid was dissolved in 10 vol% aq. MeCN with 0.1 vol% TFA and purified by semi-preparative RP-HPLC (gradient 10to100% B). After lyophilization, 5.5 mg of a purple solid **4** were obtained (23.6%).

RP-HPLC, 10→40% B, t_R=21.50 min.

HR-MS calc. for $C_{56}H_{98}N_{24}O_{16}Si_8$ m/z: 318.3222, meas. 318.3221 $[M+5H]^{5+}$.

^{1}H NMR (500 MHz, DMSO-d_6) δ: 8.91 (s, 1H), 8.72 – 8.07 (m, 2H), 8.02 – 7.67 (m, 7H), 7.67 – 6.63 (m, 29H), 3.35 (s, 89H, expected 12H), 3.09 (m, 16H, expected 14H), 3.05 – 2.90 (m, 2H), 1.69 – 1.60 (m, 2H), 1.60 – 1.44 (m, 14H), 0.78 – 0.69 (m, 2H), 0.69 – 0.50 (m, 14H).

TAMRA resonances mostly overlap with guanidinyl resonances and a strong residual water signal at ~3.53 ppm disturbs the baseline, such that the affected resonances cannot be integrated cleanly.

^{29}Si NMR (99 MHz, DMSO-d_6) δ: -66.41, -66.42.

COSS derivative 5 (TAMRA-aminoCOSS-L)

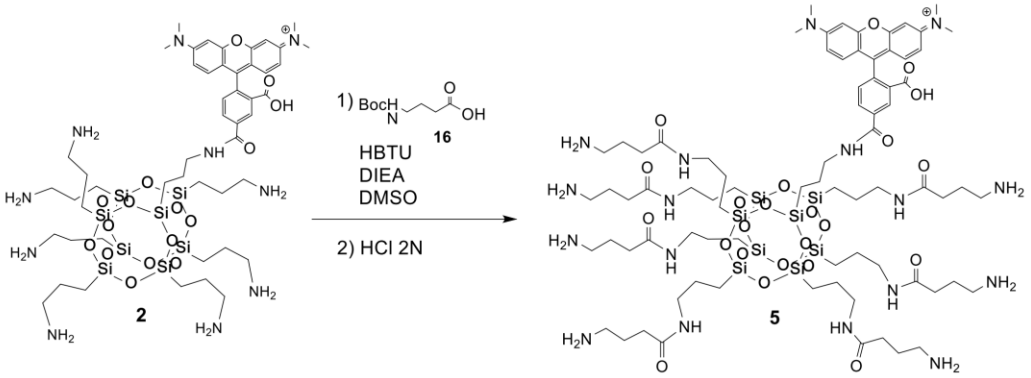

A mixture of 65.9 mg (324.3 µmol, 21 eq.) 4-Boc-aminobutyric acid (*Sigma-Aldrich*) **16**, 134.6 µL (772.2 µmol, 50 eq.) dry DIEA and 117.2 mg (308.9 µmol, 20 eq.) of HBTU were dissolved in 4 mL dry DMSO and pre-activated for 10 min at room temperature. 20 mg (15.4 µmol, 1 eq.) of TAMRA-aminoCOSS **2** were added and the mixture was stirred for 2 h. The solvent was removed by lyophilization. Boc deprotection was performed in 50 vol% aq. TFA for 7 h. The solvent was removed using a rotary evaporator and the residue was dissolved in 10 vol% aq. MeCN with 0.1 vol% TFA and purified by semi-preparative RP-HPLC (gradient 10to40% B). After lyophilization, 18.3 mg of a purple solid **5** were obtained (45.7%).

RP-HPLC, 10→40% B, t_R=19.82 min.

HR-MS calc. for $C_{77}H_{133}N_{17}O_{23}Si_8$ m/z: 378.5656 meas. 378.5661 $[M+5H]^{5+}$.

^{1}H NMR (500 MHz, DMSO-d_6) δ: 8.92 (s, 1H), 8.53 (s, 1H), 8.25 (s, 1H), 8.11 – 7.70 (m, 28H), 7.67 – 6.08 (m, 7H), 3.65 – 3.21 (m, 148H, expected 12H), 3.07 – 2.97 (m, 16H), 2.85 – 2.69 (m, 14H), 2.24 – 2.08 (m, 14H), 1.83 – 1.68 (m, 14H), 1.68 – 1.58 (m, 2H), 1.53 – 1.38 (m, 14H), 0.74 – 0.65 (m, 2H), 0.65 – 0.46 (m, 14H).

A strong residual water signal at ~3.40 ppm prevents the clean integration of some resonances.

^{29}Si NMR (99 MHz, $CDCl_3$) δ: -66.23, -66.25.

COSS derivative 6 (TAMRA-quartCOSS-L)

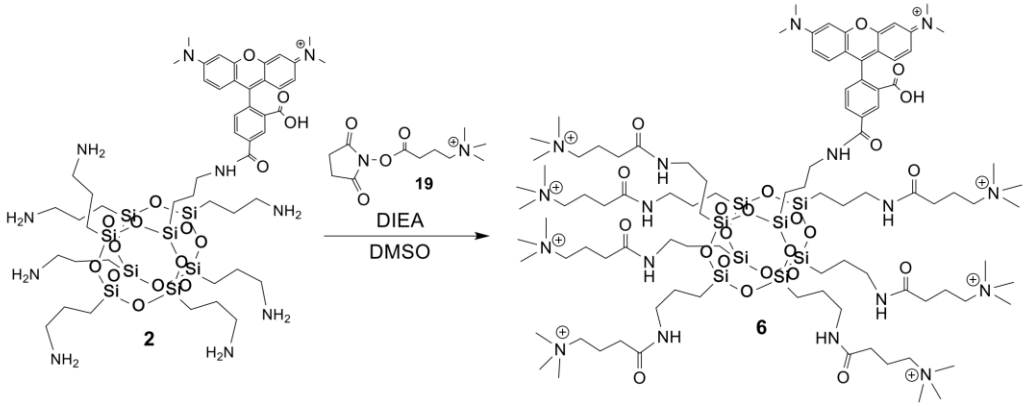

A mixture of 25 mg (19.3 µmol, 1 eq.) TAMRA-aminoCOSS **2**, 98.6 mg (324.3 µmol, 21 eq.) 4-trimethylammoniumbutyric acid NHS ester **19** and 134.4 µL (772.2 µmol, 50 eq.) dry DIEA were dissolved in 5 mL dry DMSO and stirred for 8 days. The solvent was removed by lyophilization. The residue was dissolved in 10 vol% aq. MeCN with 0.1 vol% TFA and purified by semi-preparative RP-HPLC (gradient 10to40% B). After lyophilization, 18.3 mg of a purple solid **6** were obtained (45.7%).

RP-HPLC, 10→40% B, t_R=18.87 min.

HR-MS calc. for $C_{98}H_{182}N_{17}O_{23}Si_8^{7+}$ m/z: 312.7387, meas. 312.7384 $[M]^{7+}$.

^{1}H NMR (500 MHz, DMSO-d_6) δ: 9.00 (t, J = 5.5 Hz, 1H), 8.67 (s, 1H), 8.31 (d, J = 7.9 Hz, 1H), 8.09 – 7.98 (m, 7H), 7.55 (d, J = 8.0 Hz, 1H), 7.42 – 6.59 (m, 6H), 3.37 – 3.14 (m, 28H), 3.10 – 3.01 (m, 77H), 2.15 (t, J = 7.2 Hz, 14H), 1.95 – 1.83 (m, 14H), 1.73 – 1.57 (m, 2H), 1.53 – 1.39 (m, 14H), 0.74 – 0.67 (m, 2H), 0.66 – 0.50 (m, 14H).

^{29}Si NMR (99 MHz, DMSO-d_6) δ: -66.22, -66.23, -66.25.

COSS derivative 7 (TAMRA-GuCOSS-L)

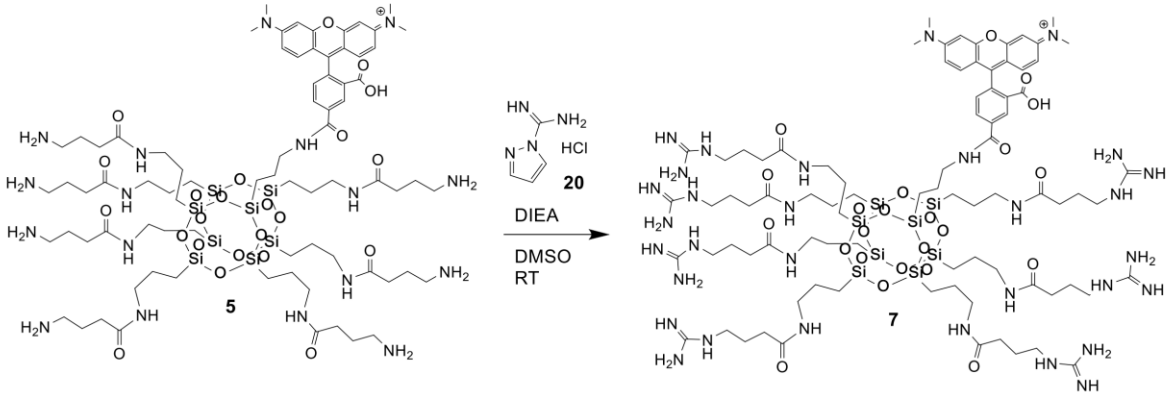

A mixture of 12 mg (6.4 µmol, 1 eq.) COSS derivative **5**, 44.1 µL (253.9 µmol, 40 eq.) dry DIEA and 22.3 mg (152.4 µmol, 24 eq.) 1*H*-pyrazole-1-carboxamidine hydrochloride **20** were dissolved in 10 mL dry DMSO and stirred for 8 days. The solvent was removed by lyophilization and the residue was dissolved in 10 vol% aq. MeCN with 0.1 vol% TFA and purified by semi-preparative RP-HPLC. After lyophilization 3.6 mg of a purple solid **7** were obtained (26%).

RP-HPLC, 10→40% B, t_R=20.9 min.

HR-MS calc. for $C_{84}H_{147}N_{31}O_{23}Si_8$ m/z: 364.6646, meas. 364.6643 $[M+6H]^{6+}$.

^{1}H NMR (500 MHz, DMSO-d_6) δ: 8.94 (s, 1H), 8.68 (s, 1H), 8.30 (d, *J* = 8.3 Hz, 1H), 7.94 (s, 7H), 7.86 – 7.75 (m, 7H), 7.68 – 6.70 (m, 28H), 3.67 – 3.44 (m, 410H, expected 12H), 3.34 – 3.31 (m, 2H), 3.17 – 3.00 (m, 28H), 2.12 (t, *J* = 7.4 Hz, 14H), 1.74 – 1.60 (m, 16H), 1.52 – 1.39 (m, 14H), 0.75 – 0.66 (m, 2H), 0.66 – 0.49 (m, 14H).

A strong residual water signal at ~3.50 ppm prevents the clean integration of some resonances.

^{29}Si NMR (99 MHz, $CDCl_3$) δ: -66.23, -66.26.

COSS derivative 8 (amino-GuCOSS)

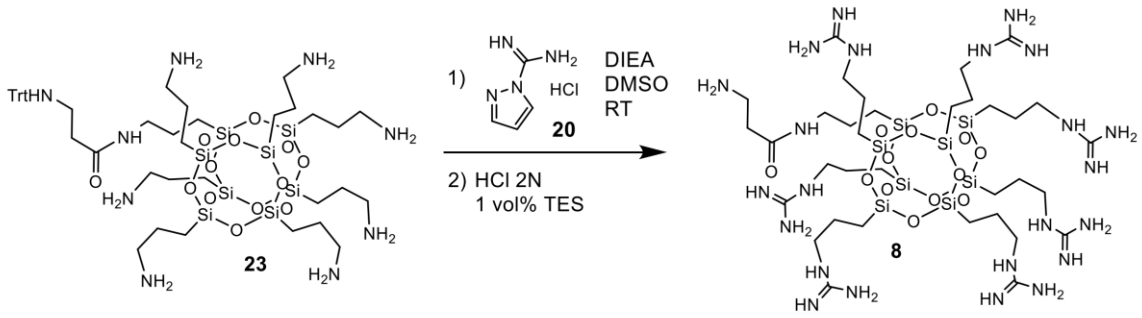

123 mg (0.103 mmol, 1 eq.) single-corner amidated and trityl-protected COSS **23**, 317 mg (2.16 mmol, 21 eq.) 1*H*-pyrazole-1-carboxamidine hydrochloride **20** and 666 mg (5.2 eq., 897 µL) dry DIEA were mixed in 5 mL dry DMSO and the mixture was stirred for 2 days at ambient temperature. The solvent was removed by lyophilization and the oily residue was suspended in dry acetonitrile. The insoluble part was washed twice with dry acetonitrile. The precipitate was dissolved in 5 vol% aq. AcOH and purified by semi-preparative RP-HPLC (gradient 0to60% B) with 0.1 vol% AcOH. After lyophilization 44.5 mg of colorless trityl-protected intermediate **24** were obtained (29%). For deprotection of the trityl protecting group, 1 mL 2 N aq. HCl and 1 mL $CHCl_3$ were added and the solution was shaken for 3 h at ambient temperature. The organic phase was removed and the aqueous phase was extracted twice with each 1 mL $CHCl_3$. The combined organic phases were abolished and 9 mL deionized water was added to the aqueous phase. The solvent was removed by lyophilization. The

remaining colorless solid was dissolved in 5 mL 5 vol% aq. AcOH and the solvent was removed by lyophilization. 37.1 mg of colorless solid **8** were obtained (99%).

Trt protected **24**:

ESI-MS calc. for $C_{53}H_{97}N_{23}O_{13}Si_8$ m/z: 745.58 meas. 745.61 $[M+2H]^{2+}$, calc. 497.39 meas. 497.32 $[M+3H]^{3+}$.

RP-HPLC, 10→60% B, t_R= 20.38 min.

^{1}H NMR (400 MHz, DMSO-d_6) δ: 8.50 (s, 7H), 8.13 (t, *J* = 5.6 Hz, 1H), 7.62 (s, 21H), 7.38 (d, *J* = 7.9 Hz, 6H), 7.29 (t, *J* = 7.6 Hz, 6H), 7.18 (t, *J* = 7.2 Hz, 3H), 3.19 – 2.95 (m, 16H), 2.72 (s, 1H), 2.39 – 2.25 (m, 2H), 2.24 – 2.09 (m, 2H), 1.61 – 1.36 (m, 16H), 0.91 – 0.27 (m, 16H).

^{29}Si NMR (79 MHz, DMSO) δ: -66.03, -66.21, -66.25, -66.32.

Amino-GuCOSS **8**:

^{1}H NMR (400 MHz, DMSO-d_6) δ: 8.07 – 7.88 (m, 8H), 7.72 – 6.91 (m, 26H, expected 23H), 3.31 – 3.14 (m, 14H), 3.11 – 3.02 (m, 2H), 3.01 – 2.91 (m, 2H), 2.67 – 2.54 (m, 2H), 1.69 – 1.34 (m, 16H), 0.95 – 0.24 (m, 16H).

COSS derivative 9 (Fluorescein-TAMRA-GuCOSS)

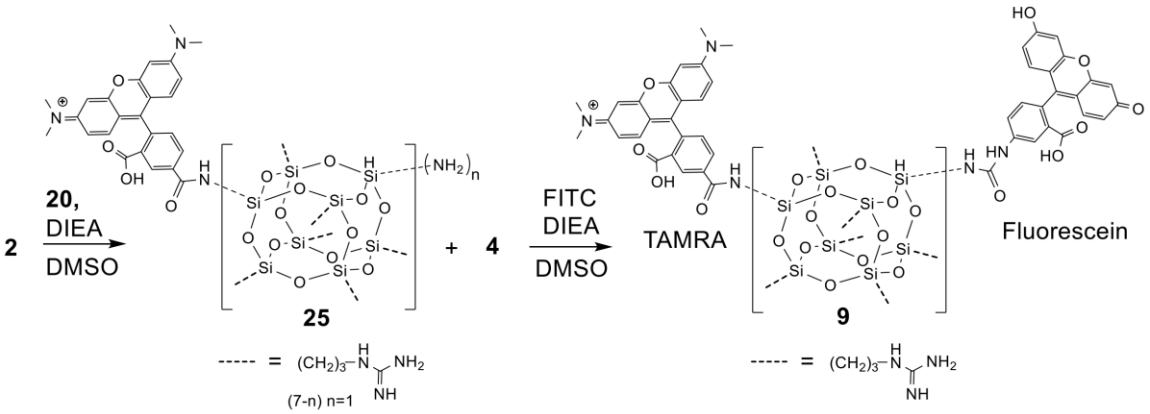

20 mg of TAMRA-aminoCOSS **2** (1 eq., 15.4 µmol), 47.5 mg of 1*H*-pyrazole-1-carboxamidine hydrochloride **20** (21 eq., 324.2 µmol) and 99.5 mg (134.5 µL, 50 eq, 770 µmol) of dry DIEA were dissolved in 5 mL dry DMSO and stirred at room temperature for 3 days. The formation of six- and sevenfold guanidinylated COSS was verified by LC-MS analysis of the reaction mixture. The mixture was freeze-dried and the oily residue was suspended in dry acetonitrile. The insoluble part was washed twice with dry acetonitrile. The purple solid was dissolved in 10 vol% aq. MeCN with 0.1 vol% TFA and purified by semi-preparative RP-HPLC (gradient 10to100% B). After lyophilization, 5.6 mg of a mixture of compound **25** and TAMRA-GuCOSS **4** were obtained. The product mixture was treated with 2.7 mg fluoresceinisothiocyanate (FITC, *Applichem*) (2 eq., 6.9 µmol) and 1.8 mg dry DIEA (2.4 µL, 4 eq., 13.9 µmol) in 2 mL

dry DMSO at ambient temperature overnight. The solvent was removed by lyophilization and the oily residue purified by RP-HPLC. After lyophilization, 1.9 mg of red solid **9** were obtained (6.6%).

RP-HPLC, 10→100% B, t_R=14.57 min.

HR-MS calc. for $C_{76}H_{107}N_{23}O_{21}SSi_8$ m/z: calc. 645.5368, meas. 645.5362 $[M+3H]^{3+}$.

TAMRA-*β*-alanine-Tat peptide 10

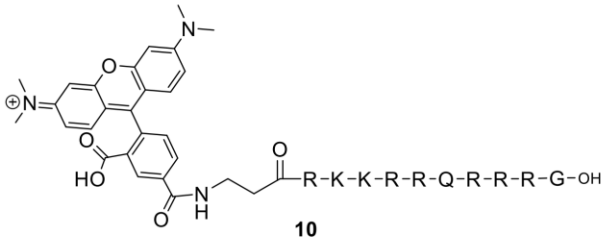

10

The synthesis was performed on 100 mg preloaded *TentaGel S AC-Gly(Fmoc)* with a binding capacity of 0.2-0.25 mmol/g (0.23 mmol, 1 eq.) by manual Fmoc-SPPS.

Afterwards 6.4 µL (36.8 µmol, 8 eq.) DIEA and 4.9 mg (9.2 µmol, 2 eq.) of TAMRA-NHS ester **33** were dissolved in a minimal amount of DMF and added to 25 mg of resin-bound peptide. The reaction mixture was gently shaken overnight at room temperature and afterwards washed four times with DMF and DCM, respectively. Cleavage and workup was performed as previously described. After lyophilization, 2.2 mg of a purple solid **10** were obtained (25.4%).

RP-HPLC, 10→40% B, t_R=17.03 min.

ESI-MS calc. for $C_{83}H_{135}N_{34}O_{17}^+$ m/z: 628.06, meas. 627.6 $[M+3H]^{3+}$, calc. 471.30 meas. 470.94 $[M+4H]^{4+}$, 377.24 meas. 376.89 $[M+5H]^{5+}$.

TAMRA-*β*-alanine-penetratin 11

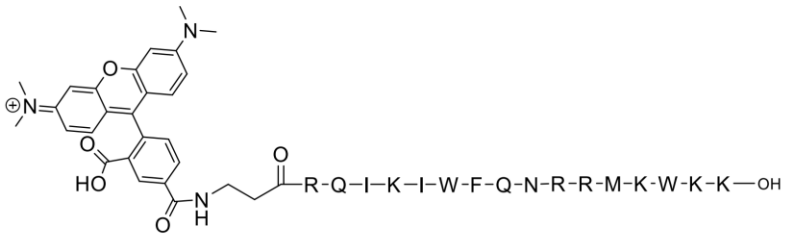

11

The synthesis was performed on 1 g preloaded *TentaGel S AC-Lys(Boc) Fmoc* with a binding capacity of 0.22 mmol/g (0.22 mmol, 1 eq.) by manual Fmoc-SPPS. After the attachment of *β*-

alanine, the resin-bound peptide was split and one-half (11 mmol) was fluorescently labeled. Therefore, 85.2 mg (114.82 µL, 0.66 mmol, 6 eq.) DIEA and 63.95 mg (0.12 mmol, 1.1 eq.) of TAMRA-NHS ester **33** were dissolved in a minimal amount of DMF and added to the resin-bound peptide. The reaction mixture was gently shaken overnight at ambient temperature and afterwards washed four times with each DMF and DCM. Cleavage and workup was performed as previously described. After lyophilization, 46 mg of a purple solid **11** were obtained (15.31%).

RP-HPLC, 10→80% B, t_R=15.41 min.

ESI-MS calc. for $C_{132}H_{194}N_{37}O_{25}S^+$ m/z: 911.43 meas. 911.1 $[M+3H]^{3+}$, calc. 683.83 meas. 683.60 $[M+4H]^{4+}$, 547.26 meas. 547.1 $[M+5H]^{5+}$.

TAMRA-β-alanine-heptaarginine 12 and TAMRA-β-alanine-decaarginine 13

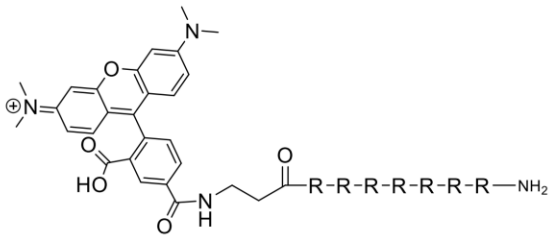

12

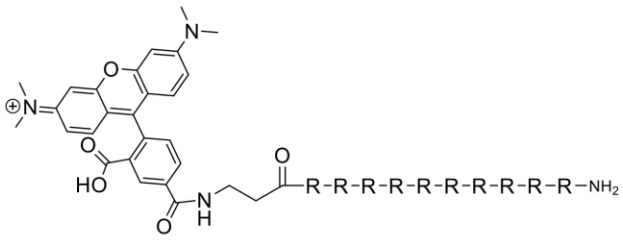

13

The synthesis was performed on 1 g preloaded *TentaGel Fmoc-Arg(Pbf)-NovaSyn TGA* resin (*Novabiochem*) with a binding capacity of 0.19 mmol/g by manual Fmoc-SPPS. After the attachment of six arginines, the resin was split and to one part additional three arginines were attached.

Afterwards, Fmoc-β-Ala was coupled to both peptides and each 0.05 mmol of the peptides were converted with TAMRA-NHS ester **33**.

To that end, 51.7 mg (69.9 µL, 0.40 mmol, 8 eq.) DIEA and 52.8 mg (0.1 mmol, 2 eq.) of TAMRA-NHS ester **33** were dissolved in a minimal amount of DMF and added to the resin-bound peptide. The reaction mixture was gently shaken overnight at room temperature and afterwards washed four times with DMF and DCM respectively. Cleavage and workup was performed as previously described. After lyophilization 19.1 mg of a purple solid **12** (24%) and 19.6 mg of purple solid **13** were obtained (19%).

RP-HPLC, 10→100% B, t_R=13.42 min for **12** and 13.12 min for **13**.

ESI-MS calc. for **12** $C_{70}H_{112}N_{32}O_{12}$ m/z: 532.29 meas. 532.57 $[M+3H]^{3+}$, 570.57 $[M+TFA+3H]^{3+}$, 608.56 $[M+2TFA+3H]^{3+}$; calc. 399.47 meas. 399.61 $[M+4H]^{4+}$, 428.13 $[M+TFA+4H]^{4+}$.

ESI-MS calc. for **13** $C_{88}H_{148}N_{44}O_{15}$ m/z: 688.49 meas. 764.71 $[M+2TFA+3H]^{3+}$, 840.79 $[M+4TFA+3H]^{3+}$, 787.76 $[M+5TFA+3H]^{3+}$, 916.78 $[M+6TFA+3H]^{3+}$; calc. 516.62 meas. 573.80 $[M+2TFA+4H]^{4+}$, 602.30 $[M+3TFA+4H]^{4+}$, 630.82 $[M+4TFA+4H]^{4+}$, 659.30 $[M+5TFA+4H]^{4+}$, 687.87 $[M+6TFA+4H]^{4+}$; calc. 413.50 meas. 459.22 $[M+2TFA+5H]^{5+}$, 482.03 $[M+3TFA+5H]^{5+}$, 504.86 $[M+4TFA+5H]^{5+}$, 527.68 $[M+5TFA+5H]^{5+}$.

Doxorubicin-GuCOSS conjugate 15

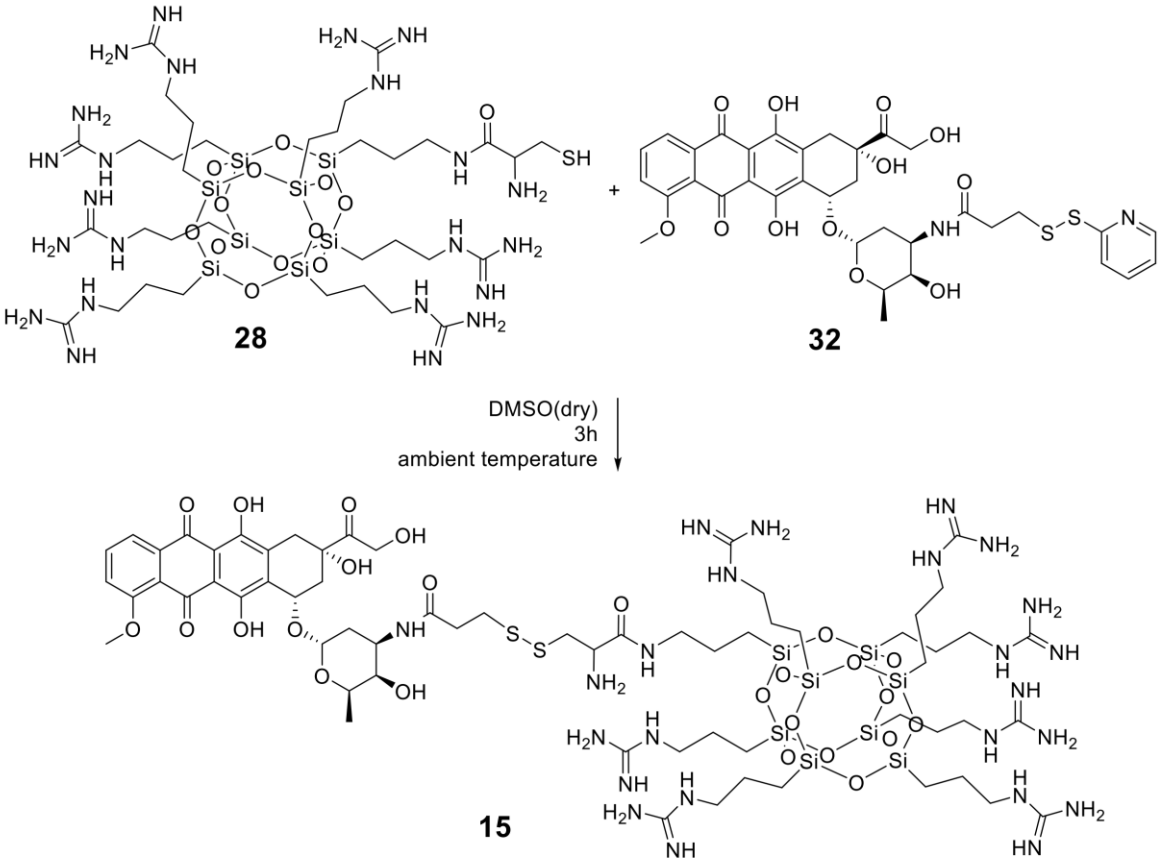

Doxorubicin-GuCOSS conjugate **15** was synthesized using 5 mg (0.0039 mmol, 1 eq.) cysteine-modified GuCOSS **28**, 3.5 mg (0.0047 mmol, 1.2 eq.) aldrithiol-activated doxorubicin **32**. **32** was dissolved in dry DMSO and **28** was added to the solution. After completion of the reaction (3 h, ambient temperature) the reaction mixture was lyophilized and purified using semi-preparative RP-HPLC with a gradient 30to100% B. After lyophilization, 1.1 mg (14.7%) of the desired product as red fluffy powder was obtained. Eluent A: 0.1% aq. acetic acid; Eluent B 90% aq. acetonitrile, 0.1% acetic acid.

RP-HPLC 0→80% B: t_R: 14.63min

HR-MS calc. for $C_{64}H_{114}N_{24}O_{25}S_2Si_8$ m/z: 477.6568 meas. 477.6562 $[M+4H]^{4+}$.

3-carboxy-*N,N,N*-trimethylpropane-1-ammonium chloride 18

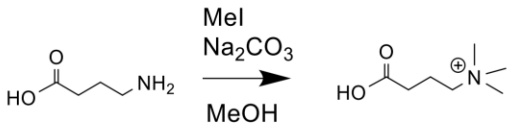

17 **18**

This synthesis was performed according to a procedure by Morano *et al.*[3] 2.2 g (21.6 mmol, 1 eq.) 4-aminobutyric acid **17** (*Alfa Aesar*) and 10 g (100 mmol, 4.6 eq.) potassium bicarbonate were combined in 250 mL of methanol under inert atmosphere. 6.9 mL (110 mmol, 5.2 eq.) methyl iodide was added and the reaction stirred for 4 days at ambient temperature. Then the solvent was removed using a rotary evaporator. The white solid was washed thrice with chloroform and dissolved in 50 mL of 6 N HCl. The solvent was removed by a rotary evaporator. The orange residue was extracted four times with acetone. The acetone was removed by using a rotary evaporator resulting in orange oil. 150 mL of ice-cold tetrahydrofuran (THF) were added and stirred for 30 min. The resulting white solid was filtered, washed twice with ice-cold THF and then dried under vacuum. 763 mg of a white precipitate **18** (19.6%) were obtained.

^{1}H NMR (500 MHz, DMSO-d6) δ: 1.81 – 1.96 (m, 2H), 2.32 (t, J = 7.1 Hz, 2H), 3.08 (s, 9H), 3.27 – 3.42 (m, 2H), 12.33 (s, 1H).

^{13}C NMR (500 MHz, DMSO-d6) δ: 17.92, 30.18, 52.26, 64.55, 173.22.

4-trimethylammoniumbutyric acid-NHS ester 19

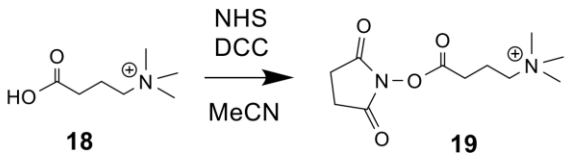

18 **19**

The synthesis was performed according to a procedure by Morano *et al.*[3] A mixture of 200 mg (1.1 mmol, 1 eq.) 3-carboxy-*N,N,N*-trimethylpropane-1-ammonium chloride **18**, 215.4 mg (1.87 mmol, 1.7 eq.) NHS and 431.6 mg (2.1 mmol, 1.9 eq.) DCC were dissolved in 8 mL dry MeCN. After complete addition at 0°C, the mixture was stirred for 16 h at ambient temperature. The reaction mixture was filtrated to remove the resulting urea derivative. The solvent was removed using a rotary evaporator. 3 mL THF were added and the solution was stirred for 5 min at 0°C. The reaction mixture was filtered and the residue was washed thrice with ice-cold THF. After solvent removal, 204.1 mg of **19** (76.2%) were obtained.

ESI-MS calc. for $C_{11}H_{19}N_2O_4^+$ m/z: 243.28, meas. 243.03 $[M+H]^+$.

_N_-Trt-protected _β_-alanine 22

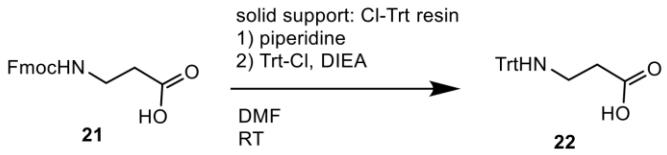

1 g 2-chlorotrityl resin (*Iris biotech GmbH*) was swollen for 1 h at ambient temperature in dry DCM. 0.995 g (3.2 mmol, 2 eq.) Fmoc-*β*-Ala and 0.825 mg (6.4 mmol, 4 eq., 1.112 mL) dry DIEA were added in 10 mL dry DCM and the mixture was shaken for 2 h at ambient temperature. The resin was washed 5 times with DCM and afterwards thrice using each 5 mL of a mixture of DCM, DIEA, and MeOH (17:2:1, *v*:*v*:*v*). The Fmoc protecting group was removed by double deprotection (20 vol% piperidine in DMF). The resin was washed with DCM and 1.784 g (6.4 mmol, 4 eq.) tritylchloride and 1.238 g (9.6 mmol, 6 eq., 1.674 mL) dry DIEA were added in 10 mL dry DCM and the mixture was shaken overnight at ambient temperature. The resin was washed 5 times with DCM. *N*-Trityl-protected *β*-alanine **22** was cleaved from the resin using 10 mL of a mixture of acetic acid, methanol, and DCM (5:1:4, *v*:*v*:*v*). The mixture was shaken for 3 h at room temperature. The solvent was removed using a rotary evaporator. 0.496 g of white solid **22** were obtained (93.5%) and used without further purification.

ESI-MS calc. for $C_{22}H_{21}NO_2$ m/z: 331.42, meas. 330.06 $[M-H]^-$.

^{1}H NMR (300 MHz, DMSO-d_6) δ: 2.20 (t, *J* = 6.7 Hz, 2H), 2.44 (t, *J* = 6.4 Hz, 2H), 2.95 (s, 1H), 7.19 (t, *J* = 7.3 Hz, 3H), 7.30 (t, *J* = 7.9 Hz, 6H), 7.41 (d, *J* = 7.2 Hz, 6H).

^{13}C-NMR (75 MHz, DMSO-d_6) δ: 34.75, 39.40, 70.29, 126.05, 127.67, 128.31, 145.96, 173.77.

COSS derivative 23 (monoTrt-aminoCOSS)

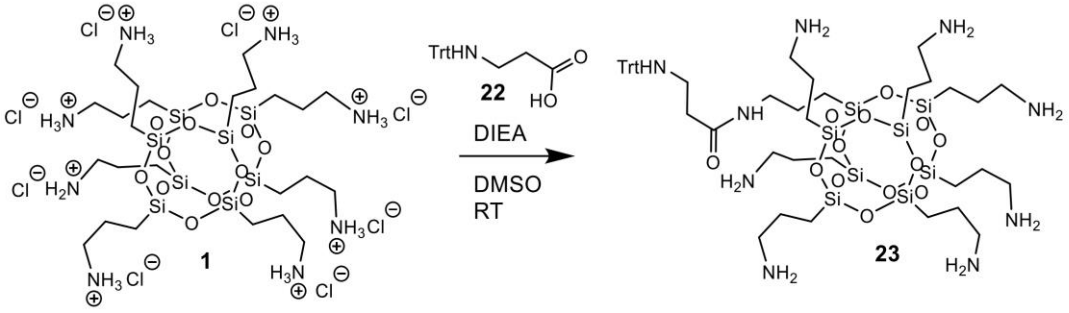

0.104 g (1.1 eq., 0.312 mmol) of β-alanine **22**, 0.148 g (1 eq., 0.284 mmol) benzotriazol-1-yl-oxytripyrrolidinophosphonium hexafluorophosphate (PyBOP) and 73.4 mg (2 eq., 0.568 mmol, 98.9 mL) dry DIEA were dissolved in 5 mL dry DMSO and shaken for 10 min at ambient temperature. After 10 min, the volume was increased to 40 mL using dry DMSO. 1 g of octaammonium COSS hydrochloride **1** was dissolved in 5 mL dry DMSO and the activated amino acid was slowly added to the vigorously stirred solution using a peristaltic pump (flow: 0.05 mL/min). The mixture was stirred for additional 2 h at room temperature and the solvent was removed by lyophilization. The oily residue was suspended in dry acetonitrile and the insoluble part was washed two times with dry acetonitrile. The precipitate was dissolved in 10 vol% aq. MeCN with 0.1 vol% AcOH and purified by semi-preparative RP-HPLC (gradient 10to100% B) with 0.1 vol% AcOH. After lyophilization 123 mg of colorless solid **23** were obtained (33%).

RP-HPLC, 10→100% B, t_R= 14.82 min.

ESI-MS calc. for $C_{46}H_{83}N_9O_{13}Si_8$ m/z: 1194.90 meas. 1194.63 $[M+H]^+$, calc. 598.45 meas. 598.26 $[M+2H]^{2+}$.

^{1}H NMR (400 MHz, DMSO-d_6) δ: 8.48 (s, 1H), 8.41 – 8.00 (m, 21H), 7.41 (s, 15H), 3.10 – 2.94 (m, 2H), 2.91 – 2.65 (m, 16H), 2.32 (s, 1H), 2.21 – 1.78 (m, 2H), 1.85 – 1.58 (m, 14H), 1.58 – 1.35 (m, 2H), 0.96 – 0.39 (m, 16H).

^{29}Si NMR (79 MHz, DMSO) δ: -65.98, -66.49, -66.52, -66.62.

3-(pyridin-2-yldisulfanyl)propanoic acid) 31

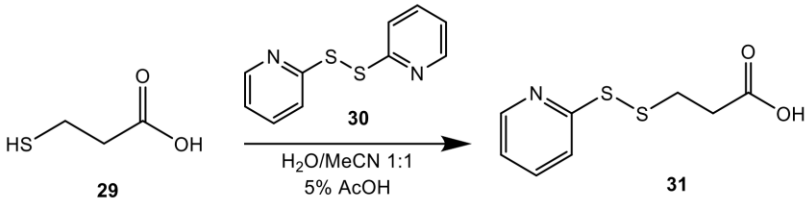

300 mg (1.3 mmol, 1 eq.) *2,2'*-dipyridyl disulfide **30** (*Aldrithiol™-2, Sigma Aldrich*) were diluted in 25.0 mL water/MeCN (1:1) with 5% acetic acid. 0.28 g (2.65 mmol, 2 eq.) 3-mercaptopropanoic acid **29** (*Sigma Aldrich*) were slowly added and the reaction mixture was stirred overnight at ambient temperature. The solvent was removed using a rotary evaporator. The precipitate was dissolved in aq. MeCN and purified by preparative RP-HPLC (gradient 10to80% B). After lyophilization, 61.9 mg of a yellow solid **31** were obtained (22.1%).

RP-HPLC, 10→100% B, t_R= 11.06min.

ESI-MS calc. for $C_8H_9NO_2S_2$ m/z: 215.29, meas. 215.94 $[M+H]^+$.

COSS derivative 27 (PG-Cys-aminoCOSS)

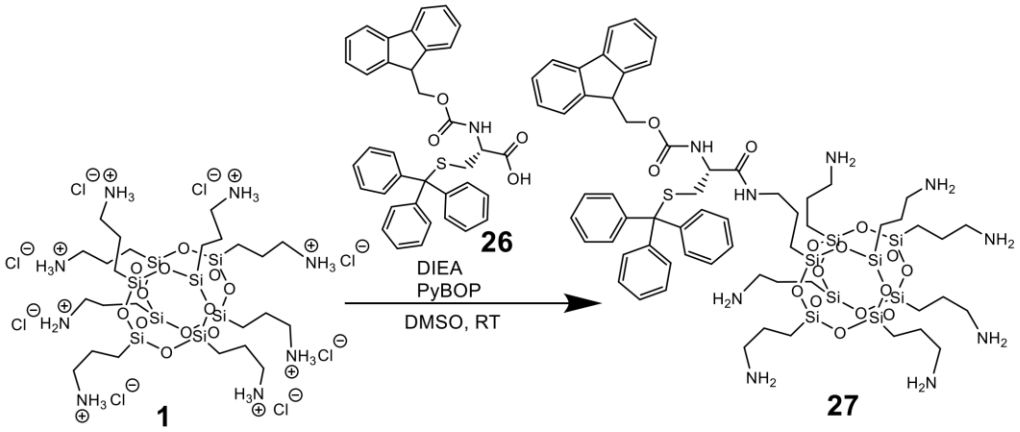

A mixture of 265.0 mg (0.45 mmol, 1 eq.) of Fmoc-Cys(Trt)-OH **26,** 1.89 mL (10.86 mmol, 24 eq.) dry DIEA and 283.0 mg (0.54 mmol, 1.2 eq.) of PyBOP was dissolved in 10 mL dry DMSO and pre-activated for 10 min. 1.06 g (0.91 mmol, 2 eq.) of octaammonium COSS hydrochloride **1** (purchased from *Hybrid Plastics* Inc., USA) were dissolved in 10.0 mL dry DMSO and vigorously stirred. The activated amino acid was added slowly using a peristaltic pump (flow: 0.05 mL/min). The mixture was stirred for additional 2 h at room temperature and the solvent was removed by lyophilization. The residue was suspended in dry acetonitrile and the insoluble part was washed twice with dry acetonitrile. The precipitate was dissolved in 10

vol% aq. MeCN with 0.1 vol% TFA and purified by semi-preparative RP-HPLC (gradient 10to50% B). After lyophilization, 145.0 mg of a white solid **27** were obtained (22.1 %).

RP-HPLC, 10→50% B, t_R= 21.5 min.

ESI-MS calc. for $C_{61}H_{93}N_9O_{15}SSi_8$ m/z: 1449.19, meas. 1449.7 $[M+H]^+$.

HR-MS calc. for $C_{61}H_{93}N_9O_{15}SSi_8$ m/z: 724.7406 measured 724.7409 $[M+2H]^{2+}$.

COSS derivative 28 (Cys-GuCOSS)

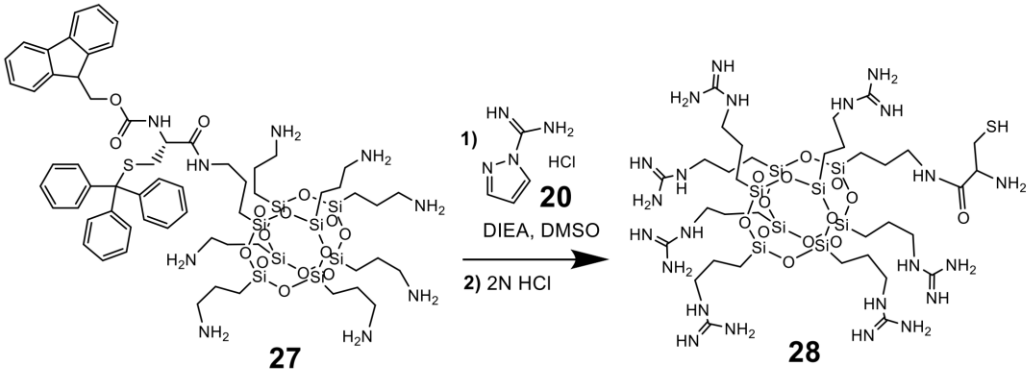

145 mg (0.12 mmol, 1 eq.) **27**, 368 mg (2.49 mmol, 21 eq.) 1*H*-pyrazole-1-carboxamidine hydrochloride **20** and 823 µL (4.73 mmol, 40 eq.) dry DIEA were mixed in 10 mL dry DMSO and the mixture was stirred for 2 days at ambient temperature (simultaneous Fmoc cleavage over the reaction course was caused by 1*H*-pyrazole formed upon guanidinylation as a by-product). Afterwards the solvent was removed by lyophilization and the oily residue was suspended in dry acetonitrile. The insoluble part was washed twice with dry acetonitrile. The precipitate was dissolved in 10 vol% aq. MeCN with 0.1 vol% TFA and purified by semi-preparative RP-HPLC (gradient 0to50% B). After lyophilization the trityl protecting group was removed by 1 mL 2 N HCl and 1 mL $CHCl_3$ and the solution was shaken for 3 h at ambient temperature. The organic phase was removed and the aqueous phase was extracted twice with each 1 mL $CHCl_3$. The combined organic phases were abolished and 9 mL deionized water was added to the aqueous phase. The solvent was removed by lyophilization. The remaining colorless solid was dissolved in 5 mL 5 vol% aq. AcOH and the solvent was removed by lyophilization. 64.0 mg of white solid **28** were obtained (42.3 %).

RP-HPLC, 0→50% B, t_R=20.12 min.

HR-MS calc. for $C_{68}H_{164}N_{46}O_{26}S_2Si_{16}$ m/z: 365.7026, meas. 365.7027 $[M+7H]^{7+}$ for the dimer.

Aldrithiol-activated doxorubicin 32

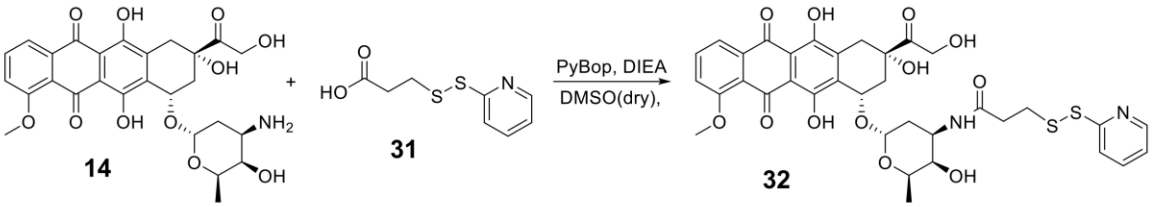

14 31 32

Aldrithiol-activated doxorubicin **32** was synthesized using 10 mg (0.018 mmol, 1 eq.) doxorubicin **14** (*Biomol GmbH*), 5.8 mg (0.027 mmol, 1.5 eq.) of **31**, 11.2 mg (0.22 mmol, 1.2 eq.) PyBop and 9.3 µL (0.054 mmol, 3 eq.) DIEA. After completion of the reaction (24 h, ambient temperature) the reaction mixture was lyophilized and purified using semi-preparative RP-HPLC with a gradient 40to100 %B. After lyophilization 8 mg (60%) of the desired product was obtained.

RP-HPLC 25→100 % B: t_R=11.95 min

ESI-MS calc. for $C_{35}H_{36}N_2O_{12}S_2$ m/z: 740.80, meas. 741.29 $[M+H]^+$.

5.3 Analytical data

COSS derivative 2 (TAMRA-aminoCOSS)

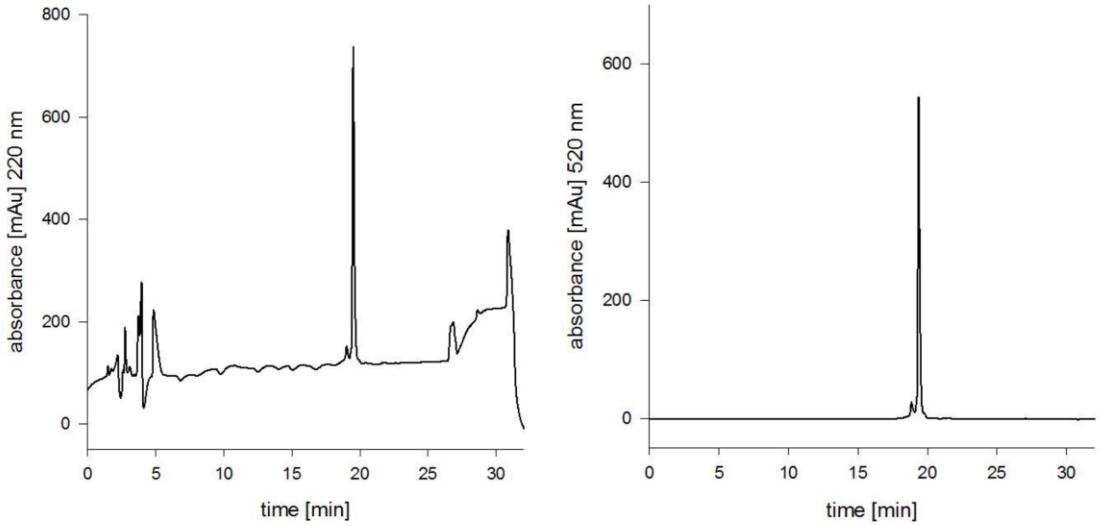

Figure S14: *Analytical HPLC diagrams of* ***2****. Left: λ=220 nm; right λ=520 nm.*

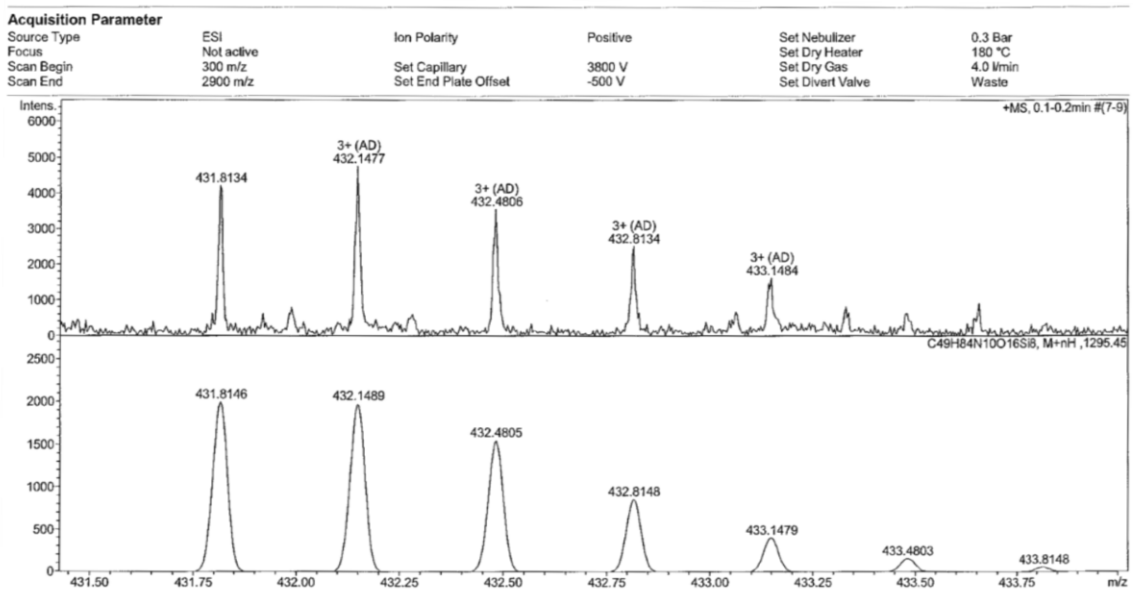

Figure S15: *HR-MS of* ***2****. m/z measured = 431.8134, m/z calculated = 431.8146* $[M+3H]^{3+}$.

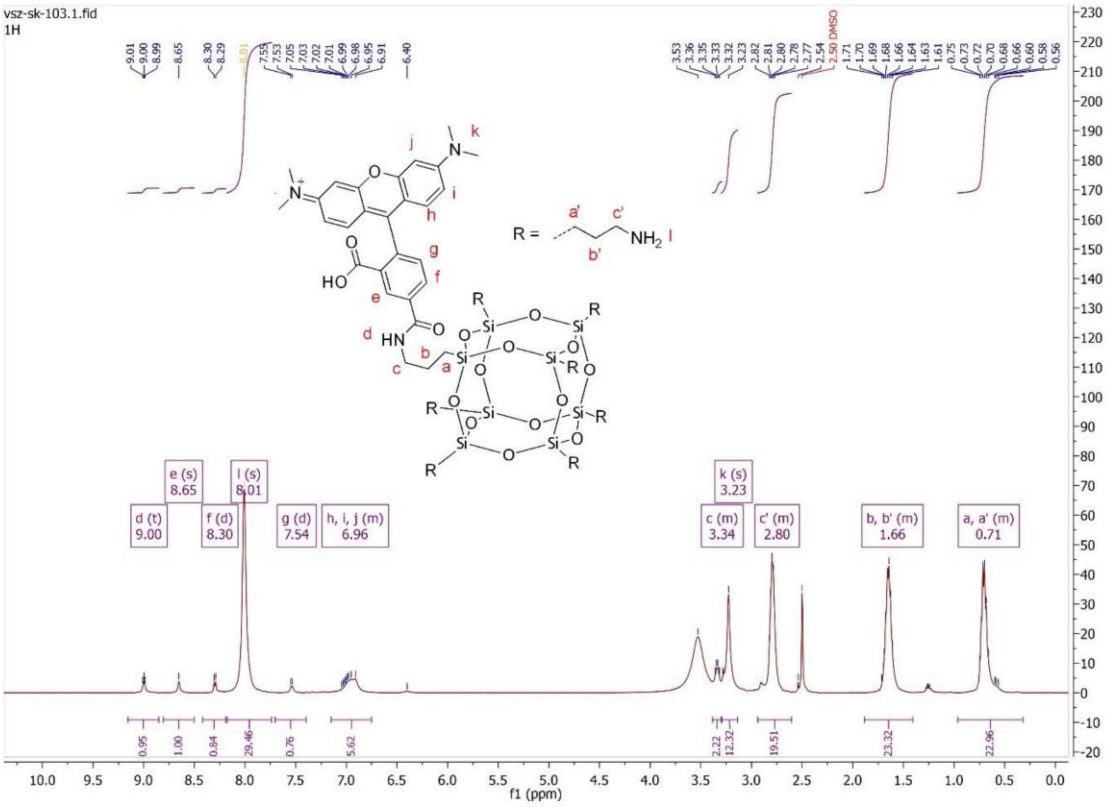

Figure S16: *^{1}H NMR of* ***2.***

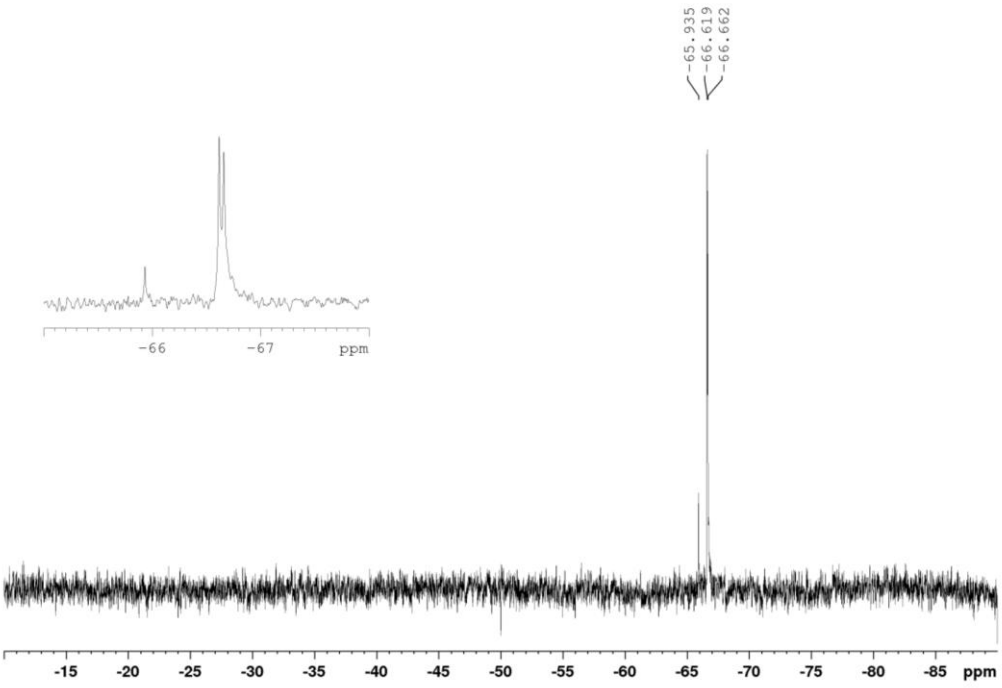

Figure S17: *^{29}Si NMR of* ***2.***

COSS derivative 3 (TAMRA-QuartCOSS)

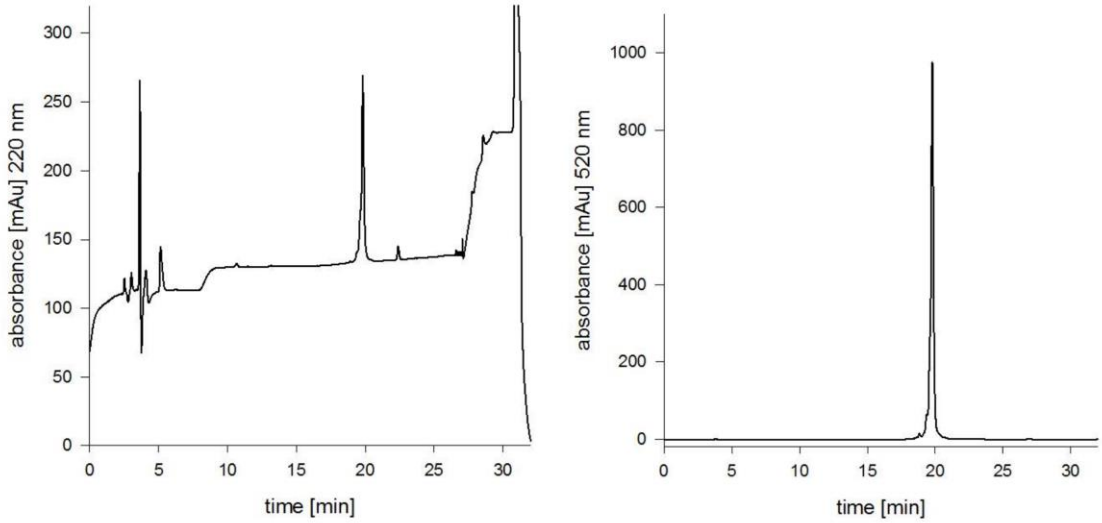

Figure S18: *Analytical HPLC diagrams of* ***3****. Left: λ=220 nm; right: λ=520 nm.*

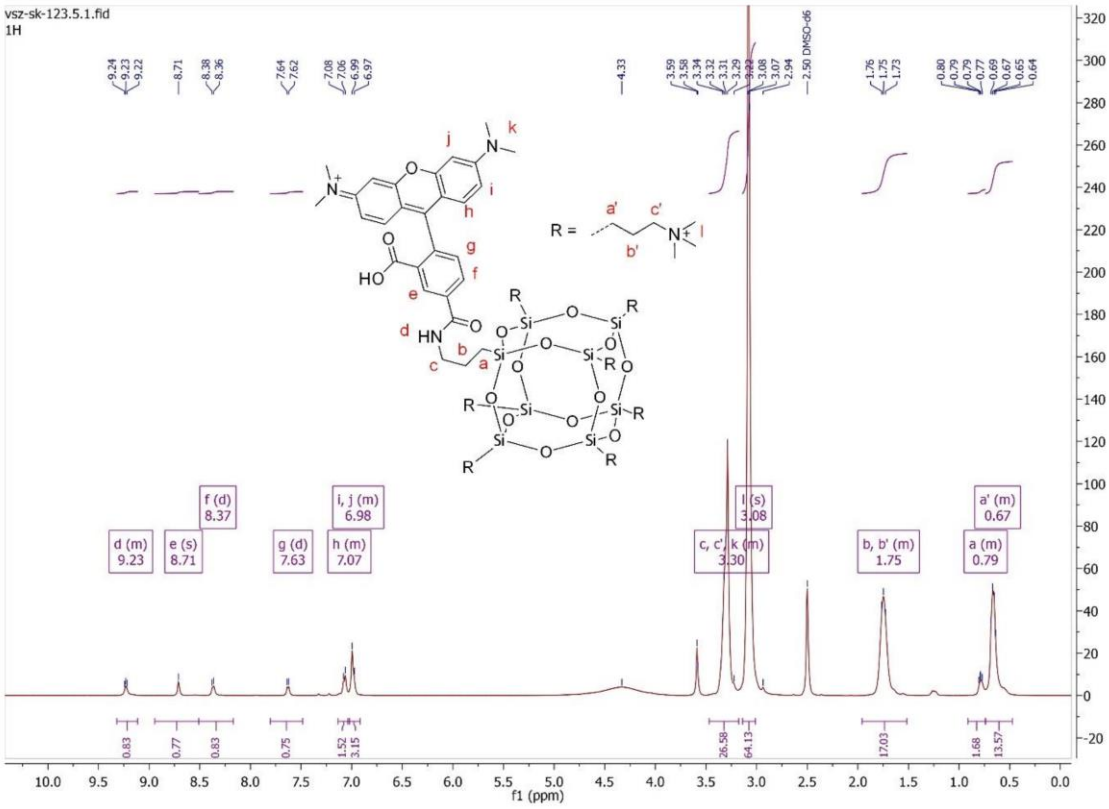

Figure S19: *^{1}H NMR of* ***3****.*

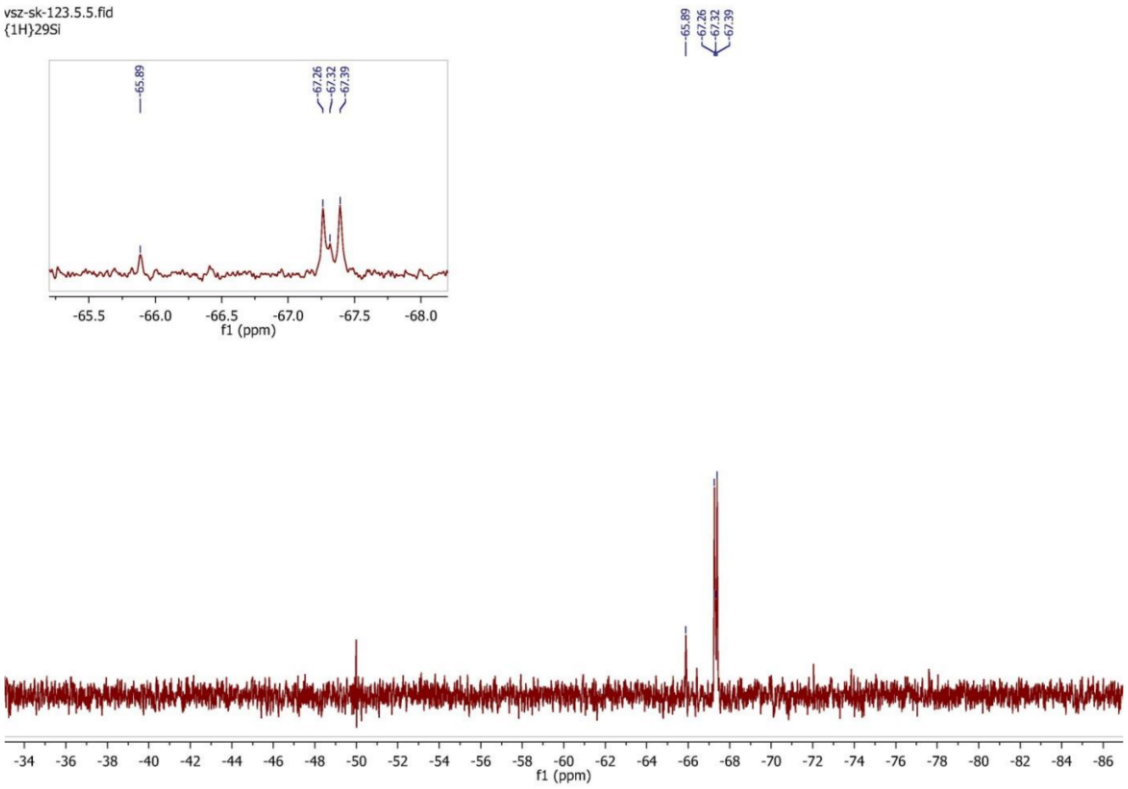

Figure S20: *^{29}Si NMR of **3**.*

COSS derivative 4 (TAMRA-GuCOSS)

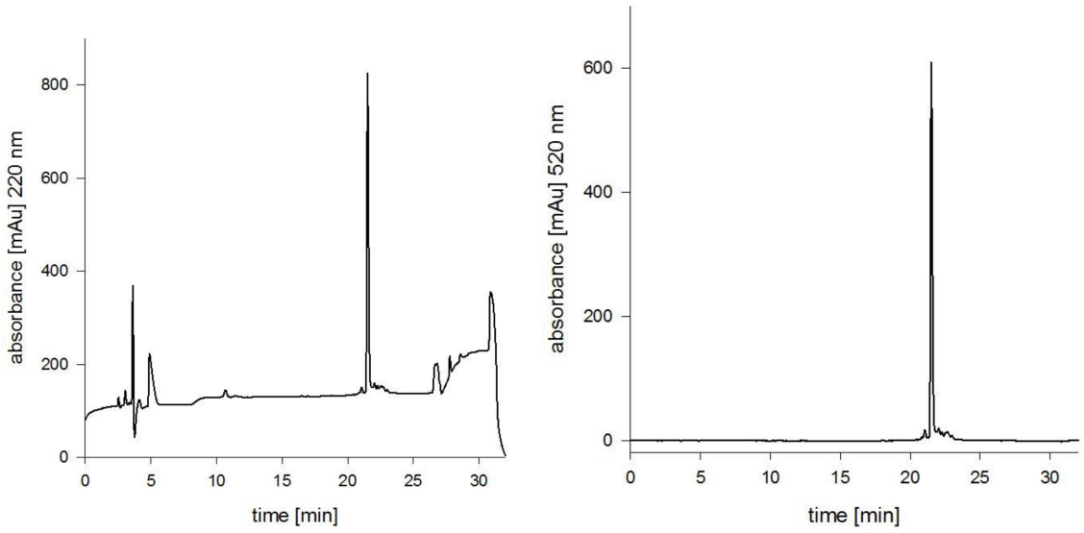

Figure S21: *Analytical HPLC diagrams of **4**. Left: λ=220 nm; right: λ=520 nm.*

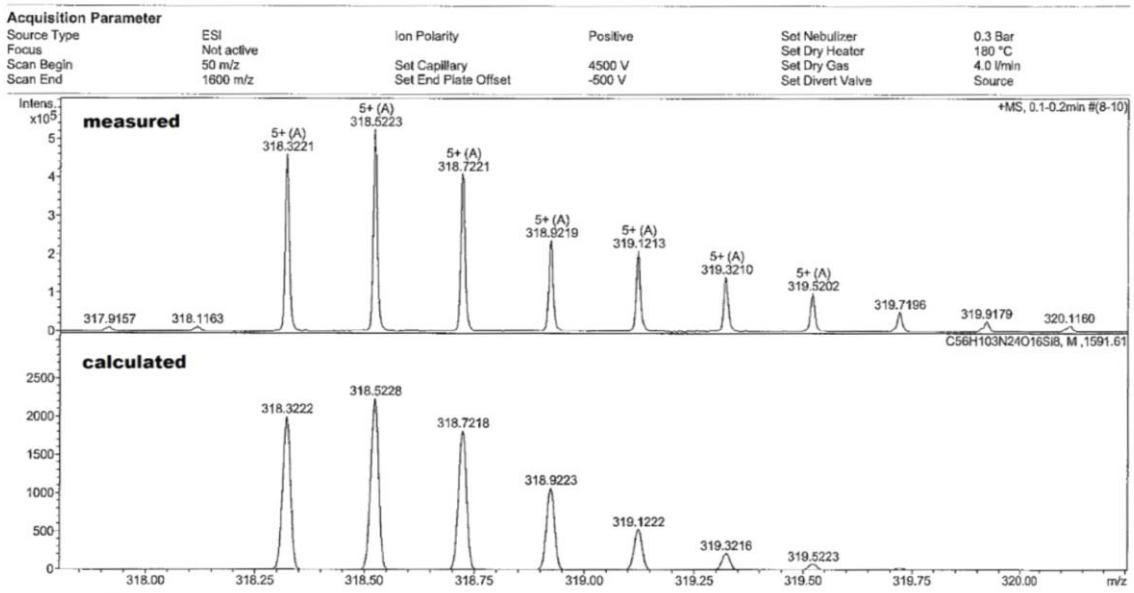

Figure S22: *HR-MS of **4**. m/z measured = 318.3221, m/z calculated = 318.3222; [M+5H]$^{5+}$.*

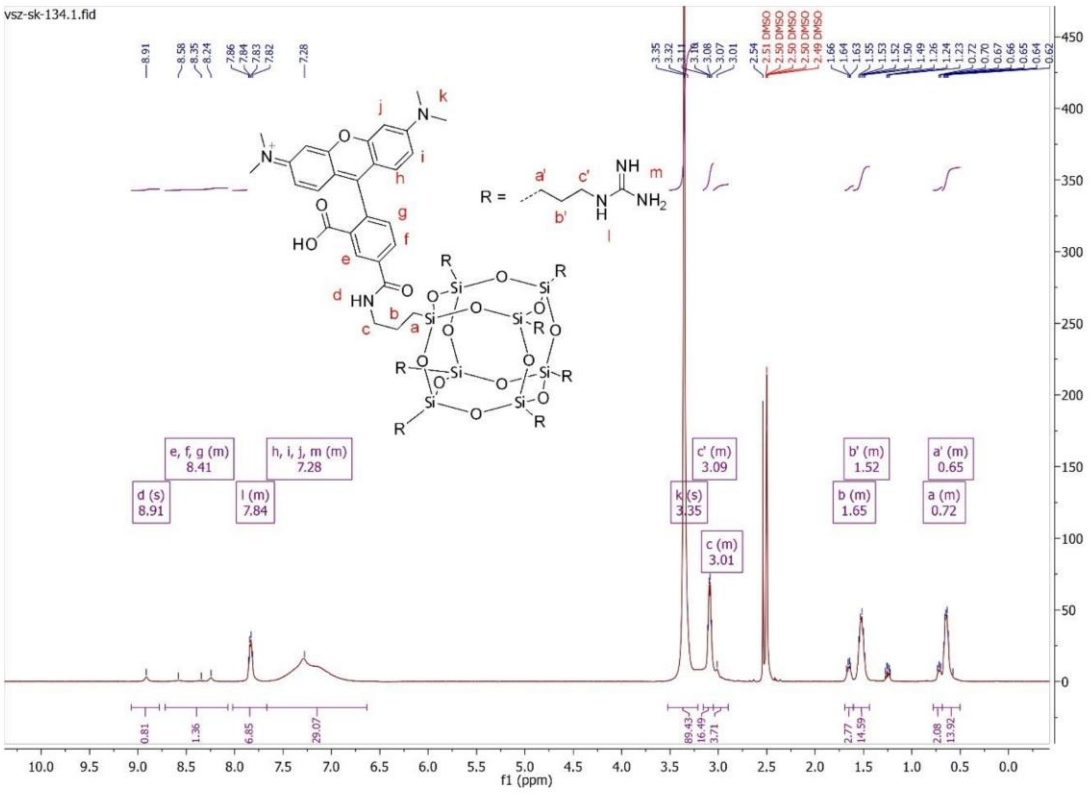

Figure S23: *^{1}H NMR of **4**.*

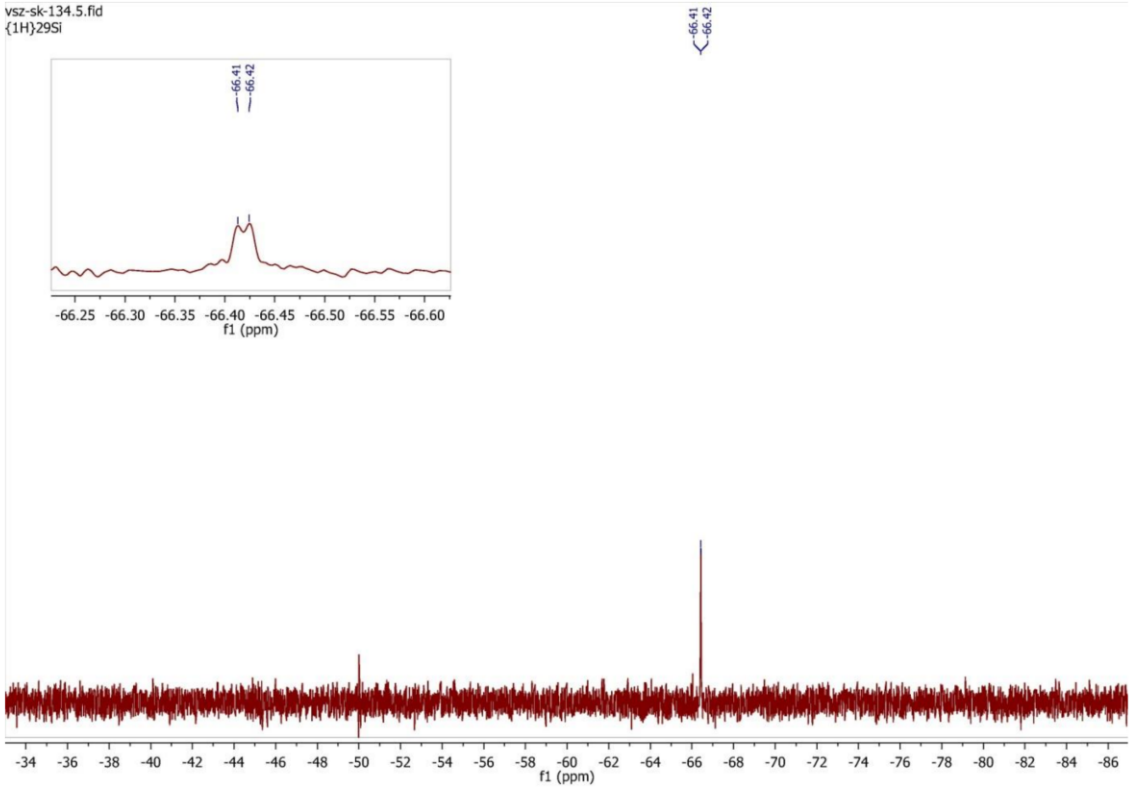

Figure S24: *^{29}Si NMR of **4**.*

COSS derivative 5 (TAMRA-aminoCOSS-L)

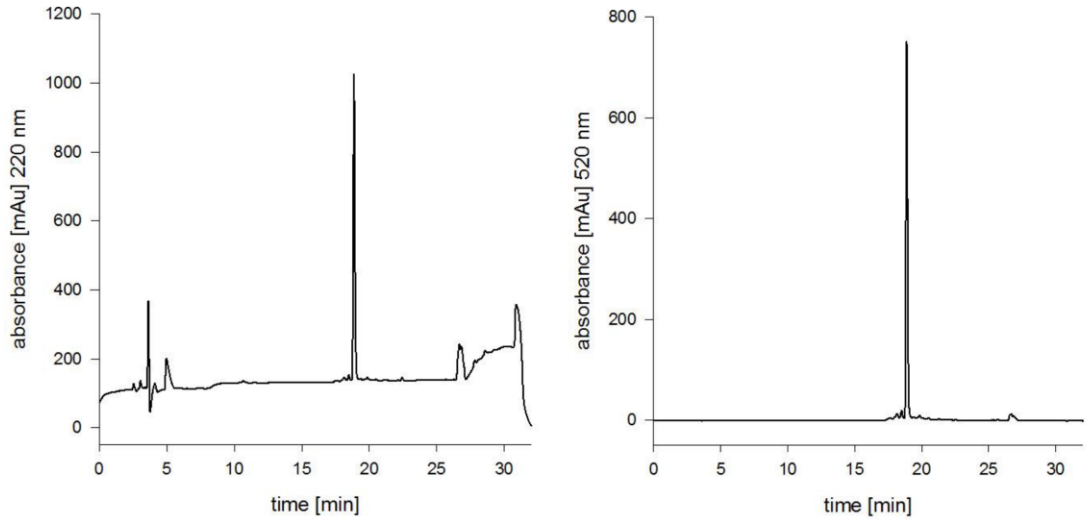

Figure S25: *Analytical HPLC diagrams of **5**. Left: λ=220 nm; right: λ=520 nm.*

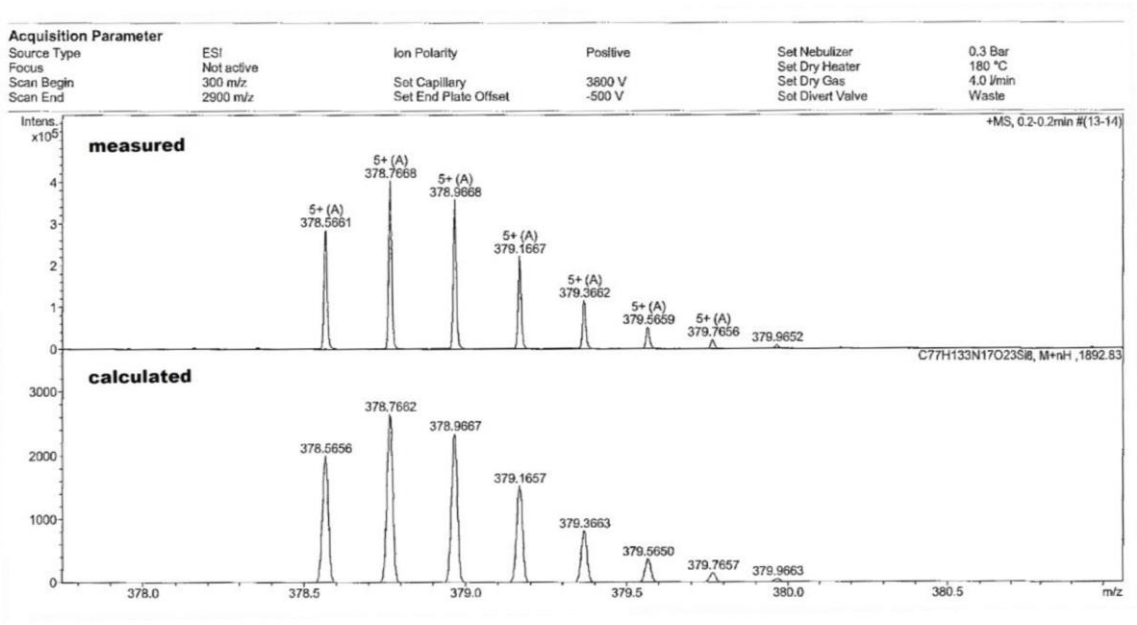

Figure S26: *HR-MS of* ***5****.Calculated for* $C_{77}H_{133}N_{17}O_{23}Si_8$ *m/z: 378.5656, measured 378.5661* $[M+5H]^{5+}$

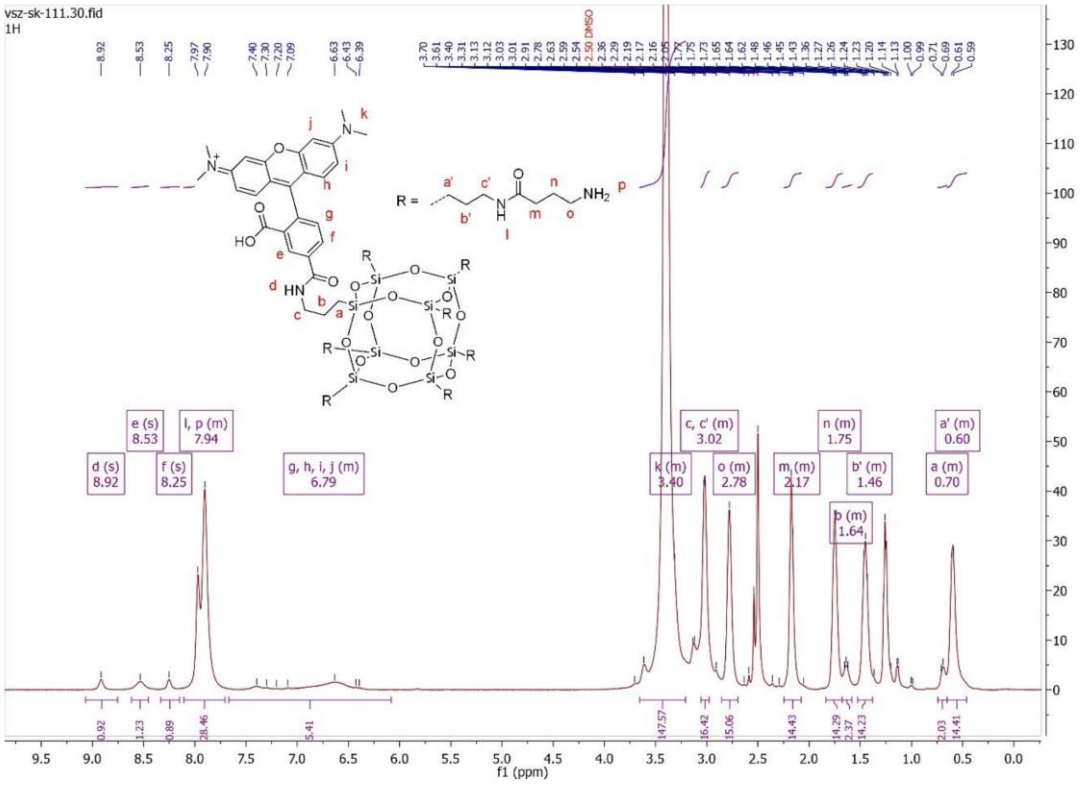

Figure S27: *^{1}H NMR of* ***5****.*

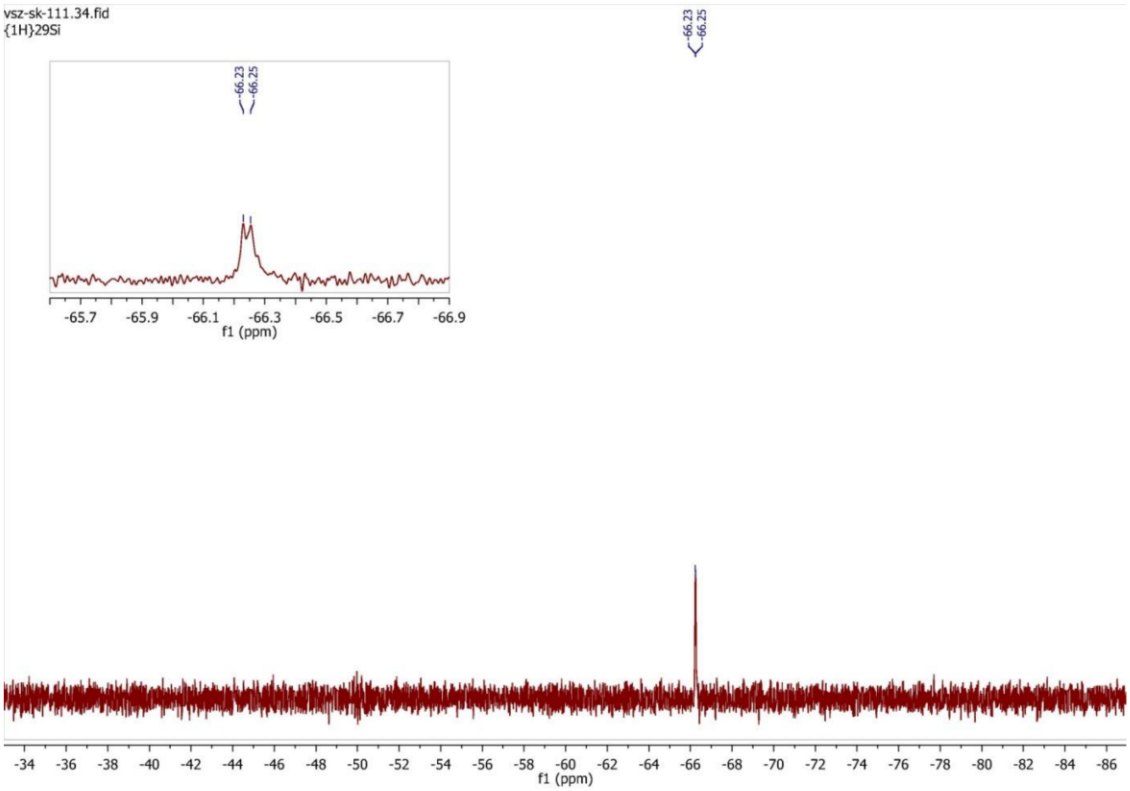

Figure S28: *^{29}Si NMR of **5**.*

COSS derivative 6 (TAMRA-quartCOSS-L)

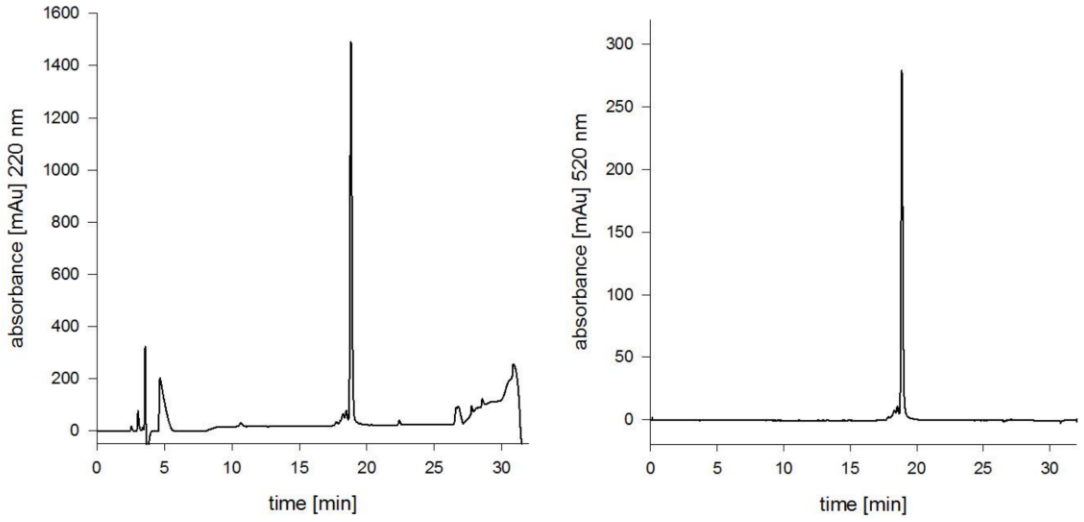

Figure S29: *Analytical HPLC diagrams of **6**. Left: λ=220 nm; right: λ=520 nm.*

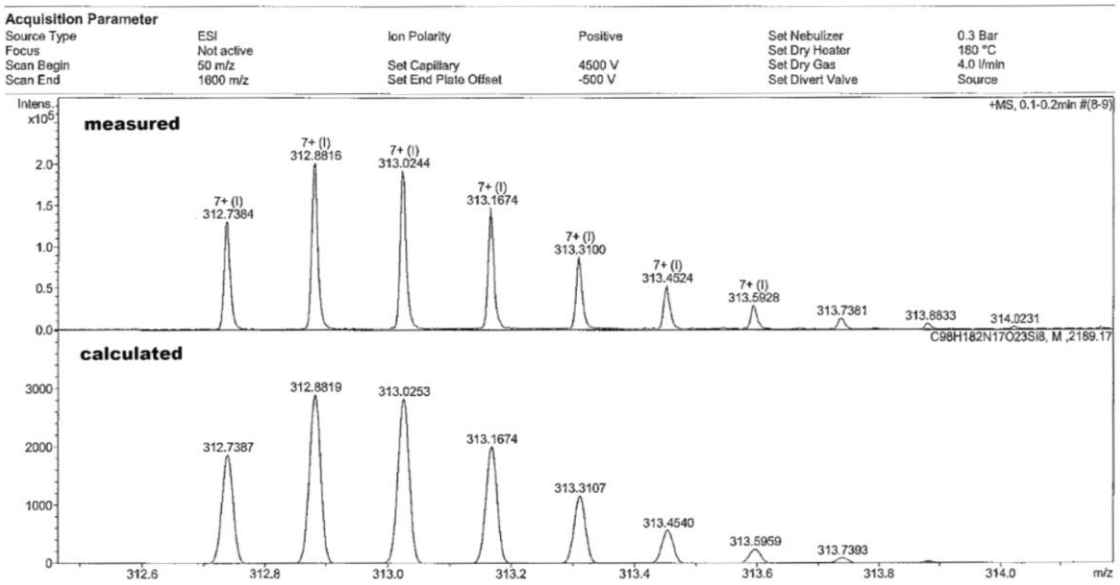

Figure S30: *HR-MS of* ***6****. Calculated for* $C_{98}H_{182}N_{17}O_{23}Si_8^{7+}$ *m/z: 312.7387, measured 312.7384* $[M]^{7+}$

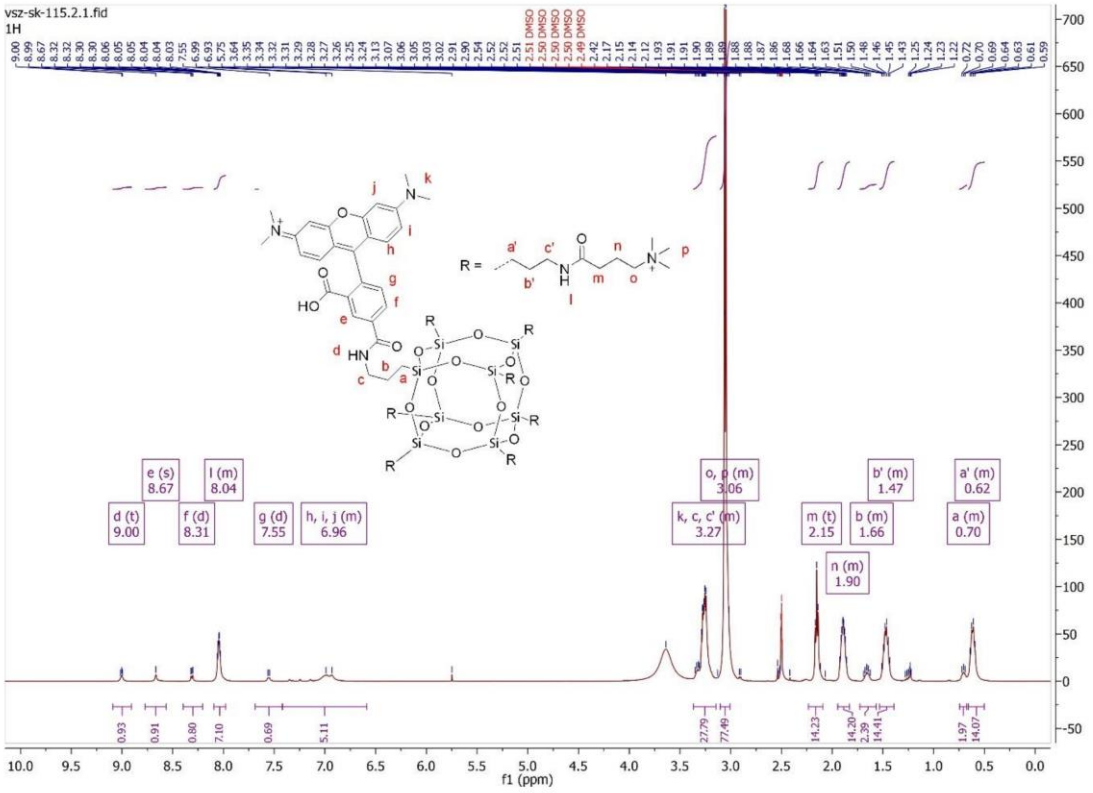

Figure S31: ^{1}*H NMR of* ***6****.*

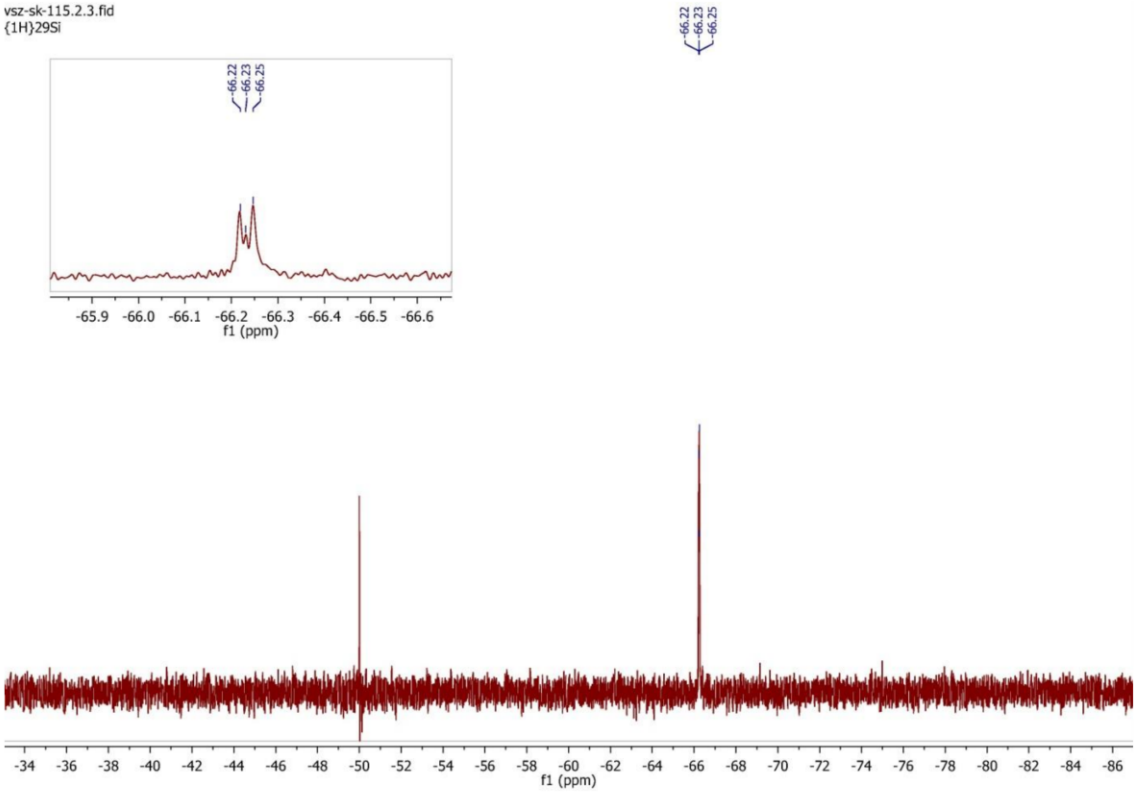

Figure S32: *^{29}Si NMR of **6**.*

COSS derivative 7 (TAMRA-GuCOSS-L)

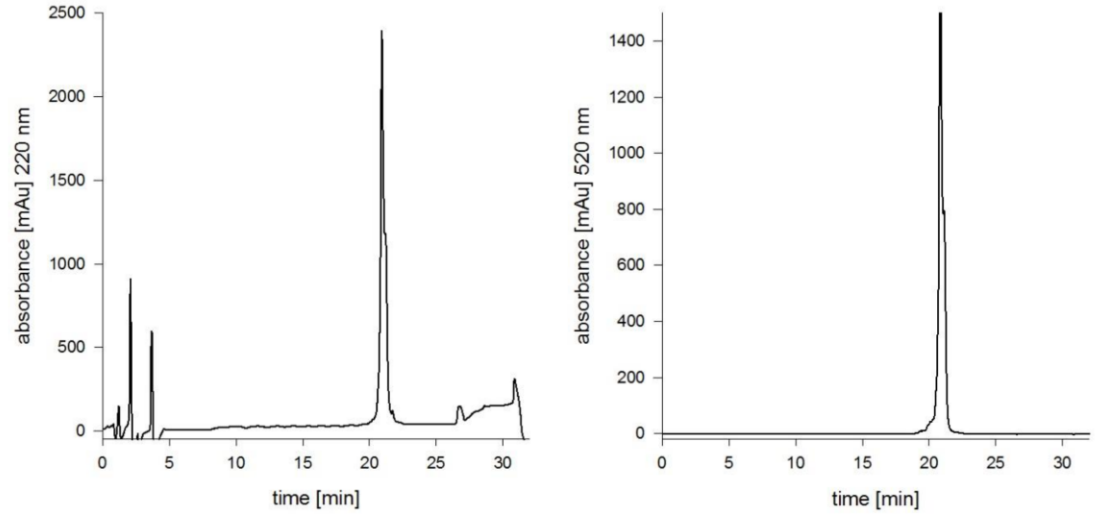

Figure S33: *Analytical HPLC diagrams of **7**. Left: λ=220 nm; right: λ=520 nm.*

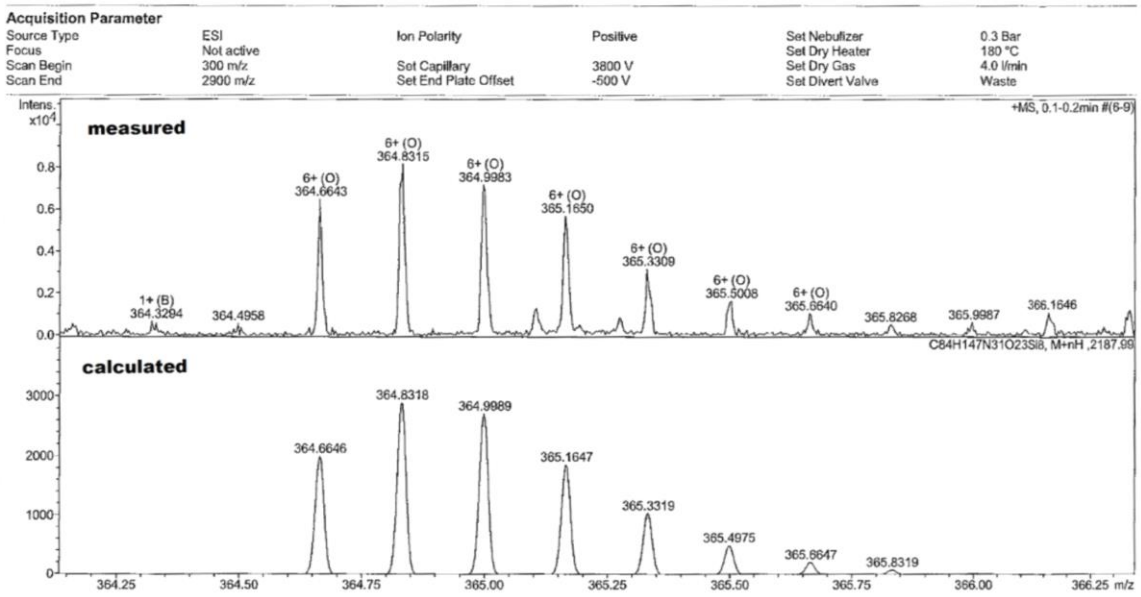

Figure S34: *HR-MS of* ***7****. Calculated for* $C_{84}H_{147}N_{31}O_{23}Si_8$ *m/z: 364.6646, measured 364.6643* $[M+6H]^{6+}$.

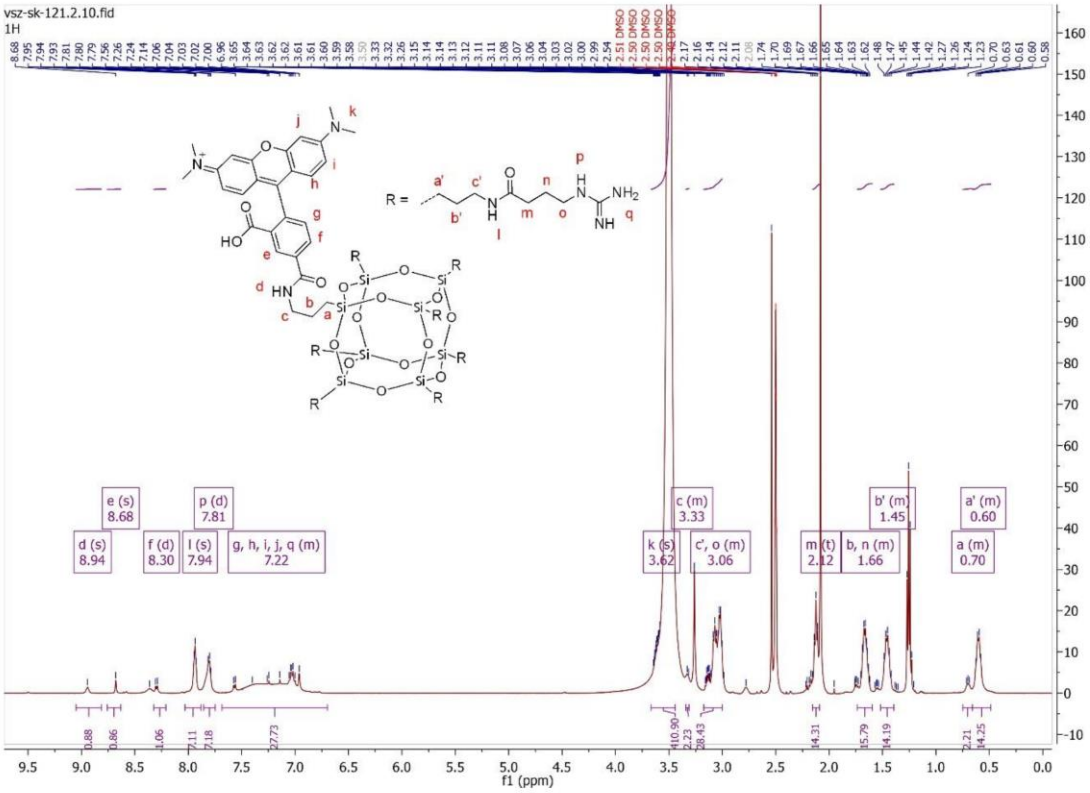

Figure S35: *^{1}H NMR of* ***7****.*

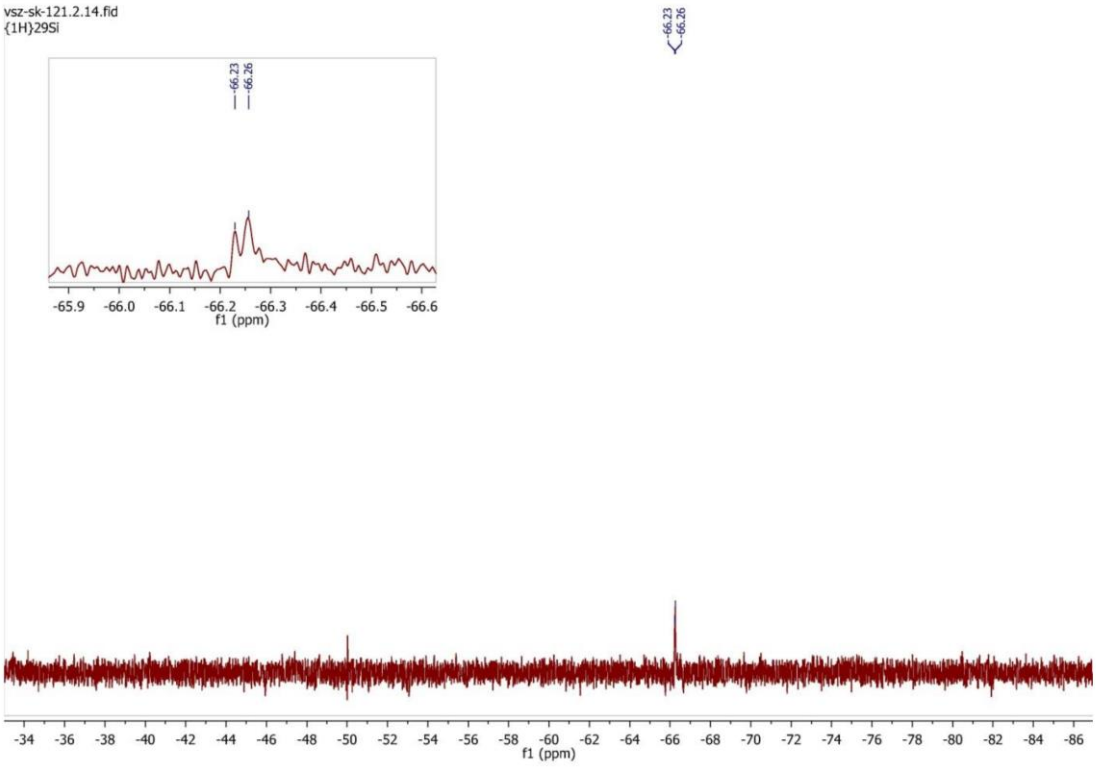

Figure S36: *^{29}Si NMR of* ***7.***

COSS derivative 8 (amino-GuCOSS)

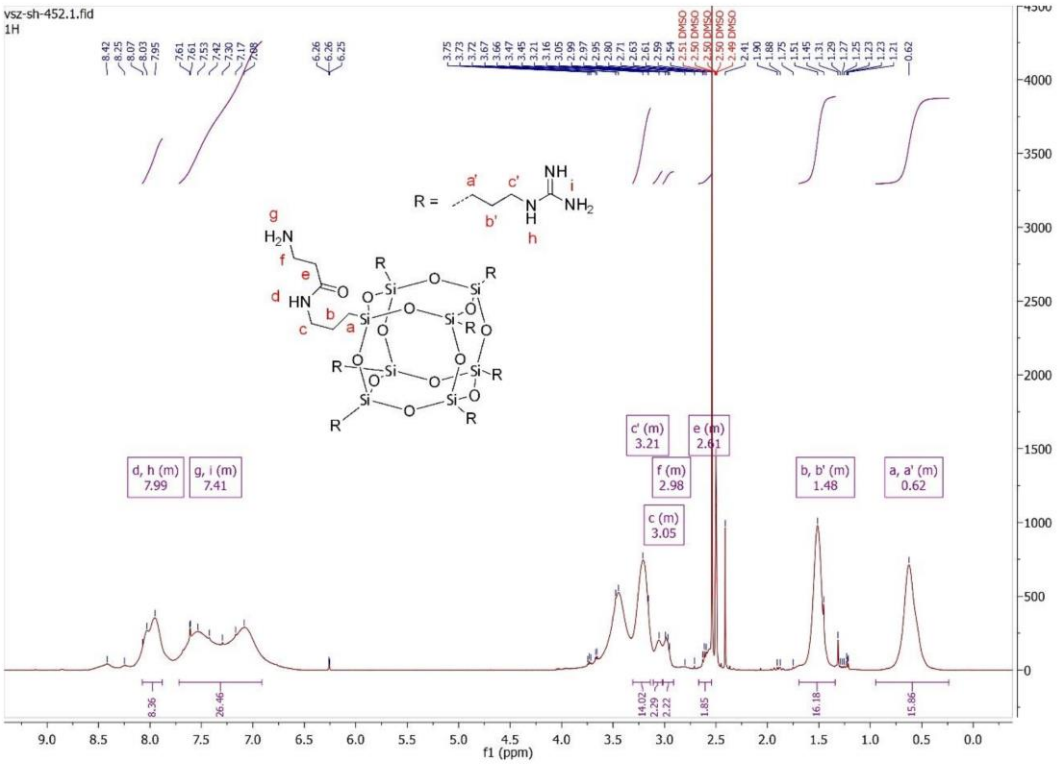

Figure S37: *^{1}H NMR of* ***8***

COSS derivative 9 (Fluorescein-TAMRA-GuCOSS)

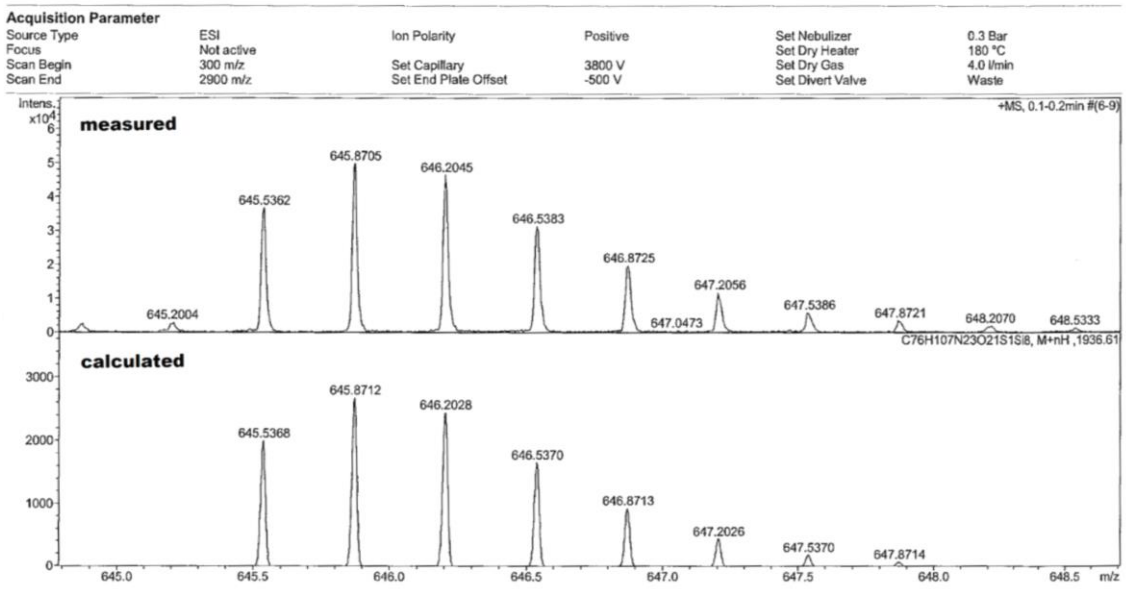

Figure S38: *HR-MS of* ***9****. Calculated for* $C_{76}H_{107}N_{23}O_{21}SSi_8$ *m/z: 645.5368, measured 645.5362* $[M+3H]^{3+}$.

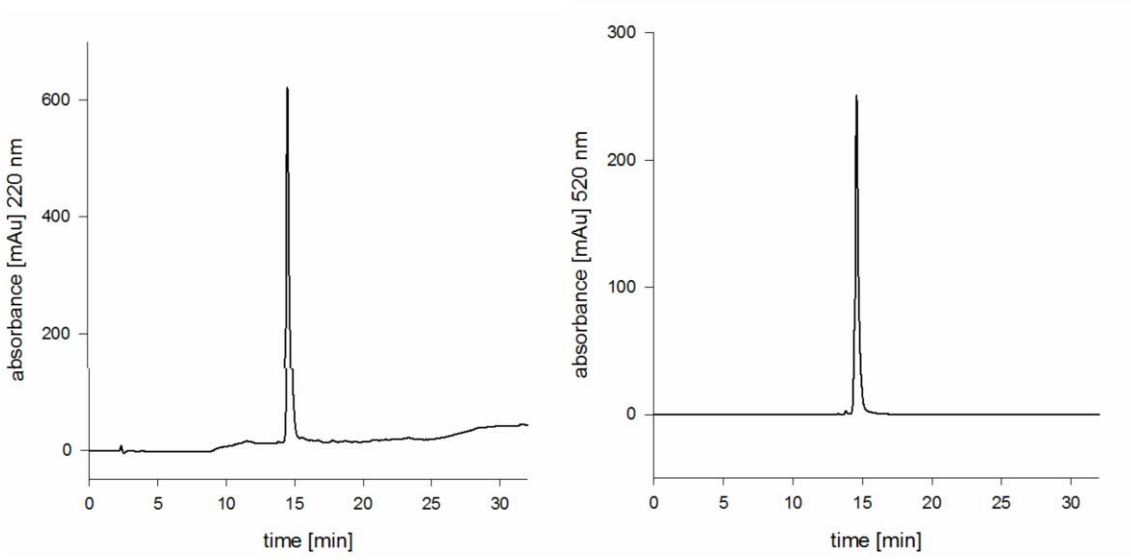

Figure S39: *Analytical HPLC diagrams of* ***9****. Left: λ=220 nm; right λ=520 nm.*

TAMRA-β-alanine-Tat peptide 10

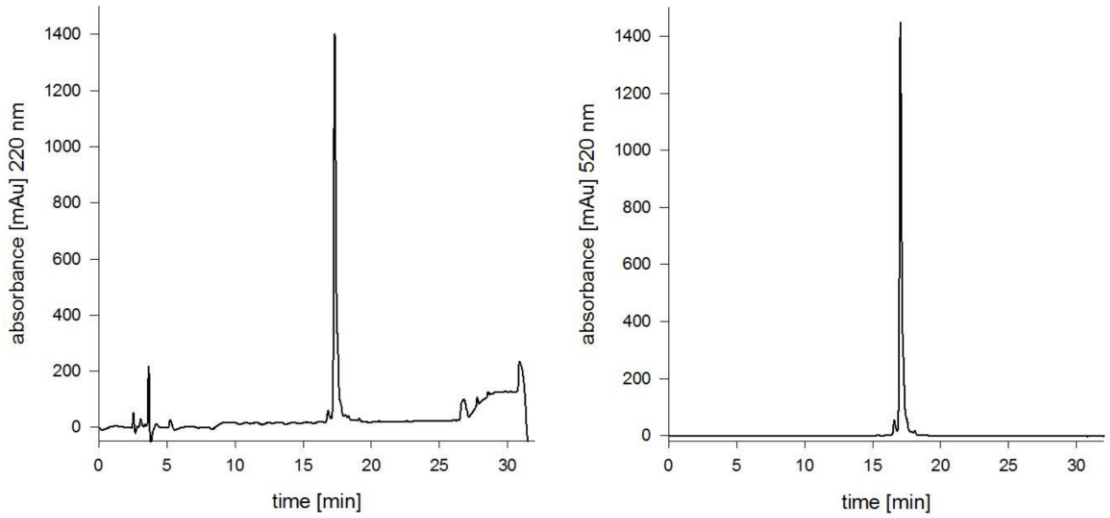

Figure S40: *Analytical HPLC diagrams of* ***10****. Left: λ=220 nm; right: λ=520 nm.*

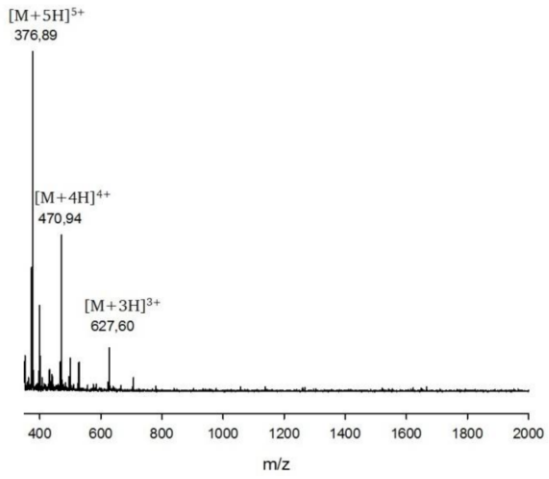

Figure S41: *ESI-MS of* ***10****. Calculated for* $C_{83}H_{135}N_{34}O_{17}^{+}$ *m/z: 628.06, measured 627.6* $[M+3H]^{3+}$*, calculated 471.30, measured 470.94* $[M+4H]^{4+}$*, calculated 377.24, measured 376.89* $[M+5H]^{5+}$*.*

TAMRA-β-alanine-Penetratin 11

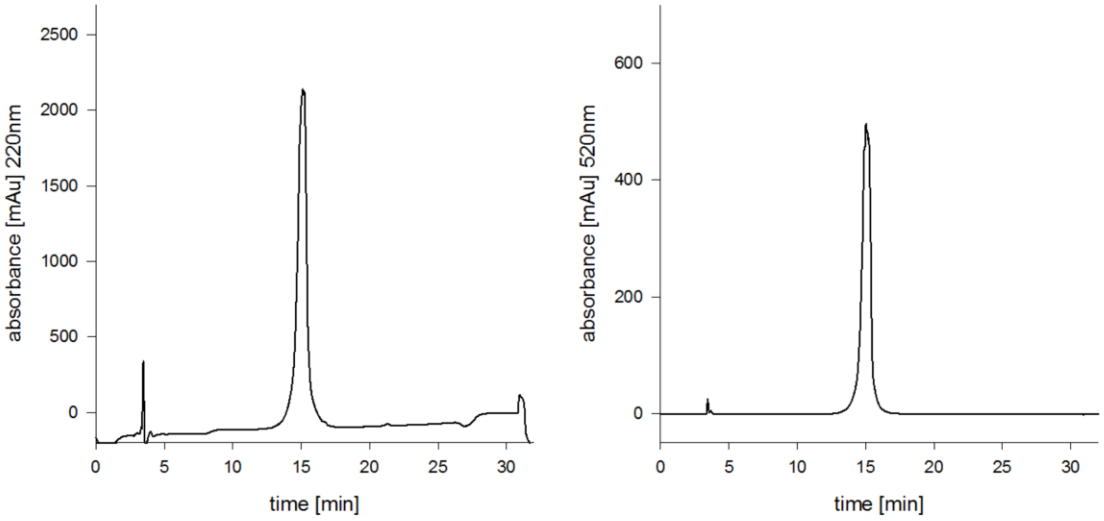

Figure S42: *Analytical HPLC diagrams of* ***11****.Left: λ=220 nm; right: λ=520 nm.*

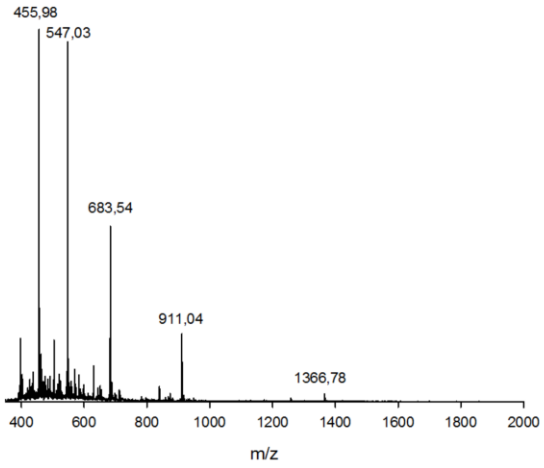

Figure S43: *ESI-MS of* ***11****. Calculated for* $C_{132}H_{194}N_{37}O_{25}S^+$ *m/z: 911.43, measured 911.1* $[M+3H]^{3+}$*, calculated 683.83, measured 683.60* $[M+4H]^{4+}$*, calculated 547.26, measured 547.1* $[M+5H]^{5+}$*.*

TAMRA-β-alanine-heptaarginine 12

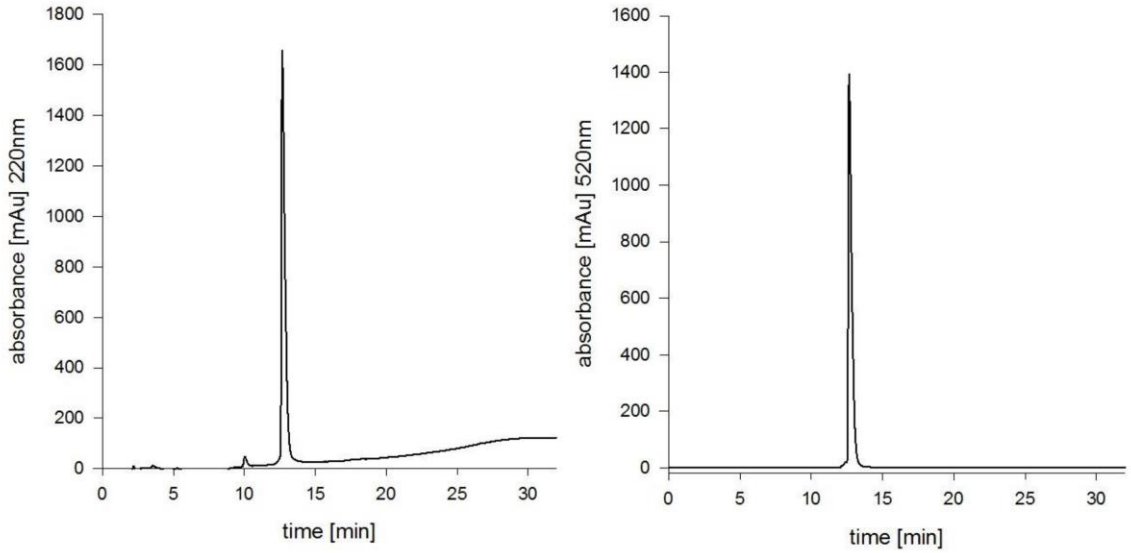

Figure S44: *Analytical HPLC diagrams* ***12****. Left: λ=220 nm; right: λ=520 nm.*

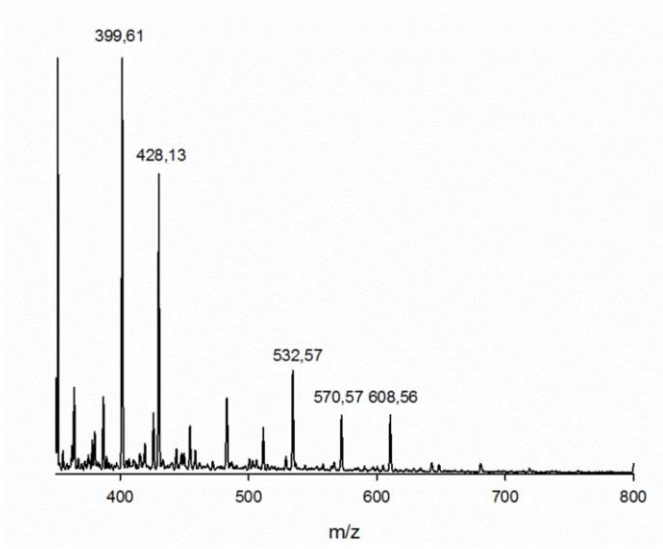

Figure S45: *ESI-MS of* ***12****. Calculated for* $C_{70}H_{112}N_{32}O_{12}$ *m/z: 532.29, measured 532.57* $[M+3H]^{3+}$*, 570.57* $[M+TFA+3H]^{3+}$*, 608.56* $[M+2TFA+3H]^{3+}$*; calculated 399.47, measured 399.61* $[M+4H]^{4+}$*, 428.13* $[M+TFA+4H]^{4+}$*.*

TAMRA-β-alanine-decaarginine 13

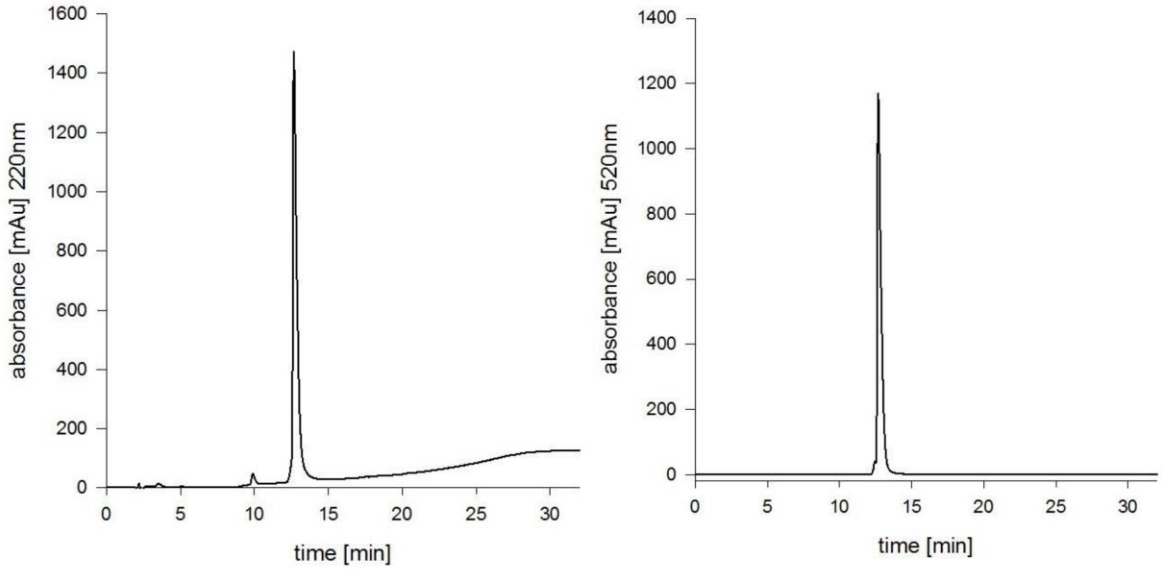

Figure S46: *Analytical HPLC diagrams of* ***13****. Left: λ=220 nm; right: λ=520 nm.*

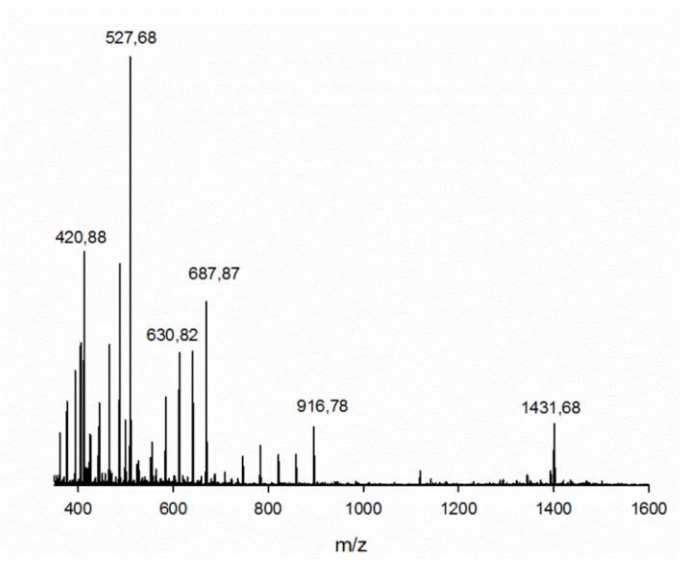

Figure S47: *ESI-MS of* ***13****. Calculated for $C_{88}H_{148}N_{44}O_{15}$ m/z: 688.49, measured 764.71 $[M+2TFA+3H]^{3+}$, 840.79 $[M+4TFA+3H]^{3+}$, 787.76 $[M+5TFA+3H]^{3+}$, 916.78 $[M+6TFA+3H]^{3+}$; calculated 516.62, measured 573.80 $[M+2TFA+4H]^{4+}$, 602.30 $[M+3TFA+4H]^{4+}$, 630.82 $[M+4TFA+4H]^{4+}$, 659.30 $[M+5TFA+4H]^{4+}$, 687.87 $[M+6TFA+4H]^{4+}$; calculated 413.50, measured 459.22 $[M+2TFA+5H]^{5+}$, 482.03 $[M+3TFA+5H]^{5+}$, 504.86 $[M+4TFA+5H]^{5+}$, 527.68 $[M+5TFA+5H]^{5+}$.*

Doxorubicin-GuCOSS derivative 15

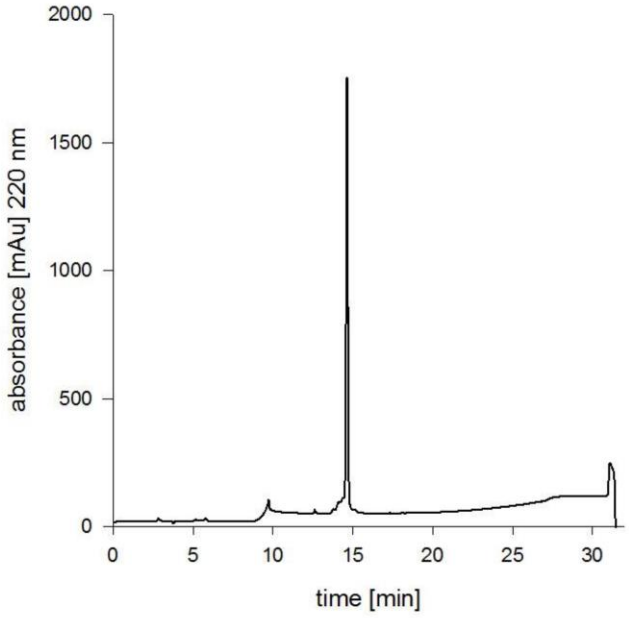

Figure S48: *Analytical HPLC diagram of* ***15****: λ=220 nm.*

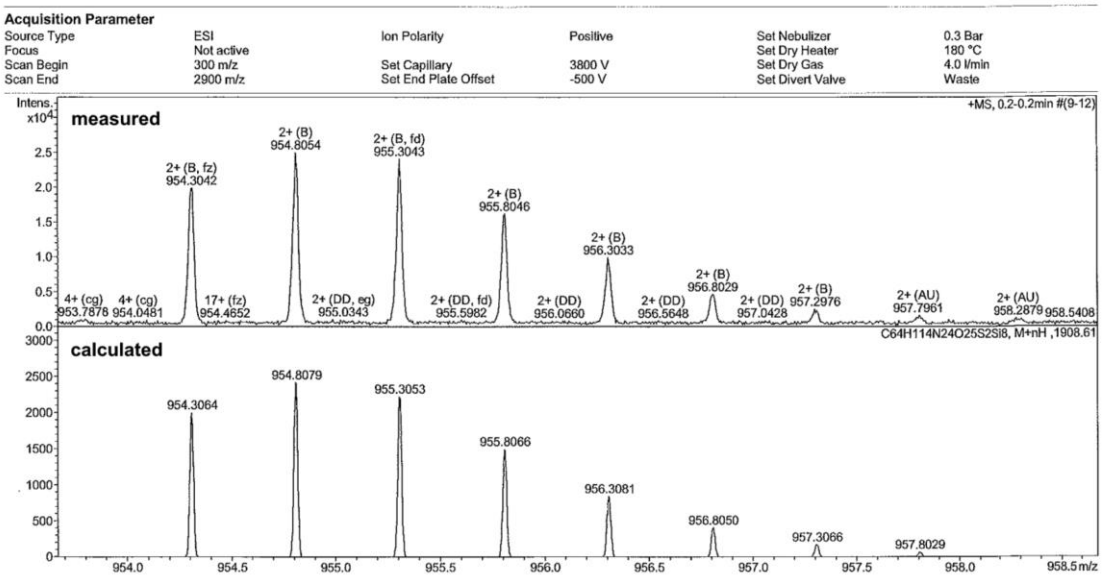

Figure S49: *HR-MS of* ***15****. Calculated for* $C_{64}H_{114}N_{24}O_{25}S_2Si_8$ *m/z: 954.3064, measured 954.3042* $[M+2H]^{2+}$.

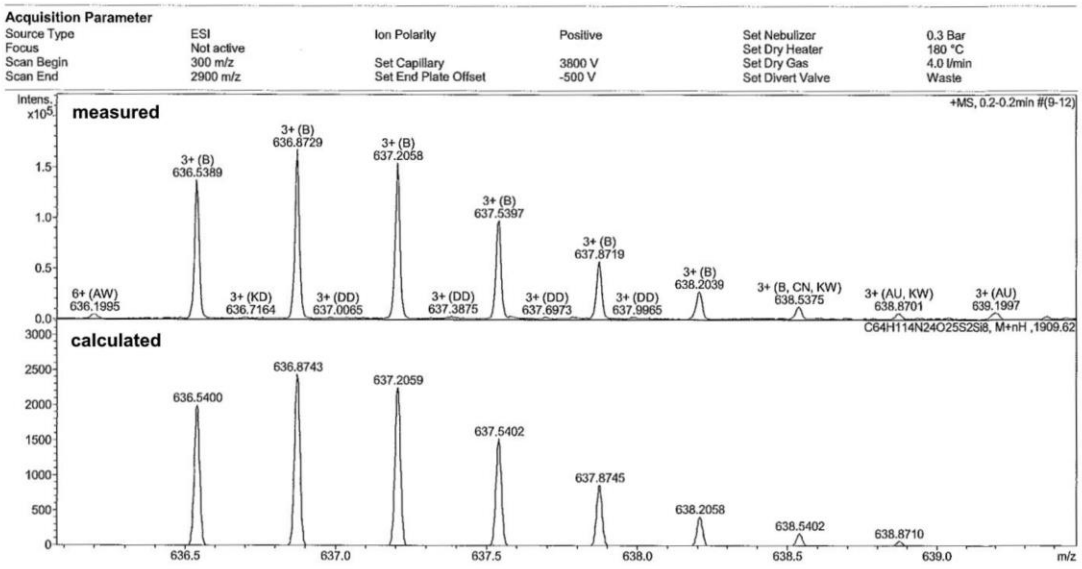

Figure S50: *HR-MS of **15**. Calculated for $C_{64}H_{114}N_{24}O_{25}S_2Si_8$ m/z: 636.5400 measured 636.5389 $[M+3H]^{3+}$.*

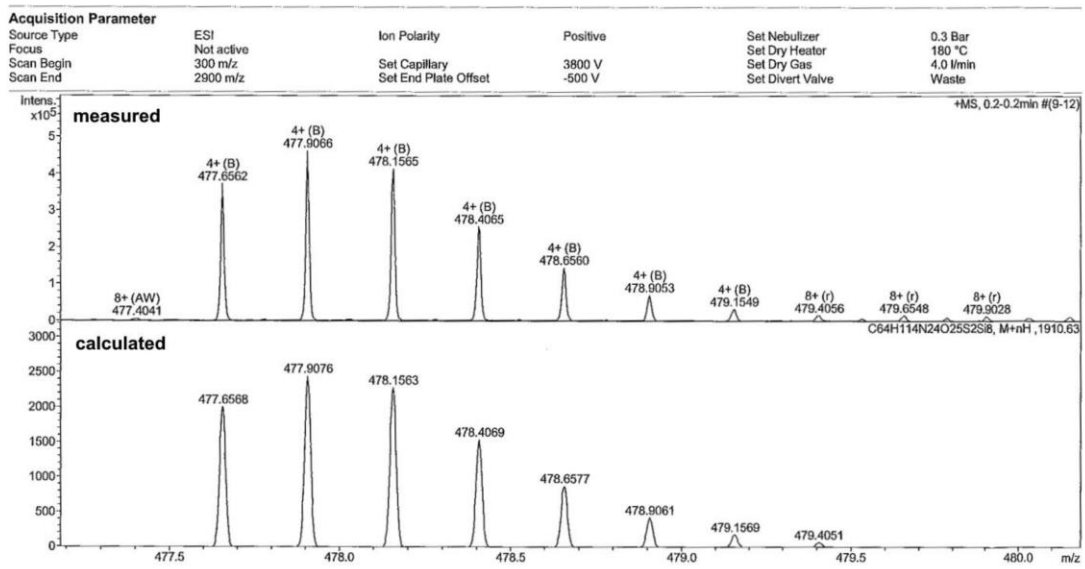

Figure S51: *HR-MS of **15**. Calculated for $C_{64}H_{114}N_{24}O_{25}S_2Si_8$ m/z: 477.6568, measured 477.6562 $[M+4H]^{4+}$.*

3-carboxy-*N,N,N*-trimethylpropane-1-ammonium chloride 18

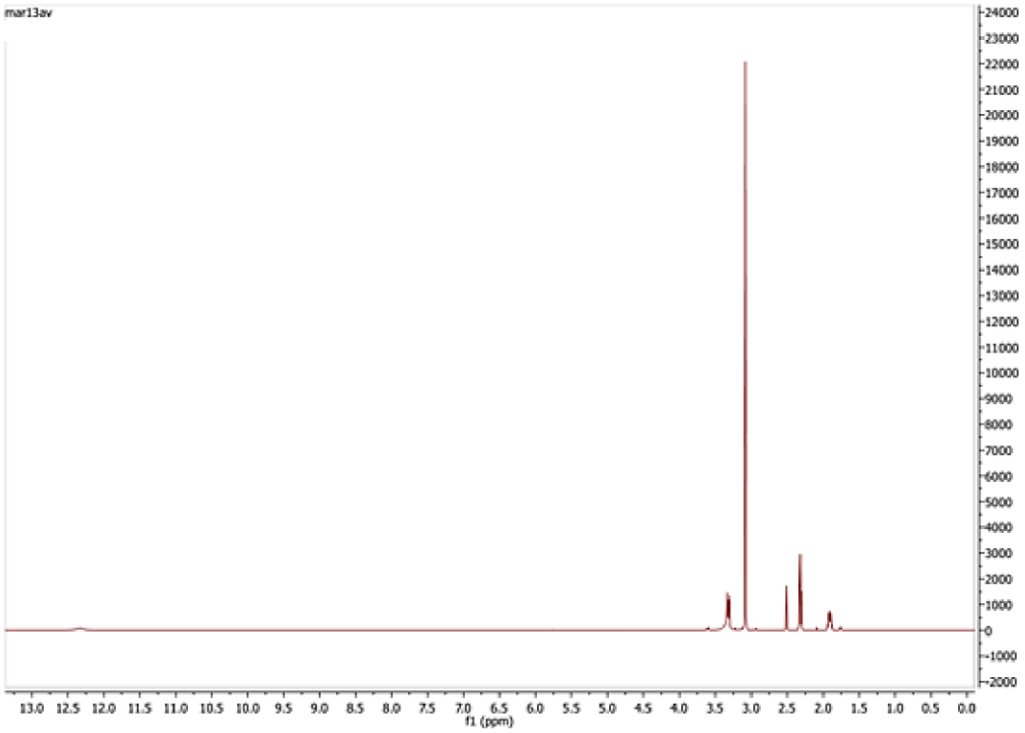

Figure S52: *^{1}H NMR of* ***18****.*

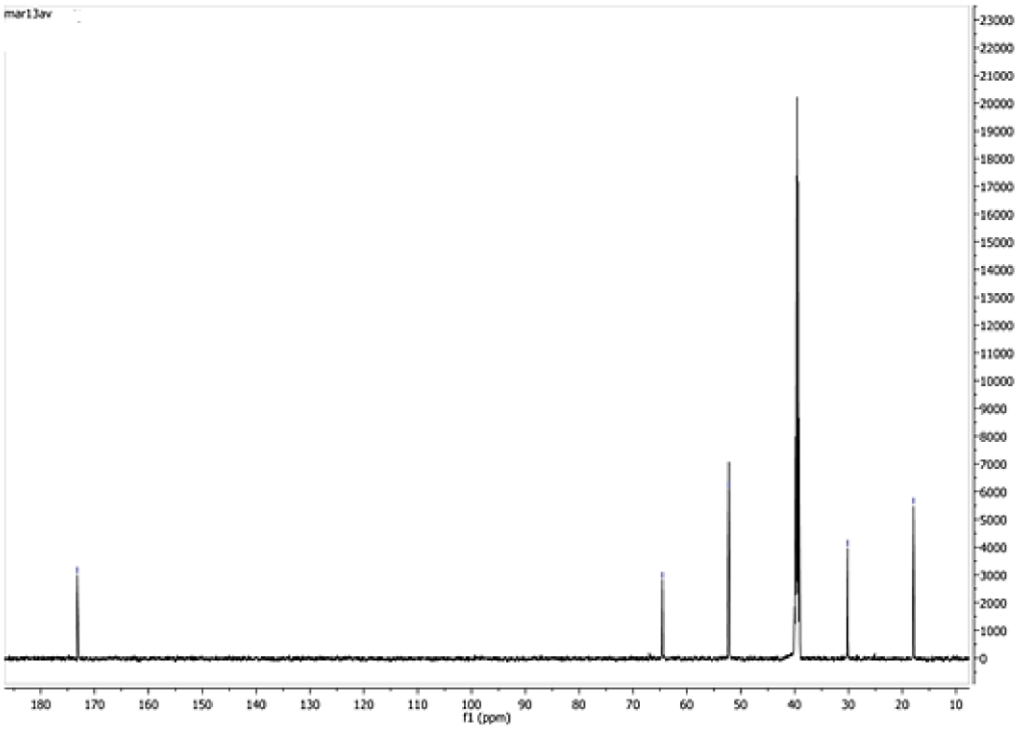

Figure S53: *^{13}C NMR of* ***18****.*

4-trimethylammoniumbutyric acid-NHS ester 19

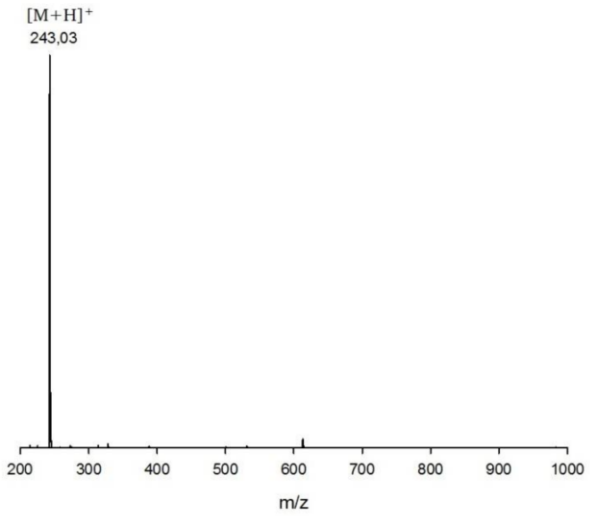

Figure S54: *ESI-MS of* ***19****. Calculated for* $C_{11}H_{19}N_2O_4^+$ *m/z: 243.28, measured 243.03* $[M+H]^+$.

N-Trt-protected β-alanine 22

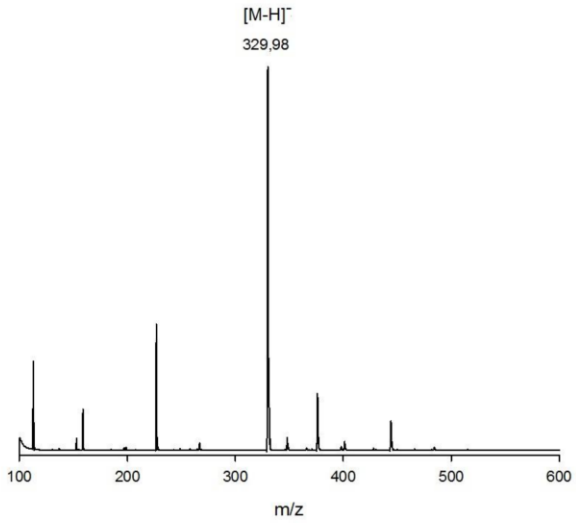

Figure S55: *ESI-MS of* ***22****. Calculated for* $C_{22}H_{21}NO_2$ *m/z: 331.42, measured 329.98* $[M-H]^-$.

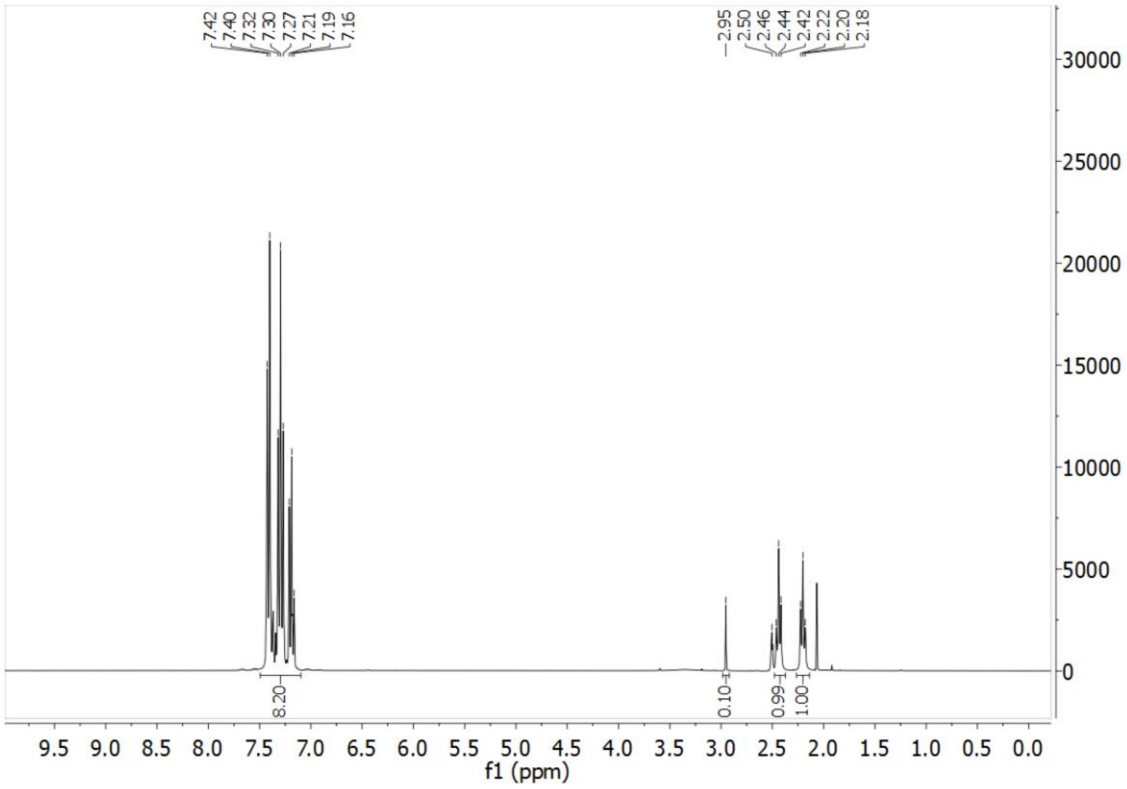

Figure S56: *^{1}H NMR of* ***22****.*

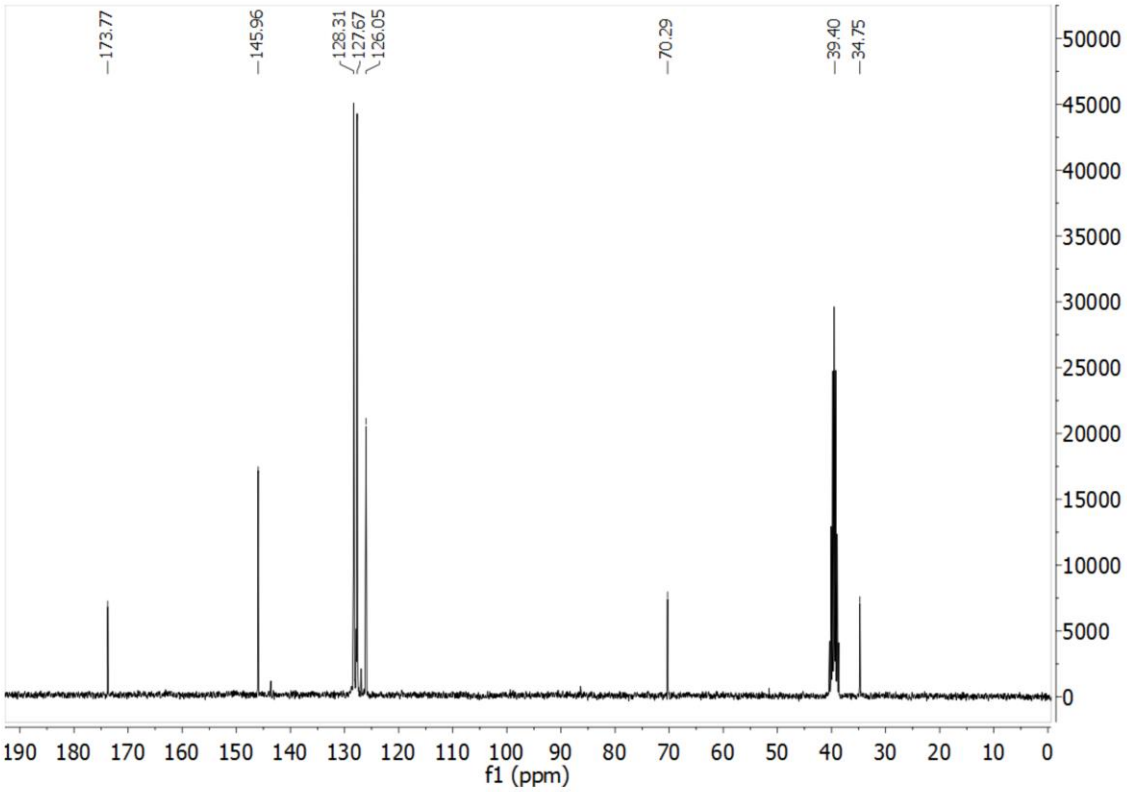

Figure S57: *^{13}C NMR of* ***22****.*

COSS derivative 23 (monoTrt-aminoCOSS)

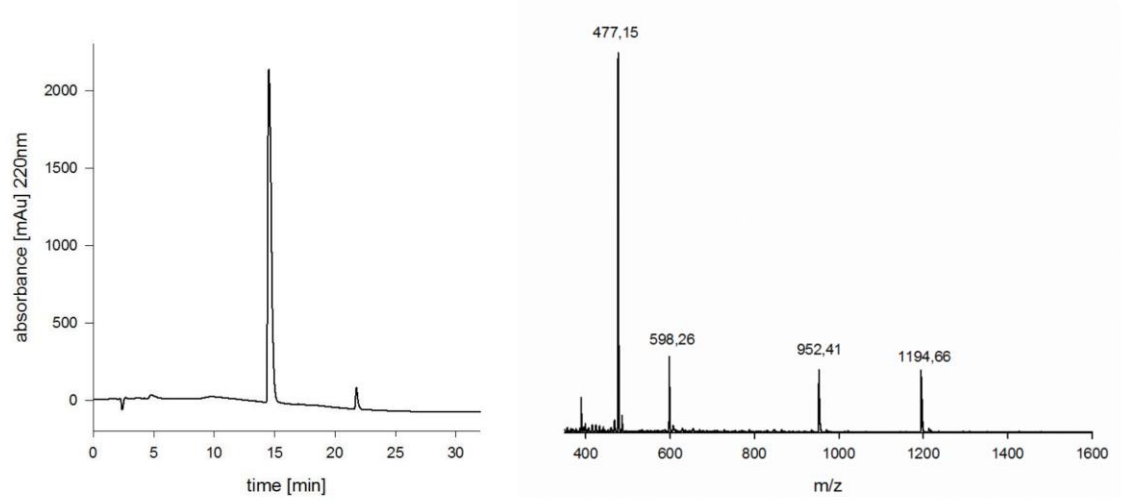

Figure S58: *Left: Analytical HPLC diagram of* ***23*** *at λ=220 nm. Right: ESI-MS spectrum of* ***23****. Calculated for* $C_{46}H_{83}N_9O_{13}Si_8$ *m/z: 1194.90, measured 1194.66* $[M+H]^+$*, calculated 598.45, measured 598.26* $[M+2H]^{2+}$*.*

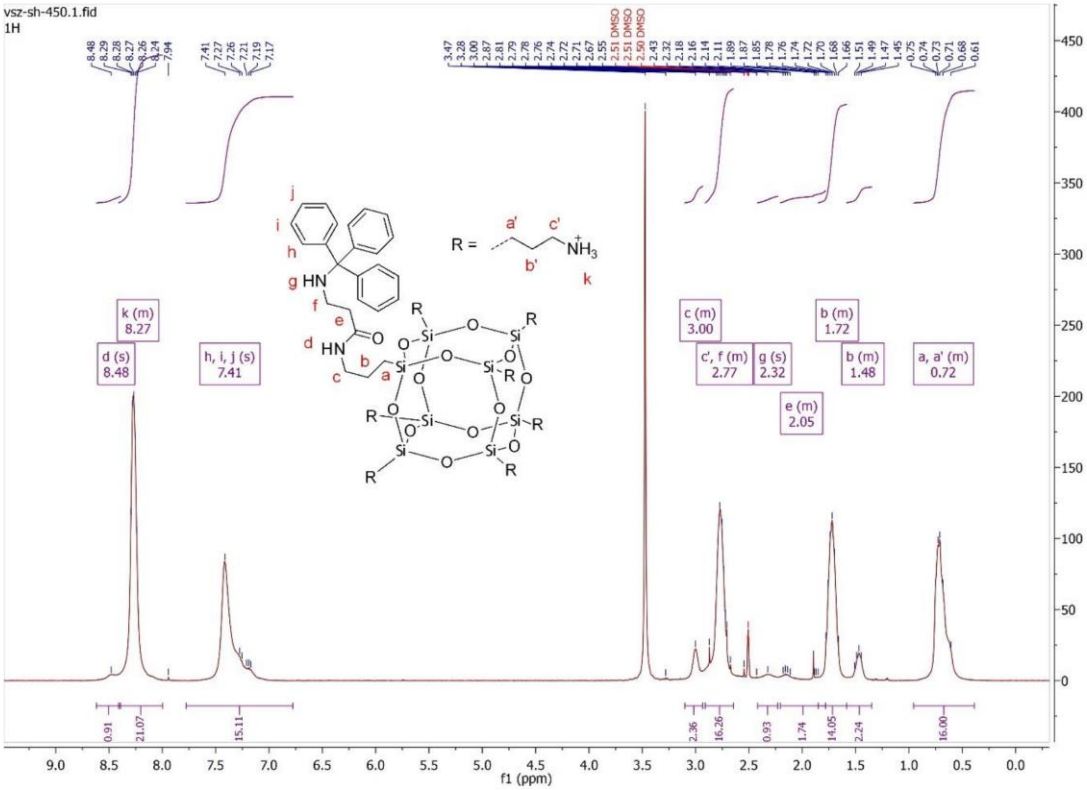

Figure S59: *^{1}H NMR spectrum of* ***23****.*

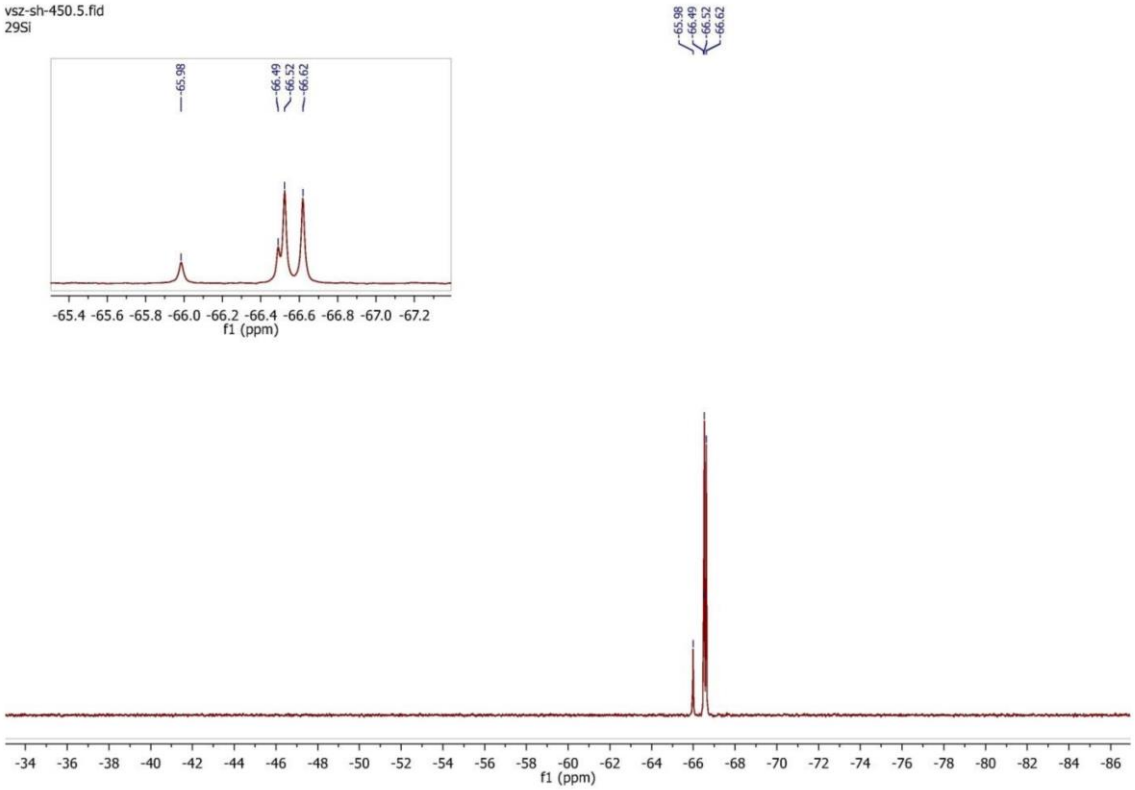

Figure S60: *^{29}Si NMR spectrum of* ***23****.*

COSS derivative 24 (Trt-protected GuCOSS)

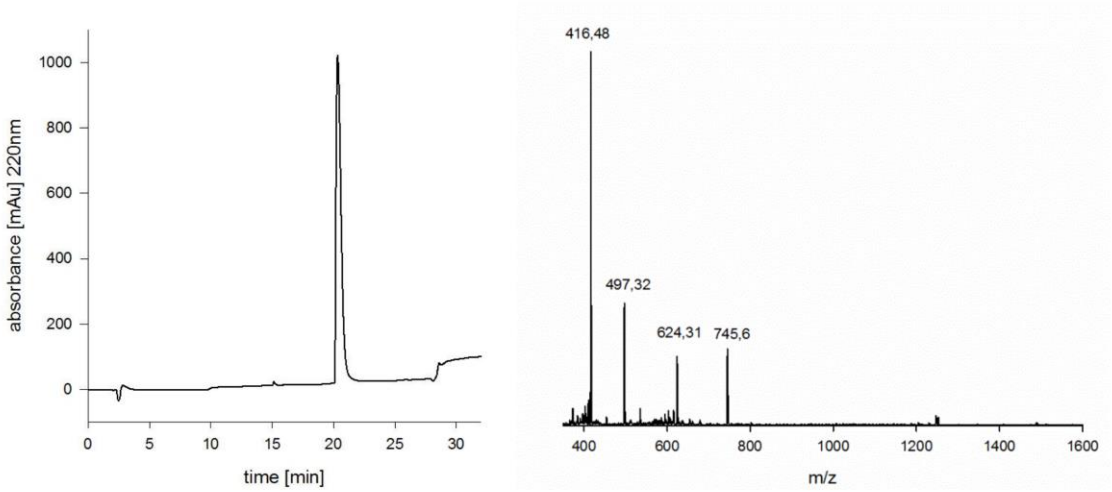

Figure S61: *Left: Analytical HPLC diagram of* ***24*** *at λ=220 nm. Right: ESI-MS of* ***24****. Calculated for $C_{53}H_{97}N_{23}O_{13}Si_8$ m/z: 745.58, measured 745.61 $[M+2H]^{2+}$, calculated 497.39, measured 497.32 $[M+3H]^{3+}$.*

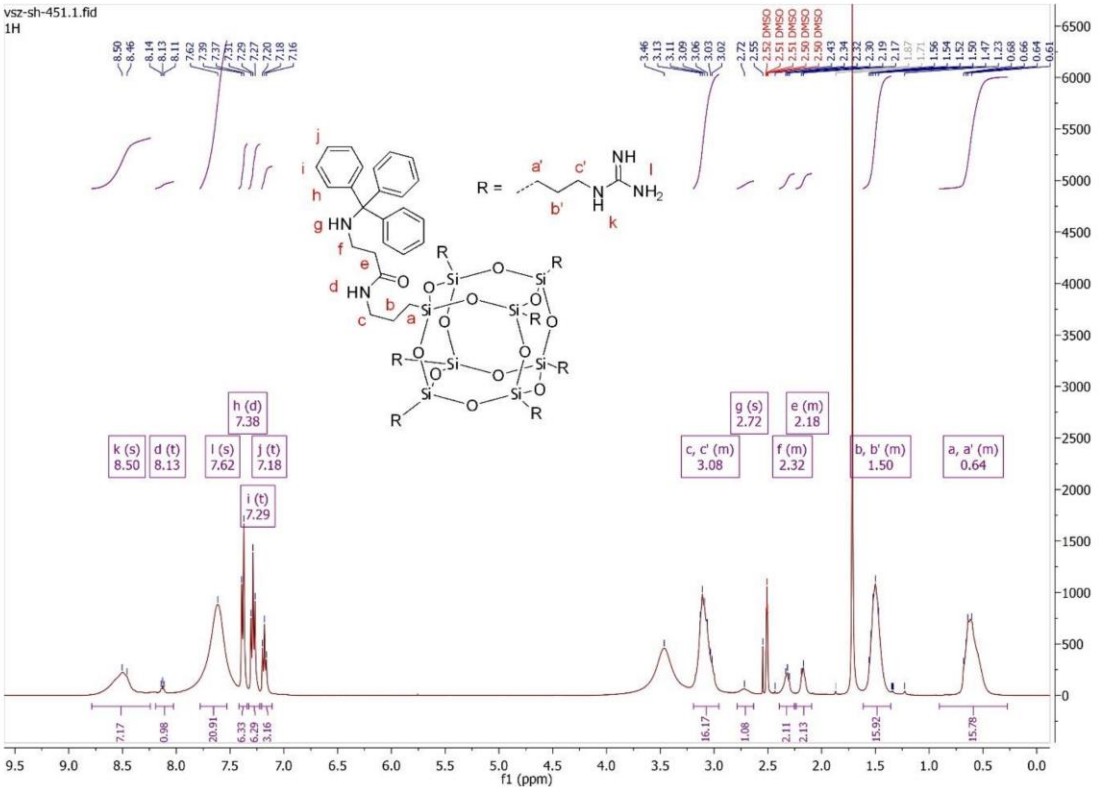

Figure S62: *^{1}H NMR spectrum of* ***24****.*

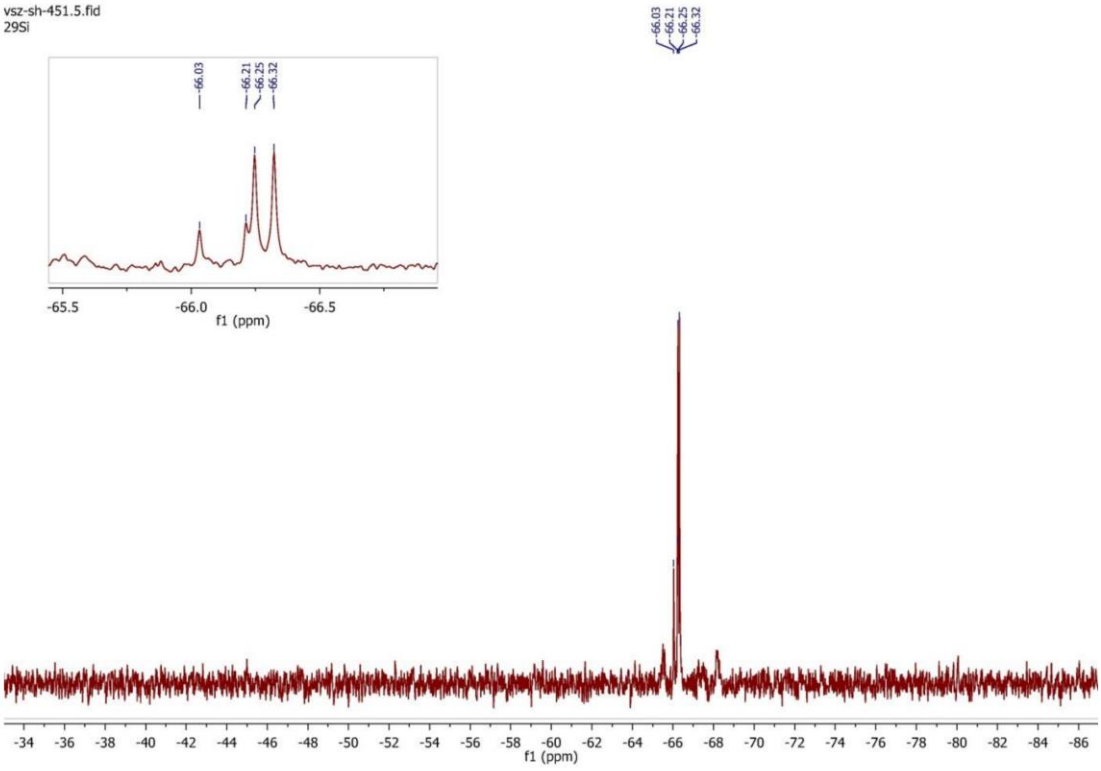

Figure S63: *^{29}Si NMR spectrum of* ***24****.*

COSS derivative 27 (PG-Cys-aminoCOSS)

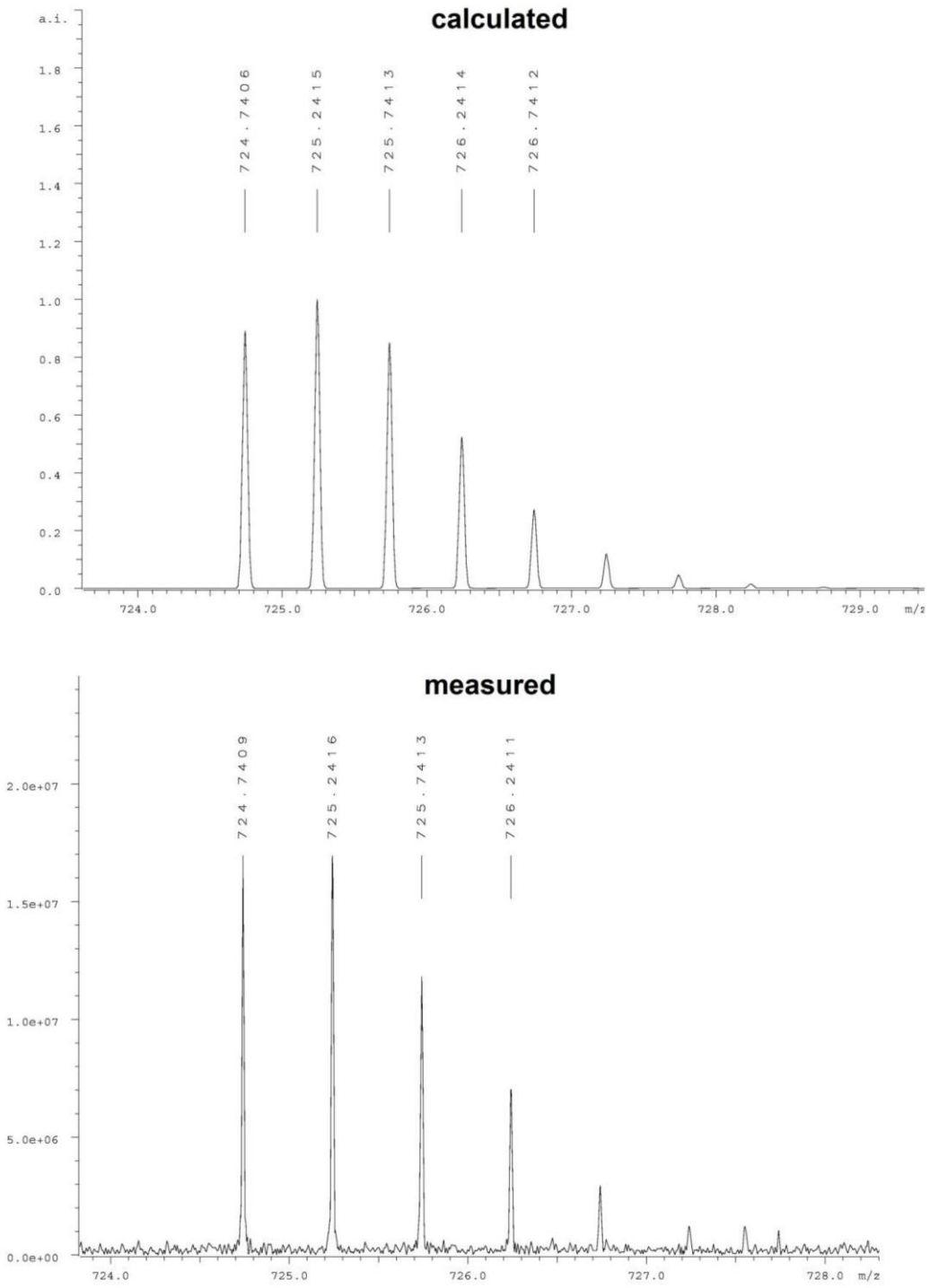

Figure S64: *HR-MS of* ***27****. Calculated for* $C_{61}H_{93}N_9O_{15}SSi_8$ *m/z: 724.7406, measured 724.7409* $[M+2H]^{2+}$.

COSS derivative 28 (Cys-GuCOSS)

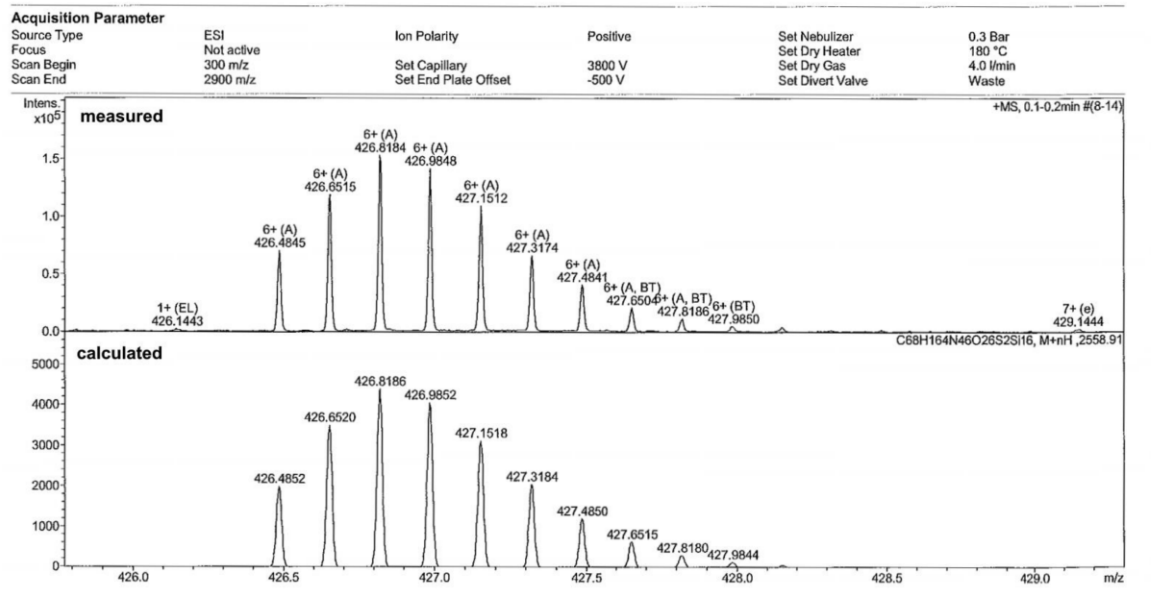

Figure S65: *HR-MS of* ***28****. Calculated for* $C_{68}H_{164}N_{46}O_{26}S_2Si_{16}$ *m/z: 426.4852, measured 426.4845* $[M+6H]^{6+}$.

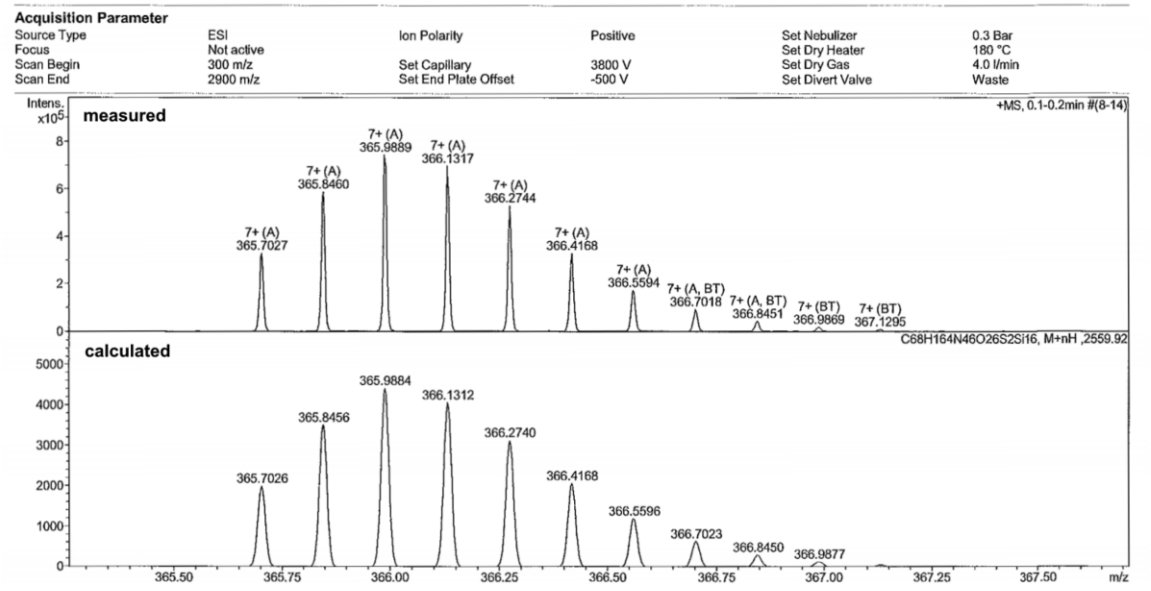

Figure S66: *HR-MS of* ***28****. Calculated for* $C_{68}H_{164}N_{46}O_{26}S_2Si_{16}$ *m/z: 365.7026, measured 365.7027* $[M+7H]^{7+}$.

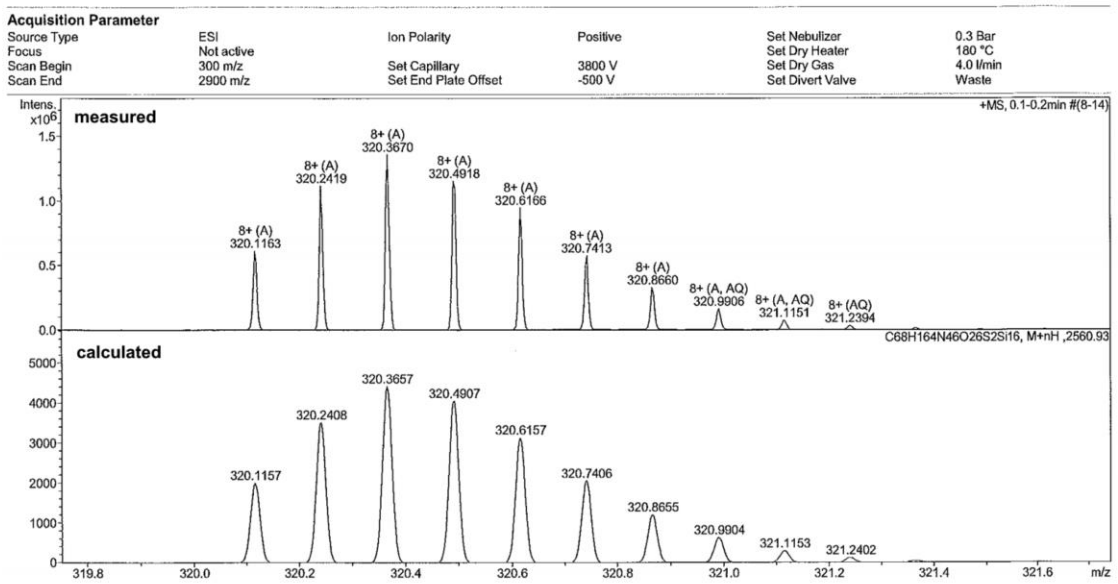

Figure S67: *HR-MS of* ***28****. Calculated for* $C_{68}H_{164}N_{46}O_{26}S_2Si_{16}$ *m/z: 320.1157, measured 320.1163* $[M+8H]^{8+}$.

3-(pyridin-2-yldisulfanyl)propanoic acid) 31

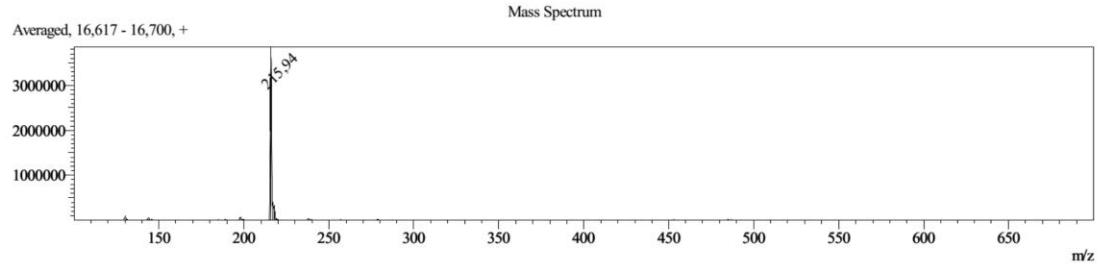

Figure S68: *ESI-MS of* ***31****. Calculated for* $C_8H_9NO_2S_2$ *m/z: 215.29, measured 215.94* $[M+H]^+$.

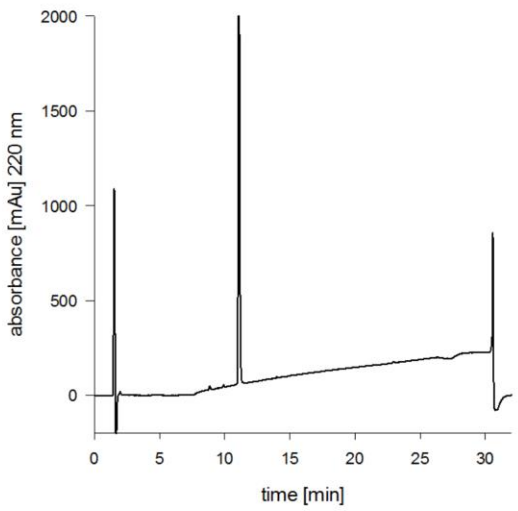

Figure S69: *Analytical HPLC diagram of* ***31****. λ=220 nm.*

Aldrithiol-activated doxorubicin 32

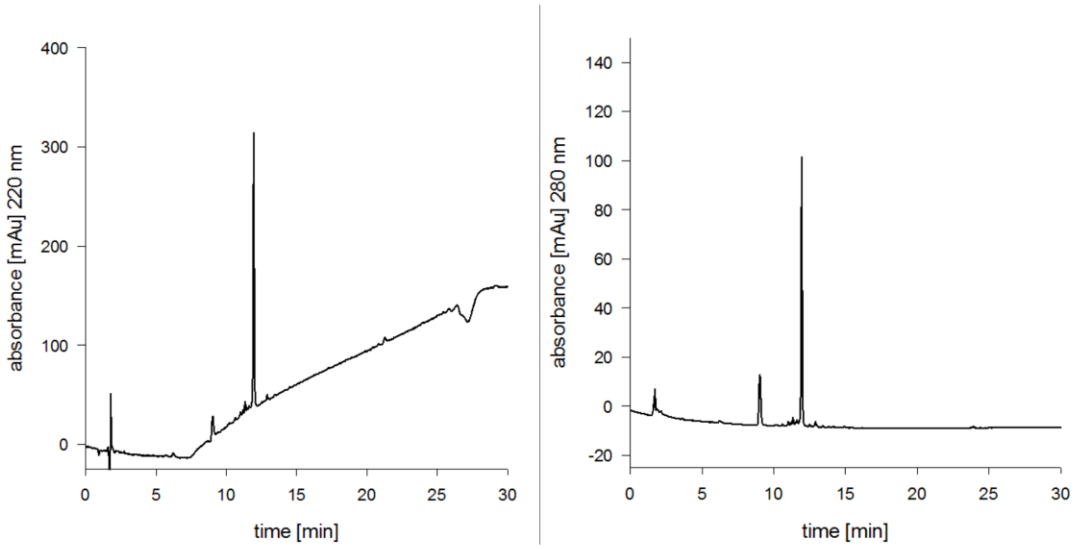

Figure S70: *Analytical HPLC diagrams of* ***32****. Left: λ=220 nm; right: λ=280 nm.*

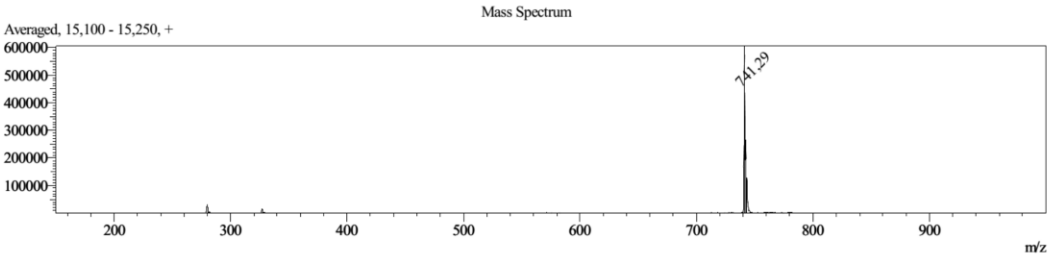

Figure S71: *ESI-MS of* ***32****. Calculated for $C_{35}H_{36}N_2O_{12}S_2$ m/z: 740.80, measured 741.29 $[M+H]^+$.*

References

[1] a) D. W. Grogan, *J. Bacteriol.* **1989**, *171*, 6710-6719; b) T. D. Brock, K. M. Brock, R. T. Belly, W. R. L., *Arch. Mikrobiol.* **1972**, *84*, 54-68.

[2] T. Hechler, F. Pfeifer, *Molecular microbiology,* **2009**, *71*, 132-145.

[3] C. Morano, X. Zhang, L. D. Fricker, *Anal. Chem.,* **2008**, *80*, 9298-9309.

Danksagung

"I can no other answer make but thanks, and thanks, and ever thanks." William Shakespeare

Es gibt unglaublich viele Personen, denen ich aufrichtig für ihre Beratung und Unterstützung in jeglicher Form danken möchte.

Zu allererst möchte ich natürlich meinem Doktorvater **Prof. Dr. Harald Kolmar** danken. Ohne Deine Unterstützung wäre diese Arbeit nicht möglich gewesen. Vielen Dank für das entgegengebrachte Vertrauen und die Freiheiten die Du mir gegeben hast Projekte auszuprobieren und auch für die vielen anregenden wissenschaftlichen Gespräche.

Prof. Dr. Siegfried Neumann, möchte ich für die Übernahme des Korreferats und für das rege Interesse und die tatkräftige Unterstützung, nicht nur bei Sulfotools, sondern auch an meiner Dissertation, sowie für viele anregende Gespräche, die mit dem Teilen seines umfangreichen Wissens persönlichen Erfahrungen verbunden waren, danken.

Bei **Prof. Dr. Markus Biesalski** und **Prof. Dr. Hans Ulrich Göringer** möchte ich mich für die Übernahme der Fachprüfungen bedanken.

Olga „Olgi" Avrutina, danke ich für die uneingeschränkte Unterstützung und dass Du Dir immer Zeit für mich genommen hast. Die „harte" Schule des Englischschreibens, die jeder Chemiker schon während des Studiums bei Dir durchlaufen muss, hat das Verfassen dieser Arbeit in dieser Form ermöglicht. Vielen Dank dafür!

Barbara „Barbarella" Diestelmann, vielen Dank für die schönen, unterhaltsamen gemeinsamen Pausen auf dem Sonnendeck und für die Freundschaft die über die Jahre entstanden ist. Natürlich auch für den Support bei Formalitäten und dem ganzen Papierkrieg.

Sebastian Hörner, mein Hörni, Dir möchte ich besonders für die langjährige Freundschaft danken, die weit über unsere gemeinsame Benchzeit hinausgeht. Ebenfalls dankbar bin ich Dir für die großartige Zusammenarbeit und langen Labornächte während unseren gemeinsamen Projekten, die vielen Konzert-, Koch- und Trinkabende, Konferenzbesuche, Arbeitsgruppenausflüge, Shopping-, Fahrrad- und Lauftouren und für die Ausflüge, vor allem der unvergessliche Madridausflug!

Thomas „Thombert" Hofmeyer danke ich für die geduldige Anleitung im biologischen Arbeiten (vor allem während meiner Diplomarbeit), die erfolgreiche Zusammenarbeit in verschiedenen Projekten, die lustigen Abende mit „el fermentero", die Konferenzbesuche, Kochkässchnitzel- und Äpplerabende, die Weinlagenwanderung und natürlich auch für den unvergesslichen Madridausflug!

Stefan Zielonka, Dir möchte ich natürlich für die tolle Zusammenarbeit im Labor, aber viel mehr eigentlich für Deine Freundschaft danken. Die unzähligen Konzertabende, die zur Erweiterung meines musikalischen Horizonts beigetragen haben, die Diskussionen/Gespräche über Musik und die Welt, die lustigen Kicker-, Koch- und Äpplerabende, die Kaffeepausen auf dem Sonnendeck, die Konferenzbesuche (PEGS Wien) und die vielen gemeinsamen Ausflüge, vielen Dank dafür!

Achim Dörner, vielen Dank für Deine Freundschaft und Deinen unglaublichen Optimismus und Deine gute Laune, mit denen Du unsere Treffen immer bereichert hast und ich freue mich auf viele weitere Kneipen(41)abende!

Sascha Knauer möchte ich für die großartige Chance danken, bei Sulfotools mitzumachen und für viele unterhaltsame Stunden bei Workshops, Wettbewerben und anderen Veranstaltungen, sowie die

gute Kooperation in gemeinsamen Projekten. Des Weiteren möchte ich auch **Niklas Koch** für die angenehme Zusammenarbeit bei Sulfotools und für die amüsanten Konzertbesuche danken.

Niklas „Nick" Weber möchte ich für die gemeinsamen Kochabende/-nächte und feuchtfröhlichen Konzertbesuche danken.

Janine „Fritzi" Becker, Du bist und bleibst die gute Seele des AK Kolmars und bist meine persönliche Klonierheldin. Vielen Dank für Deine Unterstützung auf allen Ebenen!

Vanessa „Vansa" Siegmund möchte ich für die Feierabendbierchen auf dem Sonnendeck, im Herrngarten oder Schlossgarten und schönen Gespräche danken!

Bei dem Chaostrupp **Bernhard „Perni" Valldorf**, **Stephan „Dickie" Dickgiesser**, **Heiko „Heiki" Fittler**, **Doreen „Dorn" Könning, Christian „Schröti" Schröter, Simon Krah, Julius „Jules" Grzeschick** möchte ich mich für die erfreuliche Laborzeit, die vielen „schlechtlustigen" Witze mit der Heikotränenskala, den Labor Gossip, die geschmacklich fragwürdige musikalische Unterhaltung im Labor, die Grillaktionen im Herrngarten und die feuchtfröhlichen Feiereien an der Uni bedanken!

Carolin „Caro" Mai möchte ich für die lustige und spannende Laborzeit und den unvergesslichen Madridausflug danken.

Auch bei allen ehemaligen Doktoranden, die ich nicht explizit aufgeführt habe, die aber selbstverständlich auch zu der angenehmen, amüsanten und heimischen Atmosphäre im Kolmar Labor beigetragen haben, möchte ich mich bedanken**: Sebastian „Fabi" Fabritz, Bernhard „Grobi" Glotzbach, Michael „Reini" Reinwarth, Martin Empting, Franziska „Fränzi" und Alexander „Schumi" Maass, Tim „Timää" Heiseler.**

Ebenfalls bedanken möchte ich mich bei **Cecilia „Cielie" Gorus, Andreas Christmann** und der „neuen Belegschaft" des AK Kolmars, **Thomas Pirzer, Lukas „Klaus" Deweid, Aileen Ebenig, Hendrik Schneider** und bei allen die ich vergessen habe.

Meiner Familie, **Reinhold, Ulrike** und **Timo Uth** möchte ich einen besonderen Dank aussprechen. Ihr habt mich immer unterstützt, wart und seid für mich da, habt mir meine Freiheiten gelassen und meine Entscheidungen nie in Frage gestellt, vielen Dank!!!

Last but not least, möchte ich natürlich auch meine Freunde nicht vergessen, die mich während dieser Zeit und darüber hinaus immer unterstützt haben und für mich da waren.
Petra Blank, meine Lieblings-MB, Dir möchte ich für Dein Verständnis, Dein immer offenes Ohr, den anderen Blickwinkel auf Dinge danken, sowie natürlich auch für die unzähligen gemütlichen WG-Abende, die entspannten Herrngarten-Scrabble-Sonntage, die lustigen und sehr bereichernden Gespräche.
Meinen Mädelz, **Franziska „Franzi" Zoubek, Carina „Careen" Fath, Ivana Cubelic, Marc Federmeyer** (ja, Du gehörst da auch dazu), **Katrin „Trine" Uhrig, Aleksandra „Alex" Bukowska, Catherine Kolz-Mädge, Christine „Tine" Bachmann,** möchte ich für Eure emotionale Unterstützung und für Eure Freundschaft danken, sowie für die unzähligen feuchtfröhlichen Tanznächte, Besuche, Ausflüge (besonders der Hollandtrip), Weinlieferungen, langen Telefonate und Gespräche, entspannte Clusterabende und alles was ich jetzt vergessen habe. Vielen Dank, dass Ihr für mich da seid!

Appendix

Dipl.-Ing.
Christina Uth
Schleiermacherstraße 18
64283 Darmstadt
uth@biochemie-tud.de
uth@sulfotools.com

Darmstadt,19.09.2016

Erklärung

Ich erkläre hiermit, dass ich meine Dissertation selbständig und nur mit den angegebenen Hilfsmitteln angefertigt habe.

_____

Dipl.-Ing. Christina Uth

Dipl.-Ing.
Christina Uth
Schleiermacherstraße 18
64283 Darmstadt
uth@biochemie-tud.de
uth@sulfotools.com

Darmstadt, 19.09.2016

Erklärung

Ich erkläre hiermit, noch keinen Promotionsversuch unternommen zu haben.

_____

Dipl.-Ing. Christina Uth

LEBENSLAUF	Dipl.-Ing. Christina Uth
PERSÖNLICHE DATEN	
Geburtsdatum	19. April 1983
Geburtsort	Seoul (Südkorea)
Adresse	Schleiermacherstraße 18, 64283 Darmstadt, Germany
WERDEGANG	
Seit 03/2016	Geschäftsführerin Sulfotools GmbH
Seit 09/2011	Wissenschaftliche Mitarbeiterin und postgraduales Studium an der Technischen Universität Darmstadt (AK Prof. Kolmar)
2002-2011	Chemiestudium an der Ruprecht-Karls-Universität Heidelberg und Technischen Universität Darmstadt Hauptfach: Biochemie Nebenfach: Organische Chemie Diplomarbeit: **"Towards synthetic bioconjugates for targeted delivery of a cytotoxic drug to *trypanosoma brucei*"** Abschluss: Diplom-Ingenieur (TUD)
9/2007 - 3/2008	**Auslandsstudium** Universidad Alcalá de Henares, Spanien **Forschungsprojekt in organischer Synthesechemie:** „Electroreduction of trichloroacetyl esters of aldols"
SONSTIGE AKTIVITÄTEN	
2014-2016	▪ Gewinner des deutschen *Clean Launchpad* Finales (Hessen) 2014 ▪ Teilnahme europäisches Finale Valencia (*Clean Launchpad*) 2014 ▪ Gewinner Konzeptphase Science4Life 2015 ▪ 2. Platz Science4Life Technology Slam 2015 ▪ 2. Platz Business Plan Phase Science4Life 2015 ▪ Gewinner StartGreen Award 2015, Kategorie Gründungskonzept ▪ Merck Merck Accelerator Programm 2015 ▪ Climate-KIC Accelerator 2015 Stage 1+2 ▪ EXIST-Forschungstransfer I (08/2015-01/2017)

_____

Dipl.-Ing. Christina Uth